GL01794

CENTRAL WESTERN AND HIGH CASCADES GEOLOGICAL RECONNAISSANCE, AND HEAT FLOW HOLE LOCATION RECOMMENDATIONS

NORMAN V. PETERSON
State Department of Geology and Mineral Industries

and

WALTER YOUNGQUIST
Consultant

Open File Report O-75-2, 41p.

November 1, 1975

TABLE OF CONTENTS

TABLE OF ILLUSTRATIONS

TABLE OF ILLUSTRATIONS
(continued)

TABLE OF TABLES

PURPOSE AND SCOPE OF REPORT

This report has been prepared to provide, in part, the basis for decisions as to where a Western Cascades-High Cascades heat flow drill hole program might be conducted which would produce the largest amount of good quality information for the resources available for this project. As presently envisioned, a heat flow drill hole program will be conducted in this area in 1976, and it has been assumed for the purposes of this study that approximately eight holes, each taken to a depth of about 500 feet, will be drilled. All these figures, however, are to be considered tentative, and subject to adjustment.

The area to be examined by means of this heat flow study, and the area which is the topic of this report is shown outlined on Figure 1 (next page).

The area embraces the region from and including Breitenbush Springs and southward along the western side of the Cascades from near their crest to a distance westward of about three townships. The north-south extent of this region is about 14 townships, and terminates a few miles south of the Kitson Hot Spring-McCredie Hot Spring area near Oakridge. The total area involved is somewhat in excess of 1500 square miles.

It is the purpose of this report to briefly consider the geology of this area, with special reference as to the quality of information which might be expected from heat flow holes here. Particular attention is paid to the matter of the possible effect of subsurface shallow water circulation on the data obtained. The report also proposes to reduce this larger area to several geological and geographical subdivisions for purposes of insuring that a reasonable geographic spread is obtained by the drilling program, and that ultimately a map with sufficiently well distributed points can be prepared which will give a significant picture of the heat flow variations and trends in this region.

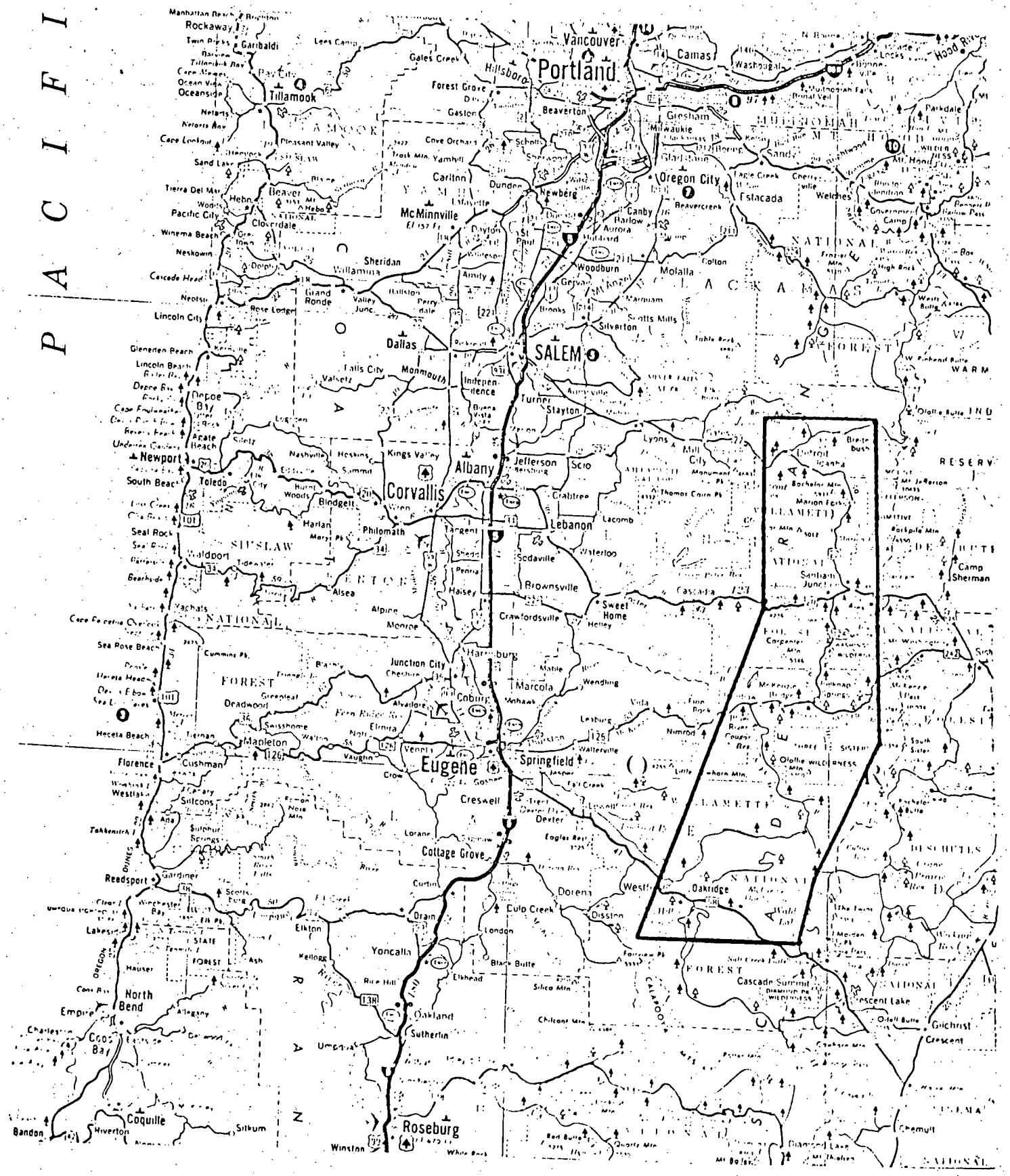

FIGURE 1. Index map showing in outline the area concerned in this report.

GEOLOGICAL RECONNAISSANCE OF THE REGION

Previous studies and present work. The Western Cascades have not been studied in any great detail except for a few local areas. The terrain is rugged, with local relief to several thousand feet. Rock exposures are poor, the vegatative cover is heavy, and the region exhibits a great variety and complexity of rock units even in a short distance. It can be conservatively stated that in many areas if there is a continuous exposure for a distance of 100 yards horizontally, it is rare that only one rock type is exposed. Commonly, several quite different rocks are present in this distance. Lacking any substantial economic reason to spend exploration money in this region to date, it has been studied only in a general way for the most part. The work of Peck, et al., 1964, remains the only large study. However, more recently Dr. Paul Hammondof Portland State University, and his students, have been doing detailed stratigraphic work in selected areas, notably in the Breitenbush Valley and adjacent terrains. In view of the designation of Breitenbush as a KGRA, and the leasing interest in this area, this is a fortunate circumstance.

During this present study, which was conducted chiefly in the month of August, 1975, all major drainages were studied, and many minor drainages were also examined. Extensive rock sampling was done, and comparisons of rock types were made directly in the field.

Peck, et al., 1964, note that natural rock outcrops in the Western Cascades make up less than 1 percent of the total area, and these exposures are confined chiefly to ridgetops and stream bottoms. More recently, an extensive series of logging roads has provided the best outcrops, and afford a relatively rapid method of geological reconnaissance and a view of most of what good rock exposures as do exist. Again, however, the total area of exposed rock relative to the total area involved is very small. When this fact is combined with the great complexity of the geology, the difficulties of preparing accurate maps in any detail quickly become apparent.

Peck, et al.,(1964, p. 1) have noted that

> "The calc-alkalic volcanic rocks of the Western Cascade Range in Oregon have a total volume of about 25,000 cubic miles, and an average composition of silicic andesite or dacite. Andesite that has a silica content of about 56 percent is the most abundant rock type; rocks containing 63 to 68 percent silica are sparse, and rocks containing 70 percent silica are moderately abundant. Most of the volcanic activity in the Cascade Range was apparently concentrated in northward-trending belts, which in general have shifted progressively eastward during the Cenozoic."

During Eocene time, volcanism took place along the Oregon coastline which at that time lay somewhat eastward of Eugene. As volcanism became more intense, the land rose, the sea retreated westward, and the volcanic activity, as noted by Peck et al., appears to have shifted gradually eastward.

More than half the Western Cascade volcanic rocks are pyroclastics, and, as has been noted, basaltic andesite, andesite, and dacite are the most common rock types. In detail, the sections consist of numerous ash flow tuffs, ash falls, interbedded lava flows, volcanic breccias and agglomerates in a very large range of fragment sizes, dikes and dike swarms, small intrusives other than dikes of various shapes and sizes, and minor pond and lake deposits formed in drainages which were interrupted by landslides, mudflows, and/or lava flows (as is the case of Clear Lake at present, formed by lava flows about 3,000 years ago which came across the upper portion of the North Fork of the McKenzie River). Tuff breccias, vitric tuffs, and related rock types, in an almost infinite variety, are abundant. Of all the various lithologic units, huge mudflows consisting of weathered ash with very poorly sorted angular to well rounded pebbles, cobbles, and boulders are one of the most common. Some typical outcrops of these

various rock types are shown in Figures 2-5.

FIGURE 2. Mudflow complex exposed in lower portion of Deer Creek Canyon, tributary to North Fork of the McKenzie River.

FIGURE 3. Mudflow exposed on west side of Cougar Reservoir, a dammed portion of South Fork of the McKenzie River.

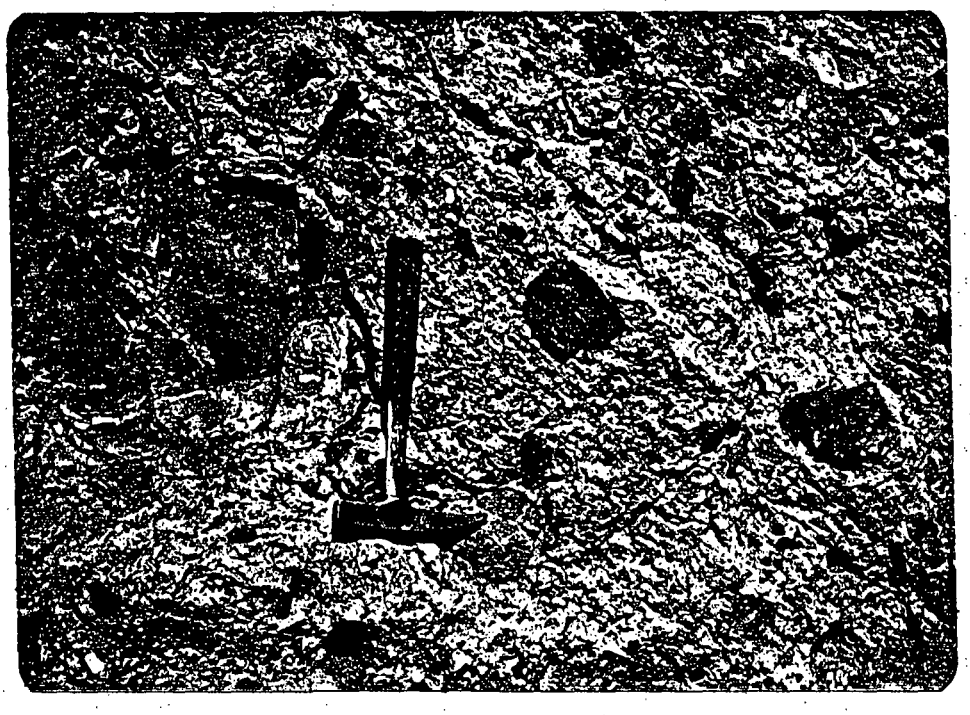

FIGURE 4. Lithified mudflow exposed in east abutment of Hills Creek dam, southeast of Oakridge, on Middle Fork Willamette River. Some rock debris in this section are 10 feet or more in long dimension. A granitic fragment was obtained from this exposure.

FIGURE 5. Lava flow which filled small gully, exposed on Lookout Ridge, which is the north valley wall of the McKenzie River, on Mill Creek road, north of the small community of Rainbow.

Some of the lava flows are thin, in places only a foot or two thick, and may occur in a series of half dozen or more flow units in a short vertical interval, as well shown by the section exposed in the spillway at the Smith River Reservoir, seen here in Figure 6.

FIGURE 6. Spillway at Smith River Reservoir, showing numerous thin lava flows interbedded with volcanic tuffs and breccias.

Some of the lava flows, however, are quite thick (to 100 feet or more), and many appear to have flowed down steep-walled narrow canyons, in some instances for distances of several miles. These massive flows now tend to stand out as steep ridges (Figure 7), as they are much more resistant to erosion than are the volcanoclastics which make up the bulk of the Western Cascades. In some instances, High Cascade lavas have flowed down valleys into the Western Cascades region for distances of a few to up to more than 10 miles and now stand

out as prominent landforms. Foley Ridge, a well-known physiographic feature northeast of McKenzie Bridge, appears to us to have had this origin.

FIGURE 7. Massive lava flow, forming prominent ridge along mid-portion of west side of Cougar Reservoir, South Fork of the McKenzie River.

Peck et al., 1964, indicate that the volcanic sequence in the Western Cascades in the vicinity of Glide, and Illahee Rock, Oregon, totals some 6,000 to 15,000 feet in thickness. Their stratigraphic section for this area is shown on Figure 8. One can only conjecture as to the thickness of the Tertiary volcanic section in the central Cascades--the area under consideration in this report, but thicknesses of 20,000 to 30,000 feet do not seem impossible.

It is noteworthy that Peck et al. were able to recognize

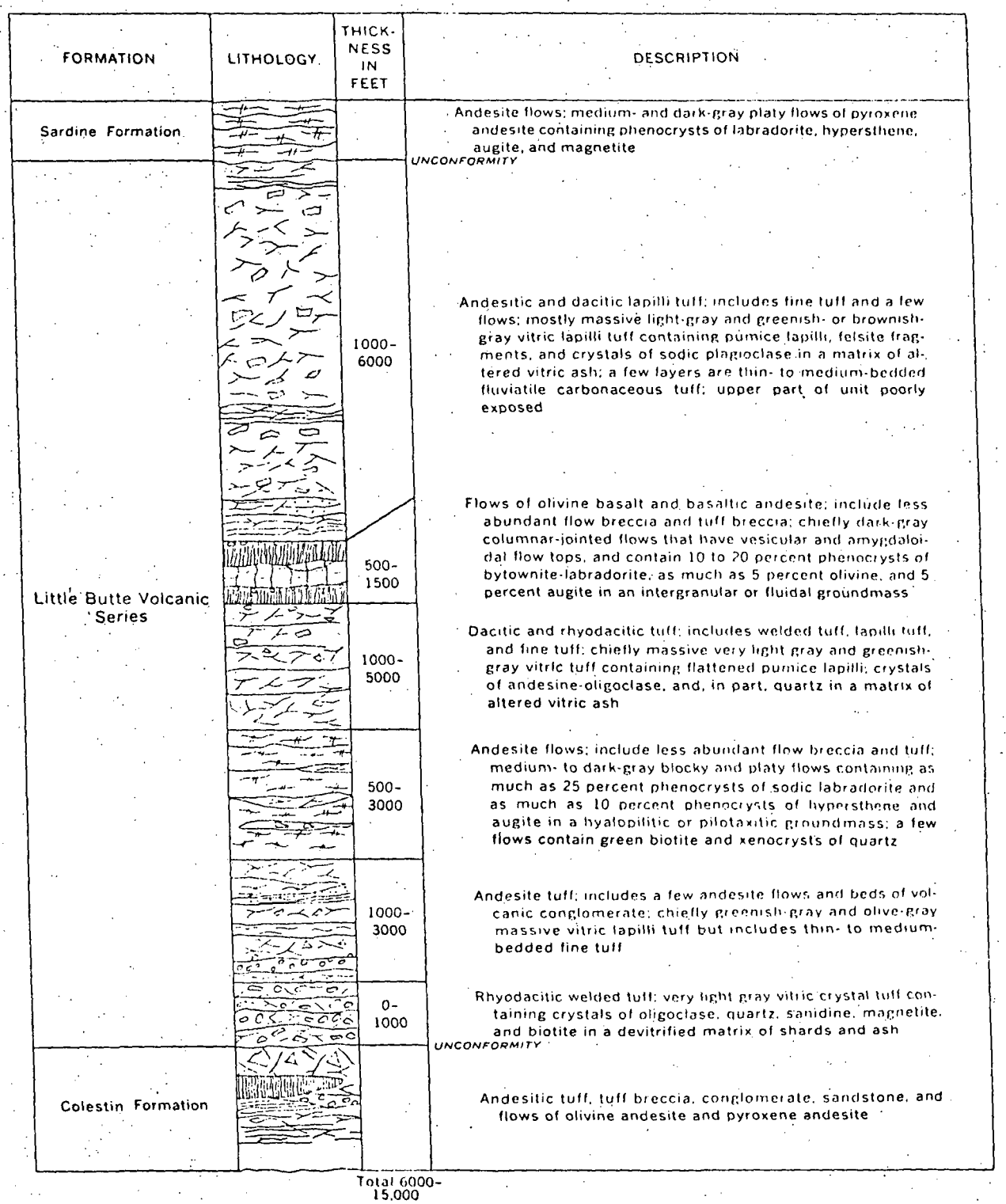

Generalized columnar section of the Little Butte Volcanic Series along the Little River and the North Umpqua River between Glide and Illahee Rock, Oreg.

FIGURE 8. A stratigraphic column of a portion of the Western Cascades, taken from Peck, et al., 1964.

only very broad subdivisions in this thick volcanic sequence. We have made consistent effort to recognize distinctive rock types and to try to carry these rock types beyond local areas in our studies, but results have been almost uniformly negative. The persistence of a given rock unit as such over any great distance (more than a few tens of miles) seems to us unlikely. On the other hand, there may have been certain episodic volcanic events during the Tertiary which for a given time might produce a characteristic rock type from numerous vents over a wide area. As our studies have been relatively local rather than regional, we are not in a position to comment on this matter with any authority. It does seem clear to us that there were numerous volcanic centers. Some were well defined, typical cones, others were fracture zones. They differed greatly in size. Numerous parasitic volcanic centers developed around larger centers. The general nature of these centers was that the more solid, large, and denser rocks and flows tended to form and remain near these centers, and the peripheral areas received the finer pyroclastics, which, upon weathering, are less durable than the coarser pyroclastics and thick flows which tended to occur and remain nearer the vents. As a result, in the erosional processes which formed the present topography of the Western Cascades, the old volcanic centers even now tend to be the higher, prominent mountain ridges and peaks, and the present valleys follow around the margins of these volcanic centers and coincide therefore to some extent with the positions of the valleys in the Tertiary. That is, the present day topography reflects to a considerable degree the topographic highs and lows which developed during Tertiary volcanism (See, for example, Figure 19, page 27 showing Crescent Mountain volcanic center in well defined present day relief).

Further evidence of this comes from the fact that logging roads around these centers expose what we believe to be, for the most part, initial dips, and a plot of these dips indicates the locations of the various centers from which these materials have come. These centers in many cases are now topographic highs. One example

of this is the very distinctive rock type described by Taylor (in Dole, 1968, p. 12) which is exposed along U. S. Highway 126 at Trail Bridge Reservoir, and which is exposed also on the ridge to the west. The rock on the ridge has a 28 degree dip to the east (Figure 9) which can be projected down to the outcrop on the valley floor along the highway, and this 28 degree dip seems clearly to be an initial dip.

FIGURE 9. Flow or welded tuff now consisting of devitrified glass, with rock fragments, dipping 28 degrees off volcanic center to the west of Trail Bridge Reservoir, North Fork of McKenzie River.

Thus, in brief, the Western Cascades consist of numerous (hundreds) of volcanic centers, some cones, some fissures, which, erupting at various times, modified the topography and drainage lines. One side of a volcanic center will commonly show quite a different stratigraphic section in detail than another side. Direction and intensity of the prevailing wind during an eruption, rainfall, the location of drainage lines, varying intensities of the eruption, the breaking out of lava on one side of a cone versus another, and differing viscosities of flows, all contributed to an exceedingly complex picture. It is difficult to visualize how any individual rock unit could persist very far over this rough and varied topography, except possibly an ash fall or ash flow tuff. Even an ash fall would

almost immediately be dissected by streams, washed down the numerous steep slopes of the region, and otherwise be modified so that its recognition and use as an horizon marker would be difficult at best.

Each volcanic center appears to have its own stratigraphic column, mingled at its periphery with sections from other adjacent volcanic centers, and with each of these centers, as just noted, exhibiting somewhat to considerably different stratigraphic sections from one side of the center to another. Cause of many of these differences undoubtedly was the rugged topography of the region in the Tertiary, as evidenced not only by the high initial dips which are still preserved, but also by the tremendous mudflows and the size and angularly of the debris which are incorporated into them.

Notable also in the Western Cascades section is the presence of a number of silicic plutons which have been mineralized in minor amounts. These include the so-called Nimrod Granite (called by Peck, et al., 1964, a quartz monzonite) of the McKenzie drainage, a granodiorite stock west of Detroit, and the plutons of the Quartzville Creek area and adjacent drainages, and other mineralized areas such as on Crhisty Creek, on the North Fork of the Middle Fork of the Willamette drainage, presumably related to a shallow pluton. A map of these intrusives, taken from Peck, et al., 1964, is shown by Figure 10.

High Cascades and Western Cascades. A distinction is commonly made between the High or Young Cascades, and the Western Cascades. Peck et al., 1964, p. 1, state:

> "The Cascade Range in Oregon comprise two physiographic divisions: The Western Cascade Range, which includes a wide, deeply dissected belt of volcanic formations making up the western slope of the range, and the High Cascade Range, which includes chiefly younger cones and lava flows forming the nearly undissected crest of the range. The volcanic rocks of the Western Cascade Range are deformed and partially altered flows and pyroclastic rocks that range in age from

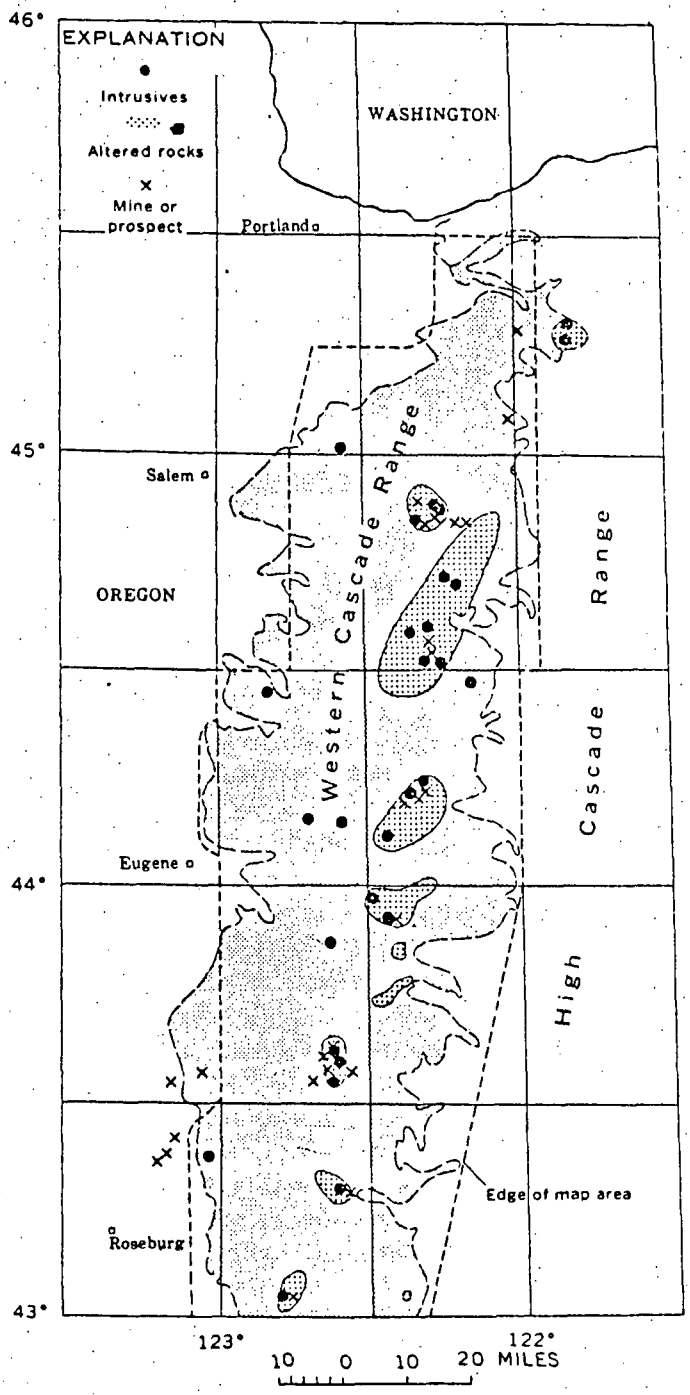

FIGURE 10. Location of diorite, quartz diorite, granodiorite, and quartz monzonite intrusives, areas of propylitically altered rocks, and mines and prospects in the Western Cascade Range in Oregon north of Latitude 43°. Western Cascade Range lightly shaded. (From Peck, et al., 1964).

late Eocene to late Miocene, as determined chiefly from fossil plants from more than 50 localities."

The divisions of High Cascades and Western Cascades, are, as Peck, et al., pointed out, physiographic divisions, and there is a question as to how sharp a geological distinction can be made between these two provinces, and how it should be done.

The High Cascade lavas lap over on to the Western Cascade complex, and in some cases tongues of High Cascade lavas run down for several miles into valleys of the Western Cascades. What are termed Western Cascade volcanics are buried beneath these younger volcanics to the east so that the eastern margin of the so-called Western Cascade volcanics is unknown. The Young or High Cascade volcanics tend to form a relatively undissected plateau surmounted by the several Pleistocene and/or Holocene volcanoes such as the Three Sisters, Mount Washington, Mount Jefferson, etc. Figure 11 is a view looking south from Sand Mountain, a series of Holocene cinder cones, on the High Cascade volcanic plateau. The slight prominence on the east (left) horizon is Scott Mountain, a shield volcano on the plateau. The dissected ridges to the west (right) in the photograph are part of the Western Cascades, and the intervening valley marked by a haze line is that of the McKenzie River.

Various lines have been drawn between High Cascade and Western Cascade rocks. Peck et al., as noted, date the Western Cascade rocks as those which are Miocene or older. Another definition, and one which can be utilized in the field with proper small geophysical equipment, is simply to draw the line between High Cascade rocks and Western Cascade rocks (or Western Cascade time) at the most recent magnetic reversal (some 690,000 years ago).

Taylor (in Dole, 1968, p. 3) states:

"In spite of the general contrast between the Western and High Cascades, their common boundary is difficult to locate. In many areas, adjacent rocks of both provinces are flat-lying, unaltered, and are similar in chemical and mineralogical composition. To resolve this problem, individual rock units must be traced from areas in which

FIGURE 11. Looking south from Sand Mountain, across the Belknap Plateau. Prominence on the left (east) horizon Scott Mountain, a shield volcano on the plateau. Dissected ridges to the right on the horizon are part of the Western Cascades. Haze area marks approximate position of the McKenzie River Valley.

the boundary is easily fixed, into areas in which the position of the boundary would be otherwise obscure. This has now been accomplished in the central Cascades and several important relations are apparent: (1) A distinctive and widespread unit of homogeneous coarse-grained basalt marks the base of the High Cascade sequence. It is usually diktytaxitic and occurs in thick sections of many thin flows. (2) A more variable, finer grained, dense basalt overlies the coarse-grained diktytaxitic section and forms the bulk of the High Cascade platform. (3) The High-Western Cascade boundary is outlined by the western limit of the coarse-grained diktytaxitic rocks. Locally, where they overlap the coarse-grained section, the fine-grained, dense basalts form the boundary. (4) A profound erosional and/or angular unconformity exists at the boundary. Coarse-grained, diktytaxitic <u>early</u> High Cascade basalt inundated eastern

foothills of previously deformed Western Cascade rocks and, in places, poured west for 10 miles through the same major valleys which penetrate the Western Cascades today. (5) If the boundary is controlled by a major north-south fault, as has been suggested by several authors, this fault is not exposed to view and has not displaced the High Cascade rocks. In fact, the principal faults along the boundary are generally less than one mile in length, trend northwest, and involve displacements of less than 100 feet. They are restricted to the Western Cascades."

We do not presume to pursue this matter of High Cascade-Western Cascade boundary in any great detail. Whatever distinction is drawn would seem to be arbitrary to some degree as this is a region where volcanism has been a more or less on-going situation since the early Tertiary, although some episodic volcanic activity may perhaps be recognized.

For our studies, the principal significant difference between the High Cascades and Western Cascades is simply the degree of weathering of the rocks. All these volcanic materials are relatively unstable under the climatic conditions of the Cascades now and apparently those of the Tertiary, and the Western Cascades rocks have, in places, been altered entirely or very nearly so to clay. All degrees of alteration occur. Also, ancient geothermal areas can be identified where either over an area of several miles, or simply locally, hydrothermal alteration has occurred, or minor mineralization has taken place. Peck et al., have marked on their map the areas of propylitically altered rock (see also our Figure 10, taken from Peck et al.). The significance of these altered and locally mineralized areas is not known with regard to geothermal matters, and exploration of one or several such areas with heat flow holes might be warranted.

In general, the High Cascade volcanics have protected the underlying rocks from present and Pleistocene erosion and also have filled the valleys in the underlying rocks so that the High Cascades west of the crest present the appearance of a broad, gently sloping plateau. Where these younger rocks stop,

and erosion has cut deeply into the Western Cascade volcanics is where the hot springs occur.

HOT SPRINGS OF THE REGION

Parallel to, but lying some distance west from the crest of the Cascades in this region is a line of hot springs. In this study, the northernmost such area is Breitenbush, and the southernmost hot spring is Kitson--the distance between these two being some 70 miles. The hot springs all occur in Western Cascade volcanic rocks, and very close to the surficial junction of the High Cascade rocks with these Western Cascade volcanics. Most of the springs occur in the lowest points in the valleys, at stream level or close to it, but there are some exceptions such as Foley Hot Springs, and Rider Hot Spring. Locations of these and other hot springs in Oregon are shown on the map by Bowen and Peterson (1970). A tabulation of the location and some characteristics of the springs which occur in the area under discussion is shown on Table 1, next page.

It should be noted that more hot springs exist than the ones shown on the map by Bowen and Peterson (1970), which was an initial preliminary map. For example, there is a hot spring in the region under consideration in this report along the west bank of the McKenzie River at river level about 200 yards downstream from the mouth of Deer Creek.

Almost all these Western Cascade hot springs, with the exception possibly of Kitson, appear to issue from a medium to coarse (with blocks up to several feet across in the case of Foley Springs) volcanic breccia facies of the Western Cascades.

Figure 12 shows a general view and Figure 13 a closer view of Foley Springs, which issue from several closely spaced vents in a hillside about 150 feet above the stream bottom of nearby Horse Creek.

Temperatures of these springs range from about 190°F down to about 90°F. Largest discharge is that of Breitenbush Springs

TABLE 1

HOT SPRINGS OF THE CENTRAL PART OF THE WESTERN CASCADES

Name	Location S	T	R	Surf. temp. °C/°F		Flow	Elevation	Use	Other information
Breitenbush	20	9S	7E	92	198	900gmp 40-60 orifices	2250'	Spa	Believed to be hot water convection system with subsf. temp. 150°C.
Deer Creek	SE22	15S	6E	est 70	158	small	1850'	None	
Belknap	NW11	16S	6E	71	160	75 gpm	1700'	Heats house and pool	Believed to be hot water convection system subsf. temp 140 C
Foley	NW28	16S	6E	79	174	25gpm	1700'	Pool	Geochem. indicates 114-135°C.
Rider	7	17S	5E	54	130	60 gpm	est.2000'	None	
Wall Creek	NW26	20S	4E	37	98	3 gpm	2080'	None	
McCredie	36	21S	4E	73	164	20 gpm	2000'	None	Several orifices in bank of Salt Creek. Geochem shows subsf. of 81°C (D. Hull, personal comm.).
Kitson	6	22S	4E	46	114	35 gpm	1575	Spa	Resort built over spring orifice.

FIGURE 12. Foley Springs, general view, on Horse Creek drainage, about 4 miles eastsoutheast of McKenzie Bridge, Lane County.

FIGURE 13. Close view of Foley Springs showing the coarse volcanic breccia from which the spring issues.

estimated to be about 900 gpm from about 40 orifices. Belknap Springs (Figure 14) is the next largest with a discharge of about 75 gpm.

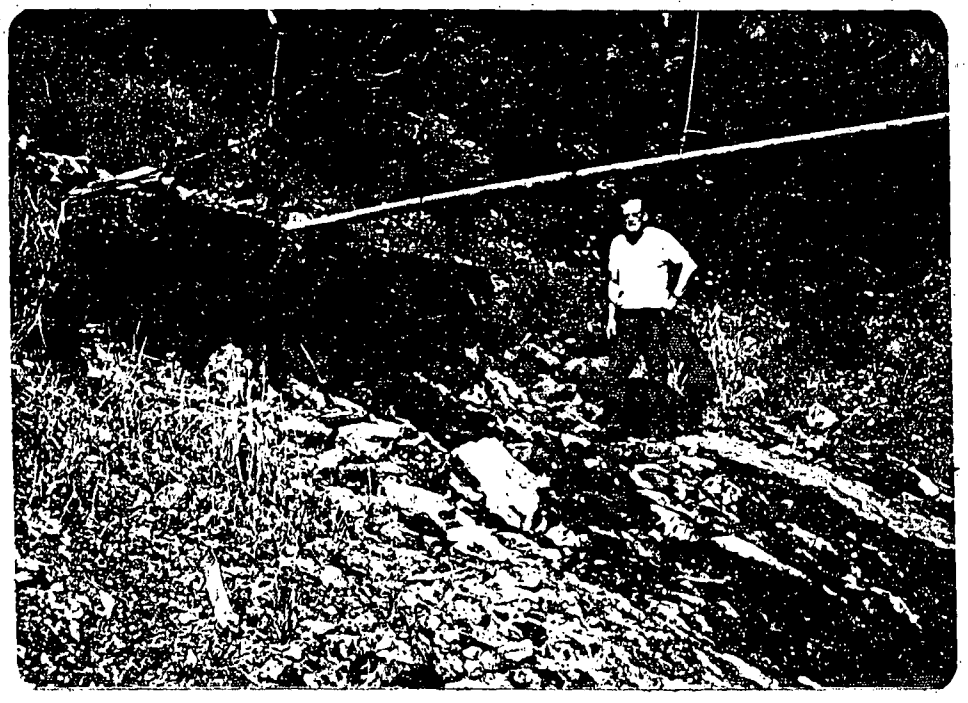

FIGURE 14. View of Belknap Springs--the main spring--which issues from volcanic breccia about 15 feet above low water on the McKenzie River. Several other smaller vents exist right at stream level. It is reported that at very low water additional hot spring vents can be detected in the river bottom. Bedrock here is volcanic breccia with fragments to about a foot in diameter.

Rider Hot Spring (Figure 15) also issues from volcanic breccia, but is unusual in that it comes from fairly high up the wall of a tributary valley (Rider Creek) to the South Fork of the McKenzie. The South Fork here is now flooded as part of Cougar Reservoir, but it is estimated that Rider Spring is about 400 feet above the old valley floor of the adjacent South Fork. All these hot springs come out within a few hundred feet, one way or another of the 1800 foot contour. The significance of this is not known, but it may represent a regional water table.

FIGURE 15. Close view of Rider Hot Spring, located near Rider Creek, a small tributary on the west side of the South Fork of the McKenzie River. S ring is about 400 feet above valley floor of nearby South Fork of Mckenzie River (before area was flooded by Cougar Reservoir).

One of the questions in regard to these springs is whether they are more or less directly over their heat sources, or do they perhaps represent isolated vents here and there which, from distances of several miles, are carrying up hot waters from geothermal systems which may lie to the east of this line of hot springs, and are related to the volcanism which has given rise to the High Cascades? A third possibility is that the entire region is one of high heatflow, and where the Cascades have been most deeply incised by erosion is where this geothermal system is leaking. No hot spring could reasonably be expected to occur in the plateau area of the High Cascades as it is underlain by young, relatively unweathered volcanic rocks, many of which are ‘a ‘a flows, highly porous and permeable. Surface drainage here is virtually non-existent. Any hot waters coming up into this volcanic complex would be diverted laterally through permeable zones and ultimately mixed with cold surface waters (rainfall here in excess of 80 inches, and snow persists into late June and early July many places). Accordingly,

such hot waters would not survive to the surface. It is remarkable, in fact, that any hot waters reach the surface, even in the valley areas, given the thick, moist, weathered cover, and the cold streams (McKenzie River is 46°F).

The volcanic rocks of the Cascades fill a broad north-south trending downwarp. Alteration by weathering and other means of the Western Cascades has resulted in what appears to be a complex which for the most part is relatively impermeable, and would act as a fairly effective seal on any hot water systems (or steam) which might lie beneath. The abundance of silicic ash, relatively easily yielding silica to solution, might suggest that it would be possible at some critical depth and temperature to have formed a silica roof over a geothermal system, and that the true nature of the hot water and/or steam systems in this area at depth is not evident from the surface indications. The hot springs which we know now at the surface may simply be recirculating relatively near-surface waters, and may be more or less sealed off from major geothermal systems at depth.

Dr. Paul Hammond and his students, in their studies in the Breitenbush area have suggested that the Western Cascades weathered volcanics do indeed act as a gigantic seal on whatever geothermal systems exist here, and we are inclined to agree with this observation. When one examines the highly altered nature of many of these volcanics, it appears that it would be only a very special circumstance--perhaps a very persistent fracture--which would allow hot water to come up through this seal.

In the McKenzie River drainage, which includes a number of hot springs (Foley, Belknap, Deer Creek, and other reported but not recorded springs), no wells deeper than a few hundred feet appear to have been drilled for any purpose, and no heat flow information is available from any of these. We have virtually no subsurface data of any kind. This general situation also exists elsewhere in the region under consideration, and therefore initiation of a heat flow drilling program will be a major advance in gaining a view of the geothermal potential of this area.

Under any circumstances, we presently know so little about the heat flow and possible hot water systems in the Cascades, and the volume of volcanics, some as young as 700 years old, is so great.

that it obviously is an attractive and worthwhile area in which to conduct extensive geothermal investigations, of which this heat flow study is but an initial step.

REGION SUBDIVISIONS

In part because of the differing geology, and in part due to the geography and the way in which the KGRA's have been designated, for purposes of this report we have recognized six subdivisions of the region under consideration. These are shown in rough sketch form on Figure 16 (next page) and are designated from north to south as:

BREITENBUSH AREA
BREITENBUSH TO SANTIAM AREA
BELKNAP AREA
WEST NORTH FORK AREA
SOUTH FORK MCKENZIE-NORTH FORK OF MIDDLE FORK OF WILLAMETTE AREA
KITSON-MCCREDIE AREA

We recommend that at least one heat flow hole be drilled in each of these areas. We have shown these tentatively recommended locations by an asterisk (*) on Figure 16. These sites are briefly described here, with specific suggestions as to where (by legal description) these heat flow holes might be located.

RECOMMENDED DRILLING LOCATIONS

Breitenbush location. This area has already been designated a KGRA. Industry information which we believe to be reliable, as well as USGS data (Circular 726 in particular) indicate that this is one of the hottest heat flow anomalies in the region under study. Because it has already been declared a KGRA and therefore is now a competitive leasing situation, no individual company is likely to spend money test drilling the area before leases are issued. This clearly seems to be a place where an agency like the Oregon State Department of Geology and Mineral Industries could make a significant contribution by drilling at least one hole, and perhaps two heat flow holes. The valley floor proper within a mile more or less of Breitenbush Hot Springs is recommended as a location. Interest in this area being as considerable as it is, another hole might be justified, and this could be a mile or two east, northeast, or

FIGURE 16
Regional subdivisions and drill site recommendations

* denotes suggested heat flow hole site

boundary of various subdivisions of this region, as recognized for this report

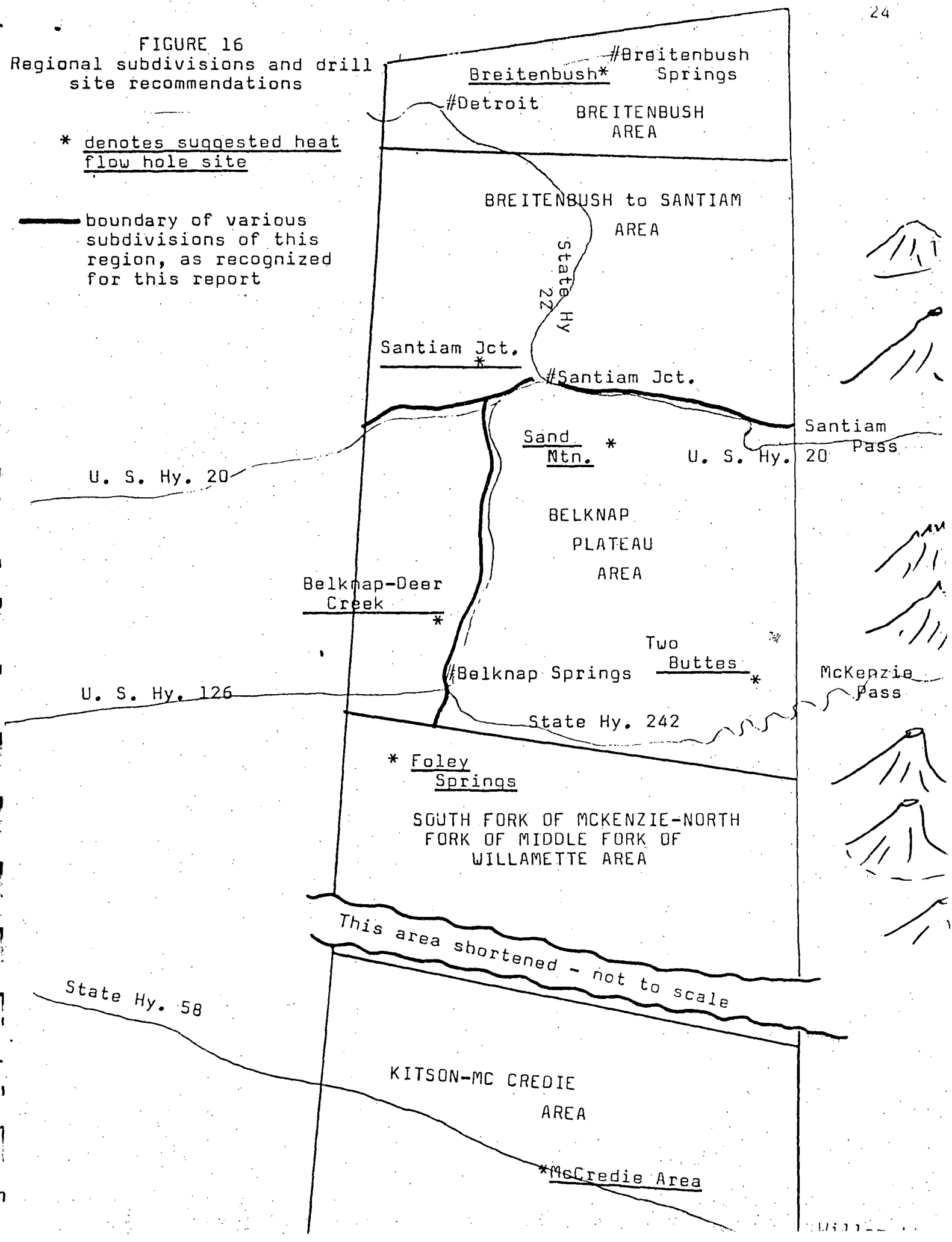

south of Breitenbush Valley. Ample access and good drill sites exist, especially south of the Breitenbush Hot Springs area. Another reason for putting two holes down in this area is the relatively good geological information we have here. As a result of the work of Dr. Paul Hammond and his students, this area is the most thoroughly studied geologically of any of the subdivisions of this region which we have established. A general view across the Breitenbush Valley, looking to the northeast, is shown in Figure 17. A close view of some of the terrain south of Breitenbush is shown in Figure 18.

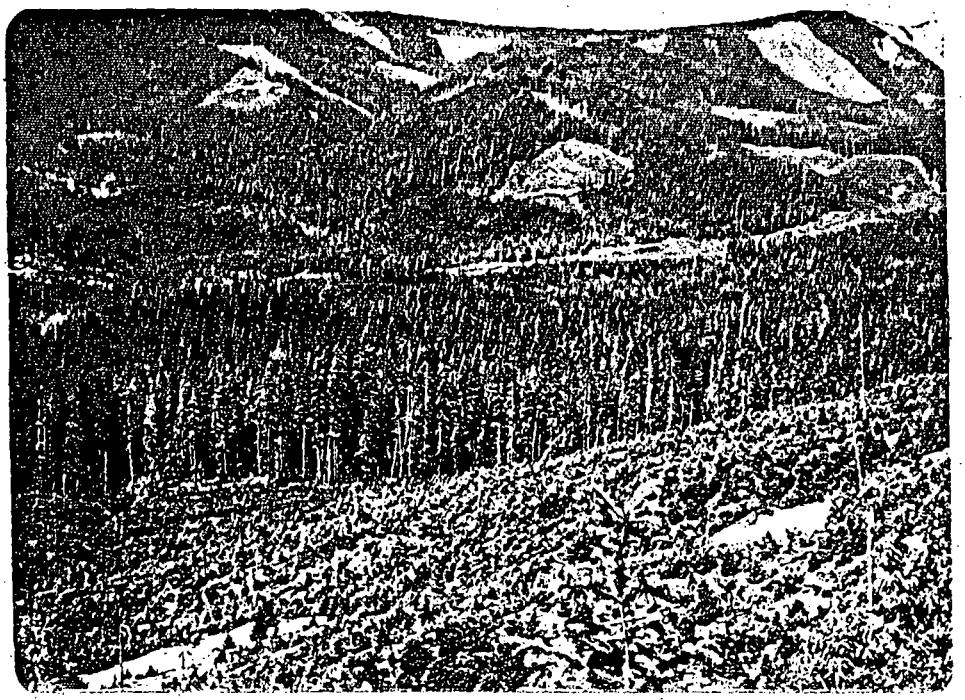

FIGURE 17. General view looking northeast across the valley of the Breitenbush River. The Breitenbush Hot Springs area proper lies slightly to the left (west) of the margin of the photograph.

Specifically, we recommend looking at a site in the south part of section 28, T 9 S, R 7 E, and/or in section 16, or 21 of the same township for one of the locations.

FIGURE 18. View of terrain, looking southeast, about 3 miles southsouthwest of Breitenbush Hot Springs.

Santiam Junction. This is an area of quite recent volcanism. It is relatively undissected with the result that little is known about the geologic section here as exposures in depth are limited. However, the several fracture systems of the area and the attendant volcanic activity here are impressive. The area is also geographically situated so as to complement information which would be obtained from a hole recommended to be drilled east of Sand Mountain (see next location). It also is almost directly on a north-south line between Breitenbush Hot Springs and the hot springs known in the southern portion of the North Fork of the McKenzie River. We recommend a location in the vicinity of section 36, T 12 S, R 6 E. The south center of this section would be satisfectory, as would the N½ section 1, T 13 S, R 6 E.

General view of this area is shown in Figure 19. Big Nash Crater is the prominence in the middle right (east) of the photograph. Photo taken looking northwest from Sand Mountain. The area of interest lies in the middle distance over the left (west) flank of Big Nash Crater in this photo. As shown on Figure 1, the area would be southeast about 1½ miles from South Pyramid Mountain.

FIGURE 19. View looking northwest from Sand Mountain. Big Nash Crater in right middle distance. Peak on left horizon is Crescent Mountain--a large volcanic center which has been breached by erosion (probably glaciation in part), or explosion, or combination of both, on the east side.

Sand Mountain. Sand Mountain is a linear series of cinder cones along a north-south fracture (See Figures 21 and 22). Volcanic activity in this area is generally less than 5000 years old, and includes such volcanic centers as Hoodoo Butte, Hayrick Butte, Sand Mountain (several craters), and Big and Little Nash craters. A location in the shallow topographic basin just east of Sand Mountain is recommended. View of this area from Sand Mountain is shown in Figure 20. A fairly detailed map showing direction of flow movement and the vents of this area is shown on Figure 22.

A map of the Santiam Junction-Sand Mountain area, taken from Howel Williams (1957) is shown on Figure 21. There is in this area an impressive amount of Holocene volcanism. Drilling here, however, is subject to the general problem that these young volcanics are highly permeable and porous and would allow water to circulate

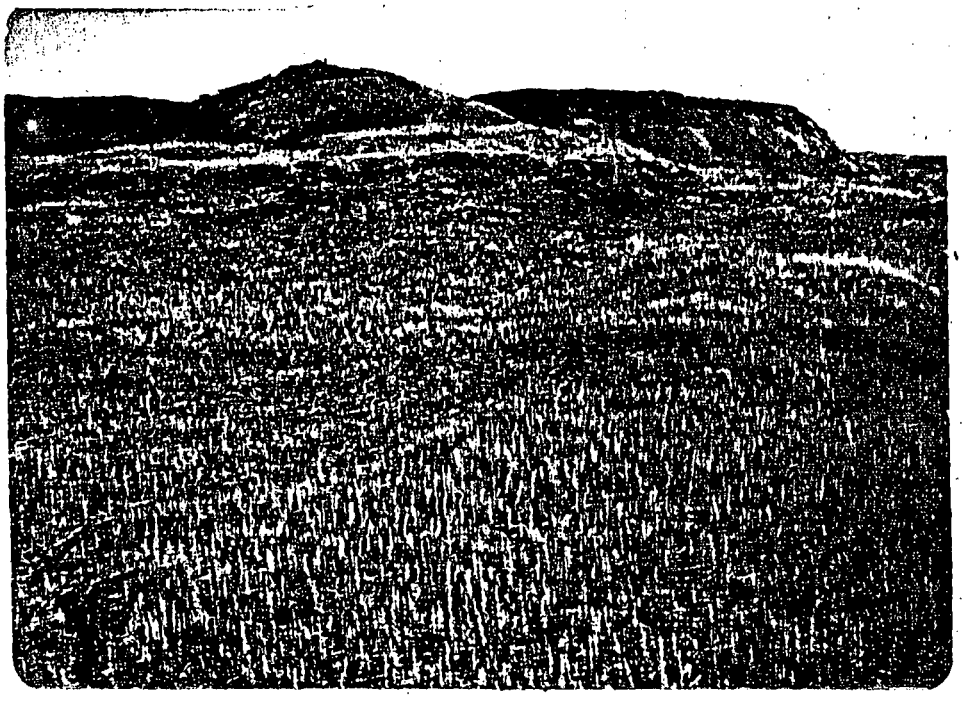

FIGURE 20. View northeast from Sand Mountain, with Hoodoo Butte the pointed peak in the middle skyline, and Hayrick Butte the flat-topped prominence to the right and slightly farther away. Basin in foreground is a cinder-ash covered plain, with a recently burned stand of jackpine (all the grey, barkless dead tree trunks--mostly still standing). Access to all of this area is very good.

through them. There is the question of how thick these porous young volcanics are. In some places even fairly extensive fields of these High Cascades volcanics prove to be fairly thin when seen in canyon wall exposures. This area is near the margin of the High Cascades volcanic field and the flows might not be particularly thick. In any case, at some place these lava fields with their attendant Holocene vents should be drilled, and the Santiam Junction-Sand Mountain area would seem to be a logical place.

The less than 5000 year age date on the volcanism in the Sand Mountain area makes it an interesting site to test. Most available information suggests that these basaltic volcanic centers derive their heat and materials from fairly deep in the Earth's crust, and rise through narrow dike-like vents. High heat flow here would be significant, although it should be noted that a low heat flow might not be conclusive as to the depth of the magma chambers for, as noted, there is a question as to the

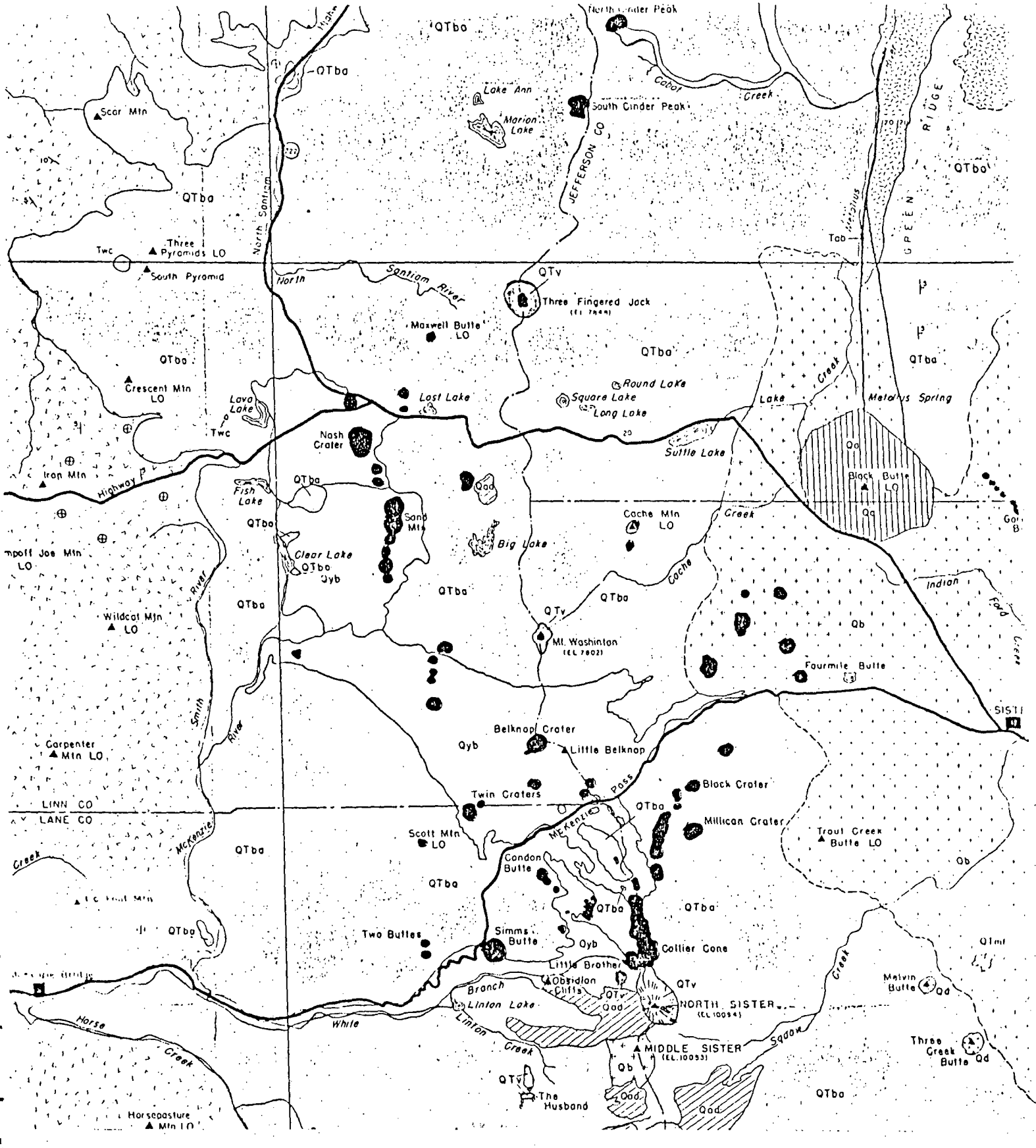

FIGURE 21. Map of Santiam Junction-Sand Mountain area, and Belknap Plateau area, map taken from Williams (1957).

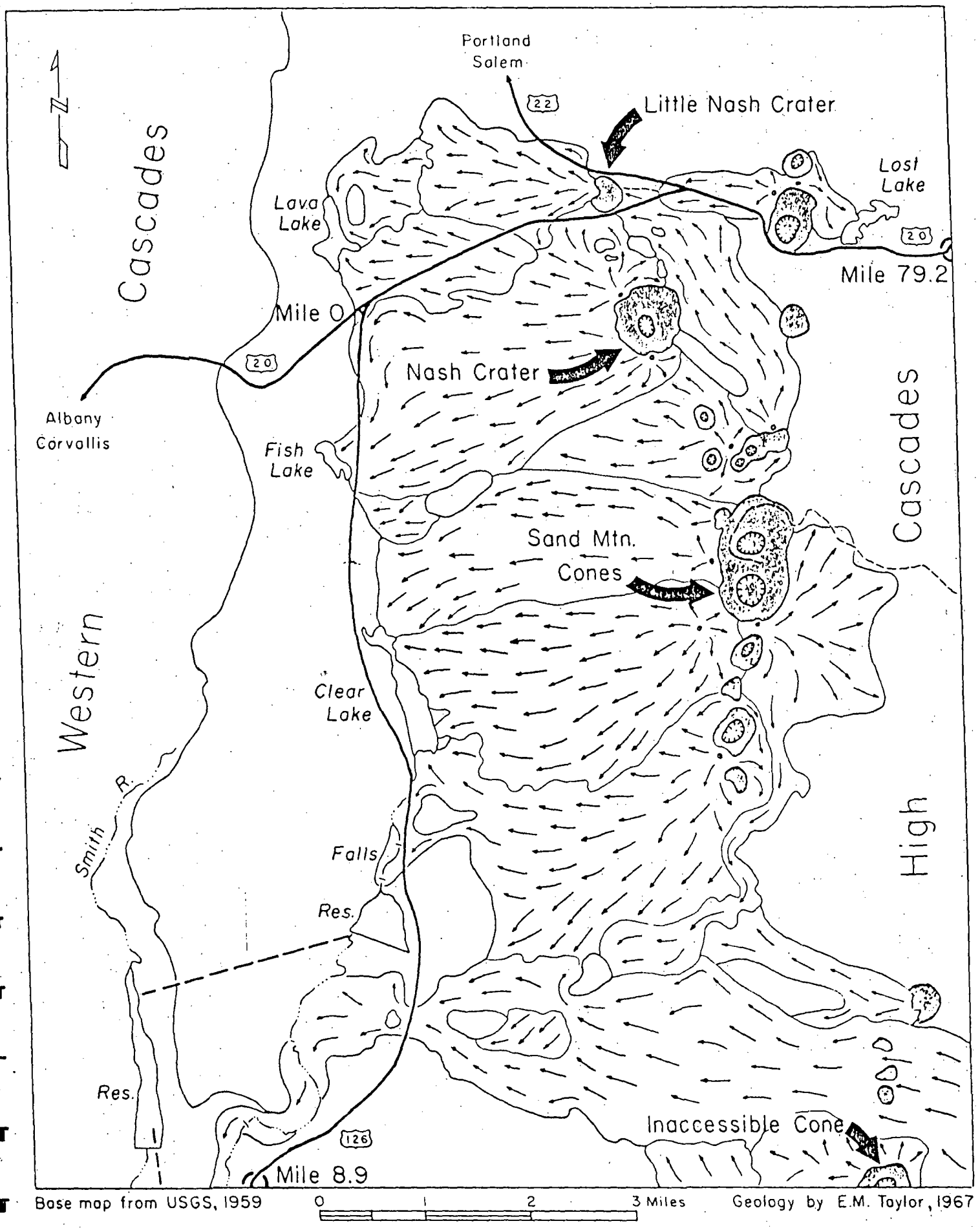

FIGURE 22. Flow directions and vents in Sand Mountain area, map from Taylor in Dole, 1968.

reliability of data in these relatively permeable and porous young volcanics. Nevertheless, this Sand Mountain area in the midst of so much very young volcanism seems a prime area in which to drill at least one heat flow hole. Most anywhere in the shallow basin east of Sand Mountain would be satisfactory. Access is excellent.

Two Buttes. This area lies at the southern end of what we have called the Belknap Plateau, so named because the flows from Belknap Crater dominate much of the area. Two Buttes are relatively young (but somewhat dissected) volcanic cones, and adjacent Deer Butte is perhaps slightly older (see Figure 21 for locations of these features). This recommended drill site represents the closest practical drill location in this region to the Three Sisters volcanic area of relatively recent activity. A view of this Two Buttes area from across the North Fork of the McKenzie River near Frissell Point is shown in Figure 23. The large valley in the foreground is that of Scott Creek. Deer Butte lies in line with the south base of the Middle Sister, and Two Buttes are the two small peaks to the north (left) of Deer Butte. A location perhaps in E½ section 9, or W½ section 10, T 16 S, R 7 E is suggested. This entire plateau would afford numerous sites for geothermal plant locations. There are no identified distinctive recreational features of this region. It is undergoing extensive logging and recently a well developed system of logging roads has been developed here. A view of a recent shelterwood cut, showing some of the terrain of the plateau, is present in Figure 24. Photograph was taken in section 3, T 15 S, R 7 E.

Deer Creek-Belknap area. This area has a number of hot springs of which only Belknap shows on the preliminary map by Bowen and Peterson. The springs show a marked north-south alignment, in agreement with the general trend of hot springs in this region. There is a hot spring about 200 yards downstream from the mouth of Deer Creek, along the west bank of the North Fork of the McKenzie River. This is about six miles north of Belknap Hot Springs. A location is suggested between these two springs, and in fact a good site exists. It lies just

FIGURE 23. View of Belknap Plateau from west, looking across valley of North Fork of McKenzie River. Large valley in right foreground is that of Scott Creek. Deer Butte is single peak in line with south base of Middle Sister, and Two Buttes are the two small buttes to the north (left) of Deer Butte.

FIGURE 24. Shelterwood cut NW$\frac{1}{4}$ section 3, T 15 S, R 7 E, Linn County, on mid-portion of Belknap Plateau. Ample sites exist in this area for geothermal plants if resource can be found.

west of the bridge over the North Fork of the McKenzie River on the Frissell Point road. This location is in NE¼ section 2, T 16 S, R 6 E, Lane County. A second location in this general area might be on the private land of John Bigelow who has 160 acres a short distance west of Belknap Springs. He has tentatively offered his acreage for a drill hole site. Again, as in the case of Breitenbush, this Belknap Springs area has been designated a KGRA. The State Department of Geology and Mineral Industries is a logical vehicle for doing heat flow drilling here, and it would be useful to have such data available before any KGRA sales are decided upon, or held.

Foley Springs. This is a fairly hot spring (174°F) and is part of the Belknap area KGRA. General view of this spring is shown in Figure 12, page 19. A number of lease applications have been filed in the vicinity of Foley Springs and adjacent Foley Ridge. A location somewhere between the springs and the ridge is suggested, perhaps in E½ section 28, or W½ section 27, T 16 S, R 6 E. The location should be as far north as possible to get between Foley Springs and Foley Ridge. Note, however, that topography here in the Horse Creek Valley will be somewhat of a problem and will limit location possibilities.

Kitson-McCredie area. This geothermal area, at the southern end of our study region, is somewhat isolated from the rest of the thermal areas, and as such it provides a significant point geographically for a heat flow map of this region. It includes not only Kitson and McCredie hot springs, but also a warm spring in the valley of Wall Creek, tributary to Salmon Creek. With the McCredie Springs designated as a KGRA and with three thermal springs in this area, it is worthy of a heat flow hole. We recommend the easily accessible McCredie Springs area, which is also the area of the hottest of the three springs. Numerous drill sites exist within a mile or two of these springs which emerge from three or four fairly closely spaced vents in a volcanic breccia along the north edge of Salt Creek, about 50 yards south from State Highway 58 (Willamette Pass highway).

SUMMARY OF SUGGESTED DRILLING LOCATIONS

In total, we have suggested seven locations which are, in summary:

1. Breitenbush area, sections 16, 21, or 28, T 9 S, R 7 E.
2. Santiam Junction, south center section 36, T 12 S, R 6 E, or N½ section 1, T 13 S, R 6 E.
3. Sand Mountain, just east or northeast of Sand Mountain which is a few miles southeast of Santiam Junction.
4. Two Buttes, E½ section 9, or W½ section 10, T 16 S, R 7 E.
5. Deer Creek-Belknap area, NE¼ section 2, T 16 S, R 6 E, with another possible location on property of John Bigelow, west of Belknap Springs. Bigelow's property is in section 10, T 16 S, R 6 E.
6. Foley Springs, E½ section 28, or W½ section 27, T 16 S, R 6 E. Topography limits locations.
7. Kitson-McCredie area, within a mile or so of McCredie Hot Springs which are in NW½ section 36, T 21 S, R 4 E, Lane County.

To bring this total to eight, the following possibilities are offered:

1. Drill an additional hole in the Breitenbush area, with one being put in the valley proper, and one in the surrounding hills, preferably south.
2. Drill the additional hole recommended in the Deer Creek-Belknap area.
3. Drill one of the mineralized zones showing hydrothermal activity in the past such as up Christy Creek (off North Fork of Middle Fork of Willamette River), or in the Quartzville Creek area near Detroit.

DRILLING PROBLEMS AND QUALITY OF RESULTS

It is evident that much drilling will be done largely through suc volcanic debris as shown in Figure 25. Difficulty may be encountered if some of these boulders or angular debris rotate or cave into the hole during drilling. A bridge or stuck bit could result. However,

FIGURE 25. Volcanic debris in Tertiary mudflow, along Horse Creek road, southeast of Foley Springs. Tremendous volumes of this same general sort of material characterize much of the Western Cascades.

much of this material is rather highly indurated and this problem could prove to be minimal.

The question of whether or not shallow subsurface cold water flows will erase any heat anomalies present has been considered frequently during our field investigations. In general, the holes will be located so that at total depth they are likely to be in Western Cascade volcanic materials. These are relatively impermeable as far as we can determine. Where water does emerge it appears to come from local pockets or trains of relatively unweathered materials in contrast to most of the rock materials in the section. There is no general sheet flow evident through these volcanics in their presently weathered form. We are inclined to the view that there will be no problem of any large scale erasure of heat flow anomalies by

near-surface cold water flow in Western Cascade volcanics. Some such problems could occur, however, in the younger or High Cascade rocks. For example, streams of water emerge from what Taylor (in Dole, 1968) has identified as thin High Cascade diktytaxitic flows in the lower High Cascades volcanics in a road cut at Trail Bridge Reservoir (Figure 26).

FIGURE 26. Road cut and emerging water streams from thin diktytaxitic flows in the lower High Cascade volcanics, in road cut at Trail Bridge Reservoir, North Fork of the McKenzie River.

It is recommended that, where possible, the lowest topographic point consistent with a good bedrock location and avoiding shallow subsurface water flow be utilized for the drill site. Also, a fairly detailed local geological study should be made of each area before final drill site determination is made.

All things considered, many suitable heat flow drilling sites appear to exist, well located geologically and geographically, in the region under consideration. Geological conditions suggest that

the quality of information which might be obtained from 500-foot holes should be quite good, and we believe implementation of the drilling program as outlined here will be a scientifically efficient use of funds, and will result in a significant contribution to knowledge of heat flow, and of probable geothermal potentials of this region.

SUMMARY AND CONCLUSIONS

The Western Cascades and the High Cascades, in total, represent a volume of igneous rocks which can be measured in many thousands of cubic miles. Geological evolution of this region involved the activity of many hundreds if not thousands of volcanic centers, great and small, and the details of stratigraphy are very complex in detail. Only in a broad way can the stratigraphy be defined and outlined at present. Pyroclastics and especially mudflow breccias on a very large scale make up more than half the volume of materials of this region. Numerous volcanic centers can still be clearly identified. Steep dips and large quantities of huge clastic debris indicate that the region was one of high relief as it developed during the Tertiary.

Far from being strictly a basaltic province, andesite appears to be a common rock type, and other even more silicic rocks exist in some abundance. In a few places rocks which approach granites in texture and composition exist, as, for example, the so-called Nimrod Granite on the McKenzie River drainage. Fragments of granite exist in the tuffaceous mudflow which is the abutment on the east side of Hills Creek dam. The source of this granite is not now known.

In general, the Western Cascade volcanics are more highly weathered and otherwise altered than are the High Cascade rocks. These Western Cascade rocks, in their altered form, appear now to act as a huge and quite effective seal on any geothermal systems which may exist at depth.

The region, for purposes of this report, has been divided into six subprovinces, based in part on geology, but also on the KGRA

designations, and the geography. Satisfactory drilling sites exist in all these subprovinces, and specific locations and comments about each recommended site have been made.

Drilling through the debris-filled mudflows could cause problems, although much of this material is rather highly indurated. Some problems may be encountered in drilling through the highly permeable and porous young volcanics of the High Cascades. In the Western Cascades, where most of the drilling will be done, large scale erasure of heat anomalies by sheet flow of shallow subsurface waters is not considered very likely, and, given proper diligence in locating the particular drill sites, good quality results can be expected. In the case of the High Cascade rocks, some subsurface cool water flow might be expected and could affect results. This could prove to be a substantial problem or it could be quite modest. One or two holes will not be conclusive but we do recommend that some such holes should be drilled in this initial program (Santiam Junction, Sand Mountain, and Two Buttes locations are High Cascade volcanic sites).

Implementation of this drilling program should greatly increase our knowledge of the geothermal potential of this region, and point the way to where additional and more detailed studies are likely to yield further significant scientific and also economically important results. We do know, from personal conversations, that this central Western and High Cascades area is regarded by a number of industry and academic geologists and geophysicists as "one of the prime geothermal targets in the United States." As such it deserves early and extensive investigation, of which this drilling program would be a significant step.

****

ADDENDUM

Position and prognosis for geothermal leases in Willamette National Forest. At the present time (November, 1975) the situation with regard to the federal lease applications for geothermal resources in this forest is as follows:

An overall land use plan is being evolved for the WNF, and public hearings are currently being held.

The Forest Service expects but is by no means certain that it will have all the hearings completed and a decision made by early 1976--perhaps February or March.

An environmental impact statement for geothermal for the Breitenbush area has been prepared by Allen Prigge, Forester with WNF, and is now on the desk of the District Ranger in Detroit, Oregon.

A pencil draft of the geothermal environmental impact statement for the rest of the forest has been prepared by Mr. Prigge, but he proposes to go no further with it until the Breitenbush statement has been approved in final form. Then Mr. Prigge plans to use that foremat for the environmental statement for the rest of the forest.

The WNF states (John Alcock, Forest Supervisor) that no move on geothermal environmental statements will be made until the overall land use planning program is finalized (February or March, 1976, maybe).

Possibly by March 1976, the environmental impact statement for geothermal on the Breitenbush area may come to public hearing. This might be concluded by May. The statement for the rest of the WNF could then perhaps be completed in preliminary form, heard, and then finalized by June or July (relatively optimistic time schedule).

After the Forest Service has completed its work on these environmental statements, they are sent on to the BLM in Portland. It takes the BLM, in non-competitive lease application situations, about four months to process the papers and attach the proper environmental statements and restrictions to the various lease applications and forward them on to the applicants for acceptance

or rejection. Adding up all these times, it seems unlikely that any leases will be issued to applicants before late summer or early fall 1976. This would seem to be the very earliest possible time; if any difficulties arise during public hearings on these environmental statements, or if the statements simply move slowly through administrative channels, this date could well move back into 1977.

****

BIBLIOGRAPHY

The principal informational sources drawn upon during this study are here listed. However, numerous maps and miscellaneous shorter reports were also utilized.

BOWEN, R. G., and PETERSON, N. V., 1970, Thermal springs and wells in Oregon: Oregon State Department of Geology and Mineral Industries, Portland, Miscelleneous Paper 14 (Map with text).

DOLE, H. M. (ed.), 1968, Andesite Conference Guidebook: Oregon State Department of Geology and Mineral Industries, Portand, Bulletin 62, 107 p.

PECK, D. L., et al., 1964, Geology of the central and northern parts of the western Cascade Range in Oregon: U. S. Geological Survey Professional Paper 449, 56 p., 1 pl. (Map).

PETERSON, N. V., and GROH, E. A. (eds.), 1964, State of Oregon Lunar Geological Field Conference Guidebook: Oregon State Department of Geology and Mineral Industries, Portland, Bulletin 57, 51 p.

TAYLOR, E. M., 1965, Recent volcanism between Three Fingered Jack and North Sister Oregon Cascade Range: The Ore Bin, Oregon State Department of Geology and Mineral Industries, p. 121-148.

WHITE, D. F., and WILLIAMS, D. L., 1975, Assessment of geothermal resources of the United States: U. S. Geological Survey circular 726.

WILLIAMS, HOWEL, 1957, A geologic map of the Bend Quadrangle, Oregon, and a reconnaissance geological map of the central portion of the High Cascade Mountains: Oregon State Department of Geology and Mineral Industries, Portland.

STATE OF OREGON
DEPARTMENT OF GEOLOGY AND MINERAL INDUSTRIES
1069 State Office Building, Portland, Oregon 97201

SPECIAL PAPER 2

FIELD GEOLOGY

OF

S.W. BROKEN TOP QUADRANGLE, OREGON

Edward M. Taylor
Associate Professor of Geology
Oregon State University

1978

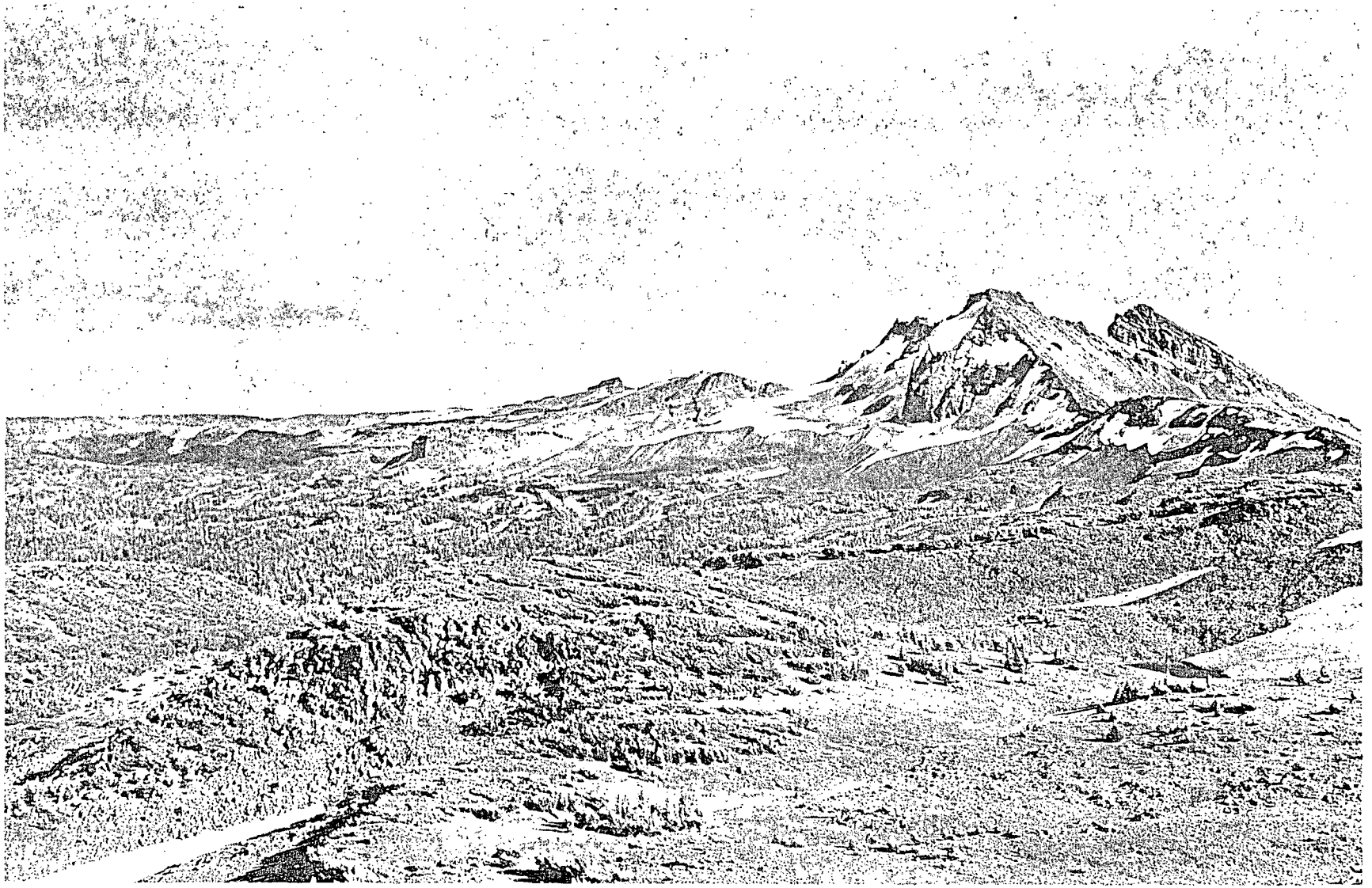

FRONTISPIECE. NORTHWEST SIDE OF BROKEN TOP VOLCANO. CENTRAL MASS CONSISTS OF INTERBEDDED AGGLOMERATE AND LAVAS CUT BY SILLS, DIKES, AND A LARGE PLUG. SURROUNDED BY HOLOCENE MORAINES AND RIDGES OF GLACIATED BASALTIC ANDESITE.

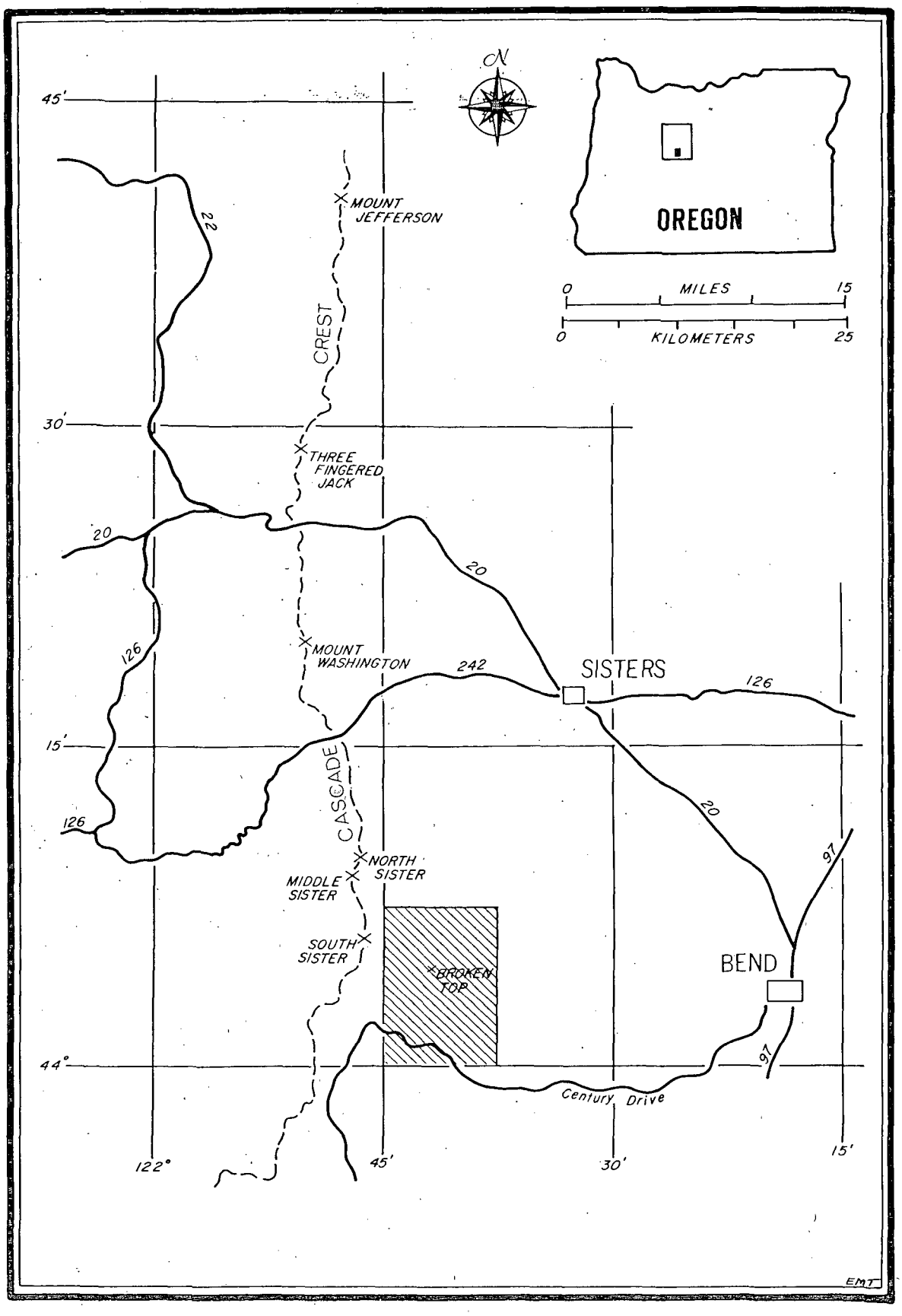

FIGURE 1. LOCATION OF S.W. BROKEN TOP QUADRANGLE.

CONTENTS

ILLUSTRATIONS

GENERAL GEOLOGY OF BROKEN TOP AND VICINITY

The 7.5-minute S.W. Broken Top quadrangle is bounded by 44° and 44°7'30" north latitude and by 121°37'30" and 121°45' west longitude in the vicinity of Broken Top volcano, 30 km west of Bend (Figure 1). The quadrangle is covered by Pleistocene and Holocene calc-alkaline volcanic and volcaniclastic rocks similar to those near the crest of the Cascade Range, approximately 10 km to the west. Basalt, basaltic andesite, andesite, dacite, and rhyodacite rock types are represented in a variety of forms including composite volcanoes, volcanic domes, lava flows, cinder cones, tuff cones, ash-flow tuffs, intrusive plugs, and dikes.

Pliocene Volcanism and Subsidence

Stratigraphic and structural records of Pliocene volcanic and tectonic activity are obscured in the S.W. Broken Top quadrangle by a thick overburden of younger rocks. However, certain inferences can be drawn from rocks of Pliocene age exposed in areas to the north and east. Within the Deschutes Formation, northeast and east of Broken Top, there is abundant evidence that a great volume of volcaniclastic material was delivered to the eastern slope of the central Cascades (Taylor, 1973) during an interval that began at least 12 million years ago and was abruptly terminated approximately 3 million years ago (Armstrong, Taylor, Hales, and Parker, 1975). This material was produced from a north-south belt of Pliocene Cascade volcanoes. Remnants of the eastern slope of the Pliocene volcanic belt are now preserved in Green Ridge north of Sisters and in other outcrops between Sisters and Bend (Peterson, Groh, Taylor, and Stensland, 1976); none of the Pliocene Source volcanoes is exposed in the modern High Cascade Range.

Extensive crustal subsidence occurred within the central Cascade volcanic belt approximately 2.5-3.5 million years ago. A complex, elongate, north-south basin was probably formed and was bordered on the east by a set of normal faults whose total displacement exceeded 1000 meters. Remnants of a north-south 700-meter fault escarpment are exposed north of Broken Top along upper Metolius River and a southern extension probably exists in the subsurface beneath Broken Top. Normal faults of northwest trend and smaller displacement were also produced at this time; the best preserved example is the Tumalo Fault between Bend and Sisters.

Construction of a Pleistocene High Cascade Platform

The late Pliocene Cascade depression was flooded (perhaps during subsidence) by basalt and basaltic andesite lavas of the early Pleistocene High Cascades. Eventually, a broad platform of overlapping shield volcanoes filled the depression and spread through low parts of the eastern escarpment; one of these shield volcanoes (Bald Peter) formed against the escarpment 2.1 million years ago. The oldest lavas along the western edge of the platform are 2.0-2.5 million years old (Armstrong and others, 1975).

The central High Cascade platform continued to develop during Pleistocene time. Ancient volcanoes of the Pliocene Cascades were completely buried and basaltic andesite volcanoes such as Three Fingered Jack, Mount Washington, North Sister, Broken Top, and a host of lesser cones and shields were constructed on the top of the platform. Volcanism of this type has persisted until recent times; for example, Bachelor Butte and associated cinder cones south of Broken Top were active 6600-12,000 years ago and Belknap Crater last erupted only 1400 years ago. The remarkable north-south alignment of volcanic vents seen in many parts of the High Cascades is probably a result of magma ascending through buried fault zones in the Pliocene rocks beneath the platform.

Faults have not been recognized within the central High Cascade platform. However, faults of small displacement and northwest trend were active northwest of Bend during

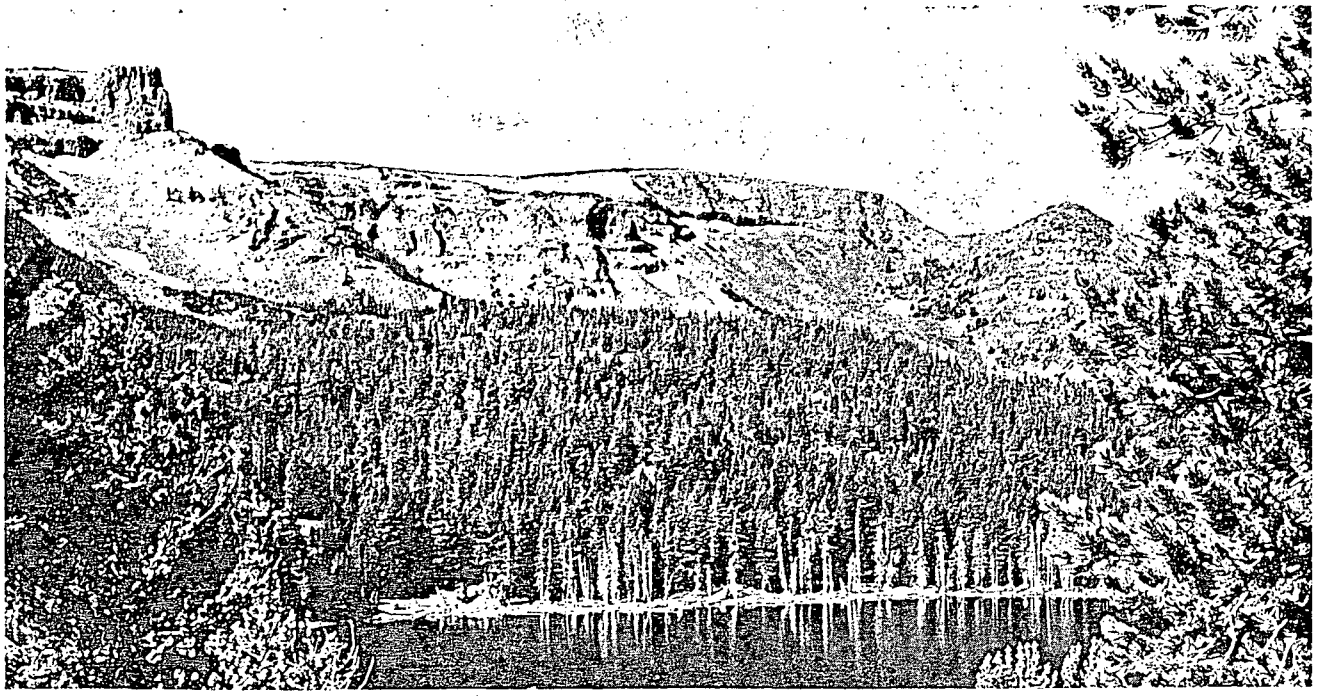

FIGURE 2. TAM MCARTHUR RIM SOUTHWEST OF THREE CREEK LAKE. RHYODACITE LAVA CAPS RIM ON LEFT AND IS OVERLAIN ON RIGHT BY BASALTIC ANDESITE LAVAS FROM BROKEN TOP.

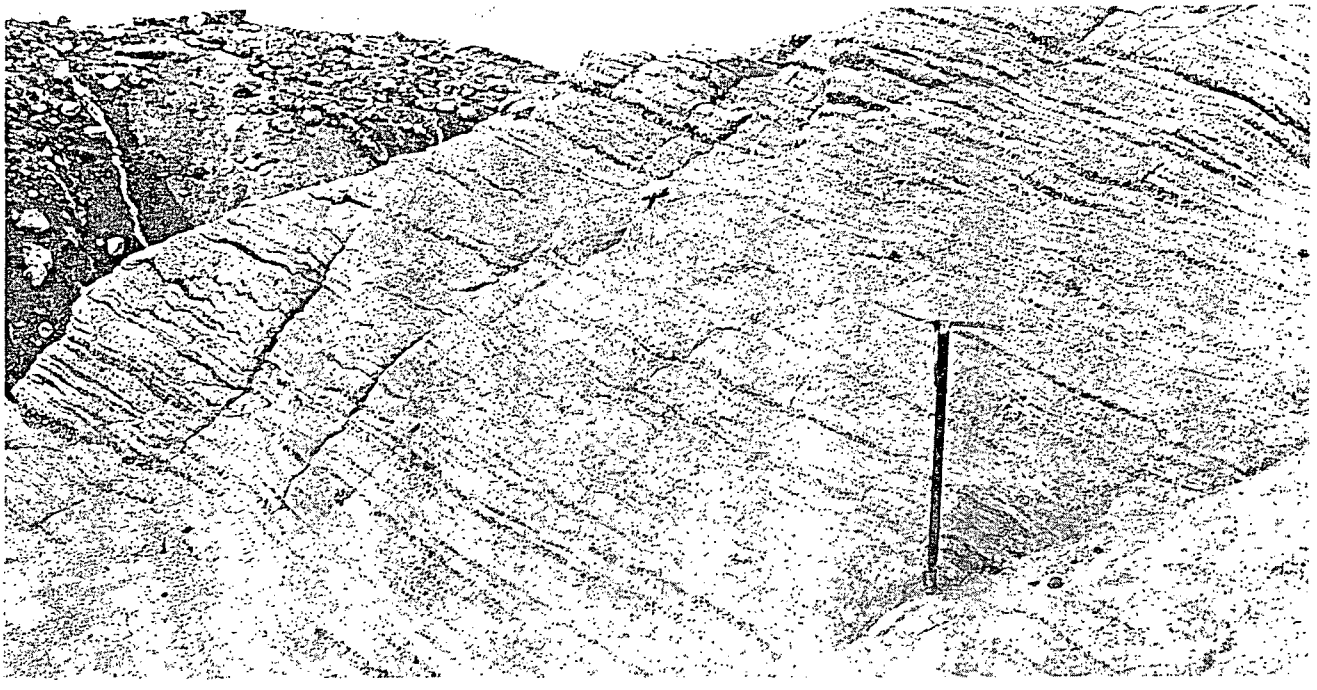

FIGURE 3. LAYERS OF ALTERED RHYODACITE PUMICE IN SILICIC TUFF CONE EXPOSED IN CANYON OF NORTH FORK TUMALO CREEK.

the Pleistocene. Parts of the Tumalo Fault were reactivated and some east-flank Cascade lavas and ash-flow tuffs were displaced. These faults appear to form a northwest extension of the Brothers Fault Zone.

A Pre-Broken Top Highland of Silicic Volcanoes

In the vicinity of S.W. Broken Top quadrangle, magmas of high-silica andesite, dacite, and rhyodacite composition reached the surface intermittently during early Pleistocene time. A broad highland of volcanic domes, silicic lavas, and ash-flow tuffs was formed on the east margin of the predominantly mafic High Cascade platform. The northeastern margin of this highland can still be seen in the steep mountain front west of Bend. Three Creek Butte, Melvin Butte, and the summits of 9 other partly buried silicic domes, together with silicic lavas in the canyons of Squaw and Tumalo Creeks are the best exposed parts of the early Pleistocene highland. In S.W. Broken Top quadrangle, the much-eroded remnants of dacitic Todd Lake Volcano and the dacite lavas exposed in lower cliffs of Tam McArthur Rim probably represent the highest and youngest parts of the highland.

Silicic volcanism in the Broken Top area appears to have abated for a time during which basalt and basaltic andesite continued to erupt, adding to the High Cascade platform and inundating parts of the silicic highland. It was at this time that the eastern slope of the Cascades between Broken Top and Bend was extensively covered by flows of mafic lava. Remnants of numerous cinder cones which mark source vents are found on the eastern slope and in the mountains. Examples are the Triangle Hill group of cones and the cone near Rim Lake, east and north of Broken Top, respectively.

Development of Broken Top Volcano

Broken Top is a complex and magnificently exposed composite volcano of basaltic andesite composition. A cone of scoria and ash accumulated near the vent and was repeatedly invaded by dikes and sills which served to strengthen the structure and probably fed numerous streams of a surrounding lava cone. The scoria, dike rocks, and lavas were all of uniform composition, crowded with phenocrysts of plagioclase, olivine, two pyroxenes, and magnetite. Silicic magmas continued to reach the surface through Broken Top vents so that andesite, dacite, and rhyodacite lavas, ash-flow tuffs, and pyroclastic-fall deposits were interbedded with basaltic andesite flows and agglomerates, from the lower flanks to the summit of the volcano.

In mid-development, the summit crater of Broken Top was enlarged to a diameter of 0.8 km, probably by subsidence. The resulting depression was filled by thin flows of basaltic andesite and most of the summit cone was eventually buried beneath a shroud of thin, vesicular lavas. Finally, after the lava conduit attained a width of 0.3-0.5 km, the magma congealed to form a central plug of micronorite. The plug and adjacent rocks were then subjected to an episode of mild hydrothermal alteration. Crowe and Nolf (1977) have recently published a similar interpretation of the development of Broken Top.

Latest Pleistocene Volcanic Activity

A 10-km alignment of rhyodacite domes extending from Devils Hill on the south to Demaris Lake on the north, was erupted during late Pleistocene time. These domes were partly buried by andesite lavas from South Sister vents. Although many additional silicic vents were active at this time in the vicinity of Three Sisters, only one small rhyodacite dome erupted east of the South Sister. It appeared at the northwest base of Broken Top; its associated air-fall pumice deposits are still preserved on the nonglaciated crest of Broken Top northwest ridge.

A northwest-trending chain of six cinder cone and lava vents erupted between Tumalo Mountain and Broken Top. Each vent produced lava similar to the glomeroporphyritic basaltic andesite of Tumalo Mountain; probably all were developed from the same magma at

FIGURE 4. CROOK GLACIER CIRQUE ON SOUTHEAST SIDE OF BROKEN TOP. APRONS OF TALUS AND HOLOCENE GLACIAL DEPOSITS MANTLE LOWER SLOPES. CIRQUE WALLS ARE CHIEFLY COMPOSED OF THIN BASALTIC ANDESITE LAVA FLOWS AND INTERBEDDED AGGLOMERATE.

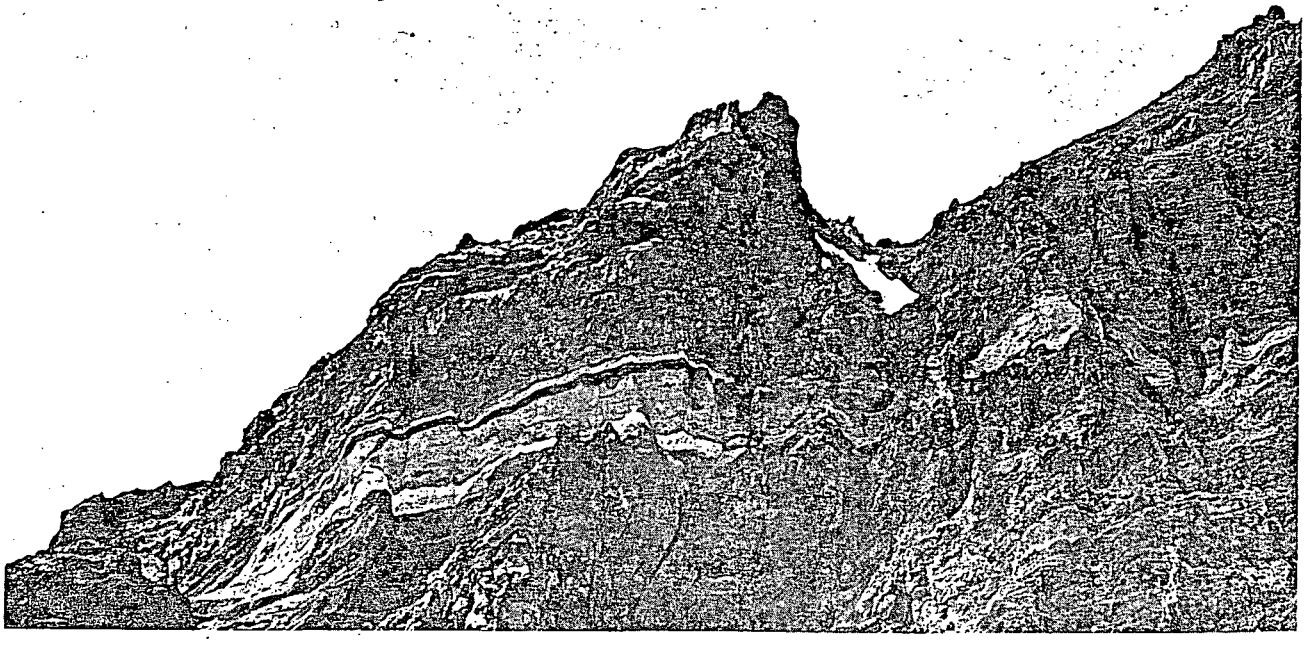

FIGURE 5. DACITIC IGNIMBRITE IN SOUTHWEST WALL OF CROOK GLACIER CIRQUE, BROKEN TOP. WHITE BASAL ZONE OF NONWELDED PUMICE IS OVERLAIN BY AN ORANGE POORLY WELDED ZONE WHICH PASSES UPWARD TO BUFF-AND-BLACK LAYERS OF NONWELDED PUMICE.

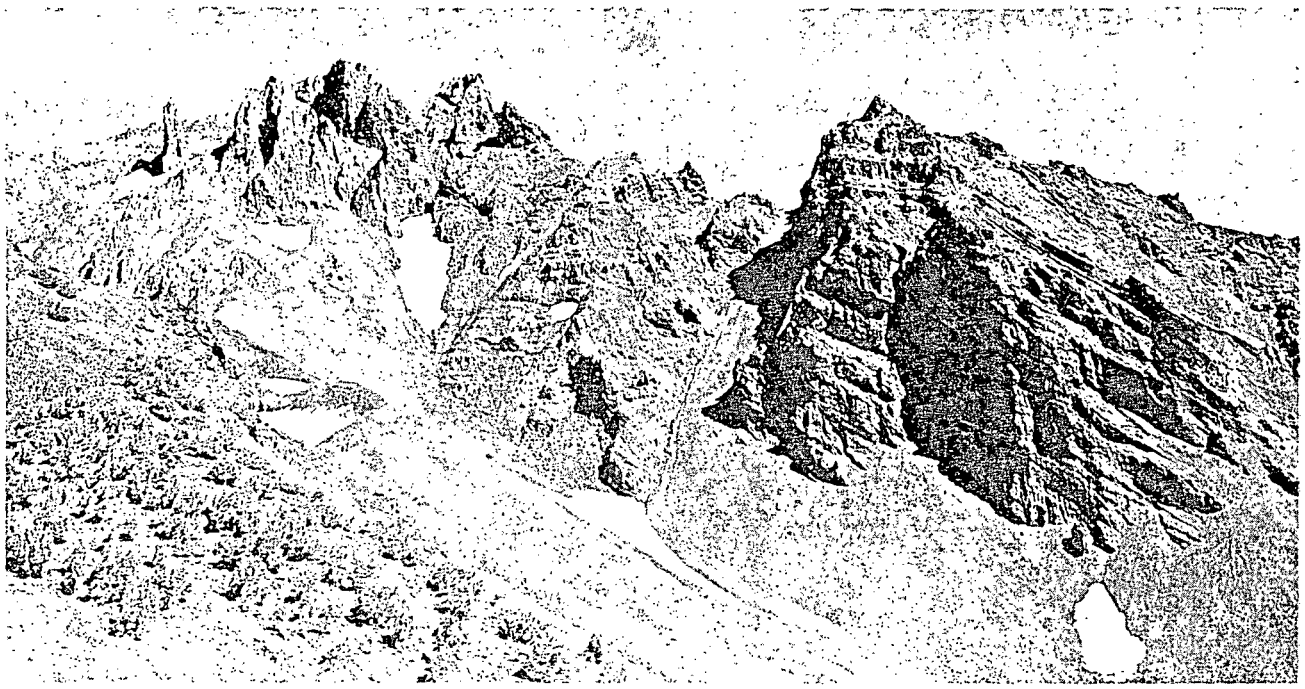

FIGURE 6. NORTHEAST WALL OF CROOK GLACIER CIRQUE, BROKEN TOP. INCLINED LAYERS OF RED AGGLOMERATE AND SCORIACEOUS LAVA OF EARLY SUMMIT CONE(RIGHT) ARE IN CONTACT WITH HORIZONTAL LAVAS WHICH FILLED A SUBSIDENCE CRATER(CENTER). IRREGULAR SURFACE OF CENTRAL CONDUIT PLUG IS EXPOSED ON THE LEFT.

FIGURE 7. SOUTHWEST WALL OF BEND GLACIER CIRQUE ON NORTH SIDE OF BROKEN TOP. DIKE CUTS DIAGONALLY ACROSS BASALTIC ANDESITE LAVAS AND INTERBEDS OF OXIDIZED AND PALAGONITIZED SCORIA. SOUTH SISTER IN BACKGROUND.

about the same time.

Basaltic magma reached the surface south of South Sister to form a set of palagonitic tuff cones which were soon buried under fresh cinders and lavas of Talupus and Katsuk Buttes. Only the lower parts of these volcanoes were eroded by latest Pleistocene glaciers.

Pleistocene Glaciation

Late Pleistocene glaciers covered all of the S.W. Broken Top quadrangle except the summit area of Tumalo Mountain and the northwest ridge crest and other prominences near the summit of Broken Top. Evidence of multiple glaciation is obscure. Pleistocene glacial deposits shown on accompanying geologic maps are probably equivalent to Suttle Lake drift of Scott (1977) and were deposited during the last episode of glaciation, ending some 12,000 years ago. Cirque basins were carved into the sides of Broken Top, Tam McArthur Rim, Todd Lake Volcano, and into the east side of Tumalo Mountain. Large tracts of striated bedrock are exposed above 7000 feet elevation; most of the debris from glacial erosion was deposited as moraines and outwash at lower elevations north, east, and south of the quadrangle. There is no evidence that eruptive activity was initiated beneath a thick cover of ice. However, some of the palagonitic tuff cones such as Talapus Butte suggest intimate and localized contact between ascending magma and ground or surface waters during the Pleistocene.

Holocene Volcanic Activity

After final retreat of Pleistocene glaciers a north-south chain of basaltic cinder cones developed south of Todd Lake and basaltic lavas moved 3 km west to Katsuk Butte. At about the same time, nearly identical magma produced Cayuse Cone and related flows from a vent 2.5 km north of Todd Lake. Still later, but before the appearance of Mazama ash from Crater Lake 6600 years ago, basaltic andesite erupted to form a small shield volcano on the north side of Bachelor Butte. The last eruption of mafic magma in S.W. Broken Top quadrangle also occurred at the north base of Bachelor Butte. A cinder cone over 150 m in height was formed and basaltic andesite lavas spread broadly to Sparks Lake basin, 5 km to the west.

Rhyodacitic ash and lapilli from eruptions of Rock Mesa at the southwest base of South Sister fell over the entire S.W. Broken Top quadrangle 2300 years ago. At a slightly later time similar material was erupted from a chain of vents on the east side of Devils Hill and from another chain of vents extending from the southeast to the northeast base of South Sister. All of these vents are now marked by domes and flows of rhyodacite, some of which moved into the west part of Broken Top quadrangle. It is clear that both mafic and silicic volcanism have continued into Holocene time and that future eruptions in this area are not unlikely.

Neoglaciation and Modern Erosion

Minor Neoglacial advances are recorded by fresh moraines and outwash fans in cirque basins on the south, east, and north sides of Broken Top summit. Outwash from Neoglacial Carver, Prouty, and Lewis Glaciers on the east flank of Middle and South Sisters is widespread in the northwest part of the Broken Top quadrangle. Some of the Neoglacial moraines are mantled by 2300-year-old rhyodacite pumice; others were formed after the pumice was deposited.

Talus aprons and talus ramparts have formed on over-steep glaciated mountain slopes and alluvium is currently accumulating in the Green Lake and Sparks Lake area. A Neoglacial moraine in the east cirque of Broken Top was breached in 1966, abruptly releasing part of a small lake (Nolf, 1966). Erosional and depositional effects of the resulting flood are still obvious over the 9-km length of affected drainage.

FIGURE 8. RHYODACITE LAVAS OF HOLOCENE NEWBERRY FLOW AND GOOSE CREEK CHAIN OF DOMES. NORTHWEST RIDGE OF BROKEN TOP ON SKYLINE.

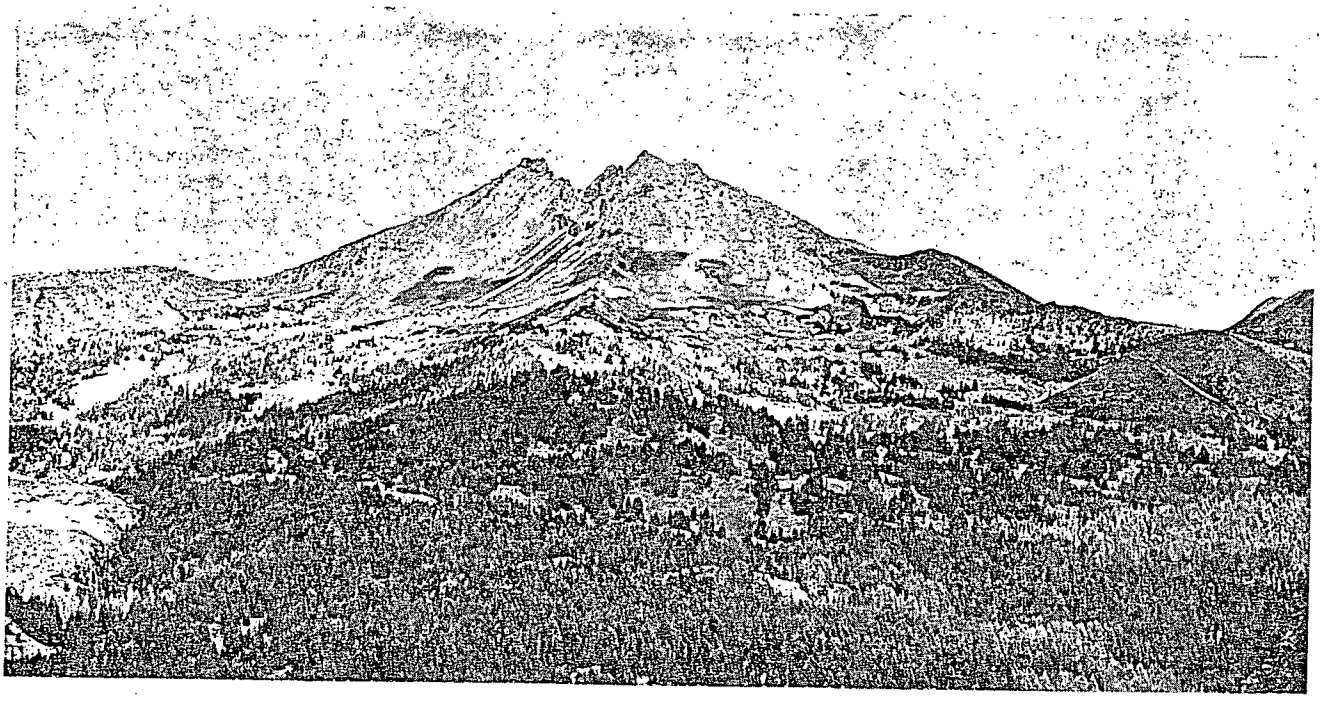

FIGURE 9. SOUTHWEST SIDE OF BROKEN TOP VOLCANO. CAYUSE CONE OF HOLOCENE BASALT(RIGHT) AND TERMINUS OF NEWBERRY RHYODACITE FLOW(LEFT).

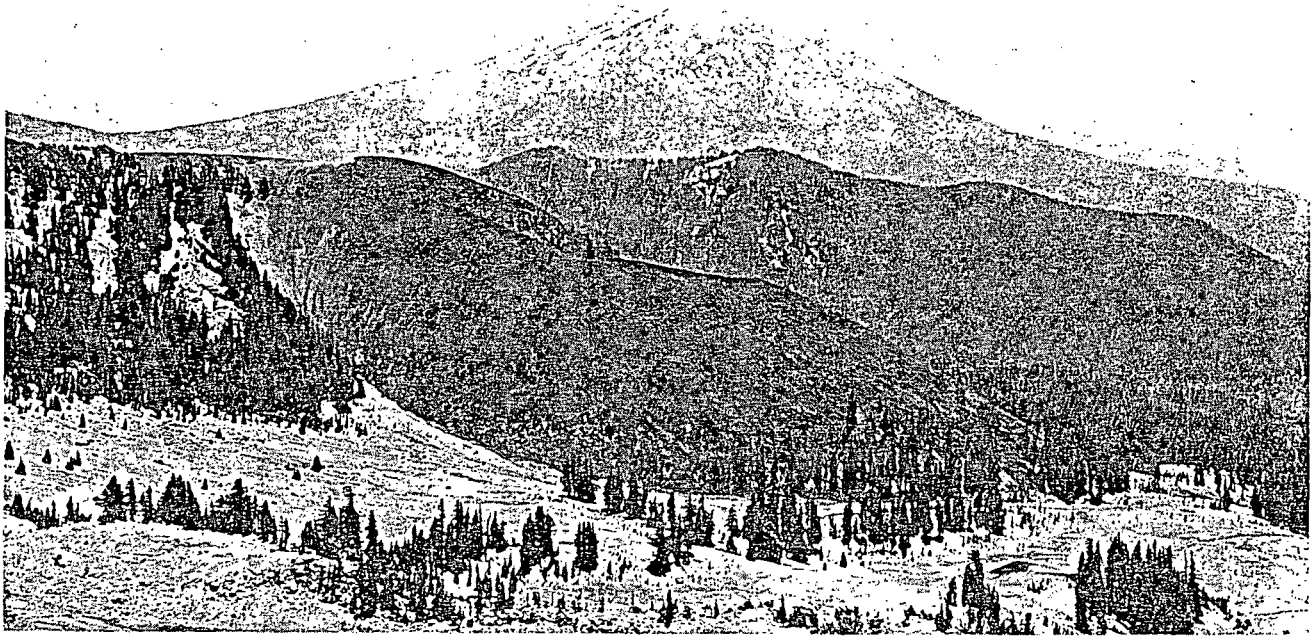

FIGURE 10. CAYUSE CONE ON SOUTHWEST SLOPE OF BROKEN TOP. TODD LAKE VOLCANO DACITE PLUG IN BACKGROUND WITH BACHELOR BUTTE ON SKYLINE.

FIGURE 11. MORAINE-DAMMED LAKE ON EAST SIDE OF BROKEN TOP. DIMINISHED IN SIZE FOLLOWING EROSIONAL BREACH IN 1966. BALL BUTTE AND TUMALO MOUNTAIN IN BACKGROUND, EXHAUSTED FIELD ASSISTANT IN FOREGROUND.

GEOLOGIC MAPS OF S.W. BROKEN TOP QUADRANGLE

The 7.5-minute S.W. Broken Top quadrangle has been divided into nine 2.5-minute rectangular areas and consecutively numbered according to the pattern shown in Figure 12. Distribution of mapped volcanic and nonvolcanic deposits within these areas is represented on the following geologic maps, Figures 14 through 22. Unit symbols are explained in the text; other symbols are given in Figure 13.

Representation of Mapped Units

In this report, symbols representing mapped volcanic rocks convey four categories of information: age, composition, occurrence, and unit number. For example, "HoDaLa3" designates the third-numbered unit of Holocene dacite lava and "PsBsPt4" designates the fourth-numbered Pleistocene basaltic tuff cone.

Age

It is unlikely that rocks older than one million years are exposed in the S.W. Broken Top quadrangle; most are younger than a few hundred-thousand years. Therefore, a paleomagnetic indication of rocks older than 700,000 years is of limited utility. Mazama ash (6600 years, Rubin and Alexander, 1960) is of widespread occurrence but few rock units within the quadrangle are younger. Most rock units in the central High Cascades can be assigned without ambiguity to either Holocene (younger than 10,000-12,000 years) or Pleistocene (10,000-12,000 to 2-3 million years) on the basis of their relationship to glaciated surfaces and glacial deposits.

Ho: Holocene deposits. Includes Neoglacial deposits, alluvium, and volcanic and volcaniclastic rocks less than 10,000-12,000 years old.

Ps: Pleistocene deposits. Includes glacial deposits, alluvium, and volcanic and volcaniclastic rocks older than 12,000 years but less than 2 million years.

Composition

At this writing, there is no universally accepted and precisely defined nomenclature applied to calc-alkaline rocks. Because many calc-alkaline Cascade rocks cannot be characterized adequately without chemical data, and because silica is a significantly variable, abundant, and easily determined constituent, it is probably the most suitable compositional parameter for classification. There is ample precedent relating an increase in silica content to the names basalt, basaltic andesite, andesite, dacite, and rhyodacite (Williams, 1942; Peck and others, 1964; Greene, 1968). In this study, five weight percent increments of silica content are assigned to basalt (48-53), basaltic andesite (53-58), andesite (58-63), dacite (63-68), and rhyodacite (68-73+)*. These values closely follow the silica subdivisions used for calc-alkaline volcanic rock series by S. R. Taylor (1969), Wise (1969), and Mackenzie and Chapell (1972); they are not in serious conflict with previously published petrographic names of rocks from the central High Cascades (Williams, 1944).

Bs Basalt, 48-53 weight percent SiO_2, H_2O-free.

BA Basaltic andesite, 53-58.

*Many High Cascade rocks contain more than 73 percent silica but none should be designated "rhyolite" unless it also contains more than 4 percent potash. Rocks that contain less than 48 percent silica might best be called "melabasalt," but they are virtually unknown in the High Cascades.

An Andesite, 58-63.

Da Dacite, 63-68.

Rd Rhyodacite, 68 or more.

Occurrence of Volcanic Deposits

Volcanic and volcaniclastic rocks in the S.W. Broken Top quadrangle occur in the form of intrusive dikes, sills, and plugs or as extrusive lava flows and volcanic domes, ash-flow deposits, ash-fall deposits, near-vent agglomerates, cinder cones, and tuff cones.

La Lavas. Includes volcanic domes, single flows, and composite flows in which pyroclastic material is subordinate.

Pc Coarse pyroclastic deposits. Includes mafic and silicic scoria and agglomerate of cinder cones and parts of composite volcanoes in which pyroclastic material is predominant; also includes pumice ramparts adjacent to volcanic domes.

Pt Tuff cones and tuff cone remnants. Includes altered (palagonitic) and fresh mafic and silicic varieties; also includes palagonitized deposits of bedded ash and lapilli in composite volcanoes.

Pf Fine-grained pyroclastic-fall deposits. Includes surficial blankets of mafic or silicic ash, generally far removed from the source vent.

Pi Ignimbritic deposits. Includes all welded and nonwelded deposits of pyroclastic-flow origin.

Id,s,p Intrusive dikes, sills, and plugs.

Occurrence of Nonvolcanic Deposits

Mapped nonvolcanic deposits are represented by symbols which designate age and occurrence only. Unit numbers are given to these deposits if they possess characteristics that require separate description.

Al Alluvium. Includes well-sorted glacial outwash, flood deposits; silt, sand, and gravel of stream and lake beds.

Gd Glacial drift. Includes till of terminal, latteral, and ground moraines, and some poorly sorted outwash near terminal moraines.

Ta Talus. Includes extensive aprons of talus, talus ramparts, and blockfields.

Sn Glacial ice, "permanent" snowfields.

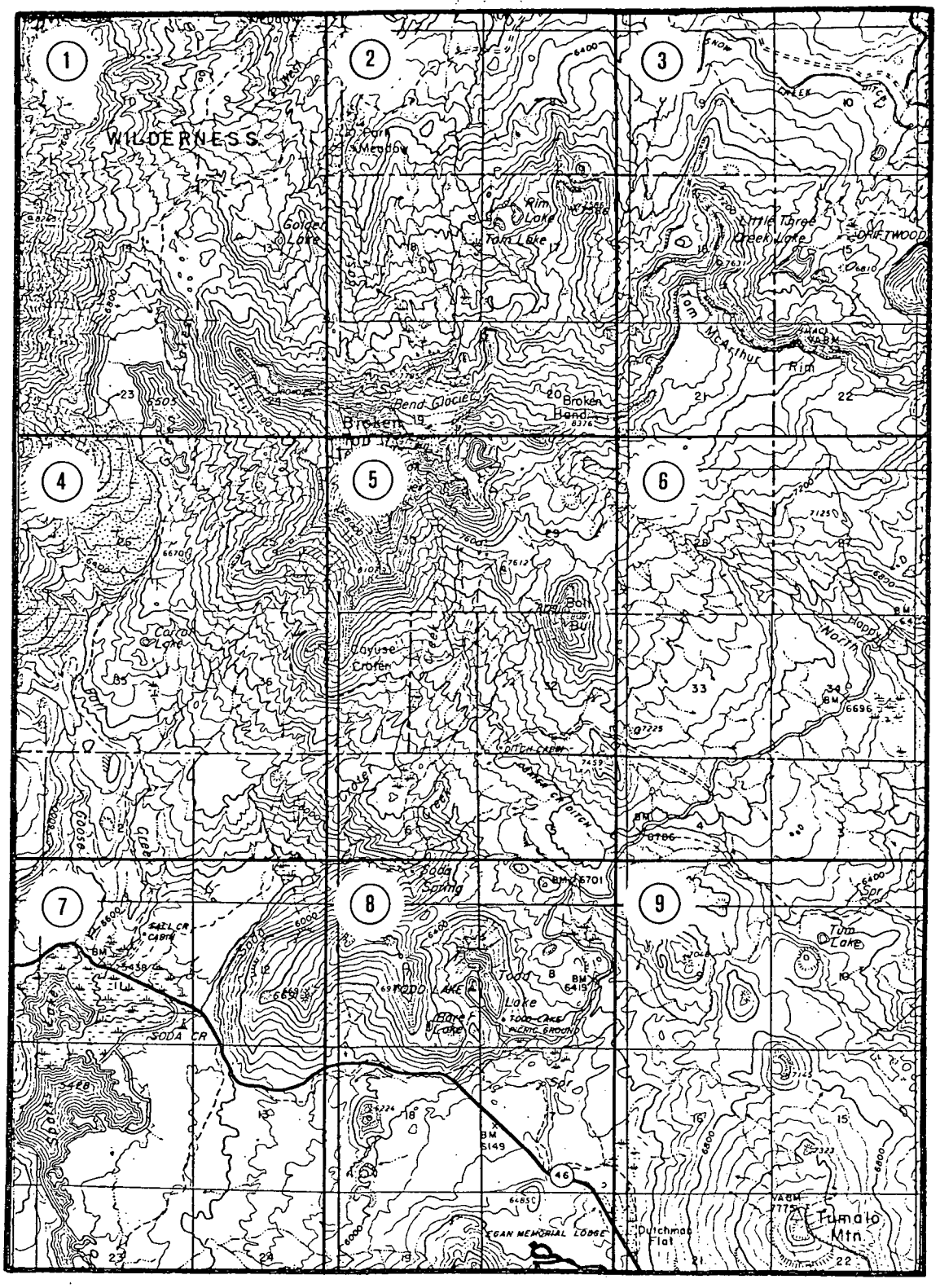

FIGURE 12. INDEX TO 9 GEOLOGIC MAPS OF S.W. BROKEN TOP QUADRANGLE.

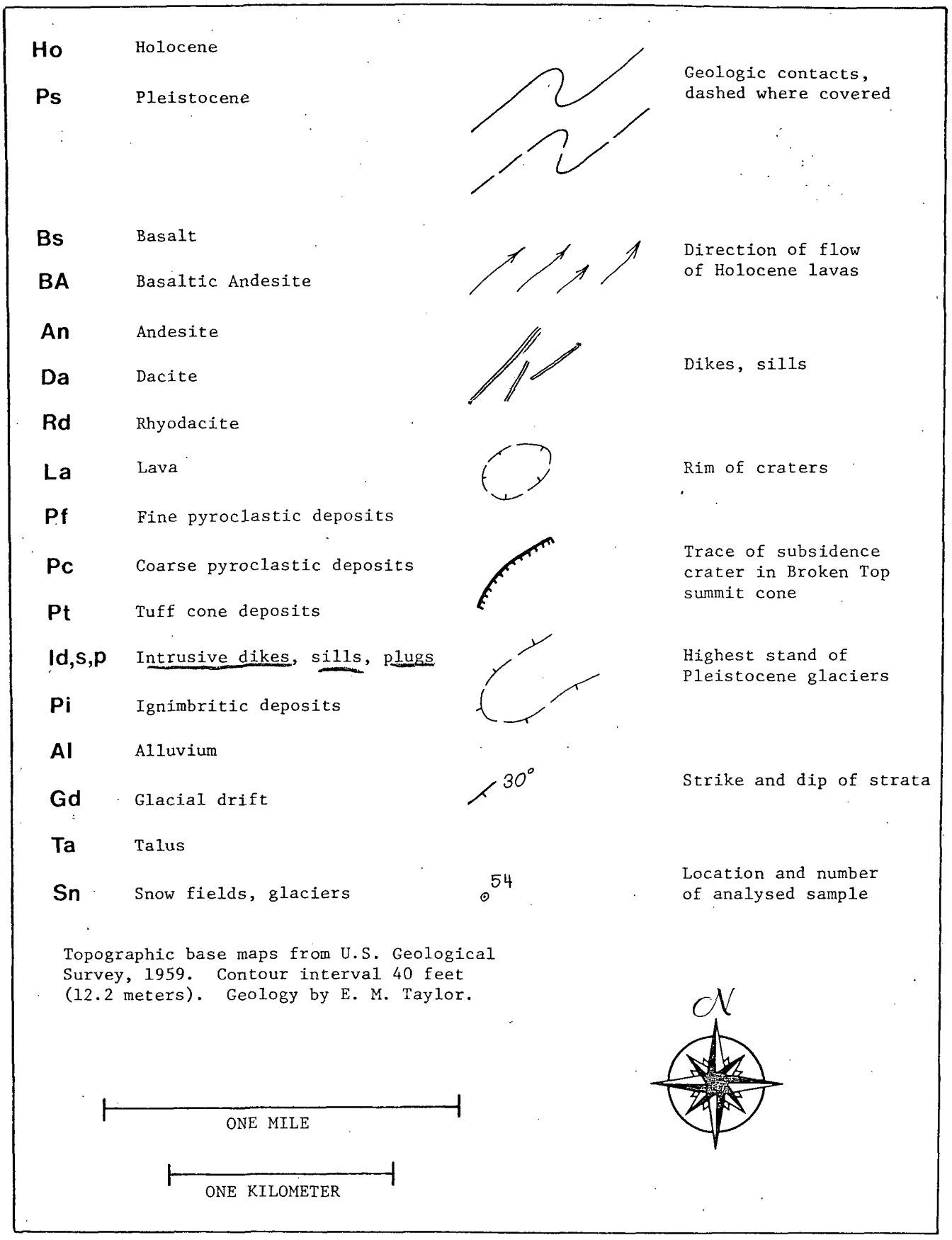

FIGURE 13. LEGEND FOR 9 GEOLOGIC MAPS OF S.W. BROKEN TOP QUADRANGLE.

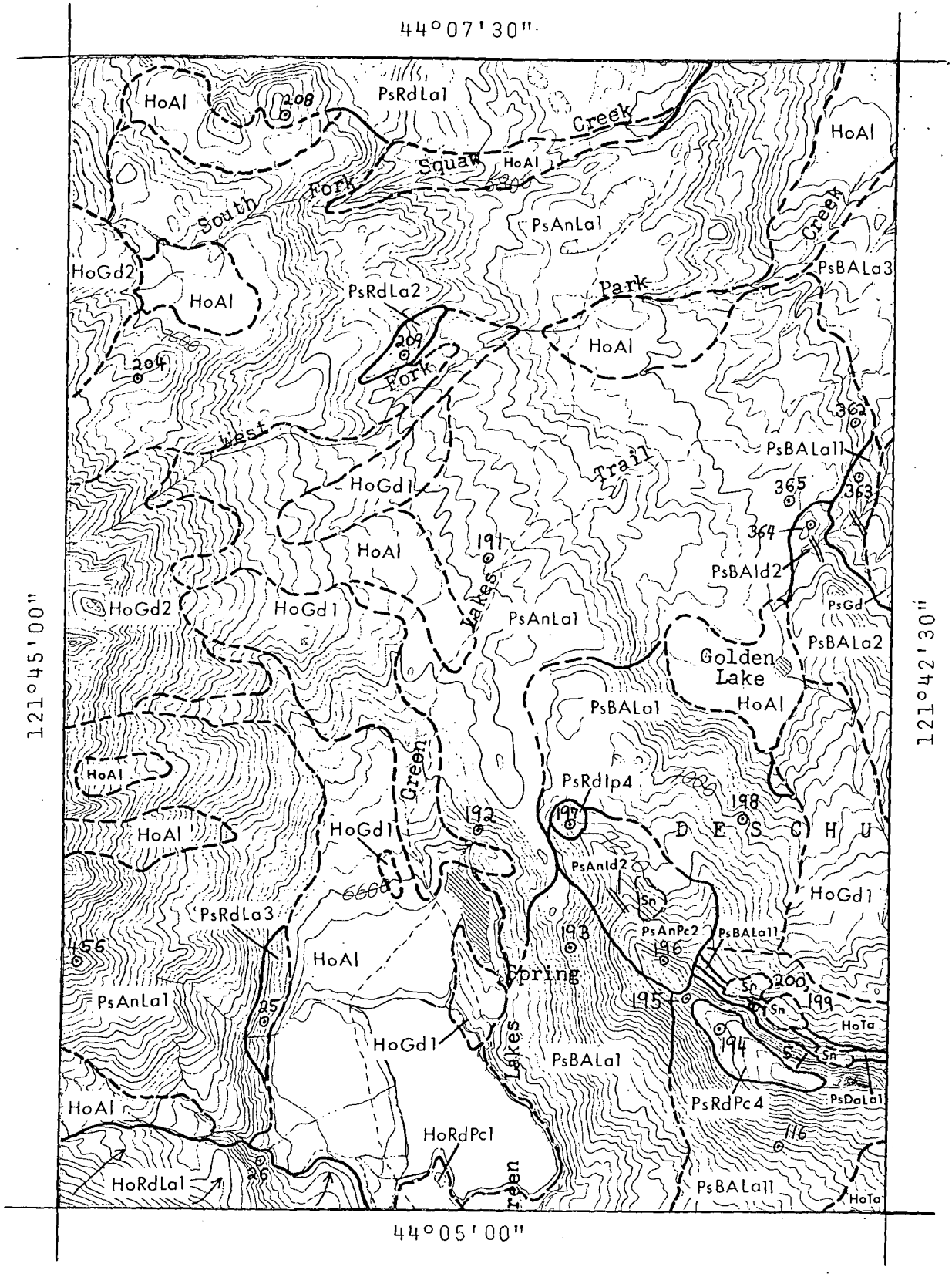

FIGURE 14. GEOLOGIC MAP NO. 1, S.W. BROKEN TOP QUADRANGLE, OREGON.

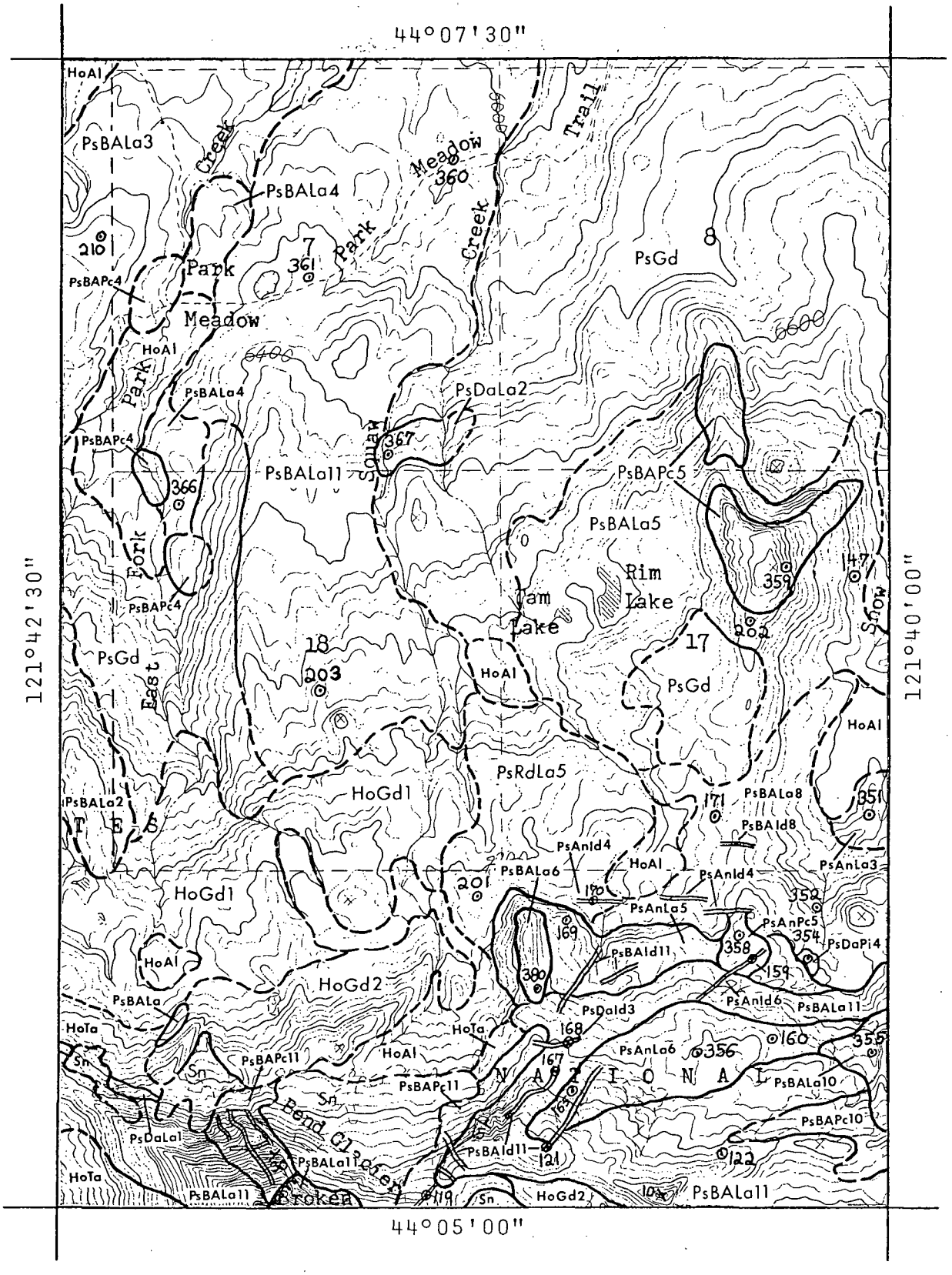

FIGURE 15. GEOLOGIC MAP NO. 2, S.W. BROKEN TOP QUADRANGLE, OREGON.

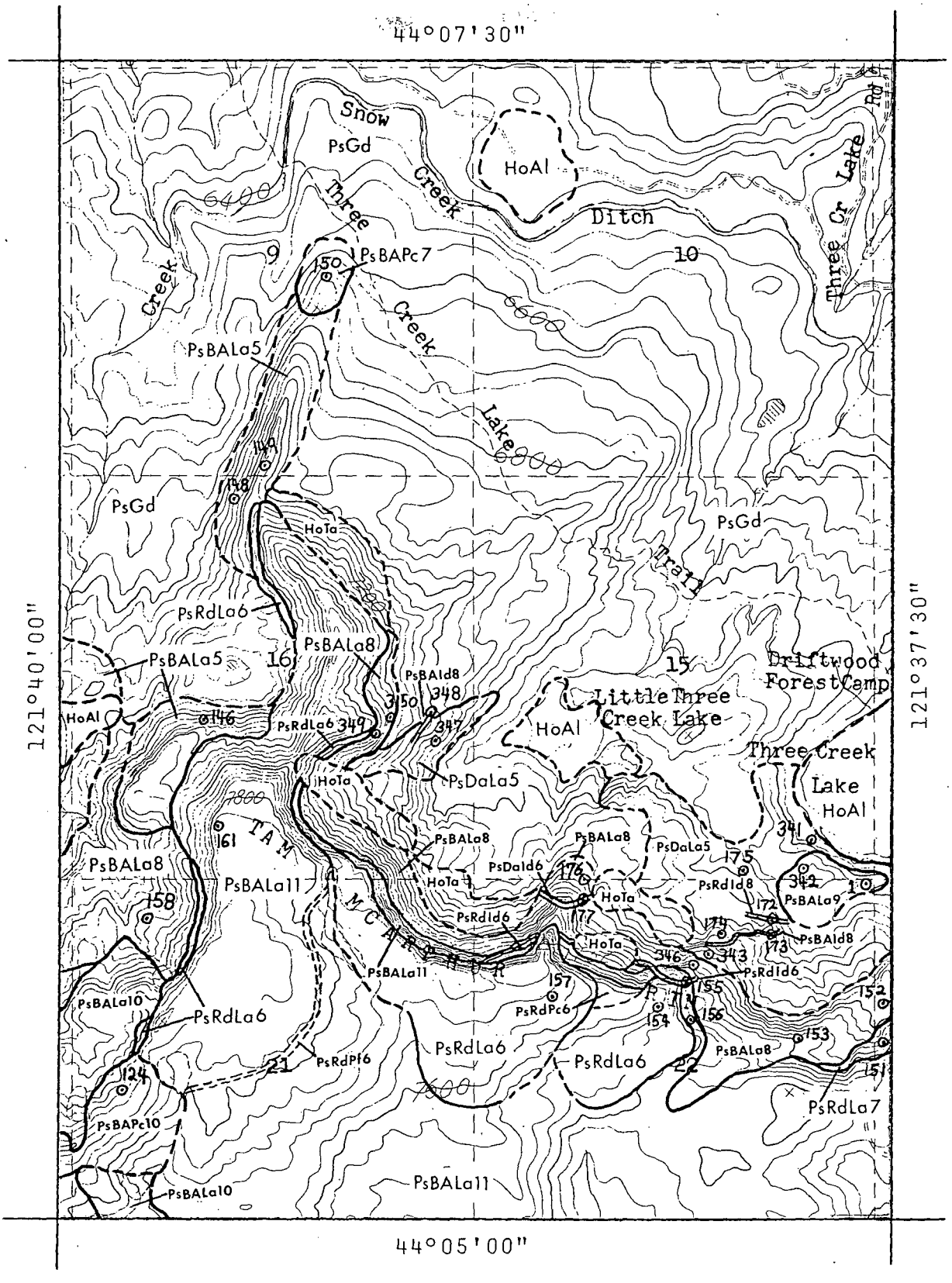

FIGURE 16. GEOLOGIC MAP NO. 3, S.W. BROKEN TOP QUADRANGLE, OREGON.

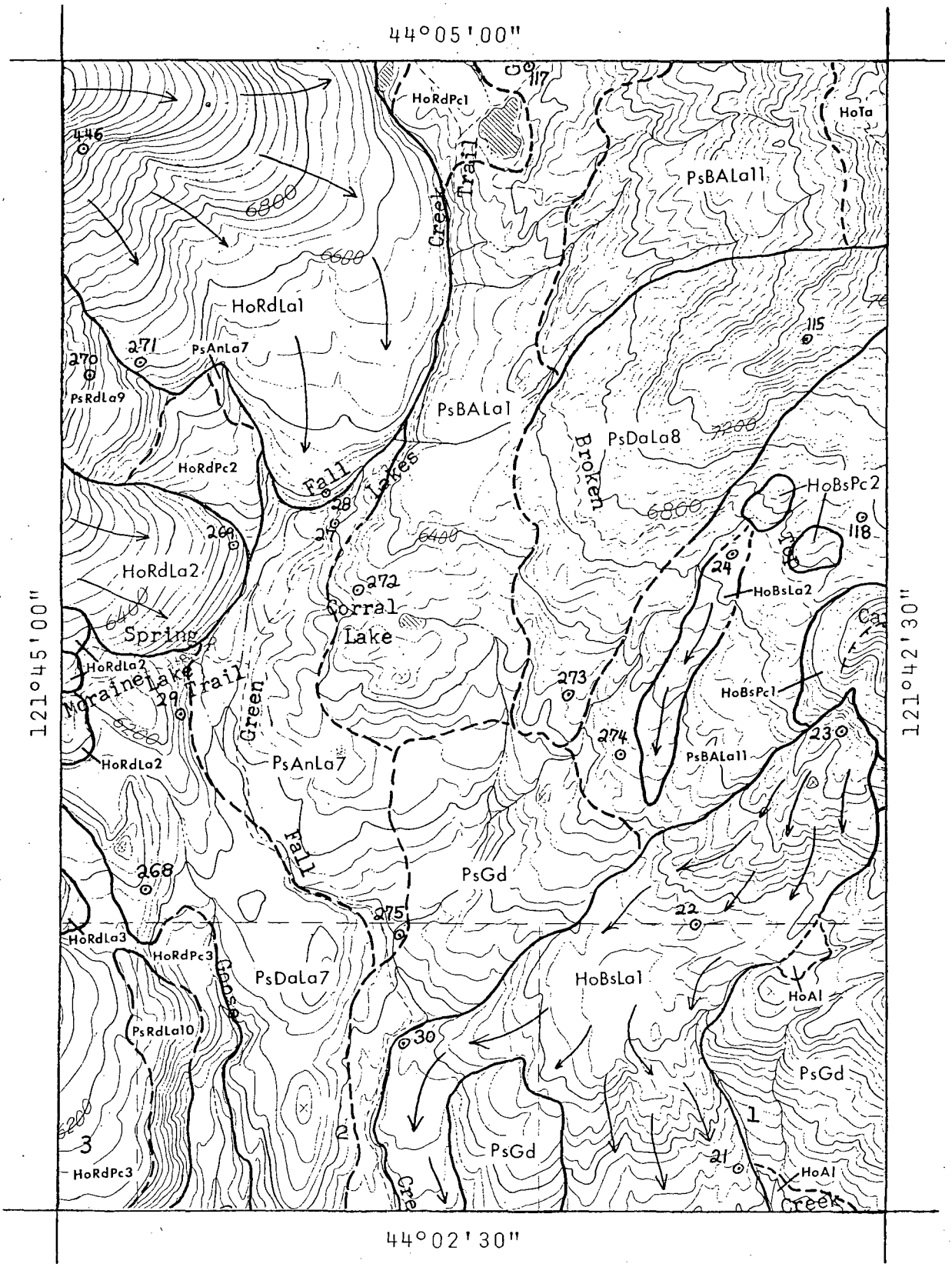

FIGURE 17. GEOLOGIC MAP NO. 4, S.W. BROKEN TOP QUADRANGLE, OREGON.

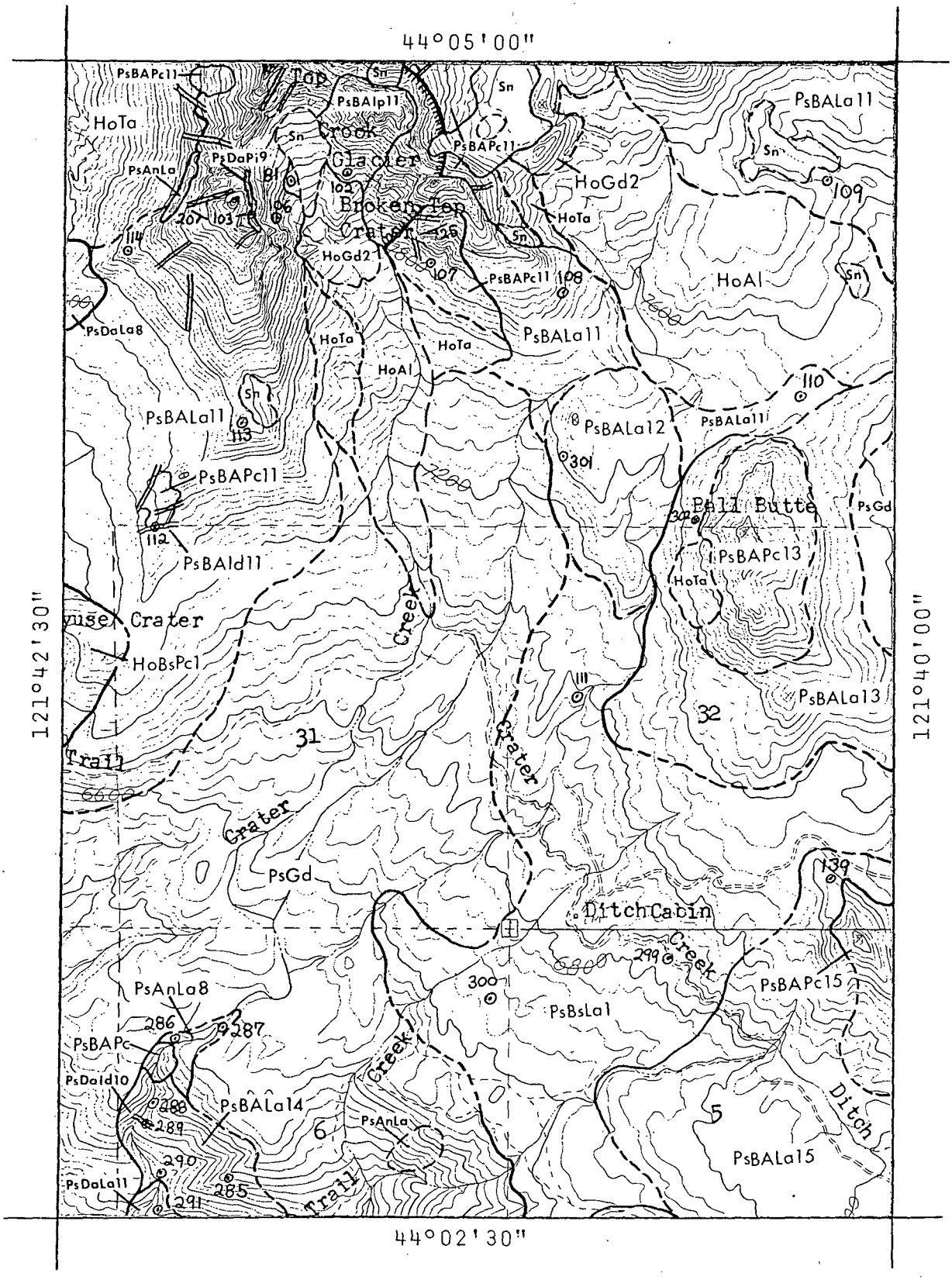

FIGURE 18. GEOLOGIC MAP NO. 5, S.W. BROKEN TOP QUADRANGLE, OREGON.

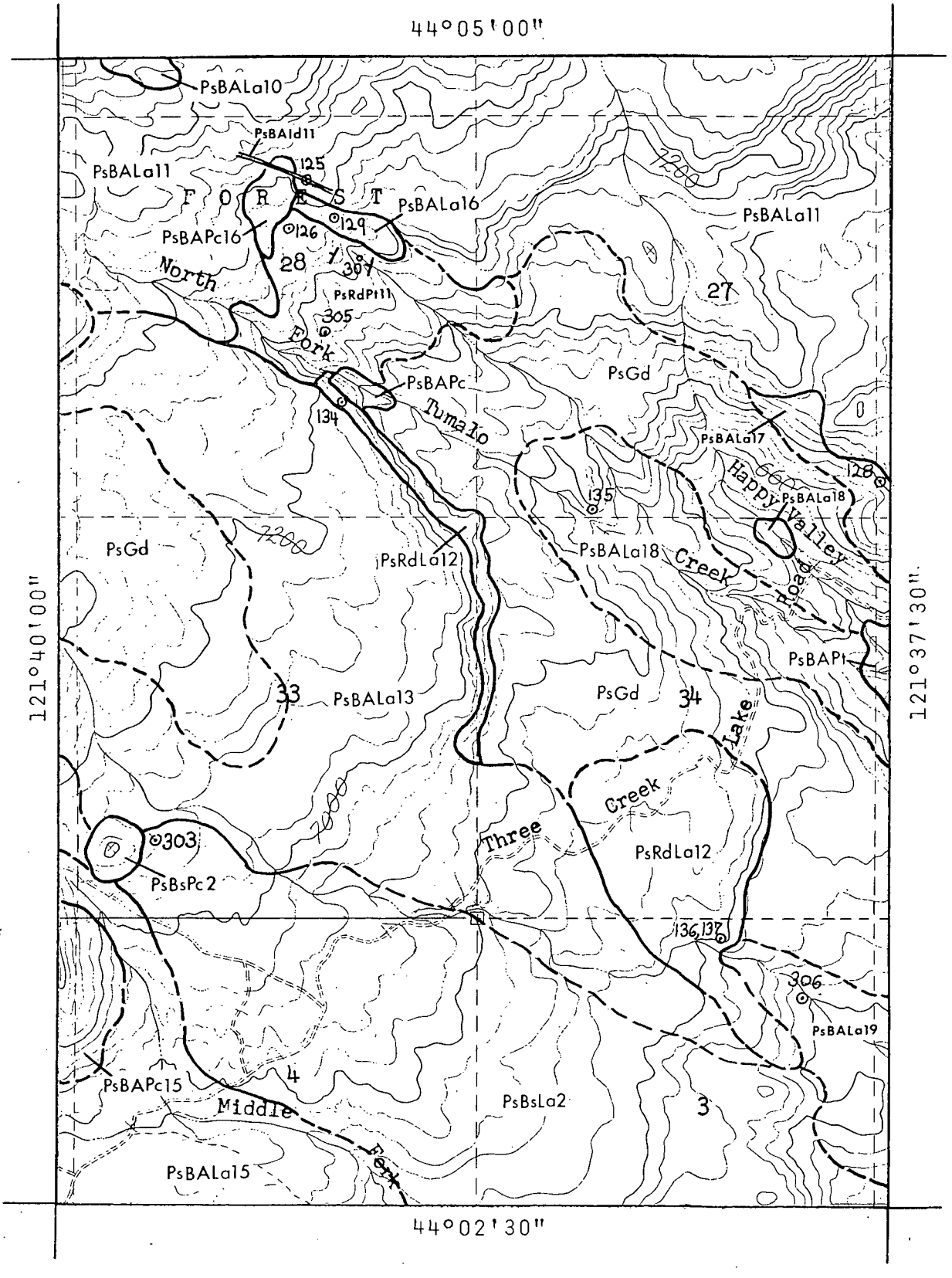

FIGURE 19. GEOLOGIC MAP NO. 6, S.W. BROKEN TOP QUADRANGLE, OREGON.

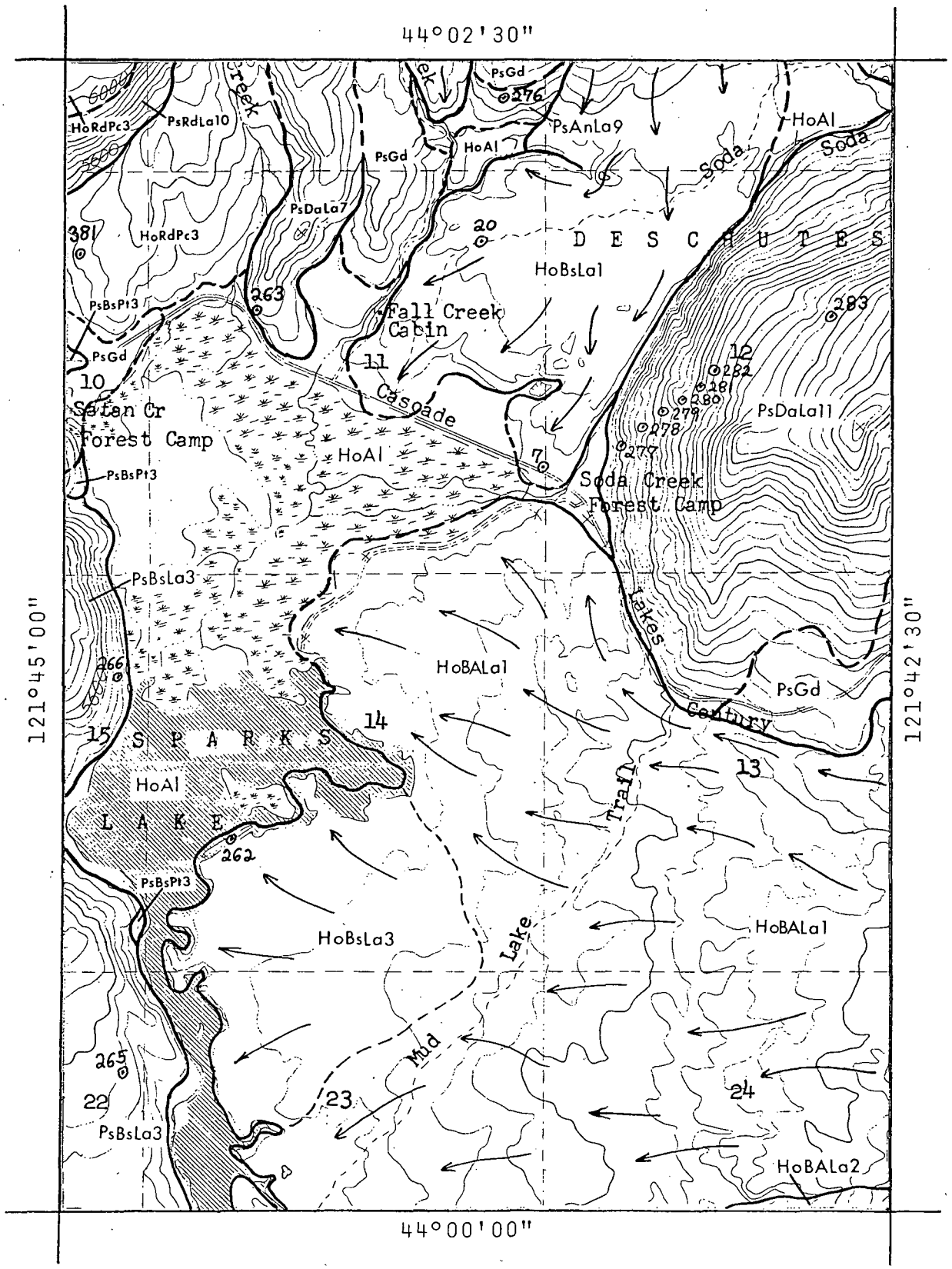

FIGURE 20. GEOLOGIC MAP NO. 7, S.W. BROKEN TOP QUADRANGLE, OREGON.

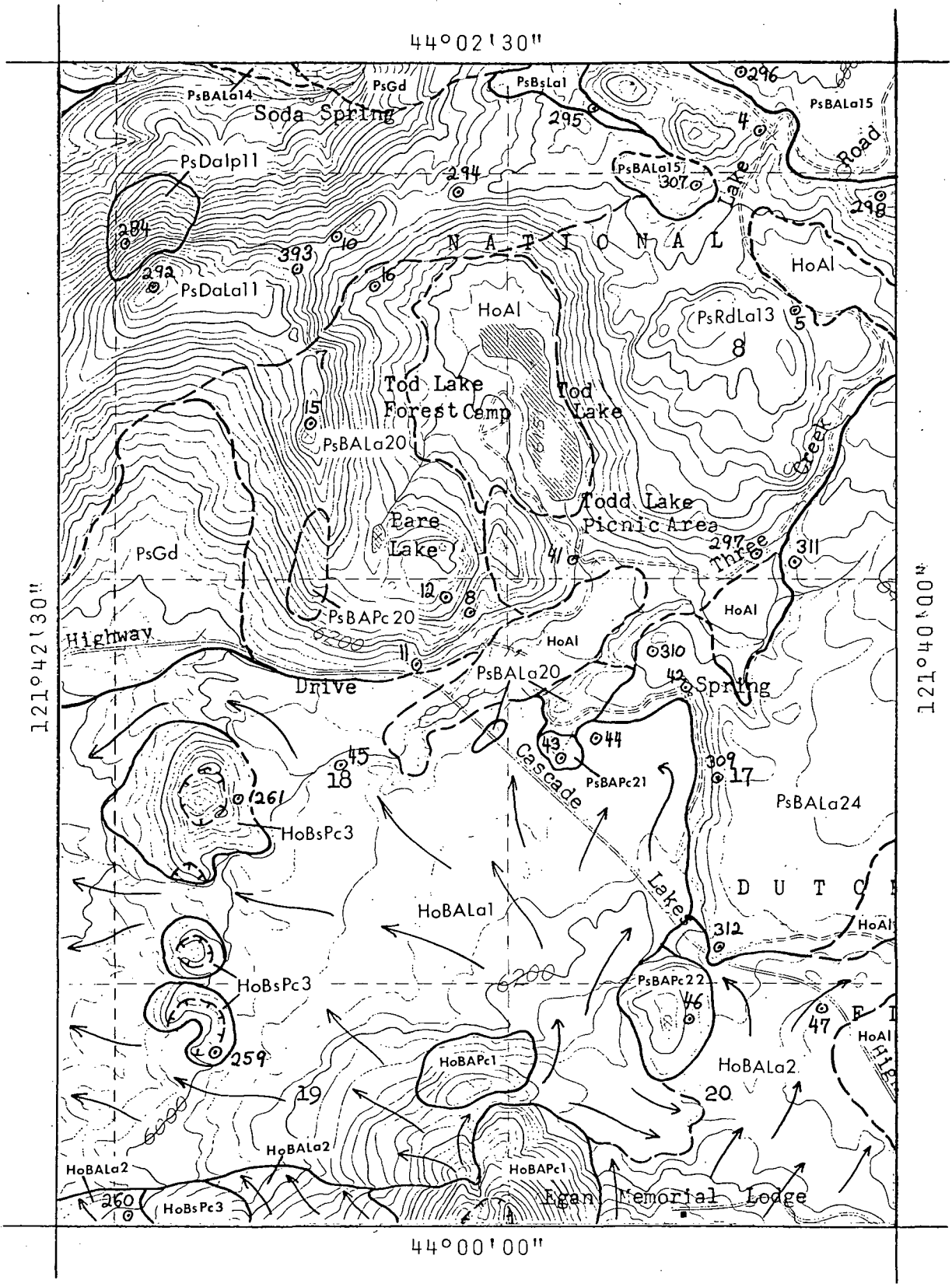

FIGURE 21. GEOLOGIC MAP NO. 8, S.W. BROKEN TOP QUADRANGLE, OREGON.

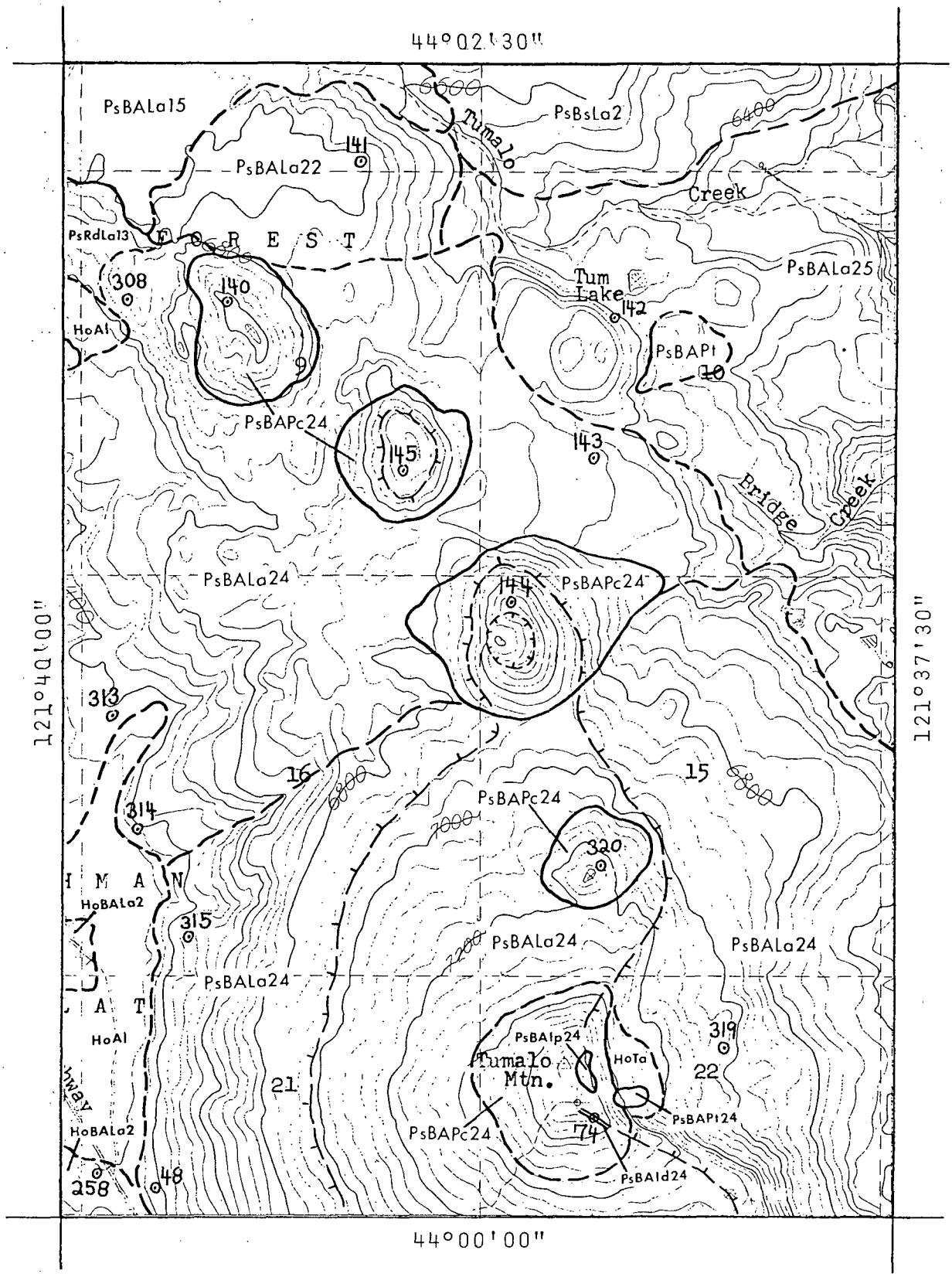

FIGURE 22. GEOLOGIC MAP NO. 9, S.W. BROKEN TOP QUADRANGLE, OREGON.

DESCRIPTIONS OF MAPPED UNITS

Salient features of mapped units are summarized below in consecutively numbered age-composition groups. Each unit is numbered on the geologic maps and appropriate geologic map numbers are included in each description. Consequently, a description of any given mapped unit is easily found and the mapped locations of each type of deposit are readily identified.

Petrographic characteristics were determined through study of thin sections, usually of fresh, nonvesicular glassy samples taken from widely separated parts of each unit. Phenocryst proportions were measured using standard point-counting techniques and are reported as volume percent of solid rock, excluding void spaces. Compositions of plagioclase are reported as mole percent An and were determined by measurement of extinction angles according to the method of combined albite and Carlsbad twins, the a-normal method, and the Michel-Levy method, in that order of preference. Charts published by Tobi (1963), Von Burri (1967), and Shelley (1975) for volcanic plagioclase were used in support of these methods, respectively.

A silica content is given for each described unit as well as the sample numbers of pertinent chemical analyses and calculated averages. All analyses are listed consecutively by sample number in Appendix 1, corresponding to Appendix 2, sample locations and geologic map numbers. Each sample site is also identified by number on the appropriate geologic map. Analytical values are expressed as weight percent oxides of the eight principal cations Si, Al, Fe, Ca, Mg, K, Na, and Ti. All iron is expressed as FeO. Each analysed sample was split from at least 0.5 kg of uniform rock powder and was converted to an anhydrous condition. A lithium borate fusion technique was used to prepare samples for x-ray emission spectrometry for Al, Fe, Ca, K, and Ti. This was followed by a silicomolybdate colorimetric method for Si and atomic absorption spectrophotometry for Mg and Na. All determinative procedures were calibrated to a set of U.S. Geological Survey analysed rock standards. Replicate analyses have established that results are reproducible to within 0.5, 0.5, 0.1, 0.1, 0.1, 0.05, 0.1, and 0.05 of the respectively tabulated values. Analyses were performed by E. M. Taylor with able assistance from Mrs. R. L. Lightfoot.

Units of Holocene Nonvolcanic Deposits

HoGd1
HoGd2 Terminal and lateral Neoglacial moraines (HoGd1) in the vicinity of Broken Top and Three Sisters which are overlain by fragments of pumice and obsidian from 2300-year-old Rock Mesa eruption, and Neoglacial moraines (HoGd2) which are not.

Units of Holocene Basalt

HoBsLa1
HoBsPc1 Olivine basalt lavas from Cayuse Cone. Silica 49-51. Cone of red and black scoria 200 m high, breached on S.W. side by lavas which moved in two lobes, 4.5 km S. to Sparks Lk. and 1.3 km W. to Fall Cr. Black to gray scoriaceous aa surface with lava levees, gutters, and hummocky terrain. Phenocrysts of Ol (10-12%; up to 2.0 mm) and sparse microphenocrysts of Plag. Groundmass Plag An60-65. Not glaciated; overlain by pumice from Devils Hill Chain of Domes, Rock Mesa (2300 C-14 yrs), and Mazama ash (6600 yrs). Terminus of main lobe is buried in alluvial deposits of Sparks Lk. basin. Analyses 7, 20, 21, 22, 23, 30; average Cayuse lava, 1000. Maps 4, 7.

HoBsLa2
HoBsPc2 Olivine basalt lava and two small cones 0.2 and 0.5 km N.W. of Cayuse Cone. Silica 51-52. Narrow lava flow, 1.2 km long, issued from S.W. base of N.W. cone. Surface features, composition, mineralogy, and probable age similar to Cayuse lavas and cone. Analysis 24. Map 4.

HoBsLa3 HoBsPc3 Olivine basalt lava and chain of cinder cones S.W. of Todd Lk. Silica 50-52. Hummocky black and gray lava surfaces composed of aa fragments. Very large, coherent, tipped blocks along flow margins. Phenocrysts of Ol (11-12%; up to 1 mm) with sparse microphenocrysts of Plag. Pilotaxitic groundmass of An 65-70 Plag microlites in subophitic intergrowth with Cpx. Two-km N-S alignment of 4 cinder cones with remnants of 5 vents. Black and red cinders, spatter, and bombs. Partly exposed flows from these cones probably exist in the basaltic andesite lava fields to the W. but are mapped separately only along E. side of Sparks Lk. Cones and lavas not glaciated; overlain by pumice from Rock Mesa and ash from Mazama. Also overlain by basaltic andesite lavas from Bachelor Bu. and from cone at N. base of Bachelor Bu. Analyses 259, 261, 262; average, 1001. Maps 7, 8.

Units of Holocene Basaltic Andesite

HoBALa1 HoBAPc1 Basaltic andesite lavas which extend from source cone at N. base of Bachelor Bu., 4.5 km W. to Sparks Lk. Silica 54-55. Hummocky, scoriaceous, black and gray lava surfaces with lava levees, blocky near source. Microphenocrysts of Plag and Ol (both <1%). Groundmass pilotaxitic intergranular, Plag microlites An 40-45. Cone of red and black cinders and spatter was breached on N.W. side. Lavas and cone not glaciated; overlain by Rock Mesa pumice and Mazama ash. Terminus of flow is partly buried in alluvium of Sparks Lk. basin and alluvium has been deposited on the lava field S. of Todd Lk. Lavas and cone rest on lavas from Bachelor Bu. Analyses 44, 45; average, 1002. Maps 7, 8, and Quad. S.

HoBALa2 Olivine- and clinopyroxene-bearing glomerophyric basaltic andesite lavas S.W. and W. of Dutchman Flat, not mapped separately. Silica 54-57. From adventive shield at 7800' elev. on N. side of Bachelor Bu. Flow surface black to gray, blocky to aa with pressure ridges. Phenocrysts and glomerocrysts of Plag (12-15%; partly resorbed with normal oscillatory zones from An 75 core to An 45 rim; up to 2 mm), Ol and Cpx (both approximately 2%; up to 1 mm). In some flows olivine is surrounded by narrow jackets of granular pyroxene. Groundmass Plag An 40-45; hyaloophitic to intergranular. Not glaciated; overlain by Rock Mesa pumice, Mazama ash, and lavas from cone at N. base of Bachelor Bu. Rests upon lavas and cone chain S.W. of Todd Lake. Analyses 47, 258, 260; average, 1003. Maps 7, 8, 9 and Quad. S.

Units of Holocene Rhyodacite

HoRdLa1 HoRdPc1 Orthopyroxene-bearing rhyodacite lava and pumice deposits from Newberry vent. Flow 3 km long, 1.5 km wide. Blocky surface with extensive pressure ridge system. Blocks composed of black, flow-banded obsidian and white, partly inflated crust. Spherulitic in part. S.W. 1/4 of flow contains mixed red and black glass. Phenocrysts of Plag (7-9%; An 35-45, normally zoned and extensively resorbed; up to 3 mm), Opx (0.5-1.5%; very small), Mag and fresh Hb (both sparse and very small). Not glaciated; Newberry flow rests upon early pumiceous deposits from Newberry vent and from Rock Mesa (2300 C-14 yrs.). Overlain by pumice from nearby Goose Cr. chain of domes. Analyses 26, 28, 271, 446; average Newberry, Goose Cr., Devils Hill chains of domes, 1004. Maps 1, 3, Quad. W.

HoRdLa2 HoRdPc2 Orthopyroxene-bearing rhyodacite lava and pumice deposits from Goose Cr. chain of domes. Silica 72-73. Five domes, 10 vents, 2.0 km long, aligned N.10W. Surface of domes and marginal crumble breccia composed of gray, partly inflated blocks. Plag phenocrysts up to 12%; otherwise mineralogy and texture identical to Newberry flow. Pumice ramparts on W. side of domes; elsewhere overlain by domes and lava flow. Goose Cr. pumice rests upon Newberry flow and is underlain by pumice from Rock Mesa. Analyses 269, 445, 447; average Newberry, Goose Cr., Devils Hill chains of domes, 1004. Map 4 and Quad. W.

HoRdLa3 HoRdPc3 Orthopyroxene-bearing rhyodacite lava and pumice deposits from Devils Hill chain of domes. SiO_2 71-72. Four domes, 5 vents, 2.4 km long. aligned N.3W. Lithology and mineralogy identical to Goose Cr. chain of domes. Pumice depo-

sits thicker and more extensive. Pumice rampart E. of domes is up to 50 m thick, composed of poorly sorted white-to-gray lumps and breadcrust bomb fragments up to 0.5 m in diameter. Collapse of steep-sided pumice ramparts probably contributed small pyroclastic flows to the pumice blanket in lower Goose Cr. valley. Domes, lavas, and deposits rest on pumice from Rock Mesa (2300 C-14 yrs.), but probably was produced at about the same time. Analyses 381, 448; average Newberry, Goose Cr., and Devils Hill chains of domes, 1004. Maps 4, 7, and Quad. W.

Units of Pleistocene Basalt

PsBsLa1 Olivine- and clinopyroxene-bearing basalt lavas in vicinity of Ditch Cabin, not separately mapped. Silica 52-53. Dark gray glaciated lavas from 7000' elev. S.W. of Ball Bu. to 6600' elev. on E. rim of Soda Cr. canyon. Phenocrysts and glomerocrysts of Plag (15-30%; An 50-60; up to 1 mm; larger crystals contain up to 50 close-set oscillatory normal zones ranging over approximately 10 An), Ol (6-8%; up to 1.5 mm), and Cpx (2-3%; 0.5 mm). Groundmass plag An 45. Flows 1.3 km S. of Ditch Cabin are coarse diktytaxitic microporphyries with phenocrysts of Plag (38%; An 70-80; up to 8 mm), Ol (17%; 2 mm), and Cpx (4%; 1.5 mm). Normal paleomagnetic polarity. Analyses 111, 295, 299, 300; average Ditch Cabin basalts, 1005. Maps 5, 6, 8.

PsBsLa2 PsBsPc2 Olivine-bearing basalt lava from small glaciated cinder cone remnant, 1.0 km S.E. of Ball Bu. Silica 52-52. Dark gray glaciated lava extends 3.3 km S.S.E. from source cone at 7200' elev. to 6200' elev. in Middle Fork Tumalo Cr. canyon. Phenocrysts and glomerocrysts of Plag (10-12%; An 55-65; up to 3 mm). Larger crystals contain normally zoned An 65-55 cores surrounded by repeated sets of An 60-65 oscillatory zones and rim zones to An 45. Ol (8-10%; up to 4 mm) and Cpx (<1%; small). Analysis 303. Maps 6, 9.

PsBsLa3 PsBsPt3 Olivine-bearing basalt lavas from Talapus and Katsuk Buttes. Silica 51-52. Dark gray interior, black to red scoriaceous surfaces. Principal flows were produced from a vent in saddle between Talapus and Katsuk, and from a vent on the S. side of Katsuk. Lavas have been moderately glaciated, especially at lower elevations. Phenocrysts and small glomerocrysts of Plag (17-19%; An 60-65 in cores, normal zoned to An 45 rims; up to 2 mm; larger crystals possess extensively resorbed cores) and Ol (5-7%; up to 1 mm). Groundmass Plag An 40-45. Talapus Bu. cinder cone was constructed on a large palagonitic tuff cone whose glaciated flanks are now occupied by Devils Lk. Bedded hyaloclastites are best exposed in roadcuts near Devils Lk., on the N. side of Talapus, and along the E. margin of the Talapus-Katsuk lava field. Overlain by lavas from Bachelor Bu. Analyses 264, 265, 266, 525, 526; average Talapus-Katsuk basalts, 1006. Map 7 and Quads. W, SW, S.

Units of Pleistocene Basaltic Andesite

PsBALa1 Basaltic andesite lavas between Golden, Green, and Corral Lakes, not mapped separately. Dark to light gray, blocky, glaciated. Lavas between Golden and Green Lks: Silica 53-54. Very fine grained with sparse microphenocrysts of An 50-55 Plag. Groundmass Plag An 40-45. Between Corral and Green Lks: Silica 53-57. Phenocrysts of Plag (5-12%; An 65-70 in cores with normal zones to An 50-55 rims; up to 4 mm), Ol and Cpx (both <1%; up to 0.5 mm). Overlain by Broken Top basaltic andesites and dacites. Analyses 117, 193, 198, 272. Averages 1007, 1008. Maps 1, 4.

PsBALa2 PsBAId2 Olivine- and clinopyroxene-bearing basaltic andesite lavas and dike on ridge east of Golden Lake. Silica 55-56. Platy, gray to pink. Phenocrysts of Plag (18-20%; An 70-75 in cores with delicate oscillatory normal zoning to rims of An 55; up to 4 mm), Ol (4-5%; rounded with rims of granular Mag, up to 0.5 mm), Cpx (1-2%; up to 3 mm). Groundmass Plag An 45-50. Glaciated. Analysis 364. Maps 1, 2.

PsBALa3 Orthopyroxene-bearing basaltic andesite lavas N.W. of Park Meadow. Silica 56-57. Glaciated remnants of pressure ridges. Gray to brown, scoriaceous to platy. Phenocrysts of Plag (27-29%; An 35-55, oscillatory normal zones; up to 2 mm),

Opx and microphenocrysts of Mag (both 1-2%). Sparse phenocrysts of large resorbed Plag with patchy zoning; glomerocrysts of Plag, Opx, and Cpx up to 6 mm. Groundmass Plag An 35. Overlain by andesite lavas from S. Sister. Analysis 210. Maps 1, 2, and Quad. N.

PsBALa4 PsBAPc4 Olivine-bearing basaltic andesite lavas and remnants of glaciated cones in Park Meadow area. Silica 54-55. Red to black scoriaceous lava and red cinders. Phenocrysts of Plag (24-26%; An 70-80, normal zones; up to 3 mm) and Ol (2-3%; 0.5 mm). Groundmass Plag An 60. Analysis 366. Map 2.

PsBALa5 PsBAPc5 Glaciated basaltic andesite lavas and remnant of glaciated cinder cone E. of Rim Lake. Silica 54-56; unusually high Fe, Ti. Lavas gray in blocky-to-platy interior, brown on scoriaceous surface. Cinders red. Microphenocrysts of Plag (reverse zoned from An 50 to An 60 in cores, surrounded by thin rim of An 50, up to 1.5 mm in length) with Ol and Cpx (up to 1 mm), all <1%. Very fine-grained groundmass with Plag An 50. Glaciers carved deep circular pit in N. flank of cone. Glacial debris and striations to summit. Analyses 146, 147, 148, 149, 202, 359; average, 1009. Maps 2, 3.

PsBALa6 Clinopyroxene-bearing microporphyritic basaltic andesite capping ridge at 7600' elev., 1.3 km S. of Tam Lk. Silica 57-58. Black vitrophyric to brown holocrystalline, blocky. Microphenocrysts of Plag (16-18%; reverse-zoned cores An 55-65 surrounded by a thin rim zoned normally to An 55; up to 1 mm), Cpx (1-2%; 0.5 mm), and Mag (<1%). Some of the Plag crystals are extensively resorbed. Glaciated and overlain by basaltic andesite lavas from Broken Top. Analysis 380. Map 2.

PsBAPc7 Glaciated remnant of basaltic andesite cinder cone 2.6 km N.W. of Three Cr. Lk. Silica 56-57. Red and black scoria. Phenocrysts of Plag (<1%; up to 2 mm) and Cpx (<1%; 0.4 mm). Analysis 150. Map 3.

PsBALa8 PsBAId8 Basaltic andesite lavas in cliffs of Tam McArthur Rim and Snow Creek cirque, not mapped separately. Overlain by lavas of Broken Top. Lavas on upper shelf S. of Three Cr. Lk: SiO_2 55-56. Thick blocky flows, gray interior with reddish-brown crust. Phenocrysts of Plag (16-17%; An 70-75 in core, rim zones of An 40; up to 4 mm), Ol (<1%; rounded and embayed; 0.5 mm), and Cpx (<1%; 0.4 mm). Normal paleomagnetic polarity. Analyses 152, 153; average, 1010. Map 3 and Quad. E. Lavas in Tam Mac Rim and Snow Cr. cirque: Silica 54-58. Thick blocky flows, light gray and flow banded. Sparse phenocrysts of Plag (generally <1%; An 60-65; in two habits within same rock - short and broad with reverse zoning in resorbed cores, and narrow prisms 1-2 mm long without zoning or evident resorption), Cpx, Opx, and Mag (all <1%; small). Groundmass commonly pilotaxitic intergranular with An 40 Plag. Normal paleomagnetic polarity. Analyses 158, 171, 176, 346, 349, 350, 352; average including dikes, 1011. Maps 2, 3. Dikes: Silica 54-56. Gray to black, generally 2-3 m thick and irregular in trend. Phenocrysts as in basaltic andesite lavas of Tam Mac Rim and Snow Cr. cirque. Analyses 173, 348. Maps 2, 3.

PsBALa9 Basaltic andesite lavas on lower shelf S. of Three Cr. Lk., not mapped separately. Interbedded with dacite lavas of PsDaLa5. Lavas on E. side of shelf: Silica 53-54. Brown to oxidized red, platy. Phenocrysts of Plag (15%; An 70-75, zoning oscillatory but indistinct in most crystals, rim zone An 45; up to 5 mm), Ol (1%; rounded, enclosed in rim of granular Mag; 0.5 mm), Cpx (<1%; small). Normal paleomagnetic polarity. Analysis 1. Lavas on W. side of shelf: Silica 55-56. Gray to brown, platy. Phenocrysts of Plag (1-2%; An 40, zoning indistinct; up to 1.0 mm), Ol and Cpx (both <1%; up to 1.5 mm). Normal paleomagnetic polarity. Analysis 342. Map 3.

PsBALa10 PsBAPc10 Glaciated basaltic andesite lavas and cinder cone on crest of Broken Top E. ridge, 1.2 km S.W. of Tam McArthur Rim. Silica 53-54, high Al. Lavas blocky, gray to red. Phenocrysts of Plag (20-22%; cores of diffuse oscillatory zoning from An 80 to An 85 with rims zoned normal to An 50; some crystals extensively resorbed; up to 4 mm) and Ol (1%; 0.5 mm). Unusual abundance of well-formed volcanic bombs mixed with red cinders of cone. Lavas and cone are overlain and underlain by basaltic andesite lavas from Broken Top. Analyses 124, 355; average 1012. Maps 2, 3, 6.

PsBALa11 PsBAPc11 PsBAIp11 PsBAId11 Orthopyroxene- and olivine-bearing basaltic andesite microporphyries of Broken Top volcano, not separately represented. Silica 54-56. Gray, black, and red vesicular flows, usually 5-10 m thick, from dike, sill, and plug sources in the summit cone and from dikes on the lower slopes. The basaltic andesite lavas of Broken Top contain 25 to 60% phenocrysts, glomerocrysts, and microphenocrysts of Plag, Ol, Opx, Cpx, and Mag, usually in that order of abundance, suspended in a hyaloophitic to intergranular groundmass. Two generations of phenocrysts are commonly represented, often in the same rock. The prominent, and presumably earlier, generation consists of olivine crystals (up to 2 mm; often rounded, embayed, and partly converted to red alteration products) and plagioclase crystals (up to 4 mm; cores as calcic as An 85 but more often An 60-70, surrounded by a broad band of An 50-60 oscillatory zones which grade to a thin rim normally zoned to An 45). Irregular blebs of glass tend to be concentrated in the oscillatory band, but are sometimes distributed uniformly. The second generation consists of stout prisms of fresh orthopyroxene (up to 0.5 mm) and plagioclase (short tablets up to 1 mm long, with oscillatory zoning from An 60 to 45 in some rocks and continuous normal zoning in others). The plagioclase is usually honeycombed with irregular inclusions of glass. The chief variation in mineralogy and texture of Broken Top lavas lies in the relative proportions of these two generations of phenocrysts. Crystals of the first generation predominate in early Broken Top lavas; intermediate stages leading to a complete replacement of the first generation by the second are best represented in later lavas from higher levels in the volcano.

Broken Top dikes and sills vary from 1 to 5 m in thickness and correspond to the lavas in phenocryst composition, texture, and variability. The central plug of Broken Top, however, is approximately 0.3 by 0.6 km in diameter and varies from a fine-grained platy margin to a blocky interior of altered hypidiomorphic-granular micronorite. It is composed of Plag (78-80%; An 55 cores normally zoned to An 30 rims; av. 1-3 mm), Opx (12-14%; 0.5-1 mm), Cpx (5-6%; 0.5-1 mm), Mag (2-3%; up to 0.5 mm), and Ol (<1%; up to 1 mm; often altered to serpentine).

Broken Top basaltic andesite lavas were deposited on a glaciated platform of many separate basaltic andesite volcanoes, are interbedded with small andesitic, dacitic, and rhyodacitic lava flows and ash-flow tuffs, and are overlain by basaltic andesite lavas of the Tumalo Mtn. chain of volcanoes and by rhyodacite pumice and andesite cinders from Pleistocene vents on the N.W. ridge. Broken Top volcano has been extensively glaciated on all but the highest ridge crests. Paleomagnetic polarity was determined in nine separate lava flows representing high, intermediate, and low stratigraphic positions in Broken Top; all were normal. Analyses: (lavas) 106, 107, 108, 109, 110, 113, 114, 116, 118, 122, 156, 161, 195, 199, 203, 274, 360, 361, 363, average 1013; (dikes) 112, 119, 121, 125, 167, average 1014; (plug) 81, 101, 102, average 1015. Maps 1, 2, 3, 4, 5, 6.

PsBALa12 Olivine- and clinopyroxene-bearing basaltic andesite lava west of Ball Butte. Silica 55. Light gray, blocky. Phenocrysts of Plag (10-11%; delicate oscillatory zoning throughout cores of An 75-80, narrow rims zoned An 75-45; up to 1.5 mm), Cpx and Ol (both 2% and up to 0.5 mm). Probably the NW member of a glaciated chain of cones which extends from Tumalo Mtn to Broken Top. Analysis 301. Map 5.

PsBALa13 PsBAPc13 Clinopyroxene- and olivine-bearing basaltic andesite lava and pyroclastic deposits of Ball Butte. Silica 56-57. Lavas red to brownish gray, fine grained, blocky. Abundant microphenocrysts with sparse phenocrysts and glomerocrysts of Plag (12-13%; An 55-60, delicate oscillatory zoning of very limited compositional range; up to 3.0 mm), Cpx and Ol (both 1-2% and up to 1.0 mm). Olivine is embayed and surrounded by granules of Cpx and Mag. Some of the glomerocrysts are associated with an altered amphibole, minute shreds of biotite, and anhedral alkali feldspar. Groundmass intergranular with Plag An 45. Red cinder cone is approximately 200 m high, nearly buried beneath lavas from summit vents, and has been extensively glaciated. Ball Bu. lavas are overlain by basaltic andesite lavas from glaciated center 0.8 km NW (PsBALa 12). Analysis 302. Maps 5, 6.

PsBALa14 Basaltic andesite lavas exposed in ravine north of Soda Creek, W. Sec. 6, not mapped separately. Silica 54-58. Thick units of red flow breccia and gray lava containing phenocrysts of Plag (2-3%; An 70 without zoning, An 45-60 with nor-

mal zoning; both types up to 1 mm), Ol and Cpx (both <1%; small). Underlain by thinner flows of porphyritic basaltic andesite and palagonitic breccia interbeds. Entire sequence rests upon lavas from Todd Lake volcano. Analyses 285, 288, 290. Maps 5, 8.

PsBALa15 PsBAPc15 Clinopyroxene- and olivine-bearing basaltic andesite lavas from glaciated cinder cone remnant, 1.5 km S.E. of Ball Butte. Silica 55-56. Light gray glaciated lavas extend from source cone at 6700' elev., 1.5 km S. to approximately 6700' elev. Phenocrysts and glomerocrysts of Plag (8-12%; cores of An 70-55 with normal and reverse sets of oscillatory zones surrounded by narrow rims zoned normal to An 50; up to 2 mm), Ol (1-3%; up to 0.5 mm), Cpx (1-2%; up to 0.5 mm). Mag in glomerocrysts with Plag and Cpx. Groundmass intergranular, pilotaxitic in part, Plag An 45. Analyses 139, 296, 307; average 1016. Maps 5, 6, 8, 9.

PsBALa16 PsBAPc16 Basaltic andesite lava flow, 0.5 km long, from small glaciated cinder cone north of upper North Fork Tumalo Creek. Silica 55. Lavas gray to black, vesicular; cinders black and red. Sparse phenocrysts of Plag (An 35-40, resorbed; up to 1.0 mm; accompanied by crystals of An 55-60, not resorbed; up to 2 mm), Cpx and Ol (both <1%; up to 0.5 mm) in a fine pilotaxitic intergranular groundmass. Analysis 129. Map 6.

PsBALa17 Basaltic andesite lavas of Happy Valley, not mapped separately. Silica 56-57. Fine grained, platy, black to gray where fresh, tan to yellow where altered. Phenocrysts of Plag (An 55) and Cpx (both <1% and <1 mm). Exposed best in glaciated cliffs and on floor of Happy Valley E. of Map 6. Analysis 128.

PsBALa18 Basaltic andesite lavas of upper North Fork Tumalo Creek, not mapped separately. Silica 53-54. Glaciated flows, gray to black, blocky. Phenocrysts of Plag (4-6%; An 65 cores normal zoned to An 35 rims; up to 4 mm), Cpx (<1%; up to 0.5 mm), and sparse Mag. Small outcrop in center of Happy Valley contains partly fused pumiceous xenoliths. Analysis 135. Map 6 and Quad. E.

PsBALa19 Olivine-bearing basaltic andesite microporphyry in canyon between north and middle forks of Tumalo Creek. Silica 54-55. Black to gray scoriaceous flows, generally less than 10 m thick. Phenocrysts of Plag (40-45%; An 50-55, indistinct zoning; clouded with minute inclusions of mafic silicates and blebs of dark glass; up to 3 mm), Ol (5%; up to 1 mm), and Opx (<1%; up to 0.5 mm). Groundmass hyaloophitic with An 35 Plag. Interbeds of palagonitic breccia are common. Overlain by rhyodacitic lava of upper N. Fork Tumalo Cr. Analysis 306. Map 6 and Quad. E.

PsBALa20 PsBAPc20 Glaciated basaltic andesite lavas (not mapped separately) and remnant of glaciated basaltic andesite cone in vicinity of Bare Lake. Silica 57. Holocrystalline lavas are gray and platy to blocky, but black and less platy with increasing glass content. Red, scoriaceous flow crust near vents. Phenocrysts of Plag (<2%; An 60-70; up to 1 mm), Cpx (<1%; 0.4 mm), and traces of Mag. Some flows are nonporphyritic and some contain as much as 1% xenoliths of fine and coarse two-pyroxene dacite lavas and plug rocks. Beds of red scoriaceous agglomerate are exposed in cliffs 0.3 km W. of Bare Lk. Rests on rhyodacite lavas S. of Todd Lk. and is overlain by dacite lavas of Todd Lk. volcano. Normal paleomagnetic polarity. Analyses 8, 11, 12, 15, 16; average, 1024. Map 8.

PsBAPc21 PsBAPc22 Glaciated remnants of basaltic andesite cinder cones 1.0 km S. of Todd Lake and 0.7 km W. of Dutchman Flat. Silica 56-57. Red spatter and scoriaceous oxidized lava. Cone near Todd Lk. contains less than 1% microphenocrysts of Plag and two pyroxenes. Cone near Dutchman Flat contains only sparse microphenocrysts of Plag. Analyses 43, 46. Map 8.

PsBALa22 Clinopyroxene-bearing basaltic andesite lavas 1 km W.N.W. of Tum Lake. Silica 55-56. Gray to black, blocky. Phenocrysts of Plag (30%; An 75 cores, normal zoned to An 45 rims; up to 3 mm), Cpx (2-3%; euhedral; up to 2 mm), Ol (<1%; rounded; up to 1 mm), Mag (<1%; up to 0.5 mm). Sparse glomerocrysts reach 4 mm in diameter. Groundmass intergranular with An 40 Plag. Glaciated, overlain by lavas from cone N.W. of Tumalo Mtn. Analysis 141. Map 9.

PsBALa24 PsBAPc24 PsBAPt24 PsBAIp24 PsBAId24 Glomeroporphyritic olivine- and clinopyroxene-bearing basaltic andesite lavas, intrusive rocks, and tuff cones associated with Tumalo Mountain and three cones N.W. of Tumalo Mountain. Silica 55-56. Surfaces of nonglaciated lavas above 7000' elev. on W. flank of Tumalo Mtn. are black and scoriaceous. Elsewhere, the glaciated interior of lava flows is gray and blocky. Phenocrysts and microphenocrysts of Plag (23-26%; An 60-75, commonly zoned in two or more sets of oscillatory normal zones surrounded by a reverse zone which passes into a thin rim zoned normally to An 45; up to 2 mm), Cpx (5%; up to 1 mm), Ol (1%; 0.5 mm), and rare Opx. Glomerocrysts of Plag, Cpx, and Ol commonly reach 6 mm in diameter and make up 3-7% of the rock. Tumalo summit cone is composed of red and black cinders, bombs, and spatter with glomerocrysts of Plag, Cpx, and Ol. Fragments of white fine-grained rhyodacite up to 3 cm are included within the cinders. Glaciated eastern face of summit cone contains a small central plug with associated radial dikes and remnants of an early-formed palagonitic tuff cone. Of the cones N.W. of Tumalo Mtn., the southernmost was glaciated up to approximately 6900' elev. but still retains a breached summit crater. The middle cone was glaciated over all but the summit area; no crater survived. The northernmost cone was extensively glaciated and stands as an irregular resistant butte of thin lava flows and interbedded scoria. Normal paleomagnetic polarity. Analyses 42, 48, 74, 140, 143, 144, 145, 308, 309, 310, 311, 312, 313, 314, 315, 319, 320; average Tumalo Mtn., 1017. Maps 8, 9, and Quads E., S.E., S.

PsBALa25 Glaciated basaltic andesite lavas exposed in vicinity of Tum Lake. Silica 56. Gray, fine grained, blocky. Phenocrysts and microphenocrysts of Plag (0.5-1.0%; An 70 cores, An 45 rims; up to 1 mm; anhedral with irregular margins gradational to groundmass), Opx, Cpx, Mag (all <0.1% and less than 0.1 mm). Groundmass intergranular with An 45 Plag. Overlies remnant of palagonitic tuff cone. Analysis 142. Map 9.

Units of Pleistocene Andesite

PsAnLa1 Glaciated two-pyroxene andesite lavas from South Sister volcano, not mapped separately. Silica 59-63. Units exposed in Broken Top quadrangle possess gray to black, platy, flow-banded interiors with blocky vitrophyric margins. Phenocrysts of Plag (5-20%, most units contain 11-13%; cores An 50 normally zoned to An 35 in some units, reverse zoned from An 50 to 60 and surrounded by a narrow rim zoned to An 35 in other units; up to 3 mm). Pyroxenes total 2-4%. Cpx exceeds Opx by a factor of 1 to 4. Cpx is surrounded by narrow rims of granular pyroxene. Mag from 0.8 to 1.5%, up to 1 mm. Sparse crystals of apatite with dark pleochroic inclusions are as long as 0.5 mm in some units. In Broken Top quadrangle, these andesites overlie rhyodacites E. of Chambers Lk and basaltic andesites near Golden and Green Lks. Analyses 191, 192, 204, 250, 362, 365, 456, 458; average 1018. Map 1 and Quads. W., N.W., N.

PsAnPc2 PsAnId2 Glaciated remnant of andesite cinder cone and included dikes at 7000' to 7700' elev. on N.W. ridge of Broken Top. Silica 61. Red to black cinders, coarse spatter, and thin flowrock cut by several short dikes less than 1 m wide. At high levels in cone deposits, cinders are interbedded with lumps of white rhyodacite pumice of ridge-crest unit PsRdPc4. Cinder cone overlies N.W. margin of basaltic andesite lava from Broken Top. Analysis 196. Map 1.

PsAnLa3 Glaciated andesite lava on shelf at 7000' elev., head of Snow Creek cirque. Silica 62-63. Black vitrophyre at margins, gray platy interior. Phenocrysts and glomerocrysts of Plag (6-7%; An 45, some much-resorbed cores of An 55 contain patchy zoning; up to 1 mm), Cpx, Opx, and Mag (all <1%; 0.5 mm). Sparse olivine crystals occur separate from glomerocrysts and are rounded and embayed. Analysis 351. Maps 2, 3.

PsAnId4 Three east-west andesite dikes 1.3 km S. of Rim Lake. Silica 60-61. Gray to white, blocky, 3-4 m wide. Microphenocrysts and small glomerocrysts of Plag (2-3%; An 50-55; up to 1 mm), Cpx and Mag (both <1%; up to 0.5 mm). Mineralogy, texture, and composition are distinct from andesite dike and lavas of units PsAnLa5 and PsAnLa6, only 0.2 to 0.5 km S. Analysis 170. Map 2.

PsAnLa5 PsAnPc5 Glaciated clinopyroxene-bearing andesite lavas at 7400' elev., 1.4 km S. of Rim Lake and probable andesitic source cone at 7480' elev., on S.W. edge of Snow Creek cirque. Silica 60-61. Lava mottled and streaked in black, gray, and red. Red andesitic scoria incorporated into base of flows; small xenoliths of basaltic andesite common throughout. Phenocrysts of Plag (4-5%; An 47; up to 1 mm), Cpx (1-2%; up to 0.5 mm), Opx and Mag (both <1%; <0.5 mm). Sparse crystals of apatite and small xenocrysts of resorbed olivine. Groundmass of light-colored, coarser, pilotaxitic streaks in dark-colored, finer, intergranular matrix. Cpx within light-colored streaks is surrounded by granular rims. Cone is composed of black cinders and brown pumice. Analyses 169 (lava), 358 (cone). Map 2.

PsAnLa6 PsAnId6 Glaciated clinopyroxene-bearing andesite lavas, not mapped separately and S.W.-N.E. dike, 7600 to 8000' elev. on S.W. side of Snow Creek cirque. Silica 61-63. Phenocrysts of Plag (7-8%; oscillatory normal zones over range of An 40-45; up to 2.5 mm), Cpx (1%; 0.5 mm), Opx and Mag (both <1%; <0.5 mm). Approximately 10% of Plag phenocrysts are extensively resorbed, but are of same composition and zonation pattern. At lower E. end of outcrop is a flow unit which is slightly more mafic and contains only 1-2% Plag phenocrysts with minor pyroxenes and Mag. Mineralogical and chemical compositions of the dike are similar to the lowermost flow and it is probably a feeder. Interbedded with basaltic andesite lavas from Broken Top. Analyses 165, 356 (upper flows), 160 (lower flow), 159 (dike); average lower flow and dike, 1019; average upper flows, 1020. Map 2.

PsAnLa7 Glaciated andesite lavas west of Corral Lake not mapped separately. Silica 62-63. Gray to pink, close-set platy joints. Microphenocrysts, phenocrysts, and glomerocrysts of Plag (5-7%; An 45-50 with poorly developed normal zoning; up to 1 mm), Cpx, Opx, and Mag (all <1%; very small). Cpx is surrounded by jackets of granular pyroxene. Groundmass hyalopilitic to intergranular. Analyses 27, 275; average 1021. Map 4.

PsAnLa8 Glaciated clinopyroxene-bearing andesite lavas at head of ravine, 6400' elev., W. Sec. 6, N. of Soda Creek, not mapped separately. Silica 62-63. Flows gray to black, platy, up to 20 m thick. Phenocrysts and glomerocrysts of Plag (5-6%; An 45-50; up to 2 mm), Cpx (1-2%; 0.5 mm), Opx and Mag (both <1%; <0.5 mm). Analyses 286, 287; average 1023. Map 5.

PsAnLa9 Glaciated andesite lava at 5600' elev. on lower Fall Creek. Silica 59-60. Gray to tan, platy. Phenocrysts of Plag (11-12%; cores oscillatory zoned An 85-90 surrounded by broad rim zone An 40-45; up to 4 mm), Cpx (<1%; granular Cpx rims; up to 0.5 mm), Ol (<1%; altered; 0.5 mm), and Mag (<1%; up to 0.2 mm). Groundmass Plag An 40. Analysis 276. Map 7.

Units of Pleistocene Dacite

PsDaLa1 Clinopyroxene-bearing dacite lava interbedded with basaltic andesite flows at 7600' elev. in cliffs 1.5 km S. of Golden Lake. Silica 64-65. Platy, dark gray to brown. Microphenocrysts of Plag (3%; An 45-50 with indistinct zoning), Cpx (1-2%; 0.5 mm), and Mag (<1%; up to 0.2 mm). Overlain by lavas from Broken Top; rests on lavas similar to Broken Top lavas but of uncertain affinity. Analysis 200. Maps 1, 2.

PsDaLa2 Glaciated dacite lava E. of Squaw Creek, 1.0 km E. of Park Meadow. Silica 64. Platy, light gray to pink. Phenocrysts of Plag (6-7%; An 35 in two broad normal zones of less than 5 An range; up to 3 mm), Cpx (0.4-0.5%; up to 0.5 mm; mostly converted to granular pyroxene), Opx (0.5-0.6%; up to 1 mm; no granular rims), and Mag (0.7-0.8%; up to 0.5 mm). Opx and Cpx commonly form parallel crystal aggregates. Sparse but unusually large apatite crystals (up to 0.25 mm). Analysis 367. Map 2.

PsDaLa3 East-west dacite dike at 7800' elev., 1.8 km S. of Rim Lake. Silica 66-67. Gray interior, black glassy margins, 0.5-1 m wide. Phenocrysts of Plag (5-7%; An 35-40, normal zoning over small compositional range; up to 1 mm), Opx, Cpx, Mag (all <1%; <0.5 mm). Part of a multiple dike set dominated by basaltic andesite

(PsBAId11). Analysis 168. Map 2.

PsDaPi4 Dacite welded tuff of Snow Creek cirque. Silica 66-67. Small outcrop exposed on W. side of Snow Cr. at 7360' elev. Yellow to light brown, glassy, poorly welded eutaxitic matrix containing fragments of pink rhyodacite and gray andesite, partly collapsed black pumice lumps, and 1-2% of small Plag phenocrysts (An 45-50, normal oscillatory zones). Other phenocrysts include Cpx and Mag, both less than 1%. Much of the unit has been removed by erosion; maximum exposed thickness is only 8 m. Overlain by andesite lavas of PsAnLa5. Analysis 354. Map 2.

PsDaLa5 Glaciated dacite lavas S.W. of Three Creek Lake and W. of Little Three Creek Lake, not mapped separately. Silica 64-68. Gray to brown, platy. Phenocrysts of Plag (9-11%; An 25-30, patchy zoning in cores surrounded by oscillatory normal zones; up to 4 mm); Opx, Cpx, and Mag all <1%; 0.5 mm). Lavas from approximately 6800 to 7000' elev., 0.7 km S.W. of 3 Cr. Lk. are low-silica dacites in which phenocrysts of Plag (An 40-50), 2 pyroxenes, and Mag are all <1%. Unit includes some of the oldest lavas exposed in the Tam Mac Rim area. Normal paleomagnetic polarity. Analyses of high-silica dacites, 175, 341, 347; average 1025. Analyses of low-silica dacites, 162, 174, 343; average 1026. Map 3 and Quad. E.

PsDaId6 East-west dacite dike at base of main protrusion of Tam McArthur Rim, 1.0 km W.S.W. of Three Creek Lake. Silica 63-64. Gray interior, black glassy flow-banded margins, dike 2-3 m wide. Phenocrysts of Plag (An 50) and Cpx are sparse and very small. Chemically and mineralogically similar to higher-elevation, low-silica dacite lavas of PsDaLa5, 0.5 km S.W. Analysis 177. Map 3.

PsDaLa7 Glaciated clinopyroxene-bearing dacite lava between Goose Creek and Fall Creek. Silica 64-65. Black, glassy, columnar-jointed margins and gray to pink, holocrystalline, platy-jointed interior. Phenocrysts and glomerocrysts of Plag (7-9%; An 40-45, normal zonation in resorbed cores surrounded by reverse oscillatory zones and a thin normal rim; up to 3 mm), Cpx (0.5-1.5%; <0.5 mm; surrounded by jackets of granular pyroxene, Opx and Mag microphenocrysts both <1%. Sparse prisms of apatite up to 0.3 mm long. Overlies andesite W. of Corral Lk. and is overlain by Goose Cr. chain of Holocene domes. Normal paleomagnetic polarity. Probably from a vent near S. Sister. Analyses 29, 263, 268; average 1027. Maps 4, 7, and Quad. W.

PsDaLa8 Glaciated clinopyroxene-bearing dacite from buried vent above 7800' elev. on S.W. side of Broken Top. Silica 63-64. Flow exposed on crest of Broken Top S.W. ridge down to 6200' elev. Gray, platy, and holocrystalline interior with black, blocky, and glassy margins. Microphenocrysts, phenocrysts, and glomerocrysts of Plag (5-6%; An 40-50; up to 1.5 mm), Cpx (1-2%; surrounded by jackets of granular Cpx; 0.5 mm), Mag (<1%; 0.5 mm). Apatite prisms up to 0.5 mm long are commonly enclosed within phenocrysts and occur free in the goundmass. Groundmass hyalopilitic to intergranular with Plag An 35. Analyses 115, 273; average 1022. Maps 4, 5.

PsDaPi9 Dacite welded tuff of Broken Top summit cone. Silica 64-65. Interbedded with basaltic andesite lavas at 8600' elev. in the W. wall of Crook Glacier cirque. Outcrop approximately 8-9 m thick and 0.2 km long. White, clay-rich, poorly welded lapilli tuff in the basal three meters is composed of dacite pumice, devitrified glass shards, and particles of black and red basaltic andesite scoria. It is overlain by a zone of orange, very poorly welded, hydrated dacite pumice which contains increasing amounts of large black and glassy dacite bombs toward the top. The orange zone grades upward to 1-2 meter gray-to-black band of pumiceous lapilli and ash which contains abundant black glassy bombs. In places, a thin orange layer can be seen at the top of the deposit. Approximately 5% of plagioclase phenocrysts with minor orthopyroxene and magnetite occur in the pumice and in the glassy bombs. This unit was deposited from a small ash flow which was produced at a near-summit vent and probably moved only a short distance down the S.W. flank of Broken Top. Analysis 103. Map 5.

PsDaId10 East-west dacite dike at 6060' elev., in ravine, W. Sec 6, N. of Soda Creek. Silica 64. Gray interior, black glassy margins, 1 m wide. Phenocrysts of Plag (1-2%; An 40 normally zoned to thin rims of An 35; up to 1 mm) with Cpx, Opx, and

Mag (all <1%; up to 0.5 mm). Cuts basaltic andesite lavas and breccias of PsBALa14. Analysis 289. Map 5.

PsDaLa11 PsDaIp11 Orthopyroxene- and clinopyroxene-bearing dacite lavas, interbedded ejecta, and central plug of Todd Lake volcano. Silica 63-66. Brown to gray platy lavas with yellow to orange scoriaceous interbeds and flow tops. Pyroclastic breccias and palagonitic ejecta near source vent. Microphenocrysts, phenocrysts, and glomerocrysts of Plag (18-23%; An 40-55). Large crystals up to 4 mm are resorbed and reverse zoned from An 40 core through oscillatory zone sets to An 55. Thin rim zones are normal oscillatory to An 45. Smaller crystals up to 1 mm are zoned normal An 50-45 and are not resorbed. Also phenocrysts of Mag (2-3%; up to 0.6 mm), Cpx (1-2%; 0.5 mm), and Opx (0.5-1.5%; 0.5 mm). Stout prisms of apatite are enclosed within all phenocrystic phases. Lower level flows (especially in Soda Cr. valley) contain oxidized hornblende; higher level flows (especially near summit of Todd Lk. volcano) contain olivine within glomerocrysts. Lavas and ejecta surround a central conduit plug, 0.4 km in diameter, exposed in S. wall of Soda Cr. canyon, 1.5 km N.W. of Todd Lk. Characterized by platy margins and a blocky interior which is gray where fresh and yellow where deuteric alteration is advanced. Except for coarser groundmass, mineralogy and texture of the plug are similar to associated lavas. Todd Lk. volcano overlies basaltic andesites near Bare Lk. and rhyodacites S. and E. of Todd Lk. Overlain by basaltic andesites of PsBALa14, 15. Paleomagnetic polarity of 7 flows on W. side of volcano all normal. Analyses 10, 277, 278, 279, 280, 281, 282, 283, 291, 292, 293, 294; average 1028. Maps 5, 7, 8.

Units of Pleistocene Rhyodacite

PsRdLa1 Glaciated rhyodacite dome and flows E. of Chambers Lk. and between two branches of South Fork Squaw Creek. Silica 73. Marginal rocks are black, brown, and red, flow banded, glassy, and spherulitic in part with phenocrysts at center of spherules. Interior of flow is gray to pink, very fine grained, contains well developed platy jointing, and grades into a gray-to-white, coarser-grained, porous core. Plag phenocrysts make up less than 0.1% and seldom exceed 1 mm. They are rounded, resorbed, and embayed. Secondary silica is common in cavities. Probable source vent underlies thickest and highest part of mass just E. of Chambers Lake. Overlain by andesite lava from S. Sister. Analyses 206, 207, 208; average 1027. Map 1 and Quads. W., N.W., N.

PsRdLa2 Glaciated rhyodacite lava on N.W. bank of West Fork Park Creek, 2.5 km W. of Park Meadow. Silica 72-73. Gray to pink, vitrophyric to holocrystalline with contorted spherulitic flow bands. Phenocrysts of Plag (10-11%; An 35-40 in broad, diffuse sets of normal oscillatory zones; up to 2 mm), Opx and Mag (both <1%; 0.5 mm). Sparse crystals of fresh Hb up to 0.1 mm in length and minute crystals of zircon also occur. Probably the exposed flank of a volcanic dome, elsewhere overlain by andesite lavas from S. Sister. Analysis 209. Map 1.

PsRdLa3 Glaciated rhyodacite lava W. of Green Lake. Silica 71-72. Pink-to-gray, platy, holocrystalline interior with black, glassy, blocky margins. Occasional lithophysae and spherulites, flow banded throughout. Phenocrysts of Plag (9-10%; cores of diffuse oscillatory zones reverse from An 25 to 35, surrounded by a broad rim zoned normal An 35 to 25). Some Plag crystals are deeply embayed while others of the same composition are sharply euhedral; whole crystals up to 3 mm, many crystals broken. Opx and Mag (both <1%, 0.5 mm). Rare Hb and zircon. Probably the exhumed east margin of a glaciated volcanic dome which was buried during growth of S. Sister volcano. Analysis 25. Map 1.

PsRdIp4 PsRdPc4 Glaciated rhyodacite volcanic dome and pumice deposits on Broken Top N.W. ridge. Silica 68-69. Dome, at 7150' elev., has been reduced by glaciation to level of feeding conduit, 0.05 km in diameter. Conduit filled with dacite, black and glassy along margins with xenoliths of intermediate and mafic rocks, passing into a gray hypocrystalline interior with minute spherulites. Phenocrysts of Plag (6%; An 35; up to 1 mm), Cpx, Opx, and Mag (all <1%; 0.5 mm). Source of rhyodacite pumice on broad crest of Broken Top ridge from 7720 to 7960' elev., 1 km S.E. Deposits are crudely bedded, up to 3 m in total thickness, and contain pumice bomb fragments up to 0.5 m in

diameter. Protected from glaciation by high-standing position. Overlies Broken Top basaltic andesite lava and is mixed with andesitic cinders of cone unit PsAnPc2. Analyses 194, 197; average 1030. Map 1.

PsRdLa5 Glaciated rhyodacite lava S. of Tam Lake and E. of Upper Squaw Creek. Silica 70-71. Platy, light gray to tan. Phenocrysts of Plag (3%; An 30-35; up to 1 mm), Opx and Mag (both <1%; 0.5 mm). Overlain by andesite lava of PsAnLa5, 1.2 km S. of Tam Lk. Analysis 201. Map 2.

PsRdLa6
PsRdPc6
PsRdPf6
PsRdId6 Glaciated rhyodacite lavas with associated coarse and fine pumice deposits and feeder dikes on summit of Tam McArthur Rim, S.W. of Three Creek Lake. Silica 68-69. Glassy lavas are red, black, and flow banded; holocrystalline lavas are white. Phenocrysts of Plag (<1%; An 40-45; rounded and resorbed with patchy zoning in cores; up to 1 mm), Opx and Mag (both <1%; 0.4 mm). Abundant cristobalite in vesicles. E-W feeder dikes are exposed in cliffs of Tam Mac. Rim. They are 2-7 m wide, white and vesicular in the center with black glassy margins, and can be traced directly into flowrocks. Lavas occur in two separate flows. Eastern flow is smaller and is overlain by a much larger western flow which also crops out on the E. side of Snow Cr. valley, 1.5-2.0 km to the W. and N.W. Both lavas rest on deposits of near-vent pumice (PsRdPc6), up to 10 m thick, containing yellow, brown, and black bread-crust bombs. Pumiceous spatter is welded in part. Rhyodacite lavas and pumice are underlain and overlain by basaltic andesite lavas from Broken Top. A thin layer of pumiceous rhyodacite ash (PsRdPf6) is interbedded with Broken Top lavas near the center of Sec. 21. Normal paleomagnetic polarity. Analyses 154, 155, 157; average 1031. Map 3.

PsRdLa7 Glaciated rhyodacite lava of Tam McArthur Rim S. of Three Creek Lake. Silica 68-69. Lavas black and glassy to holocrystalline pink, platy, and lithophysal. Remnant of associated pumice cone stands at N.E. edge of flow, 0.8 km E. of E. boundary of Map 3. Phenocryst mineralogy and texture as well as bulk rock composition is nearly identical to rhyodacite 1 km to the W (PsRdLa6). However, Broken Top lavas that underlie RsRdLa6 overlie this unit. Analysis 151. Map 3 and Quad. E.

PsRdId8 East-west rhyodacite dike, 0.15 km long, at 6760' elev., 0.4 km S.W. of Three Creek Lake. Silica 68-69. White, vesicular, blocky; 2-4 m wide. Nearly identical in mineralogy, texture, and bulk-rock composition to dike feeders of Tam Mac Rim rhyodacite (PsRdId6), 0.4 km to the S.W., but direct connection to flowrocks has been removed by glacial erosion. Normal paleomagnetic polarity. Analysis 172. Map 3.

PsRdLa9 Glaciated rhyodacite lava between Holocene rhyodacite flows of Newberry and Goose Creek Chain of Domes. Silica 72. White to gray, lithoidal to glassy, flow banded. Platy interior. Phenocrysts of Plag (3%; An 35; rounded by marginal resorption; up to 1 mm), Opx and Mag (both <1%; 0.3 mm). Abundant crystallites in glass. One of many outcrops of rhyodacite on S. slopes of S. Sister. Analysis 270. Map 4 and Quad. W.

PsRdLa10 Glaciated orthopyroxene-bearing rhyodacite lava of Devils Hill. Silica 73-74. Gray to white, glassy to holocrystalline, flow banded, spherulitic. Pumiceous crust preserved near summit. Phenocrysts of Plag (7-9%; An 35; up to 1 mm), Opx (1-2%; up to 0.4 mm), and Mag (0.5%; up to 0.2 mm). Remnant of large volcanic dome. Normal paleomagnetic polarity. Analyses 449, 529; average, 1032. Maps 4, 7, and Quad. W.

PsRdPt11 Glaciated remnant of an orthopyroxene-bearing rhyodacite tuff cone on upper North Fork Tumalo Creek. Silica 68-69. Beds in tuff cone are 0.01 to 1.0 m thick, composed of white-to-yellow devitrified pumice with obsidian and rock fragments. Dip of beds in well-exposed N. part of cone is approximately 30°W. Near the top of the tuff cone sequence and best exposed on the S.W. flank, are several layers of silicic spatter 0.2 to 3 m thick which contain collapsed pumice bombs, clots of dense rhyodacite, obsidian, and accidental fragments of other volcanic rocks in a welded matrix. Phenocrysts of Plag (10-15%; An 35-40; small angular fragments) and Opx (<1%; small) occur in a largely devitrified, flow-banded glassy matrix. Within an area of approximately 0.25 km^2 S.W. of the tuff cone, bedded tuffs, welded spatter, and coarse pyroclastic breccia

have all been hydrothermally altered to clay and opaline silica. The deposits are overlain by lavas from Broken Top, Ball Butte, and a small cinder cone along the tuff cone N.W. margin. Analyses 126, 305; average, 1033. Map 6.

PsRdLal2 Glaciated aphyric rhyodacite lavas of upper North Fork Tumalo Creek. Silica 69. Black, dull-luster obsidian crusts with gray, lithoidal, platy interior. Spherulitic in part. Rare microphenocrysts of Plag in a trachytic groundmass of An 20-25 microlites. Source dike exposed in S. wall of N. Fork Tumalo Cr. at 7100' elev. Overlain by lavas from Ball Butte. Normal paleomagnetic polarity. Analyses 134, 136, 137; average 1034. Map 6.

PsRdLal3 Glaciated orthopyroxene-bearing rhyodacite lavas E. of Todd Lake, not mapped separately. Silica 68-69. Gray to pink where platy and holocrystalline, black where glassy and columnar jointed. Phenocrysts of Plag (2-7%; reverse zoned cores An 35-45, surrounded by a broad, diffuse rim zoned normal An 45-35; up to 3 mm with rounded and embayed margins), Mag (1-2%; up to 0.4 mm), Opx (1%; 0.6 mm), and Cpx (<1%; in resorbed laths up to 0.6 mm long). Several distinct flow units from overlapping volcanic domes. Overlain by basaltic andesite lavas of Bare Lk. volcano, dacite lavas of Todd Lk. volcano, and basaltic andesite lavas from cones N.W. of Tumalo Mtn. Normal paleomagnetic polarity. Analyses 4, 5, 41, 297, 298; average 1035. Maps 8, 9.

REFERENCES

Armstrong, R. L., Taylor, E. M., Hales, P. O., and Parker, D. J., 1975, K-Ar dates for volcanic rocks, central Cascade Range of Oregon: Isochron/West, No. 13, p. 5-10.

Crowe, B. and Nolf, B., 1977, Composite cone growth modeled after Broken Top, a dissected High Cascade volcano: Geol. Soc. Am. Abs. with Programs, v. 9, p. 940-941.

Greene, R. C., 1968, Petrography and petrology of volcanic rocks in the Mount Jefferson area, High Cascade Range, Oregon: U.S. Geol. Survey Bull. 1251-G, 48 p.

Mackenzie, D. E. and Chappell, B. W., 1972, Shoshonitic and calc-alkaline lavas from the Highlands of Papua New Guinea: Cont. Min. Petrol., v. 35, p. 50-62.

Nolf, B., 1966, Broken Top breaks: flood released by erosion of glacial moraine: ORE-BIN, v. 28, p. 182-188.

Peck, D. L., Griggs, A. B., Schlicker, H. G., Wells, F. G., and Dole, H. M., 1964, Geology of the central and northern parts of the Western Cascade Range in Oregon: U.S. Geol. Survey Prof. Paper 449, 56 p.

Peterson, N. V., Groh, E. A., Taylor, E. M., and Stensland, D. E., 1976, Geology and mineral resources of Deschutes County, Oregon: Ore. Dept. Geol. Min. Ind., Bull. 89, p. 1-66.

Rubin, M. and Alexander, C., 1960, U.S. Geological Survey radiocarbon dates V: Am. Jour. Sci., Radiocarbon Suppl., v. 2, p. 129-285.

Scott, W. E., 1977, Quaternary glaciation and volcanism, Metolius River area, Oregon: Geol. Soc. Am. Bull., v. 88, p. 113-124.

Shelley, D., 1975, Manual of optical mineralogy; Elsevier, Amsterdam, 239 p.

Tobi, A. C., 1963, Plagioclase determination with the aid of the extinction angles in sections normal to (010): Am. Jour. Sci., v. 261, p. 157-167.

Taylor, E. M., 1973, Geology of the Deschutes Basin: in Geologic field trips in Northern Oregon and Southern Washington: Ore. Dept. Geol. Min. Ind., Bull. 77, p. 28-32.

Taylor, S. R., 1969, Trace element chemistry of andesites and associated calc-alkaline rocks: Ore. Dept. Geol. Min. Ind. Bull. 65, p. 43-64.

Von Burri, C., Parker, R. L., and Wenk, E., 1969, Die optische orientierung der plagioclase; Birkhauser Verlag, Basel, 334 p.

Williams, H., 1942, The geology of Crater Lake National Park, Oregon: Carnegie Inst. Wash., Pub. 540, 162 p.

_____, 1944, Volcanoes of the Three Sisters region, Oregon Cascades: Univ. Calif. Pub., Dept. Geol. Sci. Bull., v. 27, p. 37-84.

_____, 1957, A geologic map of the Bend quadrangle, Oregon and a reconnaissance geologic map of the central portion of the High Cascade Mountains: Ore. Dept. Geol. and Min. Ind., map with text.

Wise, W. S., 1969, Geology and petrology of the Mt. Hood area: a study of High Cascade volcanism: Geol. Soc. Am. Bull., v. 80, p. 969-1006.

APPENDIX 1

Chemical Analyses of Rocks from S.W. Broken Top Quadrangle

	1	2	4	5	7	8	10	11
SiO2	53.6	54.5	68.6	67.7	51.1	56.9	63.5	57.2
Al2O3	19.8	17.1	15.5	15.2	17.1	16.8	16.1	16.3
FeO	8.0	8.8	3.7	4.3	8.8	8.9	6.2	9.1
CaO	8.0	9.4	2.2	2.1	9.1	7.3	4.6	7.1
MgO	4.0	4.3	0.7	0.6	8.3	3.9	2.1	3.5
K2O	0.80	0.60	2.40	2.20	0.60	0.90	2.15	1.00
Na2O	4.5	4.2	5.6	6.2	3.4	4.2	4.4	4.2
TiO2	1.15	1.10	0.65	0.65	1.05	1.20	1.05	1.50
Total	99.85	100.00	99.35	99.15	99.45	100.00	100.10	99.90

	12	15	16	17	20	21	22	23
SiO2	57.1	57.0	56.7	55.7	49.2	51.8	51.2	49.1
Al2O3	16.4	16.7	15.8	18.6	17.4	17.6	17.8	16.7
FeO	8.2	8.4	8.4	6.8	9.5	8.5	8.3	9.0
CaO	8.3	7.4	5.8	8.5	8.7	9.7	8.4	8.9
MgO	4.1	3.5	2.7	5.1	8.8	7.3	8.8	8.7
K2O	0.90	1.25	1.40	0.80	0.60	0.65	0.85	0.55
Na2O	3.9	4.2	4.8	3.2	3.9	3.1	3.1	4.3
TiO2	1.10	1.25	1.50	0.95	1.00	1.00	1.20	1.00
Total	100.00	99.70	99.10	99.65	99.10	99.65	99.65	98.25

	24	25	26	27	28	29	30	41
SiO2	51.5	71.5	72.0	62.9	72.3	64.4	51.2	69.3
Al2O3	16.6	15.5	15.0	16.3	14.9	16.3	17.1	16.3
FeO	9.1	2.4	2.4	7.0	2.6	5.6	9.4	3.5
CaO	8.7	2.1	2.1	4.5	2.1	3.8	8.0	1.9
MgO	9.7	0.4	0.5	1.2	0.4	1.5	8.8	0.5
K2O	0.60	2.90	3.10	1.55	3.10	2.25	0.65	2.45
Na2O	2.8	4.6	4.4	4.7	4.4	5.5	2.8	5.1
TiO2	1.00	0.30	0.30	1.50	0.35	1.00	1.20	0.40
Total	100.00	99.70	99.80	99.65	100.15	100.35	99.15	99.45

	42	43	44	45	46	47	48	74
SiO2	55.5	56.8	54.3	54.3	56.8	54.2	55.5	55.4
Al2O3	17.6	16.7	16.9	17.8	17.0	17.9	17.7	17.0
FeO	7.8	8.5	9.6	9.1	9.1	8.3	8.0	7.9
CaO	8.3	7.4	8.3	8.0	6.6	8.0	9.4	10.1
MgO	5.3	4.1	4.8	4.6	3.5	6.3	3.4	3.5
K2O	0.85	1.00	0.70	0.80	1.00	1.00	1.10	1.10
Na2O	3.6	3.9	3.7	4.0	4.4	3.8	4.0	4.7
TiO2	1.00	1.30	1.45	1.30	1.45	1.10	1.05	1.05
Total	99.95	99.70	99.75	99.90	99.85	100.60	100.15	100.75

	81	101	102	103	106	107	108	109
SiO2	55.5	54.3	54.5	64.7	54.8	54.4	54.0	54.6
Al2O3	18.3	18.9	18.2	15.8	18.2	18.7	18.2	17.9
FeO	7.3	7.5	7.9	5.3	7.5	7.7	7.8	7.6
CaO	8.1	7.7	7.5	3.4	8.4	8.2	7.9	8.0
MgO	5.5	5.2	4.8	2.4	4.8	4.6	6.1	5.2
K2O	0.75	0.80	0.95	2.10	0.70	0.60	0.65	0.70
Na2O	3.9	3.9	3.9	4.5	3.7	3.9	3.7	3.7
TiO2	0.80	0.90	1.05	0.95	0.95	0.90	0.95	0.90
Total	100.15	99.20	98.80	99.15	99.05	99.00	99.30	98.60

	110	111	112	113	114	115	116	117
SiO2	55.2	52.0	54.4	55.6	54.0	62.9	55.5	53.8
Al2O3	18.2	16.6	19.7	19.1	18.7	15.2	19.1	17.8
FeO	7.0	8.9	7.2	7.6	7.6	6.7	7.7	9.7
CaO	7.7	7.8	8.0	7.3	7.8	3.6	7.0	7.3
MgO	5.0	6.3	4.7	4.3	6.1	1.6	4.3	4.8
K2O	0.90	1.15	0.65	0.95	0.65	2.05	1.00	0.60
Na2O	3.8	3.7	4.0	4.2	3.8	5.7	4.3	4.4
TiO2	0.95	1.40	0.85	1.00	0.80	1.25	1.05	1.35
Total	98.75	97.85	99.50	100.05	99.45	99.00	99.95	99.75

	118	119	121	122	124	125	126	128
SiO2	55.4	53.2	54.1	54.4	53.7	53.8	69.3	56.2
Al2O3	18.0	19.3	19.8	18.7	20.0	19.5	15.3	17.1
FeO	7.2	7.8	7.2	7.4	7.7	7.6	4.3	10.1
CaO	8.0	8.0	7.9	7.9	7.8	7.8	1.9	5.9
MgO	5.2	5.0	5.1	5.8	4.1	5.1	0.4	3.2
K2O	0.75	0.75	0.65	0.85	0.85	0.70	2.10	1.20
Na2O	4.3	4.2	3.8	4.0	4.3	4.9	5.5	4.9
TiO2	0.85	1.05	0.75	0.95	1.00	0.90	0.75	1.85
Total	99.70	99.30	99.30	100.00	99.45	100.30	99.55	100.45

	129	134	135	136	137	138	139	140
SiO2	55.0	69.0	53.7	68.9	69.1	55.0	54.8	54.8
Al2O3	17.7	14.6	18.2	15.1	14.7	18.2	19.2	17.9
FeO	10.6	3.9	10.0	4.1	3.8	9.2	7.8	8.0
CaO	6.4	1.8	7.2	1.8	1.8	6.7	7.5	7.8
MgO	3.2	0.3	3.7	0.3	0.3	3.4	4.8	5.4
K2O	0.95	2.65	0.85	2.60	2.60	1.15	0.95	0.80
Na2O	4.6	6.2	4.6	6.1	6.1	4.5	4.1	3.8
TiO2	1.80	0.50	1.65	0.50	0.50	1.60	0.95	0.95
Total	100.25	98.95	99.90	99.40	98.90	99.95	100.10	99.45

	141	142	143	144	145	146	147	148
SiO2	55.3	56.0	55.3	55.0	53.9	55.6	53.5	54.7
Al2O3	20.5	16.1	17.8	19.2	19.7	15.1	15.1	15.6
FeO	6.4	10.0	7.6	7.7	8.0	10.3	12.1	11.0
CaO	8.3	6.6	7.7	7.7	7.7	7.3	7.1	7.1
MgO	3.6	3.6	5.6	5.0	5.6	3.5	3.8	3.7
K2O	0.85	1.05	0.70	0.85	0.75	1.25	0.90	0.85
Na2O	4.2	4.8	3.7	3.9	3.9	4.6	4.6	4.6
TiO2	0.90	1.70	0.95	0.95	0.95	1.80	2.00	1.95
Total	100.05	99.85	99.35	100.30	100.50	99.45	99.10	99.50

	149	150	151	152	153	154	155	156
SiO2	55.5	56.5	68.2	55.3	55.0	68.7	67.9	54.3
Al2O3	15.5	16.6	15.3	18.1	18.1	15.5	16.2	18.0
FeO	11.4	8.8	4.7	8.4	8.4	4.1	3.9	7.7
CaO	7.0	6.6	1.7	7.9	7.3	1.7	1.6	8.0
MgO	3.2	3.8	0.7	3.8	4.0	0.4	0.5	6.1
K2O	0.85	1.00	2.55	0.80	0.95	2.60	2.65	0.75
Na2O	4.6	4.6	6.2	4.1	4.4	6.0	5.9	3.8
TiO2	1.95	1.20	0.50	1.10	1.10	0.55	0.55	0.90
Total	100.00	99.10	99.85	99.50	99.25	99.55	99.20	99.55

	157	158	159	160	161	162	165	167
SiO2	68.6	56.0	61.7	60.7	54.2	65.3	62.4	55.7
Al2O3	16.1	15.8	15.4	15.1	18.0	16.0	17.2	19.7
FeO	4.0	10.1	7.3	8.7	7.8	5.5	6.5	8.0
CaO	1.4	5.8	4.0	4.2	7.6	2.9	3.4	6.5
MgO	0.7	3.9	1.7	1.9	5.5	1.1	0.9	3.2
K2O	2.65	1.15	2.00	1.95	0.80	2.15	1.90	1.10
Na2O	6.00	4.8	5.3	5.2	3.7	5.7	5.7	4.3
TiO2	0.60	1.50	1.45	1.45	0.80	0.95	1.05	1.05
Total	100.05	99.05	98.85	99.20	98.40	99.60	99.05	99.55

	168	169	170	171	172	173	174	175
SiO2	66.3	60.8	60.5	58.5	68.2	55.6	64.1	66.9
Al2O3	15.9	17.5	15.7	16.1	15.9	16.6	16.0	15.7
FeO	5.5	7.0	7.8	8.0	3.9	9.8	6.1	5.0
CaO	2.8	3.6	5.4	5.5	1.8	6.7	3.1	2.3
MgO	0.9	1.5	2.1	2.8	0.7	3.5	0.7	0.7
K2O	2.15	1.70	1.35	1.35	2.65	0.95	1.80	2.15
Na2O	5.6	5.8	4.9	4.9	6.0	4.6	6.0	6.1
TiO2	0.95	1.25	1.40	1.45	0.50	1.25	0.85	0.65
Total	100.10	99.15	99.15	98.60	99.65	99.00	98.65	99.50

	176	177	191	192	193	194	195	196
SiO2	54.4	63.5	59.1	58.5	53.4	68.1	54.7	61.0
Al2O3	15.9	16.0	17.0	16.9	18.3	15.7	18.2	17.4
FeO	10.5	6.8	8.0	8.0	8.8	4.1	8.0	6.6
CaO	7.2	3.3	5.9	6.1	8.3	2.0	7.9	3.9
MgO	4.2	1.5	3.0	3.2	5.6	0.8	5.8	2.0
K2O	0.95	2.15	1.50	1.45	0.70	2.65	0.85	1.60
Na2O	4.5	5.7	4.9	4.6	4.0	5.8	3.9	6.0
TiO2	1.70	0.90	1.35	1.35	1.15	0.75	1.10	1.35
Total	99.35	99.85	100.75	100.10	100.25	99.90	100.45	99.85

	197	198	199	200	201	202	203	204
SiO2	68.5	54.3	54.2	64.8	70.2	55.6	53.7	60.0
Al2O3	15.7	16.5	18.2	15.9	15.1	16.5	19.0	16.8
FeO	3.6	10.7	8.5	4.9	3.3	10.0	7.4	7.8
CaO	2.0	6.9	7.8	3.7	1.3	6.8	8.1	5.2
MgO	0.8	3.6	4.6	1.5	0.3	3.7	5.4	2.5
K2O	2.40	0.90	0.90	1.80	2.60	0.95	0.80	1.60
Na2O	5.7	4.8	4.3	5.6	6.2	5.0	4.0	5.1
TiO2	0.70	2.20	1.35	1.40	0.45	1.80	1.05	1.50
Total	99.40	99.90	99.85	99.60	99.45	100.35	99.45	100.50

	206	207	208	209	210	250	258	259
SiO2	73.4	73.0	73.0	72.5	56.8	63.9	57.5	52.4
Al2O3	14.3	14.2	14.9	14.6	17.6	16.2	17.3	16.3
FeO	2.8	2.1	2.8	2.2	8.0	5.2	7.0	8.7
CaO	1.5	1.5	1.5	1.5	6.8	3.9	7.2	8.7
MgO	0.3	0.3	0.3	0.3	4.0	1.5	4.1	7.9
K2O	2.90	2.95	2.90	2.95	1.20	2.05	1.15	0.50
Na2O	4.9	4.8	4.8	5.1	4.6	5.2	4.0	3.4
TiO2	0.25	0.25	0.30	0.35	1.25	1.00	1.05	1.25
Total	100.35	99.10	100.50	99.50	100.25	98.95	99.40	99.15

	260	261	262	263	264	265	266	268
SiO2	57.0	52.5	49.7	64.9	52.4	50.8	51.9	64.3
Al2O3	17.5	15.8	16.5	15.8	18.4	17.2	17.3	16.1
FeO	7.2	8.8	10.2	5.2	9.0	9.0	9.0	5.1
CaO	7.2	8.7	8.8	3.9	7.7	8.6	8.7	3.9
MgO	4.3	8.8	9.2	1.7	5.3	8.0	7.6	1.7
K2O	1.20	0.65	0.35	2.10	0.50	0.70	0.30	1.90
Na2O	3.9	3.4	3.1	5.4	3.8	3.3	3.7	5.3
TiO2	1.05	1.30	1.55	1.05	1.30	1.50	1.40	1.05
Total	99.35	99.95	99.40	100.05	98.40	99.10	99.90	99.35

	269	270	271	272	273	274	275	276
SiO2	72.3	72.0	72.0	56.3	63.5	54.8	62.0	59.5
Al2O3	14.8	15.6	15.0	16.2	15.7	18.4	16.8	16.8
FeO	2.2	2.0	2.2	8.3	6.3	6.8	6.2	6.9
CaO	1.9	1.5	2.0	7.3	3.7	8.3	3.7	6.4
MgO	0.7	0.3	0.8	3.7	1.5	5.7	1.6	3.1
K2O	2.95	2.90	2.95	0.95	1.75	0.60	1.75	1.15
Na2O	4.8	4.7	4.5	4.5	5.4	4.0	5.3	4.7
TiO2	0.30	0.25	0.30	1.55	1.35	0.95	1.35	1.30
Total	99.95	99.25	99.75	98.80	99.20	99.55	98.70	99.85

	277	278	279	280	281	282	283	284
SiO2	65.3	64.8	63.9	63.9	63.0	63.5	62.9	63.0
Al2O3	15.8	15.8	16.6	16.0	16.1	16.0	15.8	15.8
FeO	5.3	5.4	5.4	5.6	6.1	5.8	6.3	6.0
CaO	3.4	3.5	3.7	3.7	3.7	4.2	4.2	4.2
MgO	1.5	1.5	1.5	1.5	2.0	2.1	1.7	1.8
K2O	2.25	2.20	2.20	2.20	2.10	2.10	2.00	2.00
Na2O	5.3	5.1	5.1	4.9	5.0	5.2	5.1	5.2
TiO2	1.05	1.05	1.05	1.05	1.15	1.10	1.20	1.20
Total	99.90	99.35	99.45	98.85	99.15	100.00	99.20	99.20

	285	286	287	288	289	290	291	292
SiO2	57.5	61.9	62.5	56.1	63.9	55.4	65.4	65.0
Al2O3	18.1	16.1	15.8	16.7	15.5	18.7	17.9	15.6
FeO	6.9	6.6	6.7	8.6	6.4	7.0	4.2	4.8
CaO	6.9	4.4	4.4	7.3	4.2	8.4	2.8	3.9
MgO	3.2	1.7	2.0	3.8	2.0	3.9	0.8	1.8
K2O	1.15	1.65	1.65	0.95	1.75	0.80	2.35	1.90
Na2O	4.8	5.4	5.4	4.2	5.6	4.4	5.2	4.7
TiO2	1.25	1.30	1.35	1.45	1.15	1.10	0.80	1.10
Total	99.80	99.05	99.80	99.10	100.05	99.70	99.45	98.80

	293	294	295	296	297	298	299	300
SiO2	63.0	66.0	52.3	54.6	68.5	67.9	52.2	52.0
Al2O3	17.7	16.0	18.8	19.2	16.7	17.5	18.4	19.2
FeO	5.1	4.8	8.3	7.5	3.1	3.6	8.1	8.3
CaO	3.4	3.4	8.5	7.3	1.5	1.8	8.4	8.2
MgO	1.4	1.6	5.9	4.4	0.8	0.5	5.7	5.7
K2O	2.20	2.35	0.65	0.95	2.50	2.35	1.20	1.10
Na2O	5.3	4.6	3.4	4.1	6.0	6.0	3.1	3.9
TiO2	1.05	0.95	1.30	1.05	0.45	0.65	1.50	1.50
Total	99.15	99.70	99.15	99.10	99.55	100.30	98.60	99.90

	301	302	303	305	306	307	308	309
SiO2	55.0	56.0	52.6	67.0	54.6	56.0	56.5	55.1
Al2O3	19.2	17.0	16.0	16.5	17.8	17.5	18.0	17.9
FeO	7.2	6.3	8.6	4.1	7.2	7.4	7.7	6.9
CaO	7.3	7.6	8.0	2.4	7.9	7.8	7.2	8.1
MgO	4.3	5.0	7.4	0.7	6.0	4.5	4.3	5.8
K2O	1.00	1.05	1.15	2.15	0.80	0.95	0.80	0.80
Na2O	4.3	4.6	3.9	6.5	3.8	4.1	4.2	3.7
TiO2	1.05	0.90	1.40	0.65	1.00	1.30	1.10	0.95
Total	99.35	99.45	99.05	100.00	99.10	99.55	99.80	99.25

	310	311	312	313	314	315	319	320
SiO2	55.6	56.3	55.5	54.7	55.4	55.0	53.8	55.5
Al2O3	17.9	17.3	18.0	18.6	18.5	18.0	18.7	17.7
FeO	7.3	7.4	7.3	7.4	7.4	7.5	8.2	7.5
CaO	8.0	8.0	8.1	7.9	8.0	8.6	8.6	7.8
MgO	5.7	5.7	5.5	5.7	4.5	4.5	4.7	5.6
K2O	0.80	0.80	0.85	0.85	1.20	1.15	1.10	0.80
Na2O	3.6	3.7	3.6	3.7	3.5	3.5	3.3	3.6
TiO2	0.95	0.95	0.95	1.00	1.25	1.05	1.10	1.05
Total	99.85	100.15	99.80	99.85	99.75	99.30	99.50	99.55

	341	342	343	346	347	348	349	350
SiO2	67.9	55.6	64.0	54.9	67.6	53.8	54.5	55.2
Al2O3	16.5	18.3	16.1	17.9	15.6	16.9	16.6	17.9
FeO	3.6	8.3	5.9	9.6	3.7	9.3	9.5	9.0
CaO	2.1	6.5	3.1	6.8	2.1	8.0	7.8	6.7
MgO	0.5	4.0	1.0	3.7	0.7	4.9	4.3	3.4
K2O	2.35	1.10	1.85	0.95	2.25	0.65	0.80	1.00
Na2O	6.3	4.8	6.2	4.6	6.2	4.5	4.4	4.5
TiO2	0.65	1.35	0.90	1.65	0.65	1.60	1.65	1.50
Total	99.90	99.95	99.05	100.10	98.80	99.65	99.55	99.20

	351	352	354	355	356	358	359	360
SiO2	62.9	57.5	66.7	54.0	62.5	60.0	55.4	55.3
Al2O3	17.2	17.9	17.6	20.5	17.2	15.6	17.1	18.0
FeO	6.1	8.0	3.9	6.7	5.8	7.8	8.5	8.0
CaO	3.7	5.6	2.4	8.3	3.5	5.4	7.5	8.3
MgO	1.5	2.6	0.8	4.2	1.3	2.5	4.1	5.0
K2O	1.80	1.40	2.10	0.90	2.10	1.50	0.90	0.50
Na2O	5.4	4.7	5.9	4.0	5.6	5.0	4.5	4.5
TiO2	1.15	1.50	0.80	1.00	1.10	1.45	1.25	1.05
Total	99.75	99.20	100.20	99.60	99.10	99.25	99.25	100.65

	361	362	363	364	365	366	367	380
SiO2	55.0	62.0	56.0	55.5	61.3	54.4	63.8	57.6
Al2O3	17.8	16.3	17.6	17.3	17.6	18.6	16.8	16.7
FeO	7.5	6.0	7.2	7.3	6.1	7.4	4.9	9.4
CaO	8.3	4.7	7.9	8.4	5.1	8.6	3.8	6.4
MgO	5.1	2.5	4.7	5.7	2.4	5.0	1.3	3.3
K2O	0.55	1.80	0.80	0.80	1.80	0.70	1.85	1.00
Na2O	4.2	4.8	4.2	3.8	4.8	4.2	6.1	4.6
TiO2	1.05	1.00	0.90	0.95	1.05	1.00	0.95	1.45
Total	99.50	99.10	99.30	99.75	100.15	99.90	99.50	100.45

	381	445	446	447	448	449	456	458
SiO2	71.7	72.9	72.3	72.3	71.6	73.2	63.0	62.7
Al2O3	14.9	14.2	14.9	15.0	15.0	14.2	16.0	16.5
FeO	2.9	2.5	2.4	2.6	3.0	2.3	6.3	6.4
CaO	2.1	2.0	2.0	1.9	1.9	1.4	5.1	5.2
MgO	0.8	0.5	0.4	0.5	0.8	0.3	2.0	1.8
K2O	2.90	3.10	3.05	3.10	3.00	3.10	1.70	1.90
Na2O	4.6	4.3	4.2	4.2	4.3	4.3	4.5	4.2
TiO2	0.30	0.30	0.35	0.35	0.30	0.30	1.10	1.10
Total	100.20	99.80	99.60	99.95	99.90	99.10	99.70	99.80

	525	526	529	1000	1001	1002	1003	1004
SiO2	52.1	52.5	74.3	50.7	51.5	54.3	56.2	72.2
Al2O3	17.7	17.6	14.6	17.2	16.2	17.4	17.6	14.9
FeO	10.1	9.7	2.5	8.9	9.2	9.4	7.5	2.5
CaO	7.7	7.7	1.4	8.8	8.7	8.2	7.5	2.0
MgO	5.1	4.8	0.1	8.6	8.6	4.7	4.9	0.6
K2O	0.50	0.65	2.65	0.65	0.50	0.75	1.10	3.05
Na2O	3.6	3.8	4.0	3.3	3.3	3.9	3.9	4.4
TiO2	1.50	1.30	0.25	1.05	1.35	1.40	1.05	0.30
Total	98.30	98.05	99.80	99.20	99.35	100.05	99.75	99.95

	1005	1006	1007	1008	1009	1010	1011	1012
SiO2	52.1	52.0	53.9	55.0	54.9	55.2	55.6	53.9
Al2O3	18.3	17.6	17.4	17.0	16.0	18.1	16.8	20.3
FeO	8.4	9.4	9.8	9.0	10.6	8.4	9.3	7.2
CaO	8.2	8.1	7.6	7.3	7.1	7.6	6.7	8.1
MgO	5.9	6.2	4.6	4.3	3.7	3.9	3.7	4.2
K2O	1.00	0.55	0.80	0.80	0.90	0.90	1.00	0.90
Na2O	3.5	3.6	4.4	4.5	4.7	4.3	4.6	4.2
TiO2	1.45	1.40	1.65	1.45	1.80	1.10	1.55	1.00
Total	98.85	98.85	100.15	99.35	99.70	99.50	99.25	99.80

	1013	1014	1015	1016	1017	1018	1019	1020
SiO2	54.7	54.2	54.8	55.1	55.2	61.3	61.2	62.5
Al2O3	18.4	19.6	18.5	18.6	18.1	16.7	15.3	17.2
FeO	7.6	7.6	7.6	7.6	7.6	6.7	8.0	6.2
CaO	7.9	7.6	7.7	7.6	8.2	5.2	4.1	3.5
MgO	5.2	4.6	5.2	4.6	5.0	2.4	1.8	1.1
K2O	0.75	0.75	0.85	0.95	0.90	1.75	2.00	2.00
Na2O	4.4	4.2	3.9	4.1	3.8	4.8	5.3	5.7
TiO2	0.95	0.90	0.90	1.10	1.00	1.20	1.45	1.10
Total	99.90	99.45	99.45	99.65	99.80	100.05	99.15	99.30

	1021	1022	1023	1024	1025	1026	1027	1028
SiO2	62.5	63.2	62.2	57.0	67.5	64.5	64.5	64.1
Al2O3	16.6	15.5	16.0	16.4	15.9	16.0	16.1	16.2
FeO	6.6	6.5	6.7	8.6	4.1	5.8	5.3	5.5
CaO	4.1	3.7	4.4	7.2	2.2	3.0	3.9	3.7
MgO	1.4	1.6	1.9	3.5	0.6	0.9	1.6	1.6
K2O	1.65	1.90	1.65	1.10	2.25	1.95	2.10	2.15
Na2O	5.5	5.6	5.4	4.3	6.2	6.0	5.4	5.0
TiO2	1.45	1.30	1.35	1.30	0.65	0.90	1.05	1.05
Total	98.40	99.30	99.60	99.40	99.40	99.05	99.95	99.30

	1029	1030	1031	1032	1033	1034	1035
SiO2	73.1	68.3	68.4	73.8	68.2	69.0	68.4
Al2O3	14.5	15.7	15.9	14.4	15.9	14.8	16.2
FeO	2.6	3.9	4.0	2.4	4.2	3.9	3.6
CaO	1.5	2.0	1.6	1.4	2.2	1.8	1.9
MgO	0.3	0.8	0.5	0.2	0.6	0.3	0.6
K2O	2.90	2.55	2.65	2.90	2.15	2.60	2.40
Na2O	4.8	5.8	6.0	4.2	6.0	6.1	5.8
TiO2	0.25	0.75	0.55	0.30	0.70	0.50	0.55
Total	99.95	99.80	99.60	99.60	99.65	99.00	99.45

APPENDIX 2

Locations of Analysed Rocks, S.W. Broken Top Quadrangle

1. Platy lava at 6620' elev., corner sec 14,15,22,23, 0.1 km S. of 3-Ck. Lk. Map 2.
2. Platy lava in cliffs of E. Tam Mac Rim at 6800' elev, 0.1 km E. of E. edge of Map 3.
4. Columnar-jointed glassy margin of glaciated lava in cut of 3-Cr. Lk. Rd., 0.1 km N. of boundary sec 8,5. Map 8.
5. Platy lava at 6560' elev, S. of 3-Cr. Lk. Rd., N. center sec 8. Map 8.
7. Terminous of Cayuse flow, roadcut at Soda Cr. and Century Dr. Map 7.
8. Top of platy lava in cliffs at 6320' elev, 0.6 km E. of Bare Lk. Map 8.
10. Lava from ridge crest at 6650' elev, 0.6 km N.W. of Todd Lk. Map 8.
11. Base of platy lava in cliffs at 6200' elev, 0.5 km S.E. of Bare Lk. Map 8.
12. Lava at top of S.E.-facing cliffs at 6490' elev, 0.4 km S.E. of Bare Lk. Map 8.
15. Lava from ridge crest at 6920' elev, 0.9 km W. of Todd Lk. Map 8.
16. Platy lava at 6380' elev, S.E. side of ridge N.W. of Todd Lk. Map 8.
17. Thin vesicular lava from summit of hill, E. Tam Mac Rim, W. center sec 23, 0.2 km W. of Map 3.
20. Cayuse flow at 5480' elev, Soda Cr. Tr. in N.E. corner sec 11. Map 7.
21. E. margin Cayuse flow at 5760' elev, 0.6 km N. of Soda Cr. Map 4.
22. Center of Cayuse flow, 1.0 km downstream from Cayuse Cone. Map 4.
23. Lava from head of Cayuse flow in gutter at S. base of Cayuse Cone. Map 4.
24. Lava from head of flow at 6700' elev S.W. base of small source cone 0.5 km N.W. of Cayuse Cone. Map 4.
25. Margin of black vitrophyre, 6680' elev, 0.5 km W. of Green Lk. Map 1.
26. Glassy lava from E. margin of Newberry flow, 0.6 km W. of Green Lk. Map 1.
27. Platy lava at 6200' elev, S.E. side of Fall Cr. opposite S. tip of Newberry flow. Map 4.
28. Spherulitic lava from S. tip of Newberry flow. Map 4.
29. Glassy lava from 6120' elev, 0.35 km S.W. of junction, Moraine Lk. and Green Lk. Trails. Map 4.
30. W. margin of W. lobe of Cayuse flow at 5760' elev. Map 4.
41. Lava at waterfall, 0.2 km downstream from outlet of Todd Lk. Map 8.
42. Glaciated lava from cut at spring near Old Century Drive Rd., 0.8 km S.E. of Todd Lk. Map 8.
43. Cinders from E. side of glaciated cinder cone, 1.0 km S. of Todd Lk. Map 8.
44. Lava from W. margin of N.E. lobe from cinder cone on N. slope of Bachelor Bu. Map 8.
45. Lava, 1.0 km S. of Bare Lk., center sec 18. Map 8.
46. Cinders from E. side glaciated cone, N. sec 20, 1.0 km N. of Bachelor Bu. Map 8.
47. Lava in Century Drive roadcut, W. end of Dutchman Flat. Map 8.
48. Glaciated lava at W. base of Tumalo Mtn., S.E. end of Dutchman Flat. Map 9.
74. SE-trending dike at 7680' elev, S.E. ridge of Tumalo Mtn. Map 9.
81. Fresh, coarse block from Broken Top summit plug, W. base of Crook Glacier cirque. Map 5.
101. Platy margin of Broken Top summit plug, W. base of Crook Glacier cirque. Map 5.
102. Platy margin of Broken Top summit plug, N.E. base of Crook Glacier cirque. Map 5.
103. White pumice lumps from base of welded tuff at 8600' elev, in W. wall of Crook Glacier cirque, Broken Top. Map 5.
106. Lava from lowest exposed flow in W. wall of Crook Glacier cirque, Broken Top. Map 5.
107. Oxidized lava from lowest exposed flow in E. wall of Crook Glacier cirque, Broken Top. Map 5.
108. Lava from 7800' elev on crest of Broken Top S.E. ridge. Map 5.
109. Glaciated lava at 7650' elev, 1.0 km N. of Ball Butte. Map 5.
110. Glaciated lava from 0.2 km N. of Ball Butte. Map 5.
111. Lava from Creek bed at 7000' elev, 0.5 km S.W. of Ball Butte. Map 5.
112. Lowest of 3 dikes beneath cinder cone remnant at 7600' elev, crest of Broken Top S. ridge. Map 5.
113. Lava from prominence at 8050' elev, Broken Top S. ridge. Map 5.

114. Lava at 8100' elev, crest of Broken Top S.W. ridge. Map 5.
115. Glassy crest of glaciated lava at 7520' elev, Broken Top S.W. ridge. Map 4.
116. Thin flow at 7400' elev, S. side Broken Top N.W. ridge. Map 1.
117. Glaciated lava from knoll, 0.1 km S. of Green Lk. Map 4.
118. Lava at 6960' elev, 0.3 km N. of Cayuse Cone. Map 4.
119. Dike at 8200' elev, between N. and E. arms of Bend Glacier, Broken Top. Map 2.
121. S.W. end of dike at 8280' elev in saddle of Broken Top N.E. ridge. Map 2.
122. Lava at 7080' elev, crest of Broken Top E. ridge. Map 2.
124. Cinders from cone at 7700' elev, W. sec 21, 1.3 km S.W. of Tam Mac Rim. Map 3.
125. N.W.-S.E. dike at 7440' elev, upper N. Fork Tumalo Cr. Map 6.
126. Pumice bomb from W. side of silicic tuff cone at 7320' elev, upper N. Fork Tumalo Cr. Map 6.
128. Platy lava from base of cliffs at 6840' elev, S.E. corner sec 27, N. side Happy Valley. Map 6.
129. Lava from cinder cone at 7350' elev, N. central sec 28, upper N. Fork Tumalo Cr. Map 6.
134. Obsidian from base of flow exposed in cliffs at 7160' elev, S.W. bank of N. Fork Tumalo Cr. Map 6.
135. Lava at 6800' elev, N. bank of N. Fork Tumalo Cr. Map 6.
136. Spherulitic glass from top of flow at 6600' elev, center of N. boundary sec 3. Map 6.
137. Base of flow at 6600' elev, center of N. boundary sec 3. Map 6.
138. Platy lava at 6200' elev in bed of N. Fork Tumalo Cr., 0.3 km E. of Map 6.
139. Lava at 7240' elev on N.W. side of glaciated cone, 1.0 km S. of Ball Butte. Map 5.
140. Lava at 7000' elev, N. end of glaciated cone, 3.3 km N.W. of Tumalo Mtn. Map 9.
141. Glaciated lava, 0.5 km W. of corner sec 3,4,9,10, 1.2 km N.W. of Tum Lk. Map 9.
142. Lava from cliffs 0.1 km S.S.W. of Tum Lk. Map 9.
143. Glaciated lava in S.W. sec 10, 0.8 km S.S.W. of Tum Lk. Map 9.
144. Cinders from N. rim of cone 2.0 km N. of Tumalo Mtn. Map 9.
145. Cinders from summit of cone in S.E. corner sec 9, 2.6 km N.N.W. of Tumalo Mtn. Map 9.
146. Platy lava from base of cliffs at 7200' elev, 0.2 km S. of lake, center sec 16. Map 3.
147. Lava at 6950' elev, W. side of Snow Cr. Valley, N.E. sec 17. Map 2.
148. Platy lava at 6900' elev, N. center sec 16. Map 3.
149. Oxidized lava at 7040' elev, saddle of ridge, N. boundary of sec 16. Map 3.
150. Cinders from glaciated cone at 6720' elev, center sec 9, 2.8 km N.W. of 3-Cr. Lk. Map 3.
151. Lithophysal lava at 7120' elev, E. Tam Mac Rim, 0.8 km S. of 3-Cr. Lk. Map 3.
152. Lava from glaciated shelf at 7000' elev, E. Tam Mac Rim, 0.6 km S. of 3-Cr. Lk. Map 3.
153. Lava from glaciated shelf at 7200' elev, E. Tam Mac Rim, 0.7 km S. of 3-Cr. Lk. Map 3.
154. Glassy top of flow at 7400' elev, N. center sec 22, Tam Mac Rim. Map 3.
155. Glassy margin of E. end of dike at 7240' elev, in face of Tam Mac Rim, N. center sec 22. Map 3.
156. Lava from flow below cap of Tam Mac Rim in center of sec 22. Map 3.
157. White lava at 7660' elev, 0.2 km S. of summit of Tam Mac Rim prominence in N.W. sec 22. Map 3.
158. Glaciated lava at 7450' elev, E. side Snow Cr. cirque, N.W. sec 21. Map 3.
159. N.E. end of dike at 7520' elev, S.W. Snow Cr. cirque. Map 2.
160. Platy lava at 7740' elev, head of Snow Cr. cirque. Map 2.
161. Lava from W. summit of Tam Mac Rim, S. center sec 16. Map 3.
162. Platy lava at 6760' elev, on S.E. slope of hill, 0.6 km E. of 3-Cr. Lk., 0.8 km E. of Map 3.
165. Glassy margin of platy flow at 7950' elev, S.W. head of Snow Cr. cirque. Map 2.
167. Center of platy dike at 7900' elev, S.W. head of Snow Cr. cirque. Map 2.
168. Dike at 7780' elev, S.W. head of Snow Cr. cirque. Map 2.
169. Red and gray streaked lava at 7460' elev, W. Snow Cr. cirque. Map 2.
170. Center of E.-W. dike at 7280' elev, W. Snow Cr. cirque. Map 2.

171. Blocky lava at 7280' elev, S. central sec 17, W. of Snow Cr. Map 2.
172. Center of E.-W. dike at 6760' elev, 0.3 km S.W. of 3-Cr. Lk. Map 3.
173. E. end of irregular dike at 6800' elev, below Tam Mac Rim, 0.4 km S.W. of 3-Cr. Lk. Map 3.
174. Platy lava at 6900' elev, 0.5 km S.W. of 3-Cr. Lk. Map 3.
175. Platy lava from ridge crest at 6800' elev, 0.5 km S.W. of 3-Cr. Lk. Map 3.
176. Lowest exposed lava at N. base of main protrusion of Tam Mac Rim, 0.9 km W. of 3-Cr. Lk. Map 3.
177. Glassy margin of E.-W. dike at 7100' elev at base of main protrusion of Tam Mac Rim, 1.0 km W. of 3-Cr. Lake. Map 3.
191. Glaciated lava at 6960' elev, 1.3 km N.W. of Golden Lk. at junction of Park Meadow and Green Lk. Trails. Map 1.
192. Lava from cliffs at 6760' elev, 0.2 km N.E. of Green Lk. Map 1.
193. Lava from cliffs at 7050' elev, 0.5 km N.E. of Green Lk. Map 1.
194. Fresh pumice from deposit at 7750' elev, crest of Broken Top N.W. ridge. Map 1.
195. Lava at 7750' elev on crest of Broken Top N.W. ridge. Map 1.
196. Spatter from glaciated cone at 7640' elev on Broken Top N.W. ridge. Map 1.
197. Glassy margin of glaciated volcanic dome at 7150' elev, crest of Broken Top N.W. ridge. Map 1.
198. Lava from shelf at 7020' elev, 0.6 km S.S.W. of Golden Lake. Map 1.
199. Lava from base of cliffs at 7480' elev, N. side of Broken Top N.W. ridge. Map 1.
200. Lava from middle of N.E.-facing cliffs at 7600' elev, 1.4 km S. of Golden Lk. Map 1.
201. Platy lava at 7320' elev, 1.2 km S.S.W. of Tam Lk. Map 2.
202. Lava at 7480' elev on crest of S. ridge of glaciated cone, W. side of Snow Cr. valley. Map 2.
203. Scoriaceous lava from center of sec 18, 1.5 km E. of Golden Lk. Map 2.
204. Glaciated lava at 7760' elev, ridge crest 0.7 km E. of Carver Lk. Map 1.
206. Platy lava from E. edge of E. Chambers Lk., 0.6 km W. of Map 1.
207. Spherulitic crust of glaciated volcanic dome, 0.2 km E. of E. Chambers Lk., 0.4 km W. of Map 1.
208. Holocrystalline lava at 7400' elev, glaciated volcanic dome 1.5 km E. of E. Chambers Lk. Map 1.
209. Glaciated lava at 7000' elev, N.W. side of W. Fork Park Cr., 1.6 km E. of Carver Lk. Map 1.
210. Platy lava at 6260' elev, center W. boundary sec 7, 0.5 km N. of Park Meadow. Map 2.
250. Platy lava at 5650' elev, center sec 31, 2.5 km N. of Map 2.
258. Lava from S. margin of Dutchman Flat, W. center sec 21. Map 9.
259. Bomb fragment from S. rim of third cone from N. end of chain of cones, S.W. of Todd Lk. Map 8.
260. Scoriaceous lava from center of boundary sec 18, 19. Map 8.
261. Bomb fragment from E. side quarry in N. cone of chain of cones S.W. of Todd Lk. Map 8.
262. Lava from base of marginal block along E. shore of Sparks Lk., central S.W. 1/4 sec 14. Map 7.
263. Platy lava from roadcut of Century Drive, 0.4 km W. of Fall Cr. Map 7.
264. Fresh core of palagonitized bomb from roadcut in tuff cone at N.E. base of Talapus Bu., 0.4 km W. of Map 7.
265. Lava at 5560' elev on glaciated shelf, N.E. 1/4 sec 22, S.W. of Sparks Lk. Map 7.
266. Lava at 5480' elev, N.W. edge of Sparks Lk. Map 7.
268. Lava at 6160' elev, 0.2 km N. of N.W. corner sec 2. Map 4.
269. Obsidian block from N.E. margin of Holocene lava, 0.5 km N. of Moraine and Green Lk. Trail junction. Map 4.
270. Lava from cliffs at 6800' elev between Newberrry Flow and Goose Cr. Chain of domes. Map 4.
271. Red and black banded obsidian at 6620' elev, S. margin of Newberry Flow. Map 4.
272. Glaciated lava from 6280' elev, 0.2 km N.W. of Corral Lk. Map 4.
273. Blocky lava at 6250' elev, 0.7 km S.E. of Corral Lk. Map 4.
274. Lava at 6300' elev, 1.0 km S.E. of Corral Lk. Map 4.

275. Platy lava from cliff at confluence of Fall Cr. and Corral Lk. Cr. Map 4.
276. Lava from cliffs at 5680' elev, 0.4 km E. of Fall Cr. Map 7.
277. Lava at 5600' elev, W. slope Todd Lk. volcano. Map 7.
278. Lava at 5760' elev, W. slope Todd Lk. volcano. Map 7.
279. Lava at 5840' elev, W. slope Todd Lk. volcano. Map 7.
280. Lava at 5960' elev, W. slope Todd Lk. volcano. Map 7.
281. Lava at 6040' elev, W. slope Todd Lk. volcano. Map 7.
282. Lava at 6120' elev, W. slope Todd Lk. volcano. Map 7.
283. Lava at 6360' elev, W. slope Todd Lk. volcano. Map 7.
284. Platy margin at 6500' elev along W. side of plug of Todd Lk. volcano, N.W. corner sec 7. Map 8.
285. Platy lava at 6180' elev on ridge crest W. central sec 6, N. side of Soda Cr. Canyon. Map 5.
286. Blocky lava from base of waterfall at 6320' elev in ravine, W. sec 6, N. of Soda Cr. Canyon. Map 5.
287. Lava at 6400' elev, head of ravine, W. sec. 6, N. of Soda Cr. canyon. Map 5.
288. Gray lava from base of thick flow breccia unit at 6100' elev, in ravine, W. sec 6, N. of Soda Cr. Canyon. Map 5.
289. Glassy margin of silicic dike at 6050' elev in ravine, W. sec 6, N. of Soda Cr. Canyon. Map 5.
290. Porphyritic platy lava at 6000' elev below palagonitic beds in ravine, W. sec 6, N. of Soda Cr. Canyon. Map 5.
291. Top of thick lava flow at 5800' elev, base of ravine, W. sec 6, N. of Soda Cr. Canyon. Map 5.
292. Lava from summit of Todd Lk. volcano, N.W. sec 7. Map 8.
293. Lava at 6700' elev, crest of Todd Lk. volcano N.E. ridge. Map 8.
294. Lava from saddle in ridge crest, 0.5 km N. of Todd Lk. Map. 8.
295. Coarse porphyry at 6720' elev on S.W. side of knoll, S.W. corner sec 5, 0.9 km N.E. of Todd Lk. Map 8.
296. Glaciated lava from S.-facing shelf at 6760' elev, S. central sec 5, 1.4 km N.E. of Todd Lk. Map 8.
297. Platy lava at 6280' elev in cut of 3-Cr. Lk. Rd., 0.9 km E. of Todd Lk. Map 8.
298. Platy lava at 6840' elev on glaciated knoll S. of 3-Cr. Lk. Rd., N.E. corner sec 8. Map 8.
299. Lava at 6840' elev in cut of Crater Cr. Ditch, 0.4 km E.S.E. of Ditch Cabin. Map 5.
300. Lava at 6660' elev, N.E. corner sec 6, 0.5 km S.W. of Ditch Cabin. Map 5.
301. Lava at 7400' elev, lower S.E. ridge of Broken Top. Map 5.
302. Lava at 7480' elev, base of cliffs W. face of Ball Bu. Map 5.
303. Lava at E. base of small glaciated cinder cone in S.W. corner sec 33, 1.0 km S.E. of Ball Bu. Map 6.
305. Fragment of welded spatter at 7160' elev, S. side of silicic tuff cone, upper N. Fork Tumalo Cr. Map 6.
306. Scoriaceous lava in creek bed at 6400' elev, N.E. sec 3, 1.5 km S. of Happy Valley. Map 6.
307. Glaciated lava at 6720' elev, S. base of knoll in S. central sec 5, 0.9 km N.E. of Todd Lk. Map 8.
308. Lava at 6700' elev, 0.4 km W. of glaciated cinder cone, center sec 9. Map 9.
309. Lava from cliffs at 6240' elev, E. bank of Old Century Drive road, center sec 17. Map 8.
310. Lava from summit of glaciated knoll, 0.6 km S.E. of Todd Lk. Map 8.
311. Lava from top of cliffs at 6280' elev, E. side of creek, 0.9 km E. of Todd Lk. Map 8.
312. Glaciated lava from N. side Century Drive roadcut, S. center sec 17, 0.7 km W. of Dutchman Flat. Map 8.
313. Lava at 6380' elev, W. center sec 16, N. side Dutchman Flat. Map 9.
314. Lava at 6360' elev, N.E. side Dutchman Flat. Map 9.
315. Lava at 6450' elev, W.N.W. base of Tumalo Mtn. Map 9.
319. Lava from cliffs at 7080' elev, N. central sec 22, E. flank Tumalo Mtn. Map 9.
320. Spatter from small cinder cone, 0.8 km N. of Tumalo Mtn summit. Map 9.

341. Platy lava at S.W. shore of 3-Cr. Lk. Map 3.
342. Platy lava at 6680' elev on knoll, 0.2 km S.W. of 3-Cr. Lk. Map 3.
343. Platy lava at 7040' elev, 0.6 km S.W. of 3-Cr. Lk. Map 3.
346. Blocky lava at 7160' elev below prominence of Tam Mac Rim in N. central sec 22. Map 3.
347. Platy lava at 6960' elev on shelf, 0.3 km W. of Little 3-Cr. Lk. Map 3.
348. N.E.-S.W. dike at 7060' elev, 0.4 km W. of Little 3-Cr. Lk. Map 3.
349. Blocky lava from top flow of 6 flows below vitrophyre in cliffs 0.6 km W. of Little 3-Cr. Lk. Map 3.
350. Blocky lava from basal flow of 6 flows below vitrophyre in cliffs 0.6 km W. of Little 3-Cr. Lk. Map 3.
351. Glassy base of glaciated lava at 7050' elev, 0.1 km W. of Snow Cr. Map 2.
352. Glaciated lava in bed of Snow Cr. at 7220' elev. Map 2.
354. Pumice bomb from base of welded tuff at 7360' elev, head of Snow Cr. Cirque. Map 2.
355. N.W. margin of glaciated flow from cinder cone, 7660' elev in head of Snow Cr. Cirque. Map 2.
356. Platy lava at 7840' elev, S.W. head of Snow Cr. Cirque. Map 2.
358. Pumice from cone at 7460' elev, crest of ridge W. of Snow Cr. Cirque. Map 2.
359. Lava from E. summit of glaciated cone capping ridge W. of Snow Cr. valley, N.E. sec 17. Map 2
360. Vesicular lava at 6060' elev, Park Meadow Trail, N.E. sec 7. Map 2.
361. Blocky lava at 6260' elev, Park Meadow Trail, center sec 7. Map 2.
362. Platy lava at 6560' elev in cliffs, W. side Park Meadow. Map 1.
363. Lava from cliffs at 6560' elev, 0.8 km N.N.E. of Golden Lk. Map 1.
364. Platy lava at 6600' elev on glaciated knoll, 0.6 km N. of Golden Lk. Map 1.
365. Platy lava at 6560' elev, 0.7 km N. of Golden Lk. Map 1.
366. Scoriaceous lava at 6320' elev between glaciated cinder cones, 0.6 km S. of Park Meadow. Map 2.
367. Platy lava at 6520' elev in bed of Squaw Cr., 1.0 km E. of Park Meadow. Map 2.
380. Lava cap on N.-S. ridge at 7720' elev, 1.3 km S. of Tam Lk. Map 2.
381. Large pumice lump from rampart at S.E. edge of S. dome in Devils Hill chain of domes. Map 7.
445. Pumiceous block from summit of N. dome in Goose Cr. chain of domes, 0.3 km W. of Map 4.
446. Glassy block from Newberry flow at 7260' elev, 0.5 km E. of source vent. Map 4.
447. Glassy block from S.W. margin of large central dome of Goose Cr. chain of domes, 0.2 km W. of Map 4.
448. Glassy block from N. margin of N. dome of Devils Hill chain of domes, 0.3 km W. of Map 4.
449. Spherulitic lava from W. wall of fissure, N.E. base of Devils Hill, 0.3 km W. of Map 4.
456. Lava from prominence at 7900' elev, S.E. side of S. Sister, 1.7 km W. of Green Lk. Map 1.
458. Lava from cleaver at 8600' elev at base of Prouty Glacier, N.E. side of S. Sister, 0.5 km W. of Map 1.
525. Spatter from S. rim of Talupus Bu., 0.6 km W. of Map 7.
526. Lava from glaciated cliffs at 5680' elev, N.W. side of Talupus, Bu., 0.6 km W. of Map 7.
529. Lava from summit of Devils Hill, 0.7 km W. of Map 4.
1000. Average Cayuse lavas. Analyses 7,20,21,22,23,24,30.
1001. Average of analyses 259,261,262 from Holocene lava and cone chain S.W. of Todd Lk.
1002. Average lava from cone at N. base of Bachelor Bu. Analyses 44,45.
1003. Average Bachelor Bu. Analyses 47,258,260.
1004. Average Newberry, Goose Cr., Devils Hill chains of domes. Analyses 26,28,269,271, 381,445,446,447,448.
1005. Average Ditch Cabin basalt. Analyses 111,295,299,300.
1006. Average Talupus and Katsuk Bu. lavas. Analyses 264,265,266,525,526.
1007. Average Golden Lk.-Green Lk. basaltic andesite. Analyses 193,198.
1008. Average Corral Lk.-Green Lk. basaltic andesite. Analyses 117,272.

1009. Average Rim Lk. basaltic andesite lavas. Analyses 147,148,149,202,359.
1010. Average basaltic andesite, upper shelves of 3-Cr. Lk. Analyses 152,153.
1011. Average basaltic andesite lavas and dikes of Tam Mac Rim and Snow Cr. Cirque. Analyses 158,171,173,176,346,348,349,450,352.
1012. Average basaltic andesite from cone on Broken Top E. ridge. Analyses 124,355.
1013. Average of 19 lavas from Broken Top volcano.
1014. Average Broken Top dikes. Analyses 112,119,121,125,167.
1015. Average Broken Top plug rocks. Analyses 81,101,102.
1016. Average lavas from cone S. of Ball Butte. Analyses 139,296,307.
1017. Average of 17 lavas, dikes, cinders from Tumalo Mtn. and associated cones.
1018. Average andesites, E. side S. Sister. Analyses 191,192,204,250,362,365,456,458.
1019. Average lower andesite flow and source dike, 7600' elev, W. Snow Cr. Cirque. Analyses 159,160.
1020. Average upper andesite flows, 7800' elev, W. Snow Cr. Cirque. Analyses 165,356.
1021. Average andesite W. of Corral Lk. Analyses 27,275.
1022. Average dacite from S.W. ridge of Broken Top. Analyses 115,273.
1023. Average andesite at head of ravine, W. sec 6, N. of Soda Cr. Analyses 286,287.
1024. Average basaltic andesites from Bare Lk. volcano. Analyses 8,11,12,15,16.
1025. Average high-silica dacite near 3-Cr. Lk. and Little 3-Cr. Lk. Analyses 175,341, 347.
1026. Average low-silica dacite near 3-Cr. Lk. and Little 3-Cr. Lk. Analyses 162,174, 343.
1027. Average dacite between Goose Cr. and Fall Cr. Analyses 29,263,268.
1028. Average 12 analysed lavas and 1 plug rock. Todd Lk. volcano.
1029. Average rhyodacite E. of Chambers Lks. Analyses 206,207,208.
1030. Average rhyodacite on N.W. Broken Top ridge. Analyses 194,197.
1031. Average Tam Mac Rim rhyodacite. Analyses 154,155,157.
1032. Average Devils Hill rhyodacite. Analyses 449,529.
1033. Average silicic tuff cone of upper N. Fork Tumalo Cr. Analyses 126,305.
1034. Average rhyodacite lava of upper N. Fork Tumalo Cr. Analyses 134,136,137.
1035. Average rhyodacite lava E. of Todd Lk. Analyses 4,5,41,297,298.

Taylor, 1978,

Ho	Holocene		Geologic contacts, dashed where covered
Ps	Pleistocene		
Bs	Basalt		Direction of flow of Holocene lavas
BA	Basaltic Andesite		
An	Andesite		Dikes, sills
Da	Dacite		
Rd	Rhyodacite		
La	Lava		Rim of craters
Pf	Fine pyroclastic deposits		
Pc	Coarse pyroclastic deposits		Trace of subsidence crater in Broken Top summit cone
Pt	Tuff cone deposits		
Id,s,p	Intrusive dikes, sills, plugs		Highest stand of Pleistocene glaciers
Pi	Ignimbritic deposits		
Al	Alluvium		
Gd	Glacial drift	30°	Strike and dip of strata
Ta	Talus		
Sn	Snow fields, glaciers	54	Location and number of analysed sample

Topographic base maps from U.S. Geological Survey, 1959. Contour interval 40 feet (12.2 meters). Geology by E. M. Taylor.

N

ONE MILE

ONE KILOMETER

FIGURE 13. LEGEND FOR 9 GEOLOGIC MAPS OF S.W. BROKEN TOP QUADRANGLE.

GEOCHEMICAL STUDIES OF ROCKS, WATER, AND GASES AT MT. HOOD, OREGON

OPEN-FILE REPORT O-79-2

Wollenberg and others.

FEBRUARY 1979

STATE OF OREGON

DEPARTMENT OF GEOLOGY AND MINERAL INDUSTRIES

LBL-7092 and
State of Oregon DOGAMI
Open File Report 0-79-2

GEOCHEMICAL STUDIES OF ROCKS, WATER, AND GASES AT MT. HOOD, OREGON

Harold A. Wollenberg[1]
Richard E. Bowen[2]
Harry R. Bowman[1]
Beverly Strisower[1]

February 1979

1) Lawrence Berkeley Laboratory, Earth Sciences Division
2) Consultant to State of Oregon, Department of Geology and Mineral Industries

TABLE OF CONTENTS

ABSTRACT

Mt. Hood, a composite andesitic volcano, located near Portland, Oregon, is one of several large eruptive centers which dominate the Cascade Mountains of the western United States. As part of a program of geologic, geophysical and geochemical studies to examine Mt. Hood's geothermal resource potential, samples of warm-and cold-spring water, water from a geothermal test well in Old Maid Flat, fumarolic gases, and rocks were collected and analyzed for major chemical constituents and trace elements.

The only warm-spring area on Mt Hood is Swim Springs, located on the south flank. Orifices at Swim were sampled repeatedly with little overall change noted in water chemistry between summer and winter. Oxygen and hydrogen isotope data and mixing calculations based on analyses of Swim Springs and numerous cold springs, indicate that a large component of the warm water at Swim is from near-surface runoff. Chemical geothermometry suggests that temperatures at depth in the Swim Springs system are within the range 104-170°C; the temperature of unmixed hot water may exceed 200°C. Higher-than-background chloride contents and specific conductances of cold springs on the south flank of the mountain suggest that there is a small component of thermal water in these sources.

A geothermal model of Mt. Hood is proposed wherein snow- and glacier-melt water near the summit comes in close proximity to the hot central "neck" of the mountain, manifested by the summit-crater fumaroles. The hot water migrates down-slope, mixing with cold water along its path; a small portion of the mixed warm water surfaces at Swim Springs.

We were surprised to detect the platinum-group element, iridium in warm and cold spring waters and in a sample of altered andesite. Iridium is generally considered to be associated with basic to ultrabasic igneous rocks; its association with an andesite volcano is believed to be without precedent.

ACKNOWLEDGEMENTS

The authors wish to express their appreciation to the following people for their valuable assistance on this project:

- Personnel of the State of Oregon's Department of Environmental Quality for use of earlier chemical analyses of waters in the Mt. Hood region;
- Jerry Black and Joseph Riccio of the State of Oregon's Department of Geology and Mineral Industries for assistance in collecting water samples;
- James Robison of the U.S. Geological Survey for aid in collecting samples and guidance on the hydrologic setting of Mt. Hood;
- Alfred Truesdell and Nancy Nehring of the U.S. Geological Survey for isotope analyses and analyses of constituents of fumarolic gases;
- David Johnson of the U.S. Geological Survey for aid in sampling and analyses of fumarolic gases;
- Steven Flexser of Lawrence Berkeley Laboratory for assistance in X-ray fluorescence analyses and Alan Smith of Lawrence Berkeley Laboratory for gamma-ray spectrometric analyses of radioelements.
- To Orah Goldman, the authors' thanks for many careful typings of text and tables.

This work was done under the auspices of the U.S. Department of Energy.

I. INTRODUCTION

Large volcanoes together with numerous smaller eruptive centers along the Cascade Mountains from Northern California into British Columbia (Figure 1) are evidence of a tremendous release of thermal energy along this zone. The geologic history of the Cascade Range indicates that eruptions and mountain building have taken place over a long period, and continue into the present. Mount Hood, located 80 km east of Portland (Figure 2), has a volcanic history similar to many of the other Cascade volcanoes. It has high-temperature fumaroles near its summit and a warm spring area on the south flank. These recognized thermal manifestations along with the mountain's accessibility and proximity to Portland, Oregon's main energy consuming region, make it a desirable location for the study and development of geothermal energy.

Over the past two years, a multidisciplinary study of the geologic, geochemical and geophysical features of Mount Hood that relate to the location of geothermal energy has been under the direction of the Oregon Department of Geology and Mineral Industries (DOGAMI) with funding from the U.S. Department of Energy. Earlier studies (Wise, 1968, 1969) described the geologic and tectonic framework of the region. Detailed geochemical and geophysical investigations are being conducted in the same area. A separate but related program of potential volcanic hazards of Mount Hood is being conducted concurrently by the U.S. Geological Survey (USGS) under the direction of D. R. Crandell.

Technical support of the geochemical studies of Mount Hood is supplied by the Earth Sciences Division of Lawrence Berkeley Laboratory (LBL). Geophysical studies consist of gravity and aeromagnetic surveys by Oregon State University, aerial infrared surveys by the USGS, and electrical

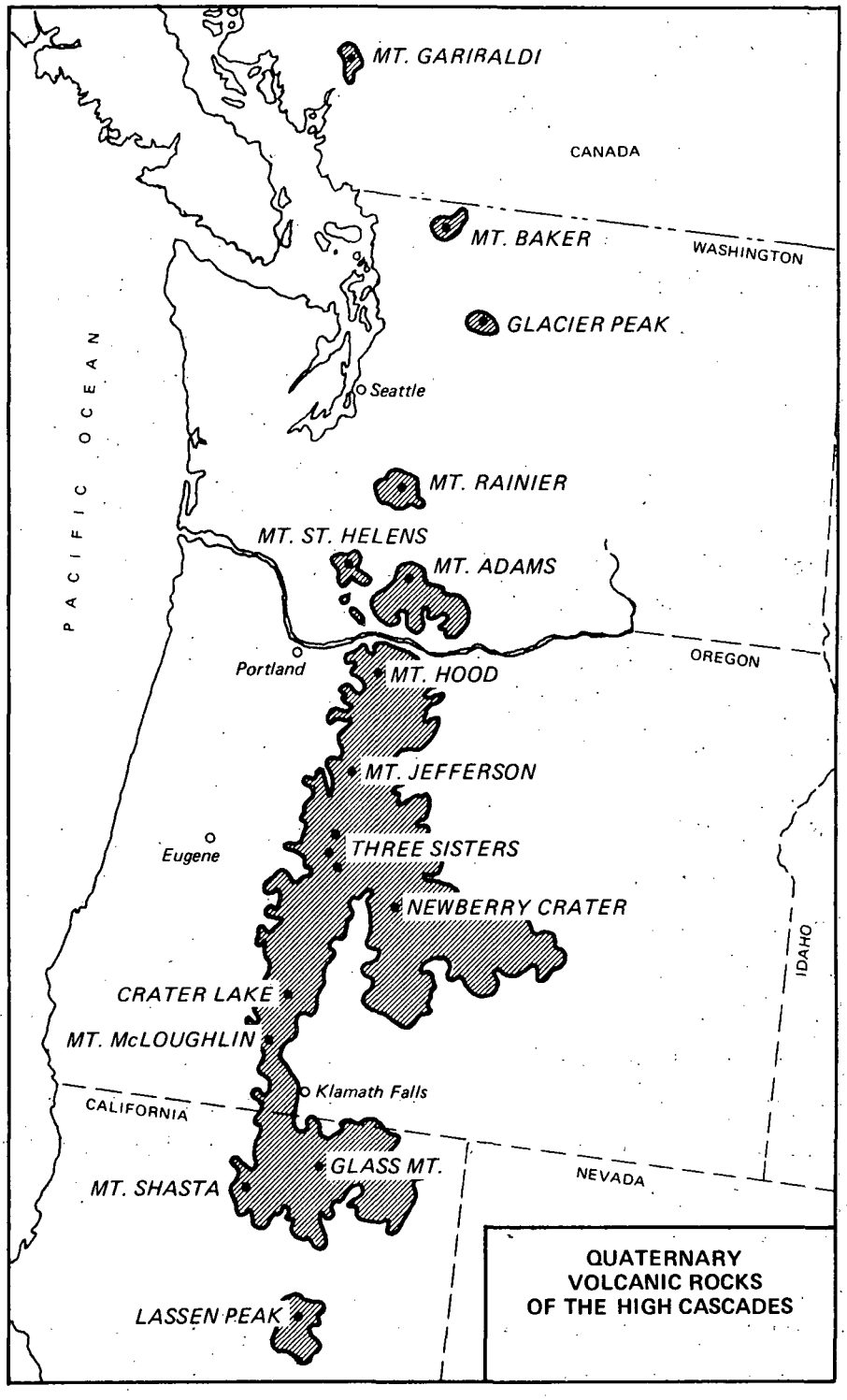

Figure 1. Regional geologic setting of Mt. Hood.

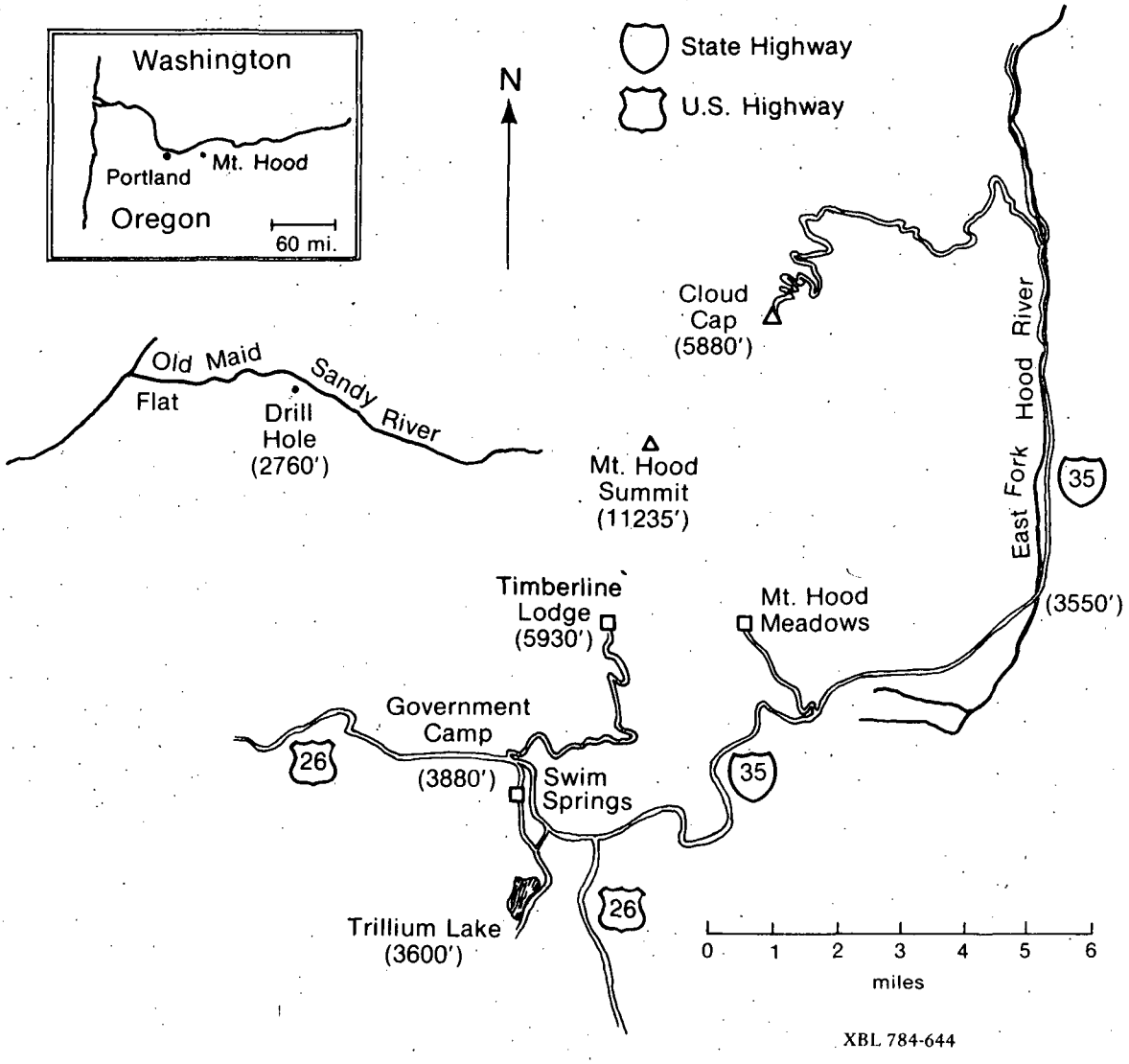

Figure 2. Location map, Mt. Hood area.

measurements by LBL (Goldstein and Mozley, 1978). Sampling and chemical analyses of rocks, gases, and ground waters in the area, including the fumaroles and the thermal and cold springs, has been a joint project between DOGAMI, USGS, and LBL. Suites of rocks typical of the area, both fresh and hydrothermally altered, have been analyzed to discern possible changes produced by the alteration. Selected water samples have been analyzed for oxygen and hydrogen isotope ratios to help determine the pathways water takes from its meteoric origin into and through the mountain's hydrologic system.

Analyses of waters from geothermal areas have proven to be very effective exploration tools. Truesdell (1975), in a comprehensive review, pointed out that several elements gave indications of minimum subsurface reservoir temperatures. The ratios between sodium, potassium, and calcium (Fournier and Truesdell, 1974) along with the silica content of warm-spring water may be definitive. A knowledge of silica contents and temperatures of cold and warm spring waters may be used to determine the amount of mixing of nonthermal waters and the reservoir temperatures before mixing.

This report emphasizes the presentation of analytical data obtained prior to October 1978. Since sampling and analyses have continued beyond that time, interpretative comments in this report are necessarily brief and should be considered as preliminary. A more detailed interpretation of the data awaits the results of continuing field sampling and laboratory analyses.

A. Geologic Setting

The regional setting of Mt. Hood is shown in Figure 1. Mt. Hood is a composite andesitic stratovolcano rising approximately 2500 meters above the surrounding terrain. It is largely Pleistocene in age with the main body of the cone constructed prior to the onset of Fraser Glaciation, about 20,000 years ago (Wise, 1968). Renewed volcanism took place about 12,000

years ago with the extrusion of several domes near the summit (Crandell and Rubin, 1977). Further episodes of extrusions near the summit about 1,600 years ago produced a series of hot avalanches that culminated in the collapse of the south rim of the crater which then topped the mountain. The collapse of the south crater wall resulted in a large debris fan that covers the south flank of the mountain (Wise, 1968). The most recent major eruption took place about 220 years ago from the Crater Rock area. At that time a series of hot avalanches cascaded down the east and west sides of the mountain, carrying incandescent debris several miles down the valleys (Crandell and Rubin, 1977). Historical eruptions were reported in 1859 and 1865 (Folsom, 1970).

Mount Hood is located along a linear trend with most of the other Cascade volcanoes of Oregon and Washington. Thayer (1937) and Callaghan (1933) have associated the lineation with a fault zone they recognized along the western edge of the High Cascades. Allen (1965) believes that the volcanoes are concentrated in a graben formed by the Hood River-Green Ridge faults on the east and the unnamed faults of Thayer and Callaghan on the west. The western fault has not been recognized in the Mount Hood area but recent drilling on the west side of Mount Hood at Old Maid Flat shows there is significant displacement of the Columbia River Basalt that may be caused by faulting.

The local geologic setting of Mount Hood is illustrated in Figure 3 (Wise, 1968). The predominant surficial material is clastic debris, of andesitic character. A plug dome of hornblende andesite, Crater Rock, was extruded about 2,000 years ago. The extensive lava flows which predated the clastic debris were predominantly hornblende andesite, while more recent extrusions on the north and northeast flanks were of olivine basalt and olivine andesite.

GEOLOGY OF THE MT. HOOD AREA, OREGON

Explanation

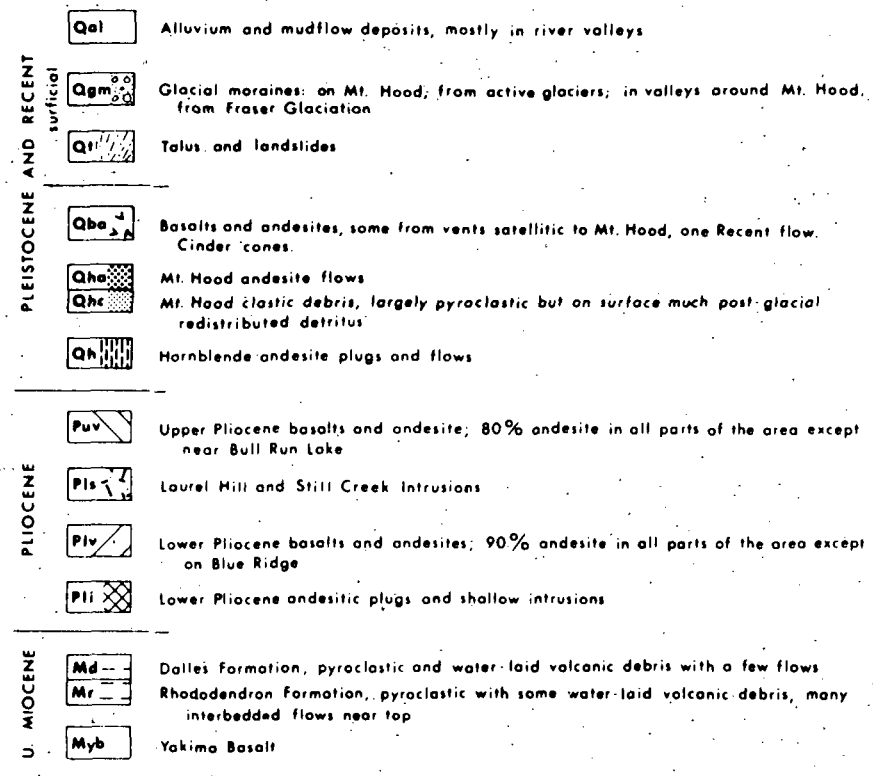

⊘ *Surface water samples*

○ *Cold spring samples*

⊕ *Well samples*

● *Warm spring samples*

▲ *Rock samples*

XBL 788-2661A

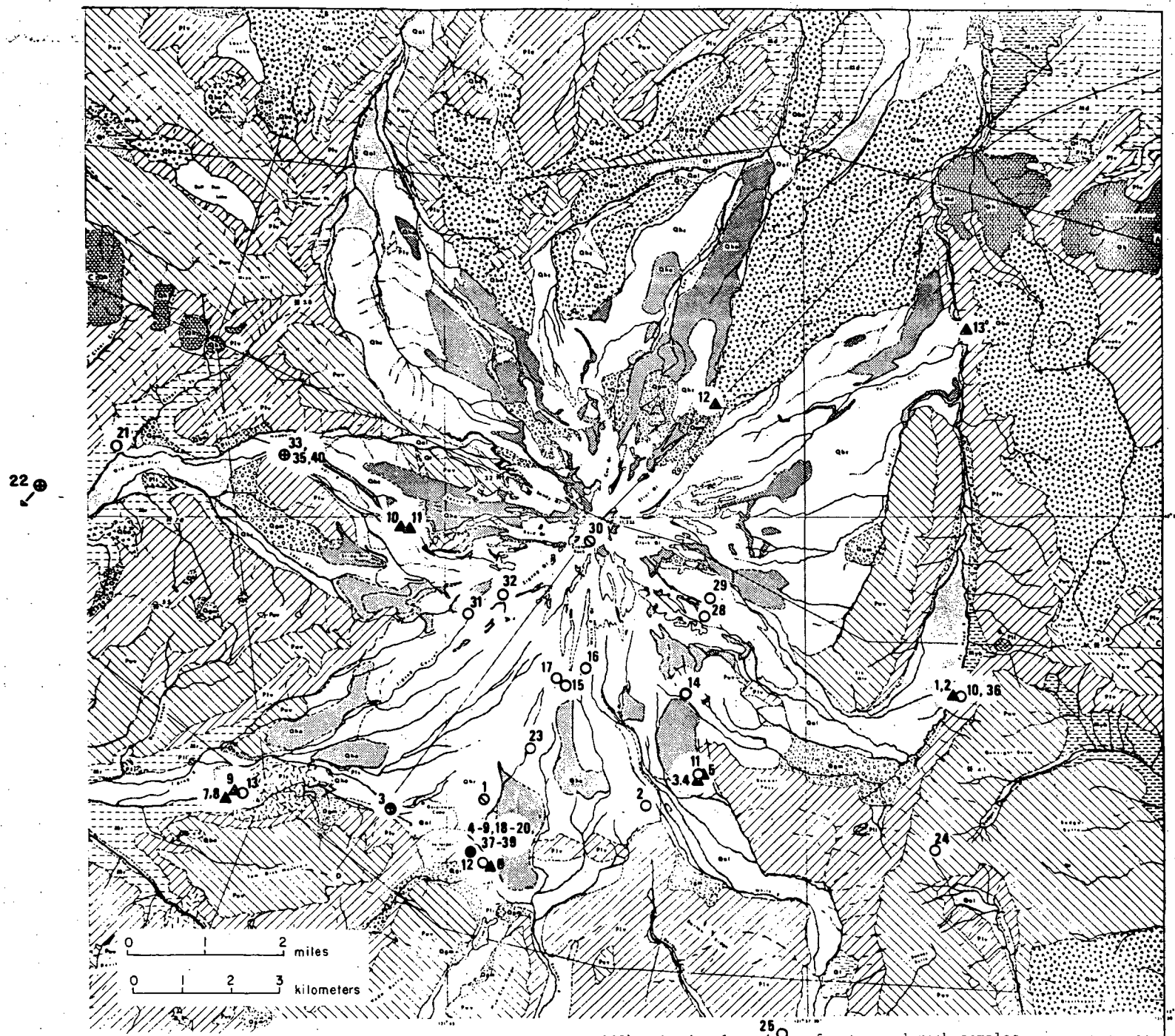

Figure 3. Local geologic setting of Mt. Hood (after Wise, 1968), showing locations of water and rock samples. XBL 788-2661

B. Hydrologic Setting*

Mt. Hood lies along the axis of the Cascade Range, and receives most of its precipitation during the fall and winter from storms that originate in the north Pacific and move southward and eastward across the range. The average annual precipitation is about 102 cm at Portland and increases to the east, to a maximum near the crest of the range. Records of the National Weather Service show that at Government Camp (Figure 2) the average is about 230 cm. Precipitation decreases rapidly to the east and is only 25 cm within 50 km of the crest.

Precipitation falling above an altitutde of about 1,500m on Mt. Hood is inferred to be within a recharge area, and ground water tends to move downward (Figure 4). The transition from recharge to discharge area is manifested by a band around the mountain where springs tend to discharge, and below which perennial streams are common. Above the band, many streams are intermittent; in smaller channels there is runoff only during spring, from melting snow.

At depths ranging to at least 250m in the vicinity of Timberline Lodge, ground water occurs in perched zones between or within andesite flows. The warm water emanating at Swim Springs may have circulated deeper than some of the perched zones, probably originating at elevations higher than Timberline Lodge. The water comes to the surface at Swim, where there is an abrupt flattening of the topographic slope (Figure 4); Mt. Hood andesite flows tend to dip down the mountain, and some permeable zones may intersect the land surface here. The Swim area also lies near a contact between Mt. Hood andesite flows or andesite debris and pre-Mt. Hood andesite and basalts (Wise, 1968); these older rocks are less permeable and may tend to direct ground water to the surface.

* Written in consultation with James Robison, U.S. Geological Survey, Menlo Park, California.

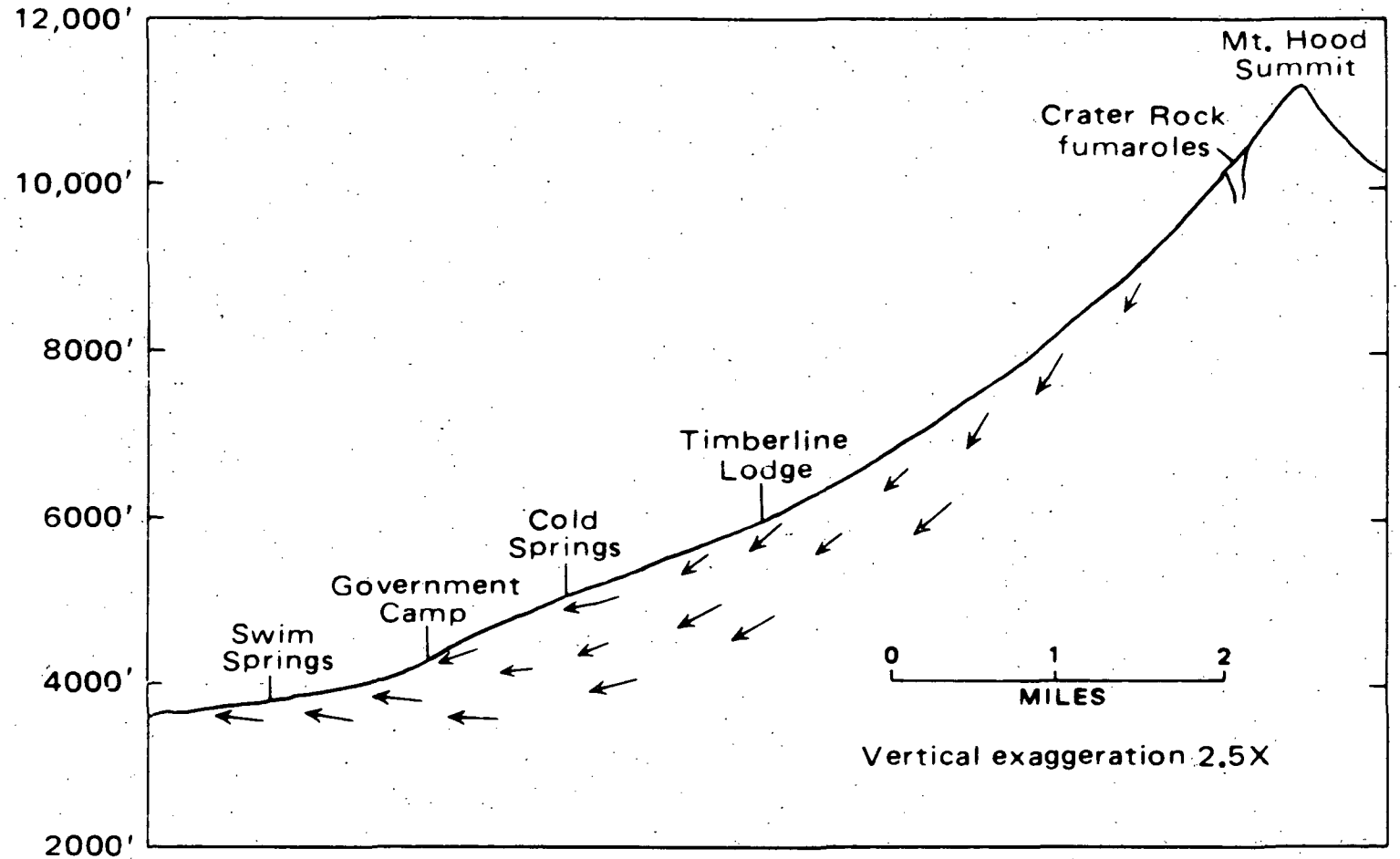

Figure 4. Inferred ground water movement on Mt. Hood.

Distribution of runoff of streams draining Mt. Hood corresponds to that of precipitation. Records of a gauging station on Salmon River, 7 miles southeast of the summit of Mt. Hood (east of Trillium Lake near highway U.S. 26) show an average runoff of about 80 cm per year for the drainage area above the gauge. Sandy River has a runoff of 178 cm above a gauge 30 km west of the summit, and the West Fork of the Hood River has a runoff of 203 cm above a station 26 km northeast of the summit. The greatest runoff in the Mt. Hood area is reflected at a station on Bull Run River, 29 km northwest of the summit, where the average is more than 305 cm. The component of any deeply-circulating ground water in most of the springs is probably very small because the runoff is large.

II. SAMPLING AND ANALYSES

Techniques used by LBL to sample waters and rocks and to analyze them for major and trace elements have been detailed in papers by Bowman and others, (1975), Hebert and Bowman (1975), and Wollenberg (1975). In this section we shall briefly describe those techniques and the techniques to determine oxygen and hydrogen isotope ratios and constituents of fumarolic gases.

A. Water

Water samples were collected at the locations shown in Figure 3; locations are referenced by latitude and longitude in Table 1. Samples included waters from cold springs and wells, the Swim Warm Springs on the south flank of the mountain (the distribution of orifices at Swim is detailed in Figure 5), and the well drilled for geothermal water on the western flank of Mt. Hood in Old Maid Flat. Samples were collected for laboratory radiometry, X-ray fluorescence, neutron activation, and mass-spectrometric analyses. For analyses of major and trace elements, sampling was done by inserting a 1/4-inch diameter tygon tube into a spring. The water was drawn

Table 1

DESCRIPTION AND LOCATION OF WATER SAMPLES

MH-1	Still Creek, crossing with Timberline Road, 0.4 mi. N. of Highway 26 junction. 45°18.1′N, 121°43.8′W.
MH-2	Spring, White River outwash; streambed strongly iron-stained. 45°18.2′N, 121°40.4′W.
MH-3	Ski Bowl, artesian well head. 45°18.1′N, 121°46.0′W.
MH-4	Swim area, "Pipeline Spring." 45°18.0′N, 121°44.6′W.
MH-5	Swim area, "Screen Spring." 45°17.9′N, 121°44.5′W.
MH-6	Swim area, east side of old swimming pool. 45°17.9′N, 121°44.6′W.
MH-7	Swim area, cistern box upstream from pool. 45°17.9′N, 121°44.6′W.
MH-8	Spring, swim area, ~100m upstream from cistern box. 45°18.0′N, 121°44.6′W.
MH-9	Swim area, northernmost spring on west branch creek. 45°18.1′N, 121°44.7′W.
MH-10	Robin Hood Quarry, small spring in central bench. 45°20.1′N, 121°34.1′W.
MH-11	Spring, roadcut on north side of Highway 35. 45°18.6′N., 121°39.6′W.
MH-12	Spring, roadcut/quarry, north side of Highway 26, 1/3 mi. NW Trillium L. turnoff. 45°17.4′N, 121°44.0′W.
MH-13	Spring, roadcut on Highway 26, above Laurel Hill Quarry. 45°18.4′N, 121°49.6′W.
MH-14	Spring, Mt. Hood Meadows below Timberline Trail. 45°20.3′N, 121°40.1′W.
MH-15	Salmon River Canyon Springs. 45°19.9′N, 121°42.2′W.
MH-16	Spring, White River Canyon. 45°20.1′N, 121°41.9′W.
MH-17	Spring, from andesite flow. 45°20.1′N, 121°42.9′W.
MH-18	"Pipeline Spring." Same location as MH-4.
MH-19	Swim area, "Screen Spring." Same location as MH-5.
MH-20	Swim area, "East side of Pool." Same location as MH-6.

Table 1 (continued)

MH-21	"Iron Spring" near bridge over Clear Creek. 45°23.5′N, 121°51.5′W.
MH-22	Slightly artesian well, Clear Creek picnic ground. 45°21.4′N, 121°56.2′W.
MH-23	Spring area below Timberline Lodge. 45°18.9′N, 121°42.9′W.
MH-24	Spring at Camp Windy. 45°24.7′N, 121°32.8′W.
MH-25	Clinger Springs. 45°16.4′N, 121°45.9′W.
MH-28	Spring on Timberline Trail, 5700 feet elevation. 45°20.0′N, 121°39.6′W.
MH-29	Cold Spring. 45°21.7′N, 121°39.6′W.
MH-30	Runoff, small lake in crater area. 45°22.1′N, 121°41.9′W.
MH-31	Spring, base of lava flow, Zigzag Canyon. 45°20.9′N, 121°44.1′W.
MH-32	Spring, base of Mississippi Head. 45°21.2′N, 121°43.6′W.
MH-33A	Old Maid Flat, NWNG Co., test hole, artesian flow, 4 days after cessation of drilling. 45°23.4′N, 121°48.5′W.
MH-33B	Old Maid Flat, NWNG Co. test hole, artesian flow, second sampling, several days later. Same location as MH-33A.
MH-35	Old Maid Flat, NWNG Co., test hole, artesian flow, sample after well had been shut-in for ~1 week. Same location as MH-33A.
MH-36	Robin Hood Quarry, same spring as in MH-10 sample.
MH-37	Swim area, east side of large pool. Same location as MH-6.
MH-38	Swim area, "Screen Spring." Same location as MH-5.
MH-39	Swim area, "Pipeline Spring." Same location as MH-4.
MH-40	Old Maid Flat, NWNG Co., test hole, artesian flow for ~36 hours following MH-35 sampling. Same location as MH-33A.

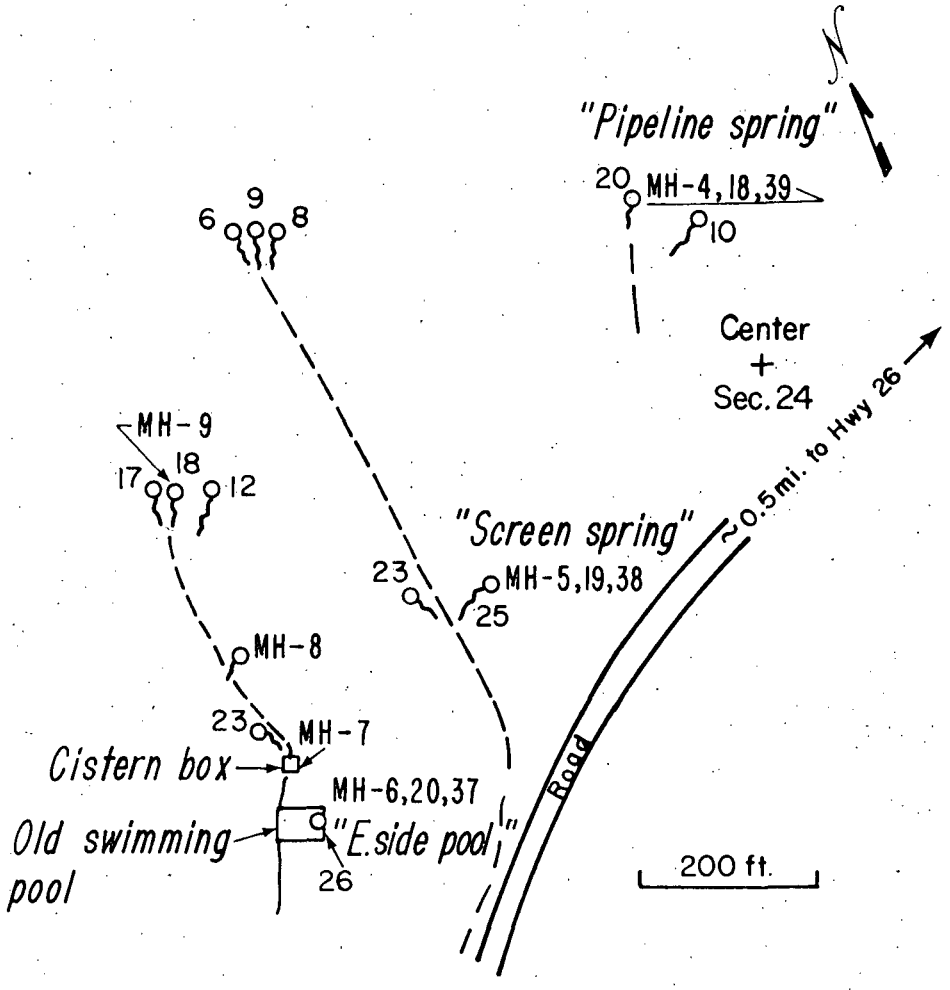

Legend:

15 Spring location with temperature (°C)

MH-7 Sample number

——— Stream

Location map, sampling sites and other springs in Swim Warm Springs area, (Sec.24, T3S., R.8½E.)

XBL 788-2660

Figure 5. The distribution of water sources at Swim Warm Springs.

through a 0.45 micron filter, using a hand-operated vacuum pump; the apparatus is shown in Figure 6. Most often, the water was introduced to the filter directly from the spring, but occasionally conditions required that samples be obtained in bottles and then filtered by pumping from the bottle in the field or laboratory. Generally, 500-ml "Nalgene" bottles were used to collect and store the samples. At the sampling site the pH of the water was measured using a color comparitor set and specific conductance measured by a portable electronic unit. Chloride contents were estimated on-site by immersing "Quantab" strips in spring or well waters.

In the laboratory the water samples were evaporated in the original collecting bottles at 80°C, and aliquots of each were taken for both neutron activation analysis and X-ray fluorescence analysis. In general, the X-ray fluorescence measurements determined the major element abundances, while neutron activation was used for the trace and minor elements. Some elements were determined by both methods so that cross-checks could be made.

For neutron activation, evaporates from water samples were made into pellets and irradiated, along with a composite standard pellet, in the TRIGA Research Reactor at the University of California, Berkeley. Nearly all elements in the samples have their counterparts in the standard, and the abundances are determined by comparing the gamma rays emitted from the unknowns with the gamma-ray spectra of the standards. This method is capable of quantitatively analyzing nearly 50 elements in a sample.

The X-ray fluorescence technique used in this study was developed by Hebert and Street (1974). In this method the evaporates were mixed with $LiBO_2$ and fused into glass discs. The major elemental abundances were determined by comparing these samples (indirectly) with USGS standard rock DTS, spiked with MgO, NaCl, $CaSO_4$ and K_2CO_3.

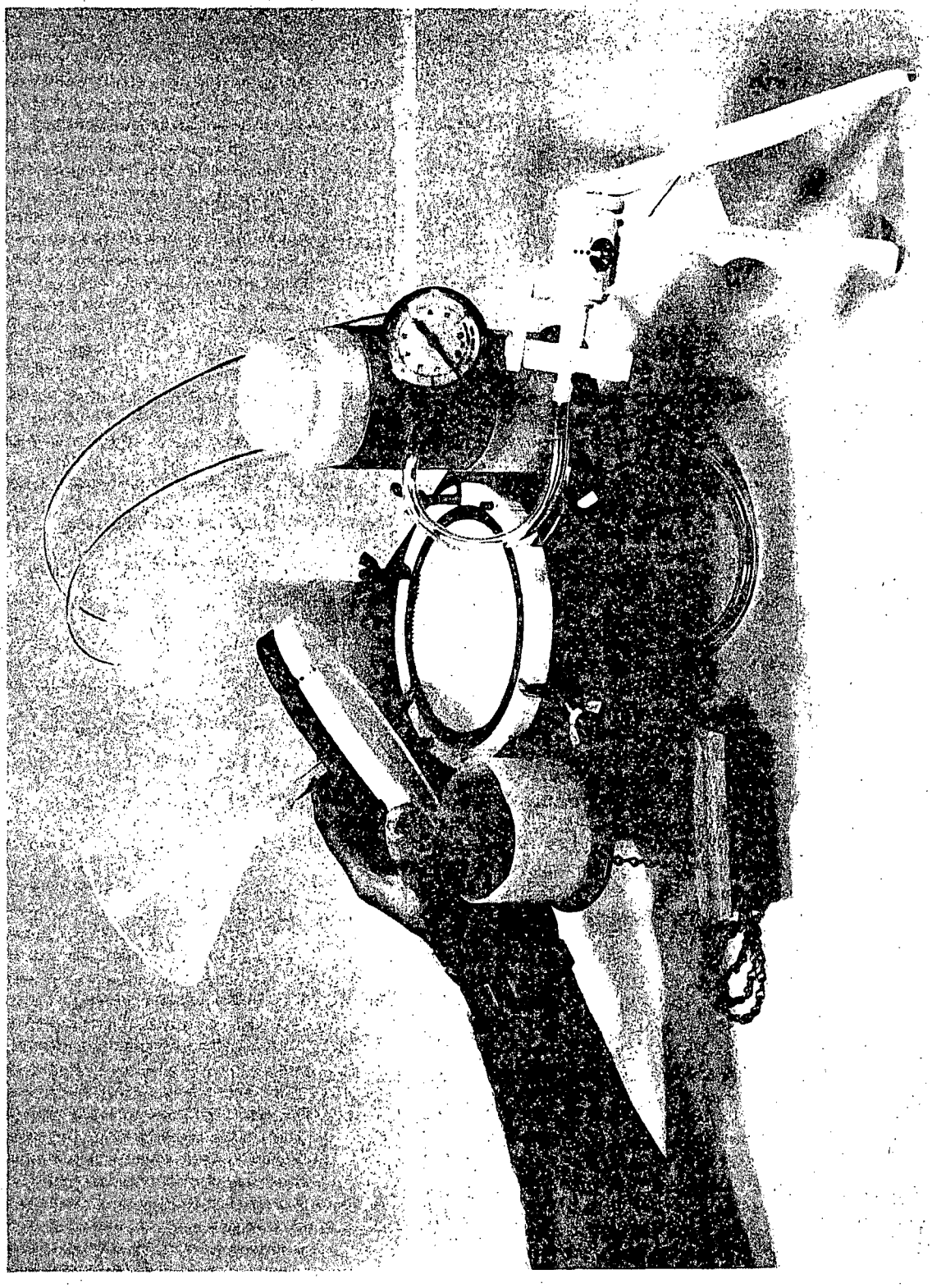

CBB 7410-7354

Figure 6. The filtering apparatus and hand pump used to collect samples in this study.

The precision of the neutron activation method depends mainly on the statistics of gamma-ray counting of the activated samples; for most elements analyzed precisions were of the order of a few percent of the abundance. Precisions and accuracies of X-ray fluorescence determinations of major elements were also a few percent of element abundances.

Samples for laboratory determination of ^{222}Rn were usually collected by filling "Nalgene" bottles with the spring water directly from the pools. This minimized radon loss which might occur if the water were drawn through the filter system. Bottles were immediately sealed, lids taped, and samples transported to the laboratory for gamma-ray pulse-height analyses. The time of sampling was noted to account for the radioactive decay of ^{222}Rn (3.8-day half-life) between sampling and gamma counting. With a reasonably short interval between sampling and counting, the sensitivity of this method is of the order of a few tens of pCi per liter of ^{222}Rn.

Samples for oxygen and hydrogen isotope determinations were obtained by filling 50 ml glass bottles directly with spring water. The bottles were tightly capped, taped, and sent via the U.S. Geological Survey, Menlo Park office, to the analytical laboratories at Saclay, France, where oxygen-16/oxygen-18 ratios and deuterium/hydrogen ratios were measured by mass spectrometry.

B. Rocks

Rock types sampled included altered and relatively fresh andesite and basalt from the flanks of Mt. Hood, a felsic dike in the Hood River Valley, and granodiorite and diorite from the Laurel Hill intrusive. Locations are shown in Figure 3, and listed in Table 2. Samples, each of the order of a kilogram, furnished adequate material for gamma spectrometric determination of uranium and thorium. At several locations gamma-ray counting rates were measured with a portable sodium-iodide crystal.

Table 2

DESCRIPTION OF ROCKS AND LOCATION OF SAMPLES

Mount Hood Rocks:

1. Felsic dike, Robin Hood Quarry
2. Basalt, Robin Hood Quarry
3. Altered Mt. Hood andesite breccia
4. Felsite dike, chloritized, with sulfide minerals
5. (pre?) Mt. Hood andesite
6. Platy Mt. Hood andesite
7. Granodiorite (?), Laurel Hill intrusive
8. Diorite (?), Laurel Hill intrusive

   } Laurel Hill Quarry

9. Altered diorite (?), Laurel Hill intrusive
10. Pliocene hornblende andesite, Sandy River
11. Altered andesite, Sandy River
12. Microporphyritic olivine andesite, Cloud Cap
13. Pliocene hornblende andesite, Hood River Canyon (Polallie Campground)

Neutron activation and X-ray fluorescence techniques for analysis of rock samples have been described, respectively, by Perlman and Asaro (1969) and Hebert and Street (1974). Crushed rock samples were pulverized and powders pelletized for reactor irradiation, and fused with lithium borate into glass discs for X-ray fluorescence. With these techniques 25 to 30 elements were determined with precisions of less than 5%; a number were determined to better than 1%.

C. Gases

Gas samples were obtained from fumaroles in the summit crater area of Mt. Hood. Three fumaroles were sampled, one of which was most likely a fumarole sampled previously by Ayres and Creswell (1951). The samples were collected by inserting the end of an $\sim$1.5m-long stainless-steel tube into the fumaroles and allowing the gas to pass into evacuated 300 ml glass bottles containing $\sim$100 ml of 4N NaOH solution. The filled bottles were transported to the laboratory of Dr. A. H. Truesdell, U.S. Geological Survey, Menlo Park, California, where they were analyzed by wet chemical methods for CO_2 and H_2S and by gas chromatography for other constituents. Sampling and analytical procedures have been described in detail by Truesdell and Nehring (1978).

III. RESULTS

Analytical data on water, rock, and gas samples are presented and preliminary interpretations discussed.

A. Water Analyses

1. Major and Trace Elements

For the purposes of this discussion, results of analyses of element contents of water are divided into two groups: those from the Swim Warm

Springs and those from the predominantly cold-water sources elsewhere in the Mt. Hood region. Three analytical laboratories are represented in this study: the Lawrence Berkeley Laboratory, the Central Laboratory of the U.S. Geological Survey, Denver, and the State of Oregon's Division of Environmental Quality.

a. Swim Warm Springs

Results of chemical analyses from successive samplings of Swim Warm Springs are presented in Tables 3a and 3b. Locations of individual orifices are shown on the map, Figure 5. Spring temperatures and the abundance of major and trace elements generally follow a geographic distribution, with the southernmost spring, "East side of pool," being warmest and having the highest chemical contents. Element abundances and temperatures are progressively lower in the "Screen" and "Pipeline" springs, which are respectively up-slope from the "East side of pool" spring. The up-slope decrease of temperature and element content is repeated in the sample sequence MH6 through MH9, from orifices along the small stream entering the pool from the northwest. The successive decreases of temperature and element content suggest that the water at "East side of pool" is the least diluted by mixing with near-surface cold waters. This suggestion is supported by data shown in Figure 7, where major- and trace-element contents are plotted against sodium. In most cases there is a linear relationship between element abundances, with the warmer springs having higher contents. Least-squre linear regression coefficients exceed 0.96 for Na versus Rb, Cs, Cl, Br and K. The strong linear correlations indicate appreciable mixing between warm and near-surface cold waters. The geochemical mixing model, discussed more fully in section III-e, indicates that over 90% of the water emanating at Swim is near-surface cold water.

Table 3a

SWIM WARM SPRINGS

	Successive Samplings										Single Sampling		
Spring	"PIPELINE"			"SCREEN"			"E. SIDE OF POOL"						
Sample	MH-4	MH-18	MH-39	MH-5	MH-19	MH-38	MH-6	MH-20	USGS	MH-37	MH-7	MH-8	MH-9
Date	6/2/77	8/22/77	2/22/78	6/2/77	8/22/77	2/22/78	6/2/77	8/22/77	8/22/77*	2/22/78	6/2/77	6/2/77	6/2/77
pH	7.5	7.5	7.5, 7.5	7.5	7.4	7.5, 7.1	7.5	7.1	7.3	7.3	7.5	7.4	7.5
Temp. °C	22	21.8	21.6	25	23.5	25.5	26	24.1	26.5	26.2	20	21	19
Sp. Cond.			820			1000			1300	1160			
									*(Robison)				
					mg/ℓ								
B	2.0	1	0.5	1.0	3	0.5	3.0	2	0.15	0.5	1	2	0.2
Na	92	84	92	95	101	105	120	114	120	126	86	62	36
Mg	34	36	38	36	30	43	40	40	51	50	30	20	13
SiO_2	75	70	75	75	91	78	80	71	92	88	70	80	60
S	54	54	58	62	65	72	63	68	~80	74	52	48	26
Cl	110	110	102	120	125	135	140	140	170	154	95	80	25
K	7.5	6	7	8	7	8	9.2	7.2	12	9	7.2	6.4	3.6
Ca	50	52	53	55	62	60	60	58	64	64	42	41	19
					µg/ℓ								
Mn	<4	<0.7	3	<5	<4	<3	<7	<5	50	<3	<6	<2	<1
Fe	70	35	(50	27	50	<12	47	<50	220	<25	18	14	14)
Ba	15	26	21	27	28)	22	37	24		27)	17	21	11
Mo	4	<2	3	3	<1.6	<5	4	<4		<7	4	5	2
Rb	17	15	17	18	19	20	23	23		23	16	14	7
Cs	0.25	0.26	0.25	0.31	0.32	0.33	0.38	0.34		0.4	0.25	0.20	0.10
Co	<0.03	<0.03	-	<0.06	<0.03	-	<0.06	<0.03		-	<0.02	<0.02	<0.02
Sb	<0.05	<0.04	<0.06	<0.03	<0.03	<0.02	<0.03	<0.05		<0.1	<0.03	<0.06	<0.02
Cr	<0.7	<0.3	<0.5	<0.7	<0.5	<1	<0.7	<0.1		<5	<0.5	<0.5	<0.4
Zn	<10	1.5	2	<10	2	3	<10	4		3	<10	<5	<5
Ag	<0.06	<0.05	<0.2	<0.06	<0.14	<0.1	<1	<0.2		<0.1	<0.1	<0.06	<0.03
Ce	<0.6	-		<0.6	-			<0.9	-		<0.7	<0.6	<0.3
Sm	0.087	0.03	<0.06	≤0.047	0.06	<0.06	0.105	0.139		<0.06	0.09	0.075	0.03
Eu	<0.011	<0.004	<0.005	<0.013	<0.006	<0.005	<0.014	<0.006		<0.006	<0.012	<0.015	<0.005
U	0.87	0.8	1.1	1.2	0.8	1.2	1.4	1.6		1.3	0.45	0.6	0.2
Ir	<0.0013	<0.0001	<0.0010	≤0.0015	<0.0001	<0.0014	≤0.0012	<0.0001		0.007	≤0.0013	≤0.0012	<0.0003
As	<8	<2	<5	<8	<3	<5	<8	<36		<5	<8	<5	<3
Br	200	134	180	220	180	220	270	280		240	180	148	48
W	<2	<1	<2	<1.5	<1	<2	≤4	<7		<2	<1	<2	<1
Sc	0.02	<0.01	0.022	0.02	0.018	<0.009	0.03	<0.01		0.015	0.014	0.012	0.010
Hf	<0.10	<0.05	<0.006	<0.12	<0.03	<0.03	<0.9	<0.07		<0.03	<0.6	<0.06	<0.010
Th	<0.02	<0.02	<0.005	<0.02	<0.02	<0.015	<0.05	<0.04		<0.10	<0.012	<0.012	<0.010
^{222}Rn (picocuries/ℓ)	172						156			161		186	

Table 3b

SWIM WARM SPRINGS

(Analyses in milligrams per liter, by
State of Oregon, Department of Environmental Quality)

Location*	Pipeline	Screen	E. Side of Pool	E. side of Pool	W. side of stream 50'N of cistern
Date	12/2/76	12/2/76	8/13/76	12/2/76	11/4/75
pH	7.3	7.3	8.1	7.5	7.4
T (C°)	20	25	26.1	25.6	--
Conductance	871	1190	1265	1300	907
Alkalinity (total as $CaCO_3$)	116	157	74	179	121
Hardness (as $CaCO_3$)	253	310	357.0	357	258.2
B	0.28	0.40	0.32	0.32	0.34
Na	79.0	114.0	98.0	136.0	79.0
Mg	29.0	44.0	28.0	48.0	40.0
SiO_2	55.4	71.6	65.5	72.3	52.1
SO_4	149.0	193.0	227.0	205.0	181.1
Cl	103.0	139.0	160.0	161.0	90.0
K	6.0	10.0	10.2	11.7	9.2
Ca	42.0	57.0	27.0	60.0	46.0
Mn	<0.05	<0.05	<0.05	<0.05	0.10
Fe (total iron)	0.05	<0.05	0.2	<0.05	<0.05
As	<0.005	<0.005	<0.005	<0.005	0.04
F	0.15	0.23	0.27	0.23	0.20
PO_4 (soluble ortho.)	0.09	0.08	0.10	0.09	0.12
Al	<0.01	<0.02	<0.02	<0.02	<0.01
Nitrogen (NH_3)	0.06	0.09	<0.01	0.05	0.03
Nitrogen (nitrite)	<0.02	<0.02	<0.02	<0.02	<0.01
Nitrogen (nitrate)	0.04	0.04	<0.02	0.03	0.01
Li	0.08	0.12	0.12	0.13	0.09
HCO_3	141	191	90	218	148

* Refer to map, Figure 5.

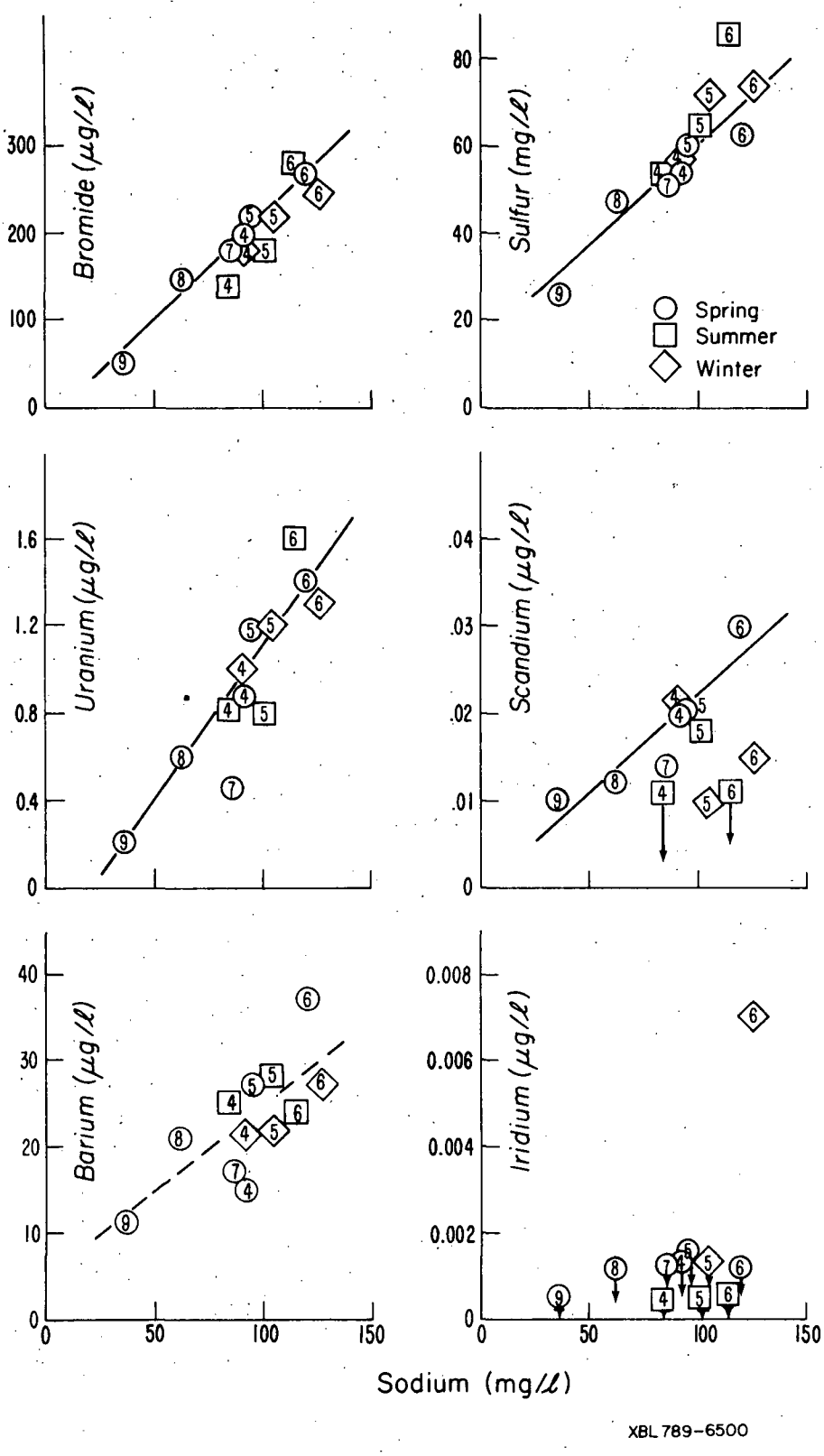

Figure 7a. Major- and trace-element contents of water from Swim Warm Springs, plotted against sodium.

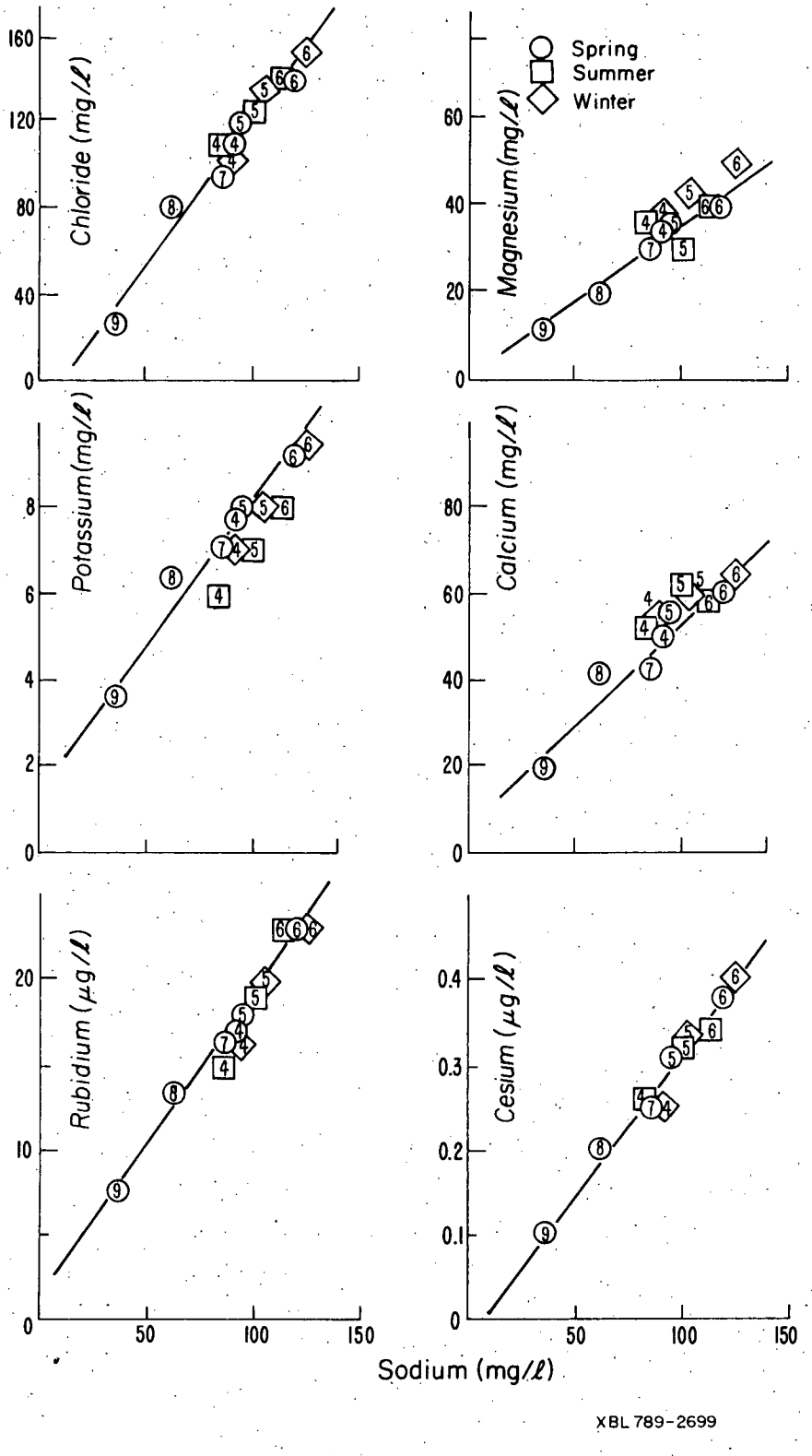

Figure 7b. Major- and trace-element contents of water from Swim Warm Springs, plotted against sodium.

The variation with time of element contents of three orifices at Swim is illustrated in Figure 8. Significant winter increases were observed in Mg and S at all three orifices, while Cl, Cl/B, Ca and Cs were greater in the winter at two of the orifices, and SiO_2, Na, Rb, and U were greater at one (but not necessarily the same) orifice. There were significant winter decreases in B at all three orifices, and in Cl, Ba, U and Br at one or another orifice. It was expected that winter samplings would yield higher contents because the surface runoff would be diminished. However, this was not substantiated because of the increase of some elements and decrease of others in the winter, with respect to the summer samplings.

The presence of the platinum-group element, iridium (0.007 µg/ℓ), in the winter sample from "East side of pool" is of interest, especially because it was not detected in the summer samples from that orifice. There were no other differences of this order in trace element abundances between summer and winter samplings. Iridium was also detected, in lower concentrations, in two cold-water sources: the iron-rich spring in White River Valley (MH 2), and the outflow of the small lake in the summit crater (MH 30). Silver is present along with iridium in these and other springs, and in the summit crater lake. A search of geochemical literature reveals that this is the first evidence of a platinum-group element being detected in geothermal or surface fresh waters.

b. Cold Springs and Wells

Results of specific conductance and chloride contents, measured in the field, are shown on Figure 9. Springs and surface waters sampled in the drainages of Still Creek, Salmon River, White River and the spring at Mt. Hood Meadows have greater abundance of Cl, and higher specific conductance than springs sampled to date on the north flank of Mt. Hood. Waters from 22 cold sources, 20 of them springs, were analyzed for major and trace elements; results of analyses, pH, and temperature measurements are listed in Table 4. With a few exceptions, the cold springs issue from andesite;

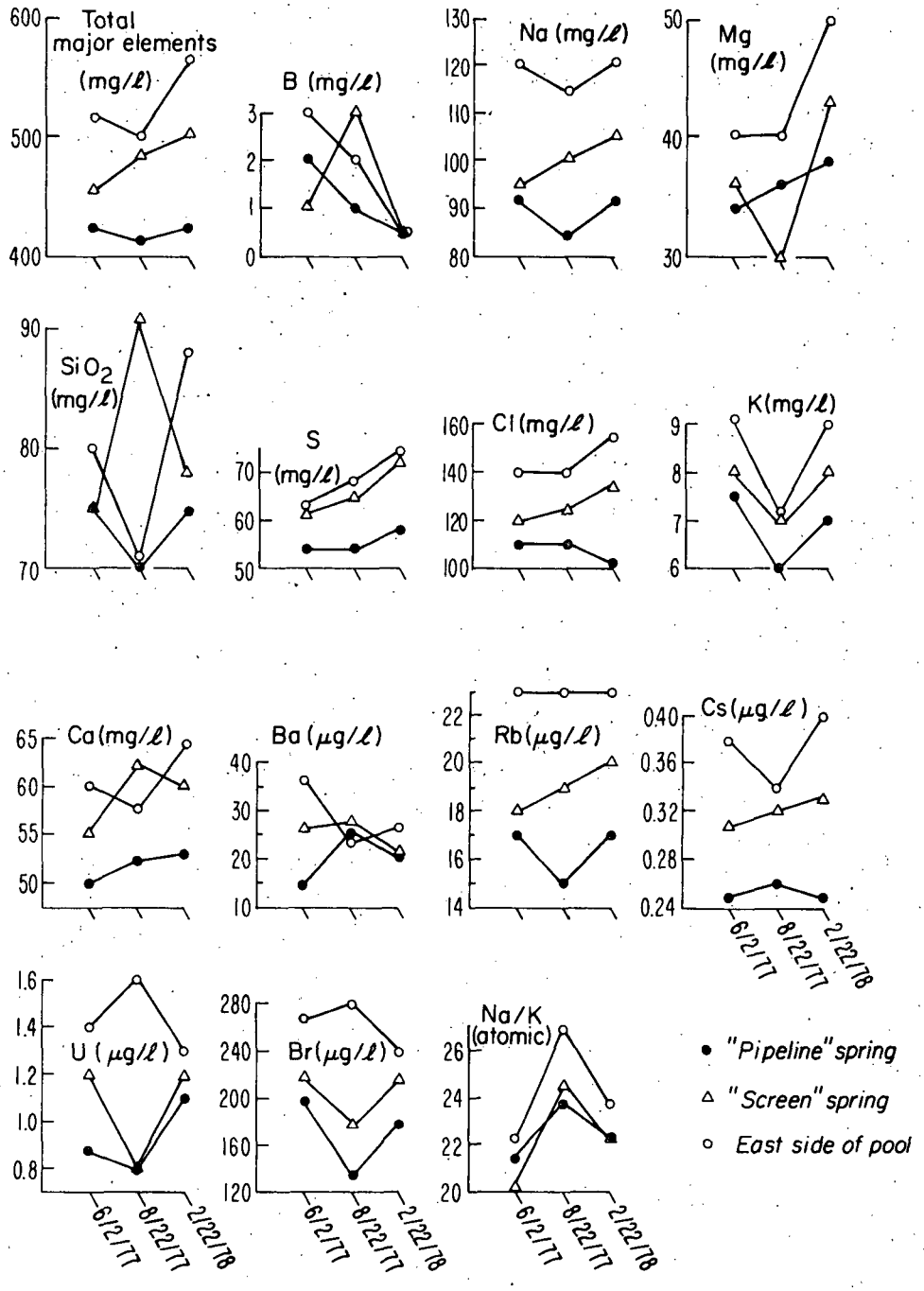

Variation in major and trace-element contents from successive samplings of three orifices at Swim Warm Springs 6/2 and 8/22/77, and 2/22/78.

XBL 789-6505

Figure 8. Element content variations with time at the three orifices at Swim Warm Springs.

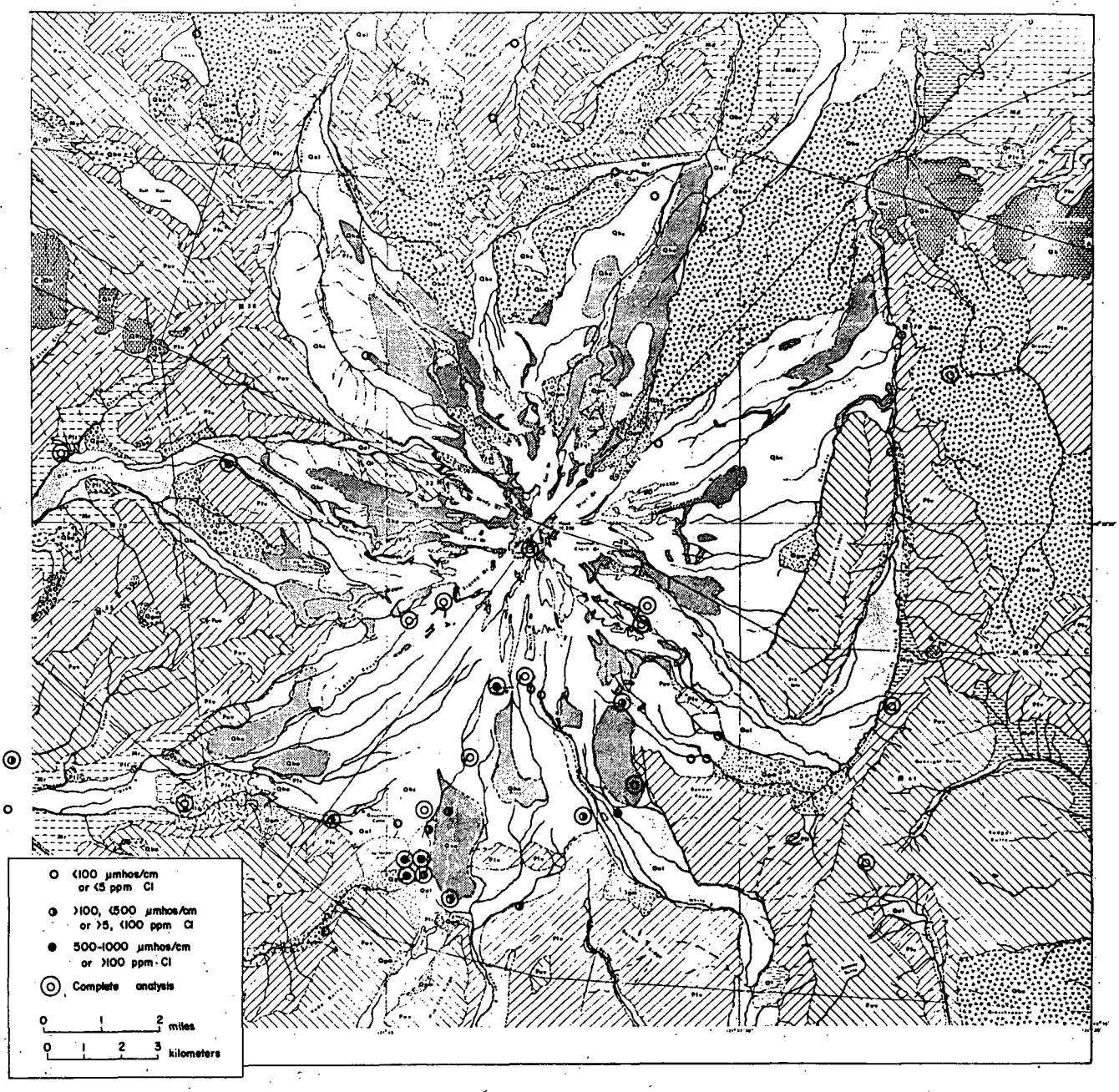

XBL 792-8468

Figure 9. Specific conductance and chloride content of waters plotted on the geologic map of Mt. Hood (after Wise, 1968).

Table 4a

Sample	MH-1	MH-2	MH-3	MH-10	MH-11	MH-12	MH-13
Date	6/1/77	6/1/77	6/2/77	6/3/77	6/4/77	6/4/77	6/4/77
pH	6.9	∿6.2	8.5	∿7.5	∿6.7	∿6.9	6.5
Temp. °C	4.5	3.5	7	7	3	5	10
			mg/ℓ				
B	3	0.5	0.2	0.5	0.3	0.2	0.5
Na	3	2.2	16	6	1.2	7	2
Mg	<0.5	<1	4	5	1	2	<0.6
SiO_2	-	-	-	-	-	30	-
S	-	-	-	-	-	3	-
Cl	1	1	2	<0.2	<0.1	5	<0.2
K	<0.7	1	2	<0.2	<0.4	1	<0.4
Ca	3	2	17	50	<0.01	0.11	0.15
			µg/ℓ				
Mn	0.7	27	2	<0.2	<0.1	1.5	4
Fe	30	2400	22		10	110	155
Ba	0.7	4	2.3	<2	5.6	3	1
Mo	0.37	0.2	3	13	≤0.06	0.02	<0.1
Rb	2.2	0.7	1.2	2	1	4	0.3
Cs	0.05	0.02	0.02	0.66	0.01	0.10	0.02
Co	0.02	0.36	<0.01	0.05	<0.02	0.05	<0.02
Sb	<0.03	0.01	0.11	2.4	<0.01	<0.01	0.02
Cr	<0.2	<0.2	<0.1	<0.3	<0.1	0.55	0.33
Zn	20	<5	120	<1	<1	8	3
Ag	<0.02	0.5	<0.03	<0.02	0.005	2.4	0.1
Ce	<0.04	0.17	< 0.2	<0.03	0.02	0.1	0.1
Sm	0.003	0.012	-	0.02	0.0018	0.012	0.009
Eu	<0.001	0.0019	<0.002	<0.004	0.0004	0.003	0.002
U	0.023	0.012	0.077	0.08	0.005	0.05	0.008
Ir	≤0.00005	0.00031	<0.00010	<0.0002	<0.0001	≤0.0002	<0.00001
As	<0.2	<4	1.4	12	<0.2	<1	<0.1
Br	2	1	3	<4	<2	6	7
W	<0.05	-	<0.2	<0.6	<0.07	<0.3	<0.1
Sc	0.031	0.023	<0.003	0.020	0.0027	0.030	0.05
Hf	<0.03	0.01	<0.03	<0.019	0.004	<0.009	<0.004
Th	<0.003	0.008	<0.005	≤0.008	≤0.0015	≤0.009	0.012

Table 4b

Sample	MH-14	MH-15	MH-16	MH-17	MH-21	MH-22	MH-23	MH-24
Date	6/5/77	7/29/77	7/29/77	7/29/77	8/2/77	8/2/77	8/3/77	8/3/77
pH	7.5	6.8	6.5	6.5	6.4	8.5	6.4	6.5
Temp. °C	8	4	10	9	4.5	10	1	3
				mg/ℓ				
B	0.5	0.5	1	0.5	0.5	3	0.5	0.5
Na	6.5	0.8	0.6	1.4	3	125	3	1.2
Mg	6	<0.3	<0.4	<0.3	2	20	1	<0.3
SiO_2	42	24	13	21	27	54	29	23
S					-			
Cl	6	0.2	0.3	0.8	1.5	25	1.3	0.5
K	3.5	0.3	0.3	0.6	<0.5	16	0.5	0.8
Ca	19	0.5	0.4	2	4	51	4	1.4
				µg/ℓ				
Mn	1.6	0.7	3	2	144	<7	0.5	2
Fe	90	38	180	100	5800	210	14	20
Ba	7	2.3	2.7	1.3	<3	10	<0.5	<1
Mo	<0.1	<0.1	<0.05	<0.04	0.13	5.5	≤0.1	<0.04
Rb	5	0.9	0.5	1.8	1.3	8	2	1.3
Cs	0.09	≤0.008	0.009	0.014	<0.04	0.06	0.06	0.01
Co	0.04	0.02	0.08	0.06	0.11	0.05	<0.01	0.03
Sb	0.01	0.01	<0.009	<0.02	0.04	0.05	0.02	<0.01
Cr	<0.4	0.23	0.45	0.23	0.7	<0.3	<0.1	0.2
Zn	1	0.8	2.5	0.8	3	4.6	<1	1
Ag	<0.07	≤0.02	≤0.6	<0.01	<0.06	<0.05	<0.04	<0.1
Ce	0.18	0.12	0.36	0.15	-	-	-	-
Sm	0.009	0.009	0.02	0.01	0.02	0.01	0.002	0.008
Eu	<0.001	<0.002	<0.004	<0.004	<0.004	<0.002	<0.001	<0.004
U	0.23	0.012	<0.02	<0.02	<0.01	0.04	0.02	<0.01
Ir	<0.0001	<0.0001	<0.0001	<0.0001	<0.0001	<0.0001	<0.0001	<0.0001
As	<0.5	<0.01	<0.1	<0.1	<0.2	<0.2	<0.2	-
Br	6	1	1	2	6	34	3	3
W	<0.1	<0.01	<0.02	<0.02	<0.05	<0.4	<0.03	<0.03
Sc	0.025	0.021	0.06	0.03	0.05	<0.01	<0.003	0.01
Hf	0.02	0.008	0.021	0.01	<0.02	<0.005	<0.001	0.007
Th	0.009	0.026	0.03	0.03	<0.01	<0.01	<0.001	0.02

Table 4c

MT. HOOD WATER SAMPLES

									Old Maid Flat Well		
	Sample	MH-25	MH-28	MH-29	MH-30	MH-31	MH-32	MH-36	MH-33B	MH-35	MH-40
	Date	8/3/77	8/24/77	8/25/77	2/30/77	9/7/77	9/7/77	2/22/78	12/19/77	2/21/78	2/22/78
	pH	6.5	7	7.4	∿4.7	6.5	6.5	7.8	10	10	10
	Temp. °C	9.5	9	6	2	10	4	4	9	6	11
						mg/ℓ					
B		0.5	0.5	0.3	0.1	1	1	0.5	10	7	7
Na		5	1.3	3.8	2.7	2	0.6	4	130	136	132
Mg		3	<0.5	<2	2.5	<1	<0.5	2	<1	<1	<1
SiO_2		47	16	61	14	28	24	10	40	34	31
S								15	23	23	25
Cl		1	<1	<1	<0.1	1	1.7	2	135	124	123
K		<0.3	<0.2	2	1	0.9	<0.2	0.1	<1	≤0.2	<0.2
Ca		11	2.7	8.6	17	3	1	43	72	11	11
						µg/ℓ					
Mn		35	8	2.5	119	2	<0.1	10	<40	<8	<7
Fe		155	64	30	1200	103	25	120	200	21	<10
Ba		<3	3.5	2	<10	<1	<1	2.3	7	<4	<2
Mo		<0.05	0.15	0.17	0.4	0.3	0.2	4	<0.7	35	37
Rb		2	0.7	4.2	<0.6	1.1	0.5	1.5	1.0	1.3	1.3
Cs		<0.02	0.02	0.03	<0.03	0.02	<0.01	0.4	0.06	0.07	0.15
Co		0.14	0.10	0.035	3.3	0.06	0.02		0.08	<0.03	
Sb		0.11	<0.01	0.01	0.06	0.06	0.03	1	0.07	0.05	<0.01
Cr		0.2	0.87	0.04	1.2	0.23	0.20	<0.2	0.5	<0.5	<0.4
Zn		1	3.5	5	2400	13	0.8	7	4	2	<0.4
Ag		<0.05	-	-	0.79	0.06	0.10	<0.2	<0.2	≤0.1	<0.07
Ce		0.095	0.048	<0.04	2.4	0.2	<0.04				
Sm		0.013	0.005	0.0036	0.37	0.016	0.0026	<0.03	0.03	<0.04	<0.04
Eu		-	<0.002	≤0.0014	0.08	0.006	<0.004	<0.003	-	<0.003	<0.004
U		<0.01	<0.005	0.027	0.063	0.01	<0.004	0.05	0.15	0.12	0.14
Ir		<0.0001	<0.0001	<0.0001	0.0004	<0.0001	<0.0001	<0.0002	≤0.0008	<0.0004	<0.0010
As								4	<2	<15	<10
Br		5	1.5	4.8	<1	2.5	1	9	115	300	280
W		≤0.1	<0.1	<0.1	0.8	0.15	<0.06	<0.5	<0.4	12	13
Sc		0.013	0.011	0.013	0.11	0.026	0.007	0.053	0.06	0.013	0.011
Hf		<0.003	<0.005	<0.008				<0.05		<0.02	<0.015
Th		<0.002	<0.004	<0.005	0.03	0.013	<0.001	<0.007	<0.03	<0.015	<0.009
Ta					0.02						
Yb					0.15						

their element abundances are lower than those of the Swim Warm Springs. Exceptions are the iron-manganese-rich spring, MH 2, emanating from glacial debris in the White River Valley, the Ca-Mg-rich water of the spring from basalt in the Robin Hood Quarry (MH 10), and Fe-Mn-rich water from the outflow of a small pond in the strongly altered fumarolic area of the summit crater. In both the Fe-Mn waters of the summit crater and White River Valley spring there were identifiable contents of iridium, though in lower abundance than in the winter sample from "East side of pool" at Swim. (Fe and Mn were both below detection limits in the sample from Swim). Water from a cold well in the Government Camp area (MH 3) is similar in character, except for its high Zn content, to cold "andesite" waters. However, a cold well near Brightwood (MH 22), most likely producing from the Rhododendron Formation, has water low in Fe and Mn and relatively high in Na and Mg, in contrast to a nearby cold spring (MH 21).

c. Old Maid Flat Geothermal Test Hole

Water samples were obtained from the artesian-flowing geothermal test hole in Old Maid Flat in December 1977 and February 1978. It is expected that the water was flowing from a depth of 450m; total depth at that time was 550m. Since that time the hole has been deepened to 1200m. The initial sample, taken only a few days followng cessation of drilling, contained unusually high contents of SiO_2, Mn, Fe, Ba, and other constituents, indicating that the sample was contaminated by drilling fluid. A sample taken 16 days later (MH 33b) contained considerably lower amounts of these constituents but somewhat greater amounts of SiO_2, Cl, Ca, Fe, and Ba than samples obtained two months later (MH 35 and MH 40). It is possible that water from the Old Maid Flat well was still slightly contaminated by drilling fluid.

d. Comparison of Water Chemistries

To facilitate comparison between the chemistries of the various water sources, major- and trace-element contents were plotted generally in order of increasing abundance in Figures 10, 11, 12, and 13. The patterns on these figures afford qualitative assessment of significant differences or similarities between water types. Mean values and standard deviations of element contents of cold waters emanating from springs in andesite and of waters from Swim Warm Springs are plotted on Figures 10 and 11. In Figure 10, which compares major elements, there is a "high" in sulfur and sodium in the warm spring water, in contrast to the cold "andesite" water where SiO_2 is relatively prominent. In the comparison of mean values of trace-element contents in both water types (Figure 11), uranium is prominent with respect to its neighbors, Sm and Cs at Swim Warm Springs. Barium stands out among the trace elements in the cold-spring waters.

Plots of major-element contents in waters from the geothermal test well in Old Maid Flat (MH 40) and the cold spring in Robin Hood Quarry (MH 10) comprise Figure 12. Similar diagrams of trace-element contents in these two sources are shown in Figure 13. The major-element pattern of the Old Maid Flat well water has a Na-S "high," similar to but considerably more accentuated than, that of the Swim Warm Spring waters (Figure 10). The trace-element pattern of Old Maid Flat well water has a sharp "high" of Mo with respect to its neighbors on the plot, Cs and Rb; Br is also accentuated. The major element pattern of cold water emanating from basalt in Robin Hood Quarry accentuates S and Ca, in contrast to the cold "andesite" waters where SiO_2 predominates. The trace element pattern of the Robin Hood Quarry water has prominences of Mo and Ba; Ba is also relatively prominent in the cold "andesite" water. Barium and calcium contents are relatively high in a sample of basalt from Robin Hood Quarry (MHR-2, Table 2), and a sample of felsic dike rock from the quarry (MHR-1) also has a relatively high Ba content.

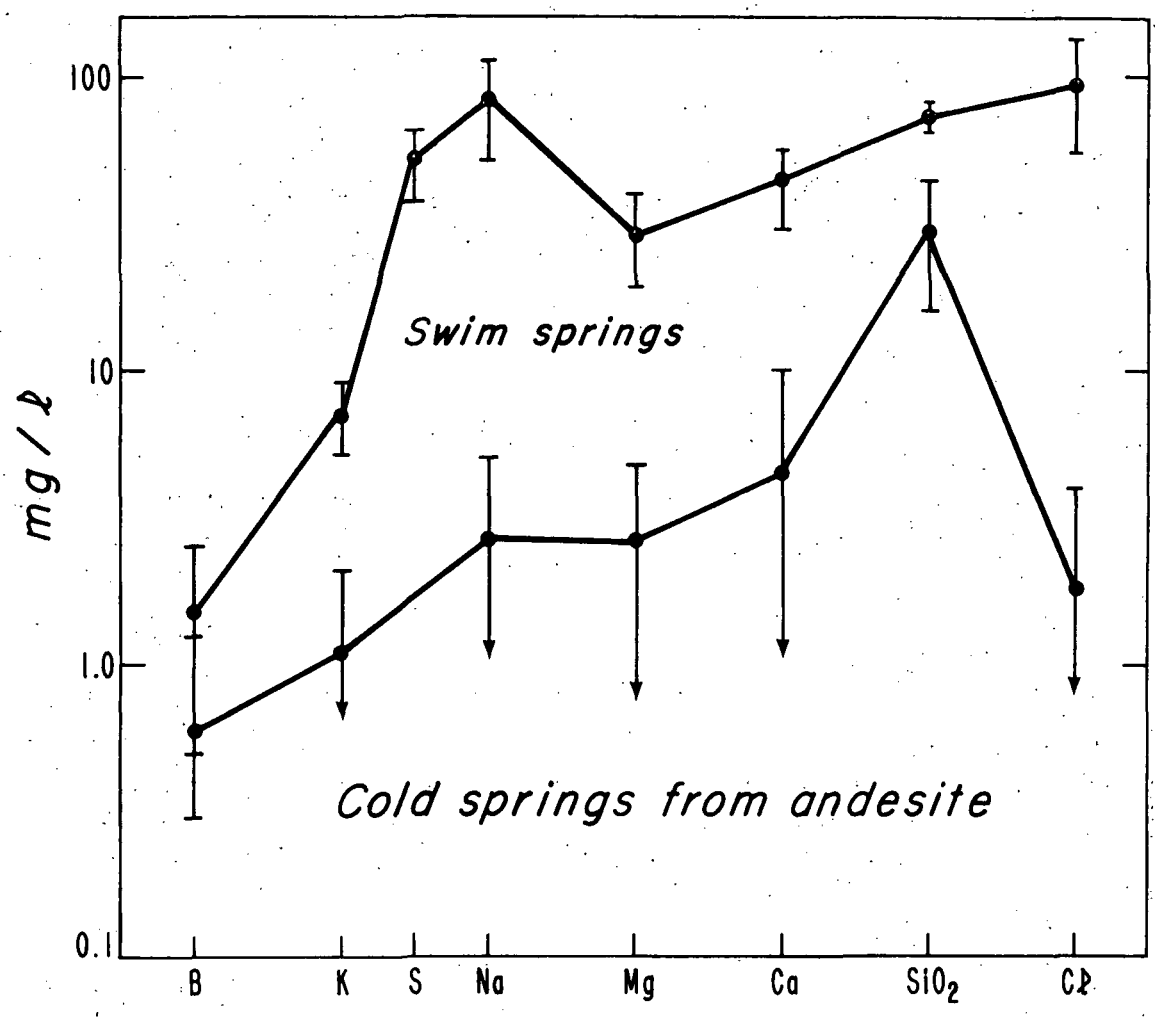

Figure 10. Major element contents of Swim Warm Springs and cold water from andesite.

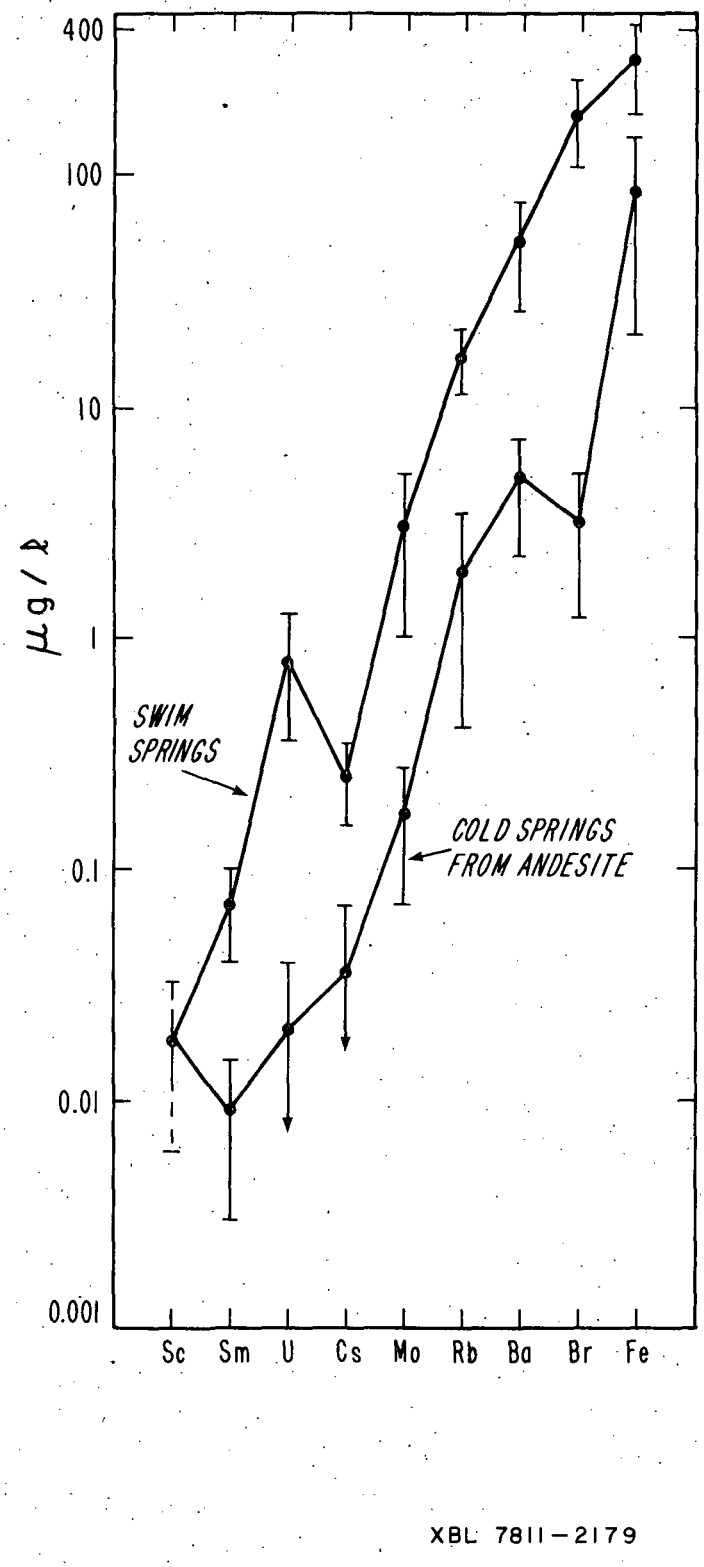

Figure 11. Trace-element contents of Swim Warm Springs and cold water from andesite.

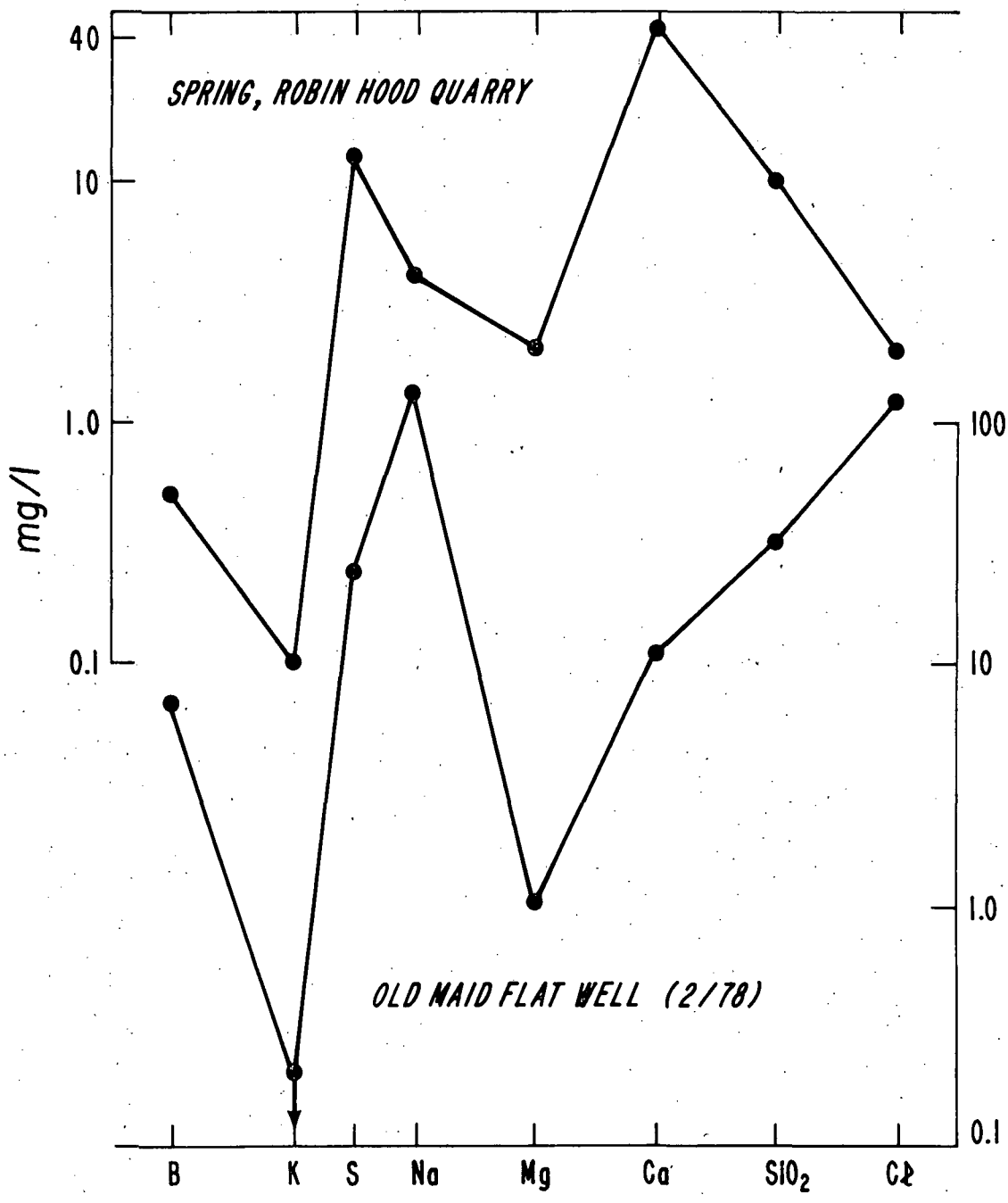

Figure 12. Major-element contents of the spring in Robin Hood Quarry and of water from the geothermal test well in Old Maid Flat.

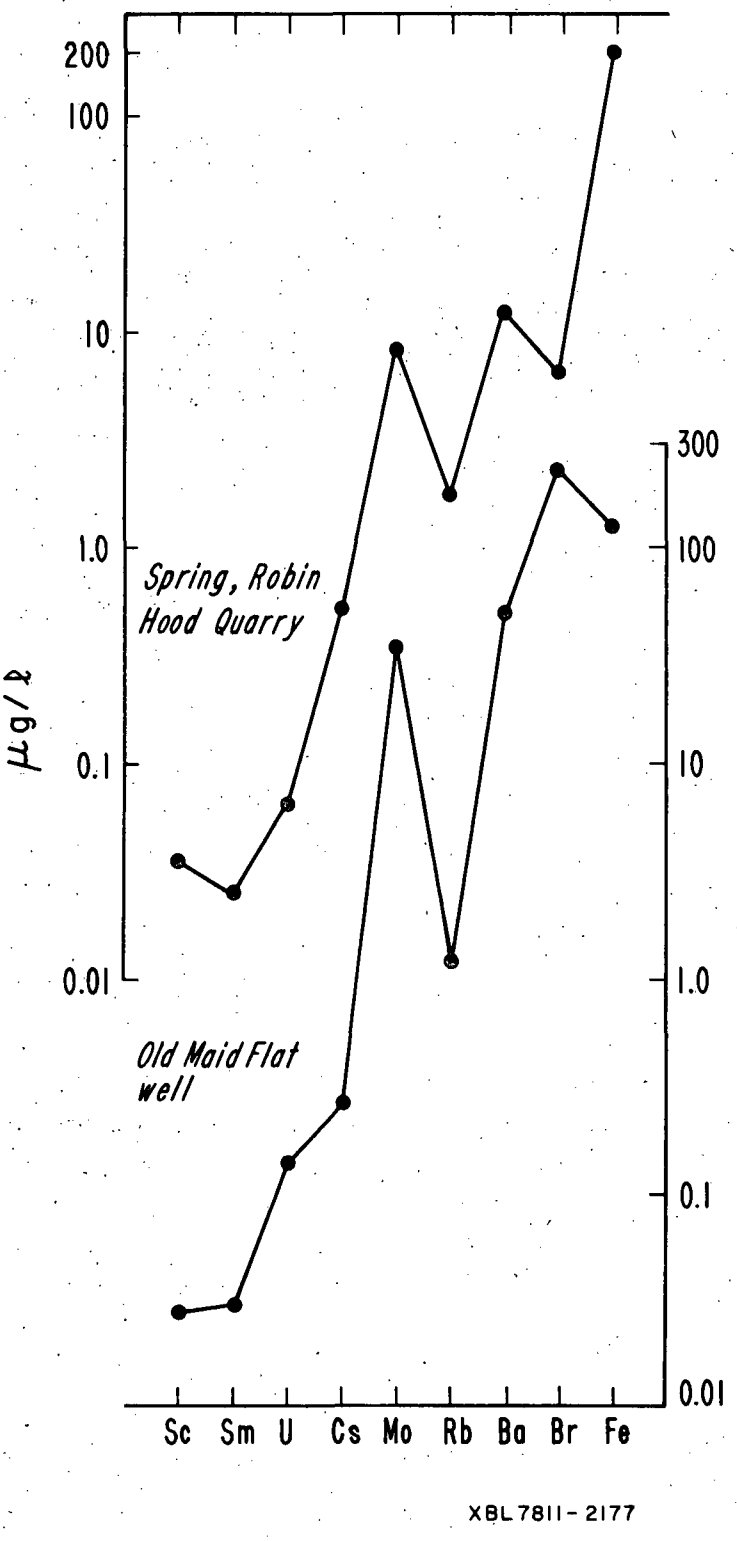

Figure 13. Trace-element content of the spring in Robin Hood Quarry and of water from the geothermal test well in Old Maid Flat.

e. Estimates of Subsurface Temperature

Major-element analyses were used to calculate the water temperature at depth within the Swim Warm Springs system. The calculations were based on chemical geothermometers afforded by the SiO_2 content of water and the ratio of Na to K, corrected for Ca (Fournier and Truesdell, 1973). The temperature of water at depth was also estimated by the ratio of oxygen isotopes in sulfate in the water (McKenzie and Truesdell, 1976), measured by N. Nehring and A. H. Truesdell at the U.S. Geological Survey, Menlo Park, California.

The temperature of hot water, unmixed with nearer-surface cold water, and the proportion of mixed cold water in Swim Warm Springs, were estimated by applying the mixing model of Fournier and Truesdell (1974). In this model simultaneous equations are employed, incorporating as factors the temperature of warm spring water, the SiO_2 content of the warm spring water, the temperature of the near-surface cold water, and the silica content of cold spring water.

The estimates of subsurface water temperature at Swim Warm Springs are summarized in Table 5. The temperatures estimated by the Na-K-Ca geothermometer and by the mixing model may be less reliable than those estimated by the silica and oxygen-isotope geothermometers, because surface flow at Swim is low. The Na-K-Ca and mixing-model temperatures should not be discounted, however, because the mixing model indicates the large proportion of near-surface cold water intuitively expected at Swim. Therefore, the agreement between the silica and oxygen-isotope temperatures indicate that the temperature at depth is, at least, within the range of 100-125°C, the temperature may be 150° to over 200°C.

The samples from the Old Maid Flat hole may contain some vestiges of drilling fluid. However, if we assume equilibrium conditions then the

Table 5

Summary of Estimated Subsurface Temperature
at Swim Warm Springs

Geothermometers	
SiO_2	100-125°C
Na-K-Ca (β = 1/3)	152-154°C
$\delta 18_O$ - SO_4	108-110°C
Silica Mixing Model[a]	
Temperature of unmixed hot water	192-240°C[b]
Fraction of cold water	0.92

a) Fournier and Truesdell, 1974.
b) Questionable because it is a low-flowing system.

silica and alkali-element ratio geothermometers give consistent temperatures of 80-90°C. The temperature measured at 450m was 33°C; a measurement of bottom-hole temperature, following completion of the hole, was 81°C.

f. Oxygen and Hydrogen Isotope Ratios

A plot of isotope ratios of hydrogen and oxygen in cold and warm spring waters comprises Figure 14. The ratios are expressed in delta values, given in mils (°/oo), and defined as:

$$\delta \text{ in } {}^{o}/_{oo} = \frac{R_{(sample)} \quad R_{(standard)}}{R(standard)} \times 1000 \qquad \text{(Hoefs, 1973)},$$

where R represents the isotope ratios of deuterium to hydrogen and $18_O/16_O$; the standard is "mean ocean water" (Craig, 1961). The points for warm and cold springs fall close to the line for meteoric waters, indicating that the warm waters are much diluted by near-surface runoff. The warm water points would be shifted to the right of the meteoric water line if a substantial component of the spring water had been in contact with rock at depth. However, the grouping of the warm water points at more negative values indicates that the source of the warm spring water is generally higher on the mountain than the sources of most of the cold springs sampled. Exceptions are the cold springs at Mt. Hood Meadows (MH 4) and a spring in Robin Hood Quarry (MH 10), which fall in the same range as the warm waters. The grouping of the points indicates that the cold waters have shorter pathways between their sources and the springs, while a component of the warm water may circulate deeply enough in the mountain to come in proximity to a hot central conduit system.

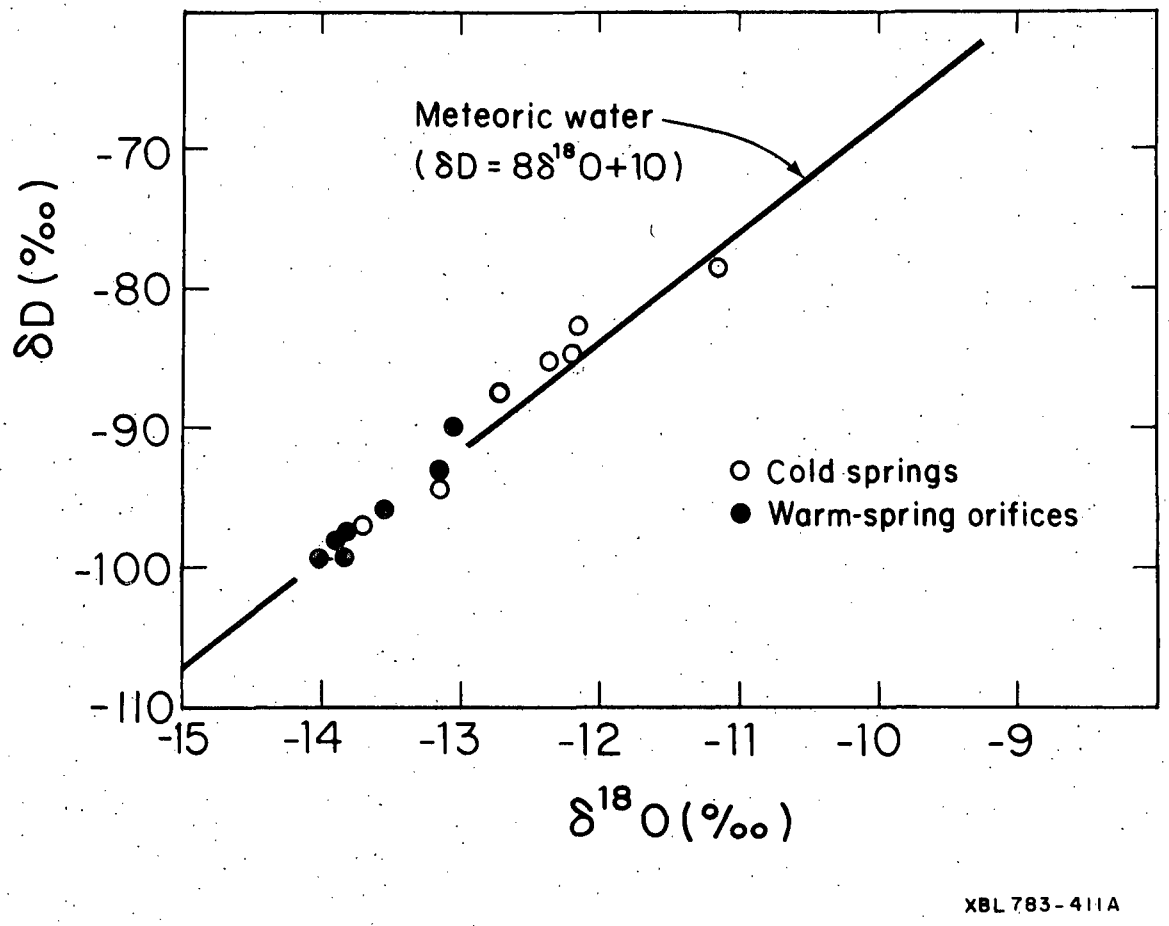

Figure 14. Isotope ratios of hydrogen and oxygen in cold and warm-spring water of Mt. Hood.

B. Rock Analyses

A limited number of samples of the igneous rock types in the Mt. Hood region were collected and analyzed. A more detailed investigation of the petrology, mineralogy, and geochemistry of Mt. Hood's extrusive rocks is presently being conducted by Craig White of the University of Oregon.

Results of major and trace-element analyses of 13 rock samples, together with brief sample descriptions, are listed in Table 6. Seven of the samples are andesite, two (MHR 3 and 11) are of appreciably altered rock. The major-element contents of the samples of relatively unaltered andesite are fairly uniform, with silica contents in the range 58-63%, Al_2O_3 17.4-17.7%, CaO 5.4-6.4%, Na_2O 3.7-4.3%, and K_2O 1.0-1.5%. There do not appear to be significant differences between chemistries of samples of Pliocene andesite from the west and east flanks of Mt. Hood (MHR 10 and 13), and the andesite of the more recent flows on the south flank of the mountain (MHR 5 and 6). This is supported by the small standard-deviations of mean values of rare-earth-element (REE) ratios (REE contents in sample/REE contents in standard chrondrite) of the unaltered andesite (Figure 15). The relatively higher Fe and Mg contents of the andesite from Cloud Cap (MHR 12) are in keeping with the presence of olivine in that rock, in comparison with other andesite samples where hornblende is the principal mafic mineral. The altered brecciated andesite sample (MHR 3) from the south flank of Mt. Hood is somewhat lower in MgO, but higher in K_2O than the fresher samples, while the strongly altered andesite (MHR 11) from the west flank of the mountain has considerably greater MgO and much less K_2O than a sample of nearby, relatively unaltered andesite (MHR 10). Both fresh and altered andesite samples from the MHR 10 and 11 localities have identifiable iridium contents, in contrast to other rock samples where the abundance of that element was well below detectability limits. It is surprising to find Ir in andesitic rocks; it is more normally associated with ultramafic rocks: peridotite, pyroxenite, and serpentinite.

Table 6a

MT. HOOD ROCK SAMPLES

Major Elements
(% by weight)

SAMPLE	1	2	3	4	5	6	7	8	9	10	11	12	13
Na_2O[(a)]	4.0	2.2	3.2	3.8	4.1	4.3	5.2	3.8	2.7	4.1	2.6	4.0	3.7
MgO[(a)]	0.3	4.0	1.6	1.2	3.1	2.9	3.7	3.3	2.4	1.7	6.5	3.1	2.8
Al_2O_3[(a)]	13.6	13.1	16.4	15.3	17.7	17.5	17.7	17.8	16.7	17.4	17.3	17.4	17.7
SiO_2[(a)]	71.7	50.3	59.3	64.9	60.4	61.5	58.1	58.0	62.3	62.8	54.8	58.3	59.8
K_2O[(a)]	3.7	1.2	2.4	3.0	1.5	1.3	1.2	0.9	1.3	1.3	0.3	1.0	1.3
CaO[(a)]	1.4	7.1	4.3	0.7	5.8	5.7	5.5	7.1	4.3	5.4	1.6	6.3	5.6
TiO_2	1.4	7.1	0.8	0.7	0.8	0.7	0.8	0.7	0.6	0.5	1.0	0.9	0.8
MnO	0.04	0.23	0.12	0.05	0.10	0.09	0.07	0.10	0.04	0.04	0.03	0.13	0.07
FeO	1.8	13.2	4.6	3.3	5.7	5.7	3.9	5.4	3.7	4.2	5.1	6.3	5.2
Cr_2O_3	0.00	0.04	0.02	0.01	0.03	0.03	0.02	0.02					
TOTAL	96.7	94.0	92.7	93.0	99.2	99.7	96.2	97.1	94.0	97.4	89.2	97.4	97.0

(a) Analyses by x-ray fluorescence.

Table 6b

MT. HOOD ROCK SAMPLES

Trace Elements
(ppm)

SAMPLE	1	2	3	4	5	6	7	8	9	10	11	12	13
Rb	120	190	40	65	20	20	30	20	40	18	<4	8	32
Cs	2	5	1	<1	<1	<1	<1	<1	2	5	0.5	<0.3	0.4
Ba	600	640	300	460	350	300	250	200	240	300	120	350	300
Hf	5.4	5.0	7.1	6.2	4.2	4.1	3.6	3.7	3.3	4.0	3.7	4.5	4.1
Cr	2	40	7	4	40	55	10	70	50	30	65	46	41
Co	3	37	7.6	5.8	19	19	16	21	13	12.8	21	21	19
Ni	<10	<30	<20	<10	30	30	<10	40	40	23	33	34	25
Sc	2.3	37.7	10.5	9.6	13.9	13.3	19.4	17.2	12.8	9.0	18	15	15
Th	15	4.5	6.6	6.2	3.7	2.4	2.4	2.4	2.3	3.0	2.2	2.1	3.6
Ta	1.3	0.84	1.1	1.0	0.57	0.54	0.54	0.51	0.54	0.65	0.51	0.62	0.59
La	25	23	25	24	19	15	10	18	13	16	13	17.5	16.2
Ce	56	52	58	53	45	33	29	44	27	36	29	40	35
Nd	15	27	26	26	15	17	15	20	14	16	16	20	18
Sm	2.6	6.3	4.8	5.2	3.6	3.2	2.8	3.9	3.0	3.1	4.0	4.3	3.4
Eu	0.66	2.2	1.5	1.3	1.4	1.3	0.83	1.3	1.1	1.1	1.0	1.4	1.1
Tb	0.41	1.0	0.71	0.76	0.49	0.46	0.52	0.47	0.45	0.45	0.60	0.55	0.47
Dy	2.5	7.9	4.9	4.9	3.2	2.9	3.7	3.3	3.3	2.5	4.4	3.8	3.0
Yb	1.7	3.7	2.7	2.6	1.6	1.5	2.1	1.8	1.6	0.95	2.1	1.9	1.4
Lu	0.22	0.54	0.35	0.32	0.19	0.18	0.24	0.27	0.21	0.14	0.27	0.25	0.19
U*	4.5	1.3	1.4	1.9	1.2	0.9	1.8	0.6	0.7	0.95**	0.76	0.61	1.05
Ir	≤0.02	≤0.003	<0.0010	<0.0010									

* By γ spectrometry
** By neutron activation

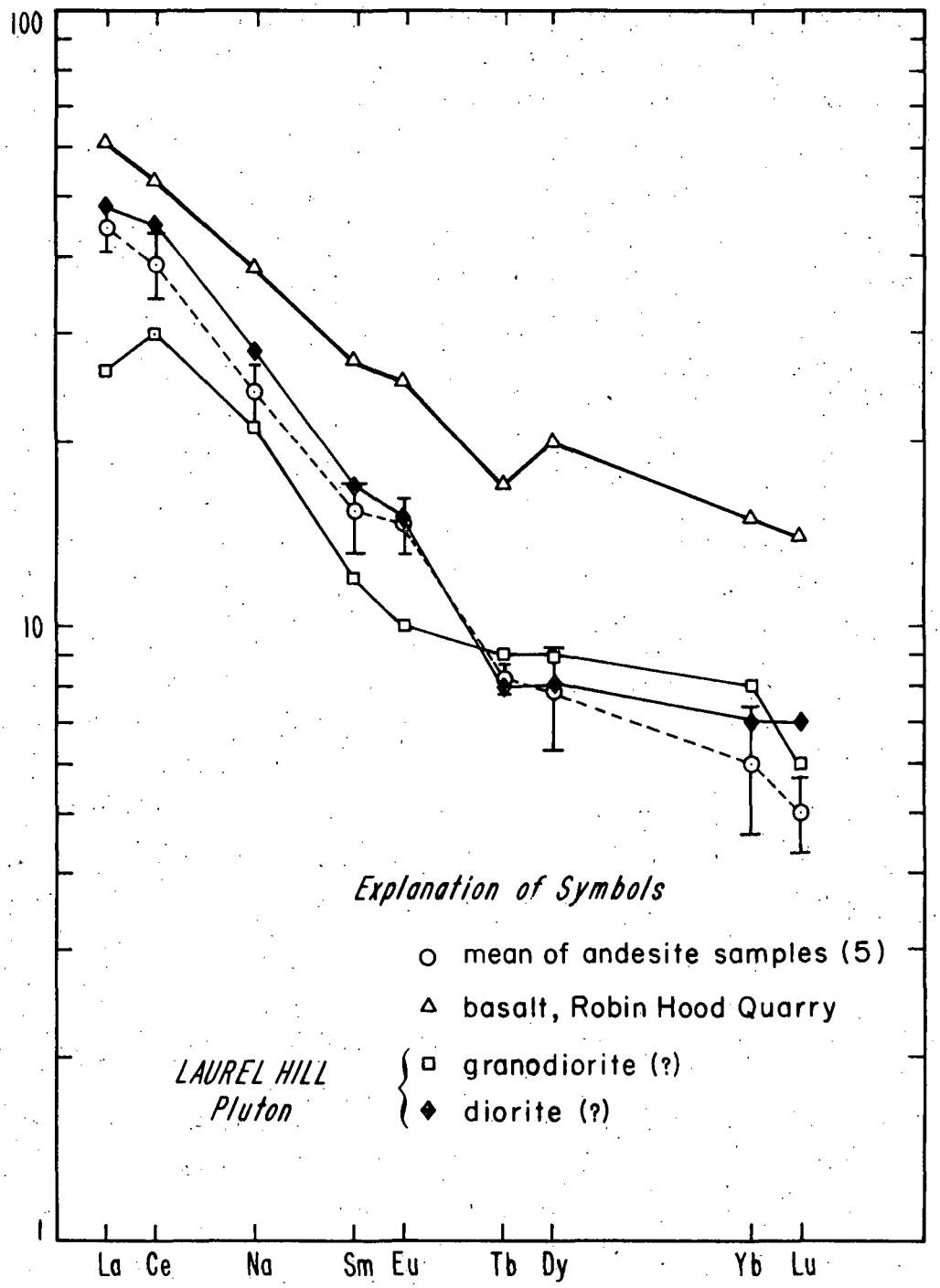

Figure 15. Rare-earth element ratios (sample/chrondrite) of rock samples from Mt. Hood.

The relatively high barium contents of the samples of felsic dike rock and basalt (MHR 1 and 2, respectively) from the Robin Hood Quarry, are reflected in the water sample from that locality (MH 10, Table 4a). The basalt has higher rare-earth-element ratios than those of the andesite or of the intrusive rocks. Comparison of major- and trace-element contents of the Robin Hood Quarry basalt with contents of Columbia River Basalt flows (Asaro and others, 1978) indicates strong similarities. An example is shown in Table 7, where sample MHR 2 is compared with basalt of the Roza flow of central Washington.

Major- and trace-element contents of the two samples of relatively unaltered intrusive rocks, diorite-granodiorite, from the Laurel Hill pluton (MHR 7 and 8), are similar to contents of the unaltered andesite samples. This is illustrated by the similarity between REE patterns of the andesite and intrusive rocks (Figure 15). A sample of altered intrusive rock from locality MHR 9 in the Laurel Hill pluton has markedly lower Na_2O, MgO and CaO, but higher SiO_2 than the unaltered samples. The similarity between the chemistries of the intrusive rocks and the andesites suggests that the intrusives may represent the roots of the Pliocene extrusive centers on the western flank of Mt. Hood. However, our sampling of andesites to date has not been extensive enough to support or deny the conclusions of Wise (1969) regarding the origin and character of the andesites of Mt. Hood.

C. Gas Analyses

Results of analyses of gases collected from two sites on Mt. Hood, Steel Cliffs and Crater Rock in the Summit Crater area, are listed in Table 8. These may be compared with analyses by Ayres and Creswell (1951) of gas samples collected in 1935 and 1951 from fumaroles near the Steel Cliffs. The bar graphs, Figure 16, permit this comparison and show that carbon dioxide predominates (88-97%) in the group of gases other than water vapor, with H_2S comprising 1 to 11% of this group. The Ayres and Creswell sample

Table 7

Major- and Trace-Element Contents of the Robin Hood Quarry and Roza Flow basalts

	Robin Hood Quarry	Roza flow
	(%)	
SiO_2	50.3	50.3
Al_2O_3	13.1	13.6
FeO	12.9	14.3
MgO	4.0	4.4
CaO	7.1	8.25
Na_2O	2.2	2.7
K_2O	1.2	1.2
TiO_2	2.5	2.6
	(ppm)	
Sc	37.7	39.0
Eu	2.2	2.67
Co	36.6	41.0
Ba	641	498
Cr	40.3	40.5

Table 8

Fumarolic Gas Analyses*

	Steel Cliffs	Crater Rock
Temperature	88-91°C	90°C
moles CO_2	0.1830	0.3056
moles H_2S	3.8368×10^{-3}	2.9228×10^{-3}
moles NH_3	1.8862×10^{-3}	1.72×10^{-3}
moles H_2O	1.1215	0
Gases other than H_2O (mole %)		
CO_2	96.85	98.43
H_2S	2.03	0.94
He	1.8×10^{-4}	4.3×10^{-3}
H_2	0.11	0.32
Ar	4.6×10^{-3}	2.0×10^{-3}
O_2	0	2.2×10^{-3}
N_2	0.87	0.25
CH_4**	1.0×10^{-3}	1.5×10^{-3}
NH_3	1.00	0.55

* Collected July 1977; analyzed by N. Nehring and A.H. Truesdell, U.S. Geological Survey, Menlo Park, California.

** Besides methane, chromatograms indicate the presence of ethene, ethane, propene, propane, 2-methyl-propane, 1-butene, n-butane, and n-pentane.

Gases other than water vapor

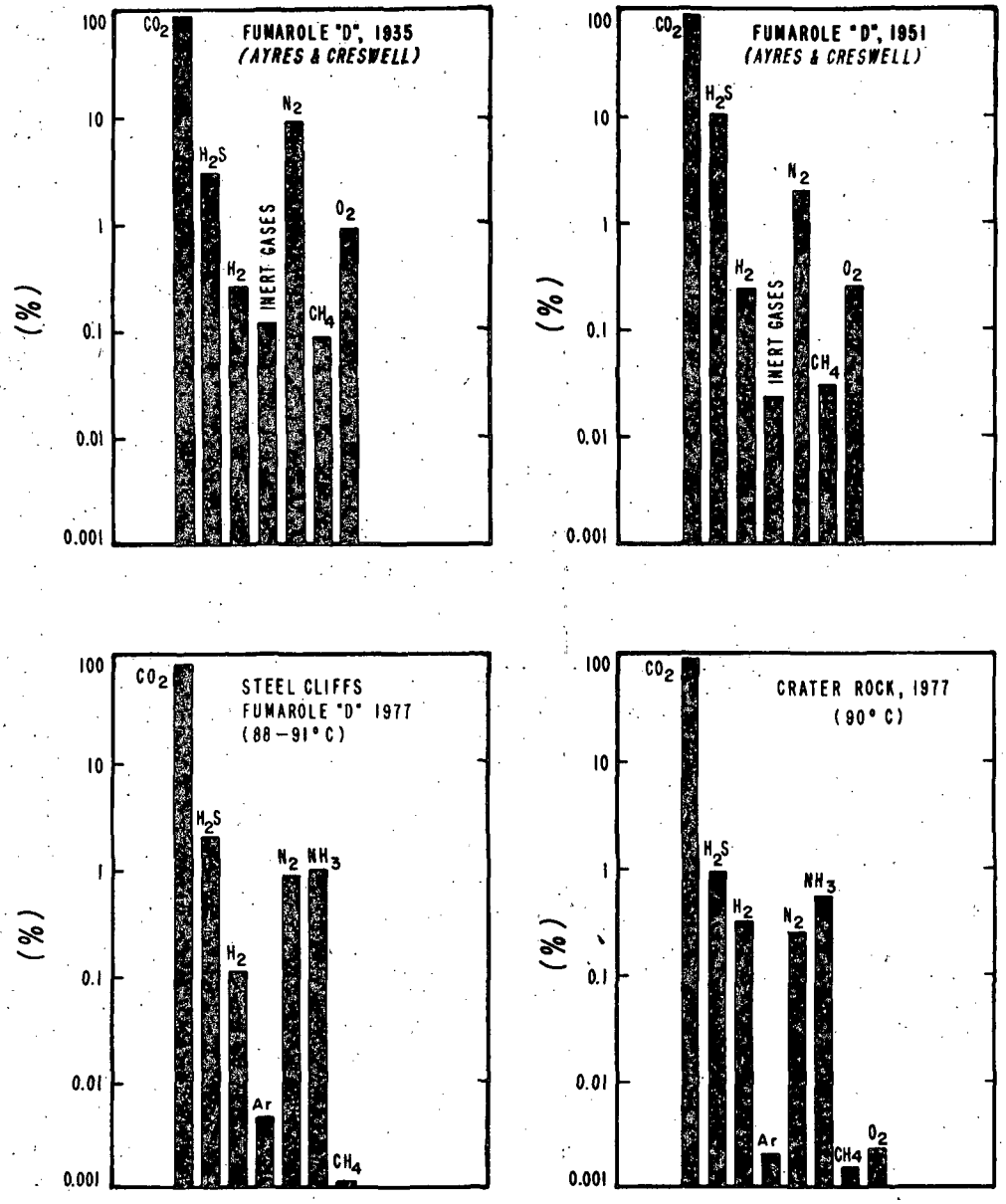

XBL 7811-2175

Figure 16. Bar graphs, showing abundances of constituents (other than water vapor) of fumarolic gases, Mt. Hood.

of 1951 differs from the 1935 sample in its relative contents of CO_2, H_2S, and other constituents. The difference between the 1951 sample and our 1977 sample is of the same order. The 1977 Steel Cliffs and Crater Rock samples have similar bar-graph patterns, with their H_2S contents substantially higher than H_2, N_2, and NH_3, which are in turn at least two orders of magnitude higher than argon.

A second set of gas samples was collected from fumaroles in the Summit Crater area in October 1978. It is expected that sufficient water vapor was collected at that time to permit analyses of stable isotope contents, providing comparison with isotope ratios in spring-water samples.

IV. ORIGIN OF WARM WATER AT SWIM SPRINGS

It is appropriate here to speculate briefly on the source of the warm water and the pathway it takes to reach Swim Springs. The most likely explanation for the occurrence of warm water at Swim is that the water has been heated higher on the mountain, has migrated downslope, mixing with cold water, and comes to the surface at Swim. Snow- and glacier-melt water near the summit may come in close proximity to the hot central neck of the mountain, manifested by the steam zone of the summit-crater fumaroles. Some of this heated water probably percolates downslope in the andesitic mud-and ash-flows, mixing with cold water along its path (Figure 17).

The oxygen-hydrogen isotope data (Figure 12) provide evidence for the high-elevation origin of the Swim water. Meteoric water deposited at higher elevations has a larger component of lighter isotopes than does water at lower elevations. This indicates that a significant proportion of the warm water originated at higher elevations than the cold spring water.

Field measurements and analyses of cold springs also suggest that there is a small thermal component in some of the cold-spring water on the south flank of Mt. Hood. Surface and spring waters in the Mt. Hood region

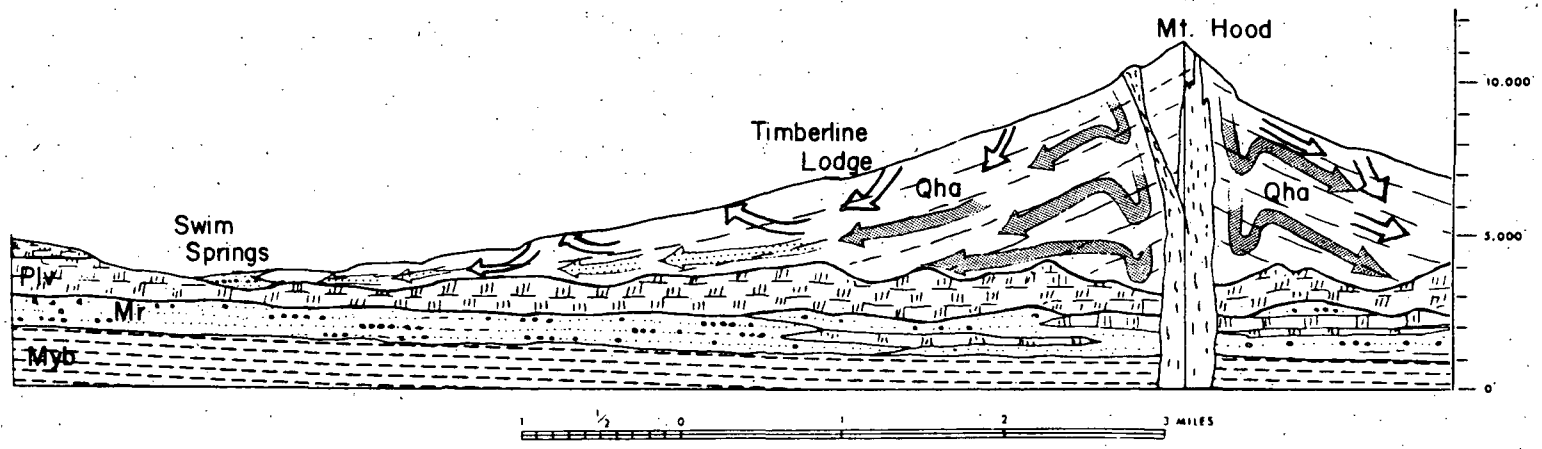

XBL 792-8469

Figure 17. North-south geologic cross section of Mt. Hood (after Wise, 1968) showing, schematically, the hypothesized circulation paths of hot water (dark arrows) heated near the volcano's central neck, mixed warm water (lighter arrows), and cold water (un-shaded arrows). The warm water emanating at Swim Springs is strongly mixed, and cold water in springs on the south flank of the mountain may contain a small component of the deeper-flowing hot water. Myb = Yakima Basalt; Mr = Rhododendron Formation; Plv = Lower Pliocene basalt and andesite; Qha = Mt. Hood andesite flows.

generally contain a few ppm of total dissolved solids, 1 to 3 ppm chloride, and have specific conductances of 30 to 70 μmohs/cm. In contrast, as is illusrated in Figure 9, several of the cold springs on the south flank, below the 6000 ft elevation, have chloride contents and/or specific conductances well in excess of these values. For comparison, undiluted geothermal waters may contain several hundred to several thousand ppm chloride and have specific conductances in the range from several hundred to several thousand μmohs/cm; at Swim, the values are ∿900 ppm total dissolved solids, ∿150 ppm chloride, and 1300 μmohs/cm specific conductance.

Another possible explanation for the presence of warm water at Swim Springs is deep circulation along a fault zone. An east-west oriented fault zone in the vicinity of Swim has been suggested from analyses of earthquake epicentral data (R. Couch, personal communication, 1977). However, to date, other geological and geophysical investigations have not confirmed the fault zone. If a fault zone were present and it contained permeable zones, these could serve as conduits for deep circulation of meteoric water. It is more likely that if a fault zone is present, it would serve as an impermeable barrier to warm water moving down-slope, causing some impoundment and the emanation at Swim Springs. That the highest temperature orifice at Swim is lowest in elevation (Figure 5) could be attributed to nearly vertical circulation associated with a fault zone. More plausible, however, is the explanation that the water emanating at the lower orifice is warm water moving down-slope from a deeper horizon in the andesite, and therefore less mixed with cold water than the water in the higher orifices. Neither the fault-zone nor the down-slope moving warm water mechanisms for Swim Springs are mutually exclusive; both could be operating.

V. CONCLUSIONS

Though this is not a final report, sufficient data have been obtained to provide some preliminary conclusions on the geochemical setting of Mt. Hood. Firmer conclusions on the usefulness of the geochemistry in evaluating the geothermal resource potential await results of analyses presently underway.

1. The warm water at Swim Springs on the south flank of Mt. Hood has a large component (~90%) of nearer-surface cold water. The flux of cold-water runoff nearly masks the surface indications of deeper-circulating hot water. The upper-slope orifices at Swim are the most diluted, those downslope are successively less diluted. The oxygen-hydrogen isotope data indicate that cold-spring waters have short pathways between their sources and the springs, while a component of the warm-spring water has its origin considerably higher on the mountain.

2. Chemical geothermometers and mixing-model calculations indicate that temperatures at depth in the Swim Springs system are within the range 104-170°C. The silica mixing model gives a range of 192-240°C for unmixed hot water.

3. The chloride contents and specific conductances of the water sources indicate that most of the cold spring waters are derived almost directly from snow melt. Relatively high chloride contents and specific conductances in some springs on the south flank of Mt. Hood indicate that these waters may circulate deeper or may mix with geothermal waters.

4. Water in the geothermal test hole in Old Maid Flat, in a sample most likely from the Rhododendron Formation, has a different chemical character from the water at Swim. Geothermometry is consistent with a temperature gradient of 60°C/km as measured in the Old Maid Flat well.

5. The Platinum-group element, iridium, is present in identifiable abundances at one orifice at Swim Warm Springs, a cold spring, and in the small lake in the summit crater area. Iridium also occurs in altered andesite at one location on the western flank of Mt. Hood. The association of Ir with an andesitic volcano is surprising; it is generally considered to be associated with basic to ultrabasic igneous rocks.

6. The similarity between major- and trace-element contents of Pliocene andesite on the west flank of the mountain and intermediate intrusive rocks of the Laurel Hill pluton in that area supports Wise's (1969) contention that the pluton represents the root zone of a center of extrusion of the andesite.

7. The basalt exposed in the Robin Hood Quarry in the Hood River Valley has major- and trace-element contents very similar to those of the Roza flow of central Washington. This supports the idea that the basalt on the east side of the valley is Columbia River Basalt, on the upward-thrown side of a north-south trending normal fault.

VI. CONTINUING ACTIVITIES

Activities underway include analyses of gas samples collected in October 1978 in the summit fumarolic area. In the sampling of 1977 we were not able to collect sufficient water vapor to permit determination of isotope ratios. The volume of water vapor collected in 1978 is sufficient for these analyses. This will afford comparison with the isotope ratios of cold- and warm-spring water reported here.

Water analyses still to be completed at the time of publication include a sample collected in October 1978 from the geothermal test hole drilled near Timberline Lodge and a set of samples collected at that time from the three orifices sampled periodically at Swim Springs. Deepening of the geothermal test hole in Old Maid Flat in the summer of 1978 may permit us to obtain a fluid sample from a deeper aquifer (most likely within the Columbia River Basalt) than the Rhododendron Formation sampled in 1977.

Samples of altered and unaltered andesite from the fumarolic area in the summit crater were collected in October 1978. These are being analyzed for major and trace elements and will indicate if iridium and silver are present in the strongly altered ground, coinciding with the presence of these elements in the runoff water from the small lake.

It is recommended that one or more geothermal test holes be drilled in the Swim Warm Springs area. These holes should be deep enough to obtain temperature measurements and fluid samples from below the zone of near-surface and shallow cold-water runoff, to permit major-, trace-element, and isotope analyses of relatively unmixed hot water. The holes should be located on the up hill gradient from the Swim system to test whether the water emanating from Swim is leakage from volcanic units higher on Mt. Hood, or whether it is from deeper circulation within a fault zone.

LIST OF FIGURES

LIST OF TABLES

BIBLIOGRAPHY

Allen, J.E., 1966. The Cascade Range volcano-tectonic depression in Oregon, in Transactions of the Lunar Geologic Field Conference, Bend, Oregon, August 1965: Oregon Department Geology and Mineral Industries, 21-23, 2 figures.

Asaro, F., H.V. Michel and C.W. Myers, 1978. A statistical evaluation of some Columbia River Basalt chemical analyses, Rockwell International Report RHO-BWI-ST-3, 62 pp.

Ayers, F.D. and A.E. Creswell, 1951. The Mount Hood fumaroles, Mazama, 33(13), 33-39.

Bowman, H.R., A.J. Hebert, H.A. Wollenberg and F. Asaro, 1976. Trace, minor and major elements in geothermal waters and associated rock formations (north-central Nevada). Proc. 2nd U.N. Symposium Develop. Use Geothermal Res., San Francisco, 20-29 May 1975, 699-702.

Callaghan, E., 1933. Some features of the volcanic sequence in the Cascade Range in Oregon: Am. Geophys. Union Trans., 14th Annual Meeting, 243-249.

Craig, H., 1961. Standard for reporting concentrations of deuterium and oxygen-18 in natural waters: Science, 133, 1833.

Crandell, D.R. and M. Rubin, 1977. Late glacial and post-glacial eruptions at Mt. Hood, Oregon: Geol. Soc. Am. Abs. with Programs, 9(4), 406.

Folsom, M.M., 1970. Volcanic eruptions: The pioneer's attitudes on the Pacific Coast from 1800 to 1875: Ore Bin, 32(4), 61-71.

Fournier, R.O. and A.H. Truesdell, 1974. Geochemical indicators of subsurface temperature, Part II: Estimation of temperature and fraction of hot water mixed with cold water: U.S. Geol. Survey Journal. Res., 2(3), 263-270.

Fournier, R.O. and A.H. Truesdell, 1973. An empirical Na-K-Ca geothermometer for natural waters: Geoch. et Cosmoch. Acta, 37, 1255-1275.

Goldstein, N.E. and E. Mozley, 1978. A telluric-magnetotelluric survey at Mt. Hood, Oregon: A preliminary study. LBL-7050, 89 pp.

Hebert, A.J. and H.R. Bowman, 1976. Nondispersive soft X-ray fluorescence analyses of rocks and waters. Proc. 2nd U.N. Symposium Develop. Use Geothermal Res., San Francisco, 20-29 May 1975, 751-755.

Hebert, A.J. and K. Street, Jr., 1974. A nondispersive soft X-ray fluorescence spectrometer for quantitative analysis of the major elements in rocks and minerals. Anal. Chem., 46, 203.

Hoefs, J., 1973. Stable isotope geochemistry. Berlin: Springer Verlag.

McKenzie, W.F. and A.H. Truesdell, 1976. Geothermal reservoir temperatures estimated from the oxygen isotope compositions of dissolved sulfate and water from hot springs and shallow drill holes: Geothermics, 5(1-4), 51-61.

Perlman, I. and F. Asaro, 1969. Pottery analysis by neutron activation, Archaeometry, 11, 21-52.

Thayer, T.P., 1937. Petrology of the later tertiary and quaternary rocks of the north-central Cascade Mountains in Oregon, with notes on similar rocks in western Nevada. Geol. Soc. Am. Bull., 48, 1611-1652.

Truesdell, A.H. and R.O. Fournier, 1976. Calculation of deep temperatures in geothermal systems from the chemistry of boiling spring waters of mixed origin. Proc. 2nd U.N. Symposium Develop. Use Geothermal Res., San Francisco, 20-29 May 1975, 837-844.

Truesdell, A.H. and N.L. Nehring, 1978. Gases and water isotopes in a geochemical section across the Larderello, Italy, geothermal field. Pageoph., 117, 1-14.

Wise, W.S., 1968. Geology of the Mt. Hood volcano. Andesite Conference Guidebook, International Upper Mantle Project, Sci. Report. 16-S; also Oregon Dept. Geol. Mineral Ind. Bull., 62, 81-98.

Wise, W.S., 1969. Geology and petrology of the Mt. Hood area: A study of the High Cascade volcanism. Geol. Soc. Am. Bull., 80, 969-1006.

Wollenberg, H.A., 1975. Sampling hot springs for radioactive and trace elements: Proc. EPA Workshop on Sampling Geothermal Effluents, Las Vegas, Nevada, 20-21 October 1975, p. 24, and Lawrence Berkeley Laboratory Report, LBL-4422.

STATE OF OREGON
DEPARTMENT OF GEOLOGY AND MINERAL INDUSTRIES
1005 State Office Building
Portland, Oregon 97201

OPEN-FILE REPORT O-82-9

Geophy

GRAVITY ANOMALIES IN THE CASCADE RANGE IN OREGON: STRUCTURAL AND THERMAL IMPLICATIONS

by

R.W. Couch, G.S. Pitts, M. Gemperle,

D.E. Braman, and C.A. Veen

Geophysics Group, School of Oceanography,

Oregon State University, Corvallis, OR 97331

1982

Funds for this research were provided by the U.S. Geological Survey under Grant Number 14-08-0001-G-393 and by the U.S. Department of Energy through the Oregon Department of Geology and Mineral Industries under Cooperative Agreement Numbers DE-FC07-79ID12044 and DE-FC07-79ET27220.

NOTICE

The Oregon Department of Geology and Mineral Industries is publishing this paper because the subject matter is consistent with the mission of the Department. To facilitate timely distribution of information, camera-ready copy submitted by the authors has not been edited by the staff of the Oregon Department of Geology and Mineral Industries.

Table of Contents

List of Illustrations

List of Illustrations (con't)

Gravity Anomalies in the Cascade Range in Oregon: Structural and Thermal Implications

by

R. Couch, G.S. Pitts, M. Gemperle
D. Braman, and C. Veen

Geophysics Group, School of Oceanography
Oregon State University, Corvallis, OR 97331

Introduction

The High Cascade Mountains, a consequence of the subduction of the Juan de Fuca Plate beneath the continental margins of northern California, Oregon, Washington, and British Columbia, extend, as a volcanic arc, from northern California to British Columbia. Lavas and pyroclastics of Miocene through Recent age, variable in both time and space, have intruded into, passed through, and covered older rocks of unknown age, structure, and composition; consequently the evolution and constitution of the Cascade Range is very complex.

Because of marked differences in the densities and depths of the different geologic units that form the Cascade Range, measurements of the earth's gravity field can outline many of the structural units and provide limits on estimations of the densities, depths and petrology of the subsurface units particularly when used in conjuction with other geophysical, geological, and geochemical data. This report summarizes gravimetric measurements made by many investigators in the Cascades and surrounding regions since approximately 1965; provides free-air, Bouguer, regional, and residual gravity maps of the Cascade Range in Oregon between 121° W. lon. and 122°30' W. lon.; and discusses some of the structural and geothermal implications of the observed anomalies.

Gravity Measurements

Measurements of the earth's gravitational acceleration, reported by Blank (1965), Blank (1968), Leutsher (1968), Thiruvathukal (1968), Griscom (1974), Griscom (1975), Hassemer and Peterson (1977), Van Deusen (1978), Blakely (1979), Couch and Gemperle (1979), Pitts (1979), Finn (1980), Braman (1981), and Veen (1981), provide the principal facts for approximately 5210 gravity stations located (Figure 1) in the Cascade Range.

All of the gravity stations are referenced to the International Gravity Base Station located at the Carnegie Institute, Washington, D.C., through a series of primary and secondary base stations established in Washington, Oregon, and California (e.g. Woollard and Rose, 1963; Berg and Thiruvathukal, 1965; Blank, 1968; Barnes, 1968; Pitts, 1979; Braman, 1981; and Veen, 1981).

The circles in Couch and others (1982)* show the location of the gravity stations in the Cascade Mountains region. The average station density for the approximately 46,000 km^2 area is one station per 9 square kilometers; however, station densities within large sectors of the survey area vary significantly. Closely spaced stations occur near Timberline Lodge on Mount Hood, along the Bonneville Power Administration transmission line between Mount Hood and Mount Jefferson, across Green Ridge east of Mount Jefferson, around Paulina and East Lakes in Newberry Caldera and along many of the roads and highways in the region. Sparsely surveyed areas include the area between Mount Hood and the Columbia River, the Western Cascades west and southwest of Mount Hood,

*Residual gravity anomaly maps from this study have been released by the Oregon Department of Geology and Mineral Industries as Geologic Map Series GMS-26 (printed on topographic base, scale 1:250,000).

the Mount Jefferson Wilderness area, the Three Sisters Wilderness area and the Klamath Graben north of Klamath Lake. The station density is more than sufficient to outline most of the major structures of the Cascade Range; however, the observed anomalies undoubtedly do not reflect many of the smaller faults, cones, hypabyssal intrusions, and other geological structures present in the region.

The high-relief of the terrain in the Cascade Range makes good position control both difficult and imperative for successful gravity measurements. U.S. Geological Survey, U.S. Coast and Geodetic Survey, Oregon State Highway, U.S. Forest Service, and Bonneville Power Administration benchmarks, spot elevations shown on U.S. Geological Survey 7.5- and 15-minute topographic maps, and measurements with aneroid altimeters provided station elevations. Geodetic leveling on Mt. Hood and stero aerophotos of Crater Lake provided the elevations of a few selected stations. Benchmark locations and U.S. Geological Survey 7.5- and 15-minute maps provided horizontal position information.

Descriptions of the position and base station control, drift and tide corrections, meter and reduction parameters and field procedures used by the investigators are contained in their respective reports. The principal facts of the measurements compiled for and described in this report are currently archived in the Geophysics Group, Oregon State University, the Defense Mapping Agency, St. Louis, Missouri, and in the National Geophysical Solar-Terrestial Data Center, Boulder, Colorado.

Calculation of the Free-air and Bouguer Gravity Anomalies

The principal facts of the gravity measurements described above were reduced to free-air anomalies using the formula:

$$FAA = OG + FAC - THG$$

where OG is the observed gravitational attraction at the station, FAC is the free-air correction for the elevation of the station with respect to sea level, and THG is the theoretical gravitational attraction on the earth spheroid as given by the 1930 International Gravity Formula. The free-air correction, as formulated by Scheibe and Howard (1964), is

$$FAC = (.09411549 - 0.000137789 \sin^2\phi)h - 0.067 * 10^{-8}h^2$$

where h = elevation of the station in feet and ϕ is the latitude of the station. The 1930 International Gravity formula (Swick, 1942; Heiskanen and Vening Meinesz, 1958) is

$$THG = 978049.0(1 + 0.0052884 \sin^2\phi - 0.0000059 \sin^2 2\phi)$$

The complete Bouguer anomaly (CBA) which takes into account the elevation of the station (FAC) and the effects of the mass of the earth between the station and the spheroid is given by the relation:

$$CBA = FAA - SBC - CC - TC$$

where SBC is the simple Bouguer correction, CC is the curvature correction, and TC is the terrain correction.

The simple Bouguer correction (Bullard, 1936) is the attraction of an infinite slab of thickness h and density ρ given by the relation

$$SBC = 2\,G\,h = 0.012774\,h$$

where G is the universal gravitational constant and h is in feet. A standard reduction density of 2.67 gm/cm^3 was used in the computation of the simple Bouguer correction and the complete Bouguer anomalies.

The curvature correction reduces the effect of the infinite slab to that of a spherical cap of radius 166.7 km and thickness h (Swick, 1942). The correction is:

$$CC = h * (1.671 * 10^{-4} + h * (-1.229 * 10^{-8} + h * (4.67 * 10^{-16}))).$$

The terrain correction (TC), which compensates for the effects of local topography on gravity measurements was made by hand from field notes on the topography out to a radial distance of 68 m (Hayford and Bowie, 1912; zones A and B) from the station using the methods of Robbins and Oliver (1970). Terrain corrections for radial distances of 68 m to 166.7 km from the station (Hayford and Bowie, 1912; zones C through O) were made by computer with a program developed by Plouff (1977). Digital topographic information, obtained from the National Cartographic Information Center (NCIC) and reduced to areal blocks of one-half minute, one minute, and three minutes, provided the data base to compute the terrain correction for each station. Digital topography was not available for all zones around several stations. Terrain corrections for those zones were calculated by hand using techniques described by Oliver and others (1969). Terrain corrections for stations from Blank (1965) and Thiruvathukal (1968) were recomputed for zones C through O (Hayford and Bowie, 1912).

Pitts (1979), Braman (1981), and Veen (1981) estimated root-mean-square uncertainties of less than 1 mgal for free-air anomalies and less than 1.5 mgal for complete Bouguer anomalies in the Cascade Mountains region. Thiruvathukal (1968) estimated uncertainties of 1 to 2 mgal for the Bouguer anomalies included in his compilation of data for the gravity map of Oregon.

Free-Air Gravity Anomalies

Pitts and Couch (1978) and Pitts (1979) prepared a free-air gravity anomaly map of the central Cascade Mountains at a scale of 1:125,000, and Couch and others (1981a) and Couch and others (1981b) have prepared free-air gravity anomaly maps of the northern and southern Cascade Mountains at a scale of 1:250,000. Figures 3, 4, and 9 show their free-air gravity anomaly maps of the north, central, and south sectors, respectively, reduced to a scale of approximately 1:1,000,000. Anomaly contours occur at 10-mgal intervals, and heavy contours occur at 50-mgal intervals. The free-air gravity anomalies range from less than -90 mgal along the Columbia River gorge to over +150 mgal on Mount Hood and the Three Sisters.

The free-air gravity anomaly reflects the total gravitational acceleration at a point and includes the total mass of the earth in the measurement. Hence the free-air gravity anomalies depend in part on station elevation and yield a free-air anomaly map which resembles the topography, especially at short wavelengths. Figures 3 and 6, however, show that the average free-air anomaly in the Willamette Valley is approximately the same as in the Deschutes Valley, although the valley east of the Cascade Mountains is more than 3,000 feet higher in elevation than the valley west of the Cascade Mountains. The free-air anomalies indicate that the extra mass of the plateau east of the mountains is compensated either by less dense crustal materials or a thicker crust east of the mountains. Calculations reported by Dehlinger and others (1968), Thiruvathukal and others (1970), and Dehlinger and others (1970) based on gravity measurements indicate the crust is 20 to 25 km thick west of the Cascade Mountains and 35 to 45 km thick east of the mountains.

Recent seismic refraction measurements in the Cascade Mountains reported by Wegener and others (1980) and Hill and others (1981) indicate the crust is 40 to 45 km thick along the axis of the Cascade Mountains in northern Oregon.

Bouguer Gravity Anomalies

Figures 4, 7, and 10 show the Bouguer gravity anomalies of the Cascade Range in northern, central, and southern Oregon respectively. The anomalies range from greater than -50 mgal near the Columbia River in the northwestern portion of the Cascade Range to less than -170 mgal in the Basin and Range Province of southeastern Oregon. The mapped Bouguer gravity anomalies exhibit a marked gravity gradient with values decreasing irregularly from northwest to southeast. The constancy of the free-air anomalies and the change in Bouguer anomalies is interpreted as compensation of the elevated terrain in eastern Oregon by an increase in the thickness of the crust. Along the western portions of the mapped anomalies in Figures 4, 7, and 10, the high gravity gradient suggests not only a relatively rapid change in crustal thickness in a short distance in the vicinity of the Western Cascades but also a change in the near-surface structures from west to east.

The Bouguer anomalies about the Three Sisters and Newberry Crater areas are less pronounced than on the free-air gravity anomaly map, whereas the anomalies about Powell Butte are very prominent. This indicates that Bouguer correction and hence the reduction density of 2.67 gm/cm^3 is nearly correct for Newberry Crater and for portions of the Sisters volcanic complex. The Three Sisters, which have only a limited number of measurements about them, appear to be overcorrected in Figure 7; hence, their average density is less than the reduction density of 2.67 gm/cm^3. The large anomaly in the vicinity of Powell Butte is due to a large subsurface body whose density is greater than the surrounding country rock.

Large mass deficiencies are indicated in the area south of the Three Sisters and west of Newberry Crater and in the area northwest of Klamath Lake. These closed negative anomalies indicate large filled or partially filled sedimentary basins.

The observed anomalies are discussed further below after discussion of spectral separation of the anomalies into their regional and residual components.

The Separation of Regional and Residual Gravity Anomalies

Bouguer gravity anomalies arise from differences in densities between the topographic features of interest and the reduction density used to compute their anomalies and to density inhomogeneities at depth. Because the observed gravitational attraction is proportional to the inverse of the distance to the source body squared, structures at greater depth produce gravity anomalies of lower amplitude and longer wavelength than similar sources at shallower depths. Hence the separation of the longer wavelength anomalies or residual anomalies assists in the interpretation of the gravity measurements with respect to the shallower structures.

Spectral separation techniques applied to the complete Bouguer gravity anomalies described above yielded the regional gravity anomalies in Figure 11 and the residual gravity anomalies in Figures 14, 15 and 16. To achieve anomaly separation, initially the data, separated into three regions as originally mapped (Figures 4, 7 and 10), were prefiltered to detrend the data (Rayner, 1971). The detrended data were then gridded using the minimum curvature technique of Briggs (1974) as described by Boler (1979) and Boler and others (1978). A grid spacing of 6 km was used to create a data matrix that included regional data outside the survey area. Periodicity of the data, necessary for the application of the fast Fourier transformation, was forced by repeating the data matrix. The gridded, periodic data were transformed using a routine of Brenner (1968) after Cooley and Tukey (1965).

Application of a "boxcar" filter described by Rayner (1971) and

Nettleton (1976) with a cosine squared taper to the transformed data yielded spectral separation. Subsequently the inverse transformation and retrending resulted in a regional gravity map for the complete matrix. These techniques were described in detail by Boler and others (1978), Pitts (1979), Braman (1981) and Veen (1981).

The residual anomaly value at each station was calculated with the relation

$$\underline{RA}(\underline{\rho}) = \underline{CBA}(\underline{\rho}) - \underline{REG}(\underline{\rho})$$

where $\underline{RA}(\underline{\rho})$ is the residual anomaly at a reduction density of $(\underline{\rho})$, $\underline{CBA}(\underline{\rho})$ is the complete Bouguer anomaly at a reduction density of $(\underline{\rho})$ and $\underline{REG}(\underline{\rho})$ is the regional anomaly at a reduction density of $(\underline{\rho})$.

A reduction density of 2.43 gm/cm^3 was selected to minimize the effects of terrain in the area of the Cascade Range outlined in Figure 1. This density is a reasonable average for the area; however, a comparison of the free-air, Bouguer and residual gravity anomalies suggests a density of 2.6 to 2.7 gm/cm^3 would yield better results for Newberry Caldera and the Yamsay Mountains, whereas a density of 2.3 gm/cm^3 would yield better results for Mt. Hood and the Three Sisters. Indeed, Couch and Gemperle (1979) show a best reduction density for Mt. Hood of 2.27 gm/cm^3. As a consequence of the large variation in actual densities of the structures of the region, care is advised in interpreting singular anomalies.

The spectral separation of the anomalies occurred at a wavelength of approximately 90 km. This wavelength of separation yields residual anomalies with wavelengths shorter than 90 km that are due to sources at depths of less than approximately 20 km. A depth of 20 km is approximately one half the thickness of the earth's crust beneath and east of the Cascade Range. Figures 14, 15 and 16 show the

residual gravity anomalies of the Cascade Range in Oregon calculated as outlined above.

Figure 11 shows a map of the regional gravity anomalies with wavelengths longer than 90 km. However, conversely, the source depths of the regional anomalies, although primarily due to deeper sources, are not limited to sources below a depth of 20 km. Near-surface geologic units of large areal extent also can produce long-wavelength anomalies that may be included in the regional gravity map.

Regional Gravity Anomalies

Figure 11 shows a map of gravity anomalies in the Cascade Range in Oregon with wavelengths longer than 90 km. The regional gravity anomalies decrease in general from the Coast Range to eastern Oregon and from the Columbia River to the Basin and Range Province of southeastern Oregon. Changes in the long wavelength components of the gravity field reflect changes in the thickness of the crust. Computations by Thiruvathukal and others (1970) and Dehlinger and others (1970) based on gravity measurements indicate that the earth's crust in the vicinity of the Coast Range and Willamette Valley is approximately 20 to 25 km thick and east of the Cascades it is 35 to 45 km thick. Hill and others (1981) interpret reflected seismic waves observed along a refraction profile in the north-central Cascade Range to indicate a crustal thickness of approximately 40 km. Their results are in good agreement with those based on gravity measurements. The crustal cross section in Figure 20 illustrates the change in crustal thickness from west to east across the Cascade Range and shows that the change in thickness occurs most rapidly beneath the Western Cascades.

The regional gravity anomalies also suggest that the earth's crust is about 30 km thick near the Columbia River north of Mt. Hood and as much as 45 km thick between the Three Sisters and Crater Lake. Southeast of Crater Lake the gravity data suggest the crust may be more than 45 km thick; however, an intermediate or transition layer may be present between the lower crust and upper mantle in the Basin and Range Province (e.g. see Cook, 1962; Pakiser, 1963). We postulate that the lower crust and upper mantle in southeastern Oregon includes the northward extension

of the intermediate layer observed by Pakiser and Hill (1963) and Eaton (1963) in the Basin and Range Province in Nevada. The crustal cross section in Figure 21 shows the intermediate layer and suggests the crust above the intermediate layer may be less than 30 km thick in southeastern Oregon.

The northward excursion of the -80-mgal regional contour about Mt. Hood and the northward excursion of the -40-mgal contour about the Three Sisters may indicate changes in the crustal thickness or structure of the lower crust beneath the volcanic centers, or alternatively the anomalies may reflect compensating masses in the upper crust complimentary to the masses that cause the positive anomalies observed about the volcanic centers mapped in Figures 3, 6, 14, and 15.

Figure 12 shows topographic and gravimetric profiles along the axis of the High Cascades between the Columbia River and the California border. The elevations along the profile increase from just above sea level at the Columbia River to almost 6000 feet between Mt. Washington and Mt. Mcloughlin except for the LaPine valley and the area about Wickiup Reservoir. The short-wavelength positive free-air gravity anomalies reflect both the topography and many local mass concentrations in the upper crust, particularly beneath the stratovolcanoes. The average free-air anomaly is positive due both to uncompensated near-surface flows and intrusions and to an "edge effect" caused by the change in crustal thickness beneath the Western Cascades. The complete Bouguer gravity anomaly decreases as the topographic elevation increases, thereby indicating the higher elevations of the Cascade Range are compensated at depth.

Figure 13 shows topographic and gravity profiles, oriented west-to-east, across six of the High Cascades volcanoes. Mt. Hood, Mt. Jefferson, South Sister, and Mt. McLoughlin exhibit similar topographic and free-air gravity anomalies. The free-air anomalies start near zero and increase in amplitude to a value approximately proportional to the volume of the respective mountain. If the central peak anomaly of South Sister is omitted, the free-air anomaly signature of South Sister, Newberry Crater, and Crater Lake are similar. The anomalies suggest a mass concentration at shallow depths beneath the summits. The Bouguer gravity anomalies show a general decrease in amplitude from north to south as in Figure 12. This long-wavelength change in the Bouguer anomaly is due to the change in crustal thickness along the axis of the Cascades. A comparison of the free-air Bouguer and residual gravity anomalies suggests that the average reduction density of 2.43 gm/cm^3 is approximately correct for Crater Lake (or Mt. Mazama), slightly too light for Mt. McLoughlin and Newberry Caldera, and too dense for Mt. Hood, South Sister, and probably Mt. Jefferson. The average density of Mt. McLoughlin is probably between 2.43 and 2.50 gm/cm^3, whereas that of Mt. Hood, South Sister, and probably Mt. Jefferson is near 2.3 gm/cm^3. The shape of the Bouguer and the residual gravity anomaly profiles suggests that each of the volcanoes has a high density core or more dense mass beneath the summit. This may take the form of a dense central conduit in Mt. Hood (Couch and Gemperle, 1979), Mt. Jefferson, South Sister, and Mt. McLoughlin; a large intrusive within the volcano or near the base of the volcano (Williams and Finn, 1981); or a series of relatively dense flows that form the base of the volcano in Newberry Caldera, Crater Lake, and South Sister.

Residual Gravity Anomalies of the Cascade Range in Oregon

The maps in GMS-26 (Couch and others, 1982) show the residual gravity anomalies of the northern, central, and southern sectors respectively of the Cascade Range in Oregon at a scale of 1:250,000, and Figures 14, 15 and 16 show the residual gravity anomalies at a scale of approximately 1:1,000,000. The gravity anomalies, whose sources are located in the upper 20 km of the earth's crust, range from less than -26 mgal north of Klamath Lake to more than 30 mgal near Terrebonne north of Redmond.

The High Cascades exhibit positive residual gravity anomalies along the volcanic arc that are more extensive than the prominent peaks. In the vicinity of Mt. Hood the anomalies are small, and although no single outstanding anomaly is coincident with the topographic peak, the region about the peak is in general a residual gravity high. This suggests that though the density of the surface features is low, more dense rock occurs at a shallow depth beneath the surficial features. The positive anonalies are in part associated with the Columbia River basalts and may outline the extent of the basalts beneath the post-Miocene rocks about and northeast of Mt. Hood. The anomalies also may indicate more dense basement rocks beneath the basalts in the vicinity of Mt. Hood. Similarly, Hill and others (1981) interpreted their seismic measurements to indicate a regional thinning of the low-velocity near-surface rocks or a doming of the "basement" within 10 km of Mt. Hood.

A prominent positive anomaly encircles and connects Newberry Caldera and the Three Sisters. The anomaly also extends northeastward from the north flank of Newberry to the area about Powell Butte, north-northwestward from the north flank of Newberry to the area about

the Three Sisters, and then north-northwestward from the Three Sisters toward Three Fingered Jack. The residual gravity anomaly pattern suggests that the Three Sisters, Newberry Caldera, and Powell Butte volcanic centers are connected at depth and further that their placement is structurally controlled by fractures or lithologic discontinuities oriented northwest-southeast and northeast-southwest.

A narrow band of contiguous gravity lows extends from southwest of Mt. Hood near 45°10' N. lat., 121°50' W. lon. to the area south of Oakridge near 43°15' N. lat., 122°20' W. lon., then southeastward through Klamath Lake to Klamath Falls, and then southward into northern California. This band of gravity lows varies in width from less than 10 km south of Oakridge and west of Mt. Jefferson to more than 20 km southwest of the Three Sisters and is interrupted only by the Mt. Hood and Mt. Mazama volcanic complexes. North of Crater Lake the lows are located along and extend across the zone of contact between the Western Cascades and the High Cascades. They cross the axis of the High Cascades at Crater Lake and extend into the Basin and Range Province of southern Oregon and into the Modoc Plateau of northern California. We interpret these gravity anomalies to indicate a large fracture system and an associated broad breccia zone that extends along the Cascade Range from the Columbia River to northern California. The gravity anomaly minima suggest that vertical displacements of 2 to 3 km occur along the west side of the fracture zone. This zone has been covered, in part, by younger volcanic deposits and lava flows of High Cascade origin and obscured by contemporary intrusions. For example, gravity anomaly highs southeast of Oakridge, west of the Three Sisters, west of Mt. Washington and west of Mt. Jefferson outline flows or intrusions

that cover or extend into the eastern side of the brecciated zone.

Steep gravity gradients east of Mt. McLoughlin outline a fault-bounded graben that extends from the southeastern flank of Mt. Mazama to the south end of Klamath Lake. Computations based on the gravity minimum of -26 mgal and a density contrast between sediments in the graben and basement rock of 0.5 gm/cm^3 suggest the sediment thickness in the graben is 1 to 1.3 km in the vicinity of Fort Klamath.

The gravity low south of the Three Sisters outlines a sediment-filled basin, herein termed the Shukash Basin, in the vicinity of Wickiup Reservoir and Lookout Mountain. An arm of the basin, herein termed the Paulina Basin, extends southeastward along the base of the western flank of Paulina Shield. Computations based on gravity data suggest that the sediment thickness is about 1 km in the basin and about 0.5 km along the southwest base of Paulina Shield. Neither of these basins is apparent on geologic maps of the area (e.g. see Peterson and others (1976) and Walker (1977). The surface geology in the area includes Holocene cinder cones and glacial debris. The circularity of the anomaly and the presence of young cinder cones in and particularly along the northern rim of the Shukash Basin suggest subsidence of an older volcanic center. The postulated sediments of the Paulina Basin may lie beneath the younger flows and tuffs of the Paulina shield.

A broad gravity low outlines the Deschutes Basin east of Three Fingered Jack and Mt. Jefferson and west of the Deschutes River. Computations based on the gravity data suggest that more than 0.5 km of sediments fill the eastern part of the basin. A relative gravity high between the two lows in the central part of the basin coincides with

Green Ridge, a tilted fault block that extends across the basin from north to south. The Deschutes Basin gravity low also extends into the area between and west and south of Redmond and Bend.

A gravity low, elongated in the east-west direction, extends eastward from the southeast flank of Mt. Hood to the White River - Tygh Valley area. The negative gravity anomaly, where it is widest, coincides generally with the Tygh Valley Formation in the Tygh Basin described by Farooqui and others (1981). The gravity data suggest the sediment thickness south of Tygh Ridge is more than 0.5 km and that the basin shoals toward the south.

Prominent positive residual gravity anomalies include the Yamsay Mt. and Newberry Mt. complexes, a marked northeast-trending high between Redmond and Madras and an easterly trending high north of Warm Springs. The configuration and areal extent of the Yamsay Mt. and Newberry Mt. anomalies suggest the structure of the complexes consists of uncompensated high-density flows that increase in number and/or thickness toward the center of the complexes. In addition or alternatively, as Williams and Finn (1981) have suggested, the mountains may include large intrusive bodies at shallow depths beneath their summits. Walker Rim, prominent on topographic and geologic maps, does not exhibit a marked residual gravity anomaly; consequently it is believed to be only a surface or near-surface structure.

The positive gravity anomaly between Redmond and Madras is on trend with the Blue Mountain anticline and is probably related to shoaling of the pre-Tertiary basement along the anticline. If this is correct, the basement uplift along the anticline ends abruptly and in effect forms the eastern edge of the Deschutes Basin. Similarly the

gravity high north of Warm Springs outlines the easterly trending anticlinal uplift associated with the outcrops of the pre-Tertiary rocks of the Mutton Mountains.

Gravity Anomaly Lineations in the Cascade Range in Oregon

Density discontinuities that occur along lithologic boundaries, such as intrusions, flow fronts, and erosional or fault contacts, often are marked by steep gravity gradients. Linear anomaly contours in steep gravity gradient areas, particularly when they extend for large distances or are co-linear with other anomaly patterns, form gravity anomaly "lineations". Although the lineations, so indicated, may mark various kinds of lithologic changes, more generally they indicate vertical displacement of geological units across normal or high-angle reverse faults. However, because of the complexity and the heterogeneity of the geology in the Cascade Range, the sparsity of field data, and the fact that many of the contacts may be covered by younger strata, we retain the term "lineation" initially to describe some of the patterns of the residual gravity anomalies.

Figures 17, 18 and 19 show the residual gravity anomalies in the Cascade Range of northern, central and southern Oregon respectively. Superimposed on the maps are lineations suggested by the anomalies. Heavy lines demark prominent lineations, and narrow lines show less prominent lineations. Prominent lineations occur along steep gravity gradients where anomaly amplitudes are large and anomaly contours are straight or where a series of high gradients of several anomalies are aligned. Less prominent lineations occur where anomalies are lower in amplitude and in gradient and where contours are more sinuous or outline structures other than those which the lineation suggests. Many other lineations are visible on the residual gravity anomaly maps, particularly those which parallel the marked lineations, but are omitted to prevent obscuring the lineations shown.

The most prominent and striking of the lineation patterns is the system of subparallel lineations that strikes about N 10° E from approximately 43°40° N. lat., southeast of Oakridge to approximately 45°30' N. lat. near Mt. Hood. This system is about 210 km (130 mi) long and about 60 km (40 mi) wide. The western boundary, although exhibiting short wavelength serations, is surprisingly straight and is located along the west side of a prominent series of contiguous gravity anomaly minima. Contrastingly, the eastern boundary is not well defined. The anomalies which suggest the location of the eastern boundary include an offset in the Mutton Mts. anomaly, the zone of contact between the Deschutes Basin and the western end of the Blue Mt. uplift, and the saddle between the gravity minima of the Shukash Basin, south of the Three Sisters, and the Paulina Basin, west of the Paulina Shield.

The N 10° E pattern of lineations in this zone is interrupted northwest of Mt. Jefferson by lineations that are oriented approximately N 15° W and that extend from near the Columbia River east of Gresham to the headwaters of the Clackamas River between Mt. Hood and Mt. Jefferson.

South of Oakridge near 43°15' N. lat. the lineations change strike to about N 20° W and extend south-southeastward apparently through the Crater Lake area to Klamath Lake. At and south of Klamath Lake some of the lineations strike about N 37° W, but many other orientations are observable also. Along the gravity minima that extend from Crater Lake to Mt. Hood, lineations that bound the gravity lows strike approximately N 40° E to N 60° E and approximately N 40° W to N 50° W. Lineations with these orientations are more numerous west of the High Cascades than are indicated on the figures. However east of the Cascades these

orientations are only suggested in the Deschutes Basin and maybe in the Shukash Basin and Mutton Mts. areas.

In the Mt. Hood area lineations are observed that are oriented approximately N 30° W, N 15° W, N 7° E and N 82° E. The Mt. Mazama area shows a similar complex lineation pattern that includes orientations of about N 80° W, N 60° W, N 0° E, N 10° E, and N 70° E.

East of the Cascade Mountains easterly lineations include the anomaly gradient east of Mt. Hood that strikes about N 82° E and includes Tygh Ridge south of The Dalles, the flanks of the Blue Mountains uplift north of Redmond, the Powell Butte anomaly, the northeast flank of Yamsay Mt., along the northeast flanks of the Newberry and the Three Sisters volcanic complexes, and a lineation that extends along the southern boundary of the Paulina Basin and the Fort Rock Basin and transects the Shukash Basin. The latter lineation is the only one that may extend west of the High Cascades.

The Northern Oregon Crustal Cross Section

Line A-A' in Figure 2 maps the location of the geophysical crustal cross section of northern Oregon. The Northern Oregon Section, Figure 20, oriented approximately normal to the Cascade Range, extends from a point in Cascadia Abyssal Plain west of Oregon to a point in central Idaho. The section intersects the Humble Wicks No. 1 well on the east side of the Willamette Valley, crosses the Cascade Range near the divide between the Clackamas and Warm Springs Rivers, crosses the Deschutes River south of Maupin, and intersects the Standard Kirkpatrick No. 1 well near Condon. Logs of the two deep wells and topographic, geologic, gravimetric, and seismic refraction observations constrain the geophysical model cross section.

Shor and others (1968) made seismic refraction measurements in Cascadia Abyssal Plain west of Oregon along lines parallel to the continental margin. Their measurements provide data on the depth and seismic velocities of the crustal layers and top of the mantle on the westernmost end of the cross section. Seismic refraction observations by Hill (1972) provide data on the crustal thickness in eastern Oregon near the east end of the cross section, and the results of a seismic refraction experiment in the Cascades reported by Wegener and others (1980) and Hill and others (1981) provide information on the velocitites and thicknesses of the crustal layers in the Cascade Range.

The gravity data described in this report provided control for the central portion of the section between 121° and 122°30' W. lon., and the regional data described by Thiruvathukal and others (1970) and Dehlinger and others (1970) provided control for the eastern and western portions of the section.

The crustal cross section assumes a two-dimensional structure, a standard mass column of 50 km (30 mi) and 6442 mgal corresponding to a zero free-air gravity anomaly (Barday, 1974) and no lateral variations in density below a depth of 50 km (30 mi) (Braman, 1981). Iterative adjustments of layer boundaries constrained by land elevations, geologic contacts, refracting horizons, and horizons determined from the well logs were made until the gravity, computed with the method of Talwani and others (1959) and Gemperle (1975), agreed with the observed free-air anomalies. This process yielded the northern Oregon geophysical cross section.

Figure 20 shows the northern Oregon geophysical cross section. The section, approximately 400 km (250 mi) long, is oriented N 84° E approximately normal to the Willamette Valley and Cascade Range and intersects the High Cascades between Mt. Hood and Mt. Jefferson about 20 km north of Breitenbush Hot Springs. The continental crust is approximately 20 km thick in the vicinity of the Coast Range and increases in thickness to about 25 km on the east side of the Willamette Valley. The crust increases in thickness eastward in the vicinity of the Western Cascades and is about 35 km thick beneath the High Cascades. In eastern Oregon the crust is about 30 km thick.

Little structural control is available for the Deschutes-Umatilla Plateau in eastern Oregon; hence the cross section shows a lower crustal unit of 2.85 gm/cm^3 overlain by a layer of 2.63 gm/cm^3. The 2.85 gm/cm^3 layer beneath the plateau is observed at 6700 feet in the Standard Kirkpatrick No. 1 well as pre-Tertiary marine rocks similar in age and origin to rocks that crop out in the John Day Mountains south of the Deschutes-Umatilla Plateau.

The cross section shows layers of 2.43 and 2.55 gm/cm^3 in the vicinity of the Humble Wicks No. 1 well which correspond to the volcanics of the Western Cascades. These layers thin westward and are covered by or interfinger with the lighter (2.25 gm/cm^3) sedimentary rocks in the Willamette Valley. These sedimentary rocks, as observed in the Humble Wicks No.1 well, are composed of Oligo-Miocene tuffs and sands with interbedded volcanic fragments (Newton, 1969). The model section indicates that two large east-dipping normal faults displace rocks of the Western Cascades approximately 10 and 20 km east of the Humble Wicks No. 1 well. The model suggests that these unmapped faults extend to at least 5 km. Miocene volcanics of the Western Cascades form the surface layer of 2.43 gm/cm^3 density. The 2.55 gm/cm^3 layer beneath the Miocene volcanics is identified in the Humble Wicks No. 1 well as rock of the Fisher and Calapooya Formations of late Eocene age (Newton, 1969). The layer of density 2.70 gm/cm^3 may correlate with the Siletz River Volcanics of the Coast Range. Newton (1969) inferred that the Siletz River Volcanics shoal eastward beneath the Humble Wicks well at a depth of approximately 3 km.

The large intrusion of density 2.80 gm/cm^3 beneath the Clackamas River correlates with the massive Detroit or Hall Ridge Pluton located north of Detroit that has been described by Hammond and others (1982). Immediately east of the pluton a seismic refraction line, shot approximately normal to the section along the High Cascades (Wegener and others, 1980; Hill and others, 1981), constrains the thickness of the crustal layers. Baldwin (1959), Peck and others (1964), and Hammond and others (1982) map the surface of the uppermost layer in this region as andesites and basalts of Pliocene to Recent age. This layer of High

Cascade rocks is low in density (2.27 gm/cm^3) and less than 1.5 km thick over most of width of the region except near the intrusion where the layer thickens to over 3 km.

The low-density material of High Cascades origin overlies material with a density 2.60 gm/cm^3. This material, indicated by the gravity and seismic refraction measurements, very likely corresponds to the early High Cascades basalt platform and/or the "Plio-Cascades" described by Taylor (1980) that extend from the Western Cascades beneath the High Cascades to the Deschutes Basin.

In the cross section the units with densities of 2.60 and 2.80 gm/cm^3 shoal along the east flank of the Cascade Range. The elevation of the high-density rocks, indicated by a positive free-air gravity anomaly, occurs in the vicinity of Beaver Butte and may be associated with the early and pre-Tertiary rocks of the Mutton Mountains anticlinorium. Pre-Tertiary marine rocks were encountered at 6700 feet in the Standard Kirkpatrick No. 1 well near Condon, Oregon, approximately 100 km east of Beaver Butte. These rocks, indicated on the section as having an average density of 2.85 gm/cm^3, may be continuous with those of 2.80 gm/cm^3 beneath the Cascades.

Geophysical Cross Section of the Cascade Range in Southern Oregon

Line C-C' in Figure 8 shows the trace of the geophysical cross section across southern Oregon, and Figure 21 shows the cross section. The Southern Oregon Section, oriented east-west approximately normal to the Cascade Range, extends from the Gorda Basin offshore of southern Oregon to a point in southern Idaho. The section passes immediately south of Mt. McLoughlin, obliquely through the northern end of Klamath Lake and intersects the Humble Thomas Creek No. 1 well east of the area mapped in Figure 8.

The gravity data described in this report provided control for the central portion of the section between 121° and 122°30' W. lon., and the data described by Thiruvathukal and others (1970) in Oregon provided regional control.

The geologic maps of Wells and Peck (1961), Peterson and McIntyre (1970), and Walker (1977) provided information on near-surface geologic units, and interface locations and seismic logs from the Humble Thomas Creek No. 1 well provided estimates of the densities of the near-surface units via empirical relations between seismic velocity and density reported by Ludwig and others (1970). Aeromagnetic measurements reported by McLain (1981), modeled using the techniques described by Lu and Keeling (1974), helped constrain the structures between 121° and 122°30' W. lon. (Veen, 1981). The model crustal cross section assumes a two-dimensional structure, a standard mass column of 50 km and 6442 mgal corresponding to a zero free-air gravity anomaly (Barday, 1974), and no lateral variations in density below a depth of 50 km (30 mi) (Veen, 1981). Iterative adjustments of layer boundaries, constrained by land elevations,

geologic contacts, and horizons determined from the well logs of the Humble Thomas Creek No. 1 well, made until the gravity of the model computed with the method of Talwani and others (1959) and Gemperle (1975) agreed with the observed free-air anomalies, yielded the Southern Oregon Geophysical Cross Section.

Thiruvathukal and others (1970) computed a crustal thickness of 40 to 50 km for south-central and southeastern Oregon using gravity measurements and a model that consisted of a constant-density crust over a constant-density mantle. Studies by Hill and Pakiser (1967), Cook (1966), Scholz and others (1971) and Priestly and Brune (1978) indicate that the structure of the Basin and Range province is more complex and is characterized by a relatively thin crust and an anomalously low-velocity low-density upper mantle. In Figure 21 we extend this concept into the northern extent of the Basin and Range Province in southeastern Oregon and indicate a computed crustal thickness of approximately 30 km in the vicinity of the cross section. This crustal thickness agrees well with the recent seismic refraction measurements of Priestly and others (1982) in northern Nevada and southeastern Oregon. Figure 21 shows a relatively low-density (3.27 gm/cm^3) layer approximately 10 km thick overlying a mantle with a density 3.32 gm/cm^3. We would expect the low-density uppermost mantle to have a compressional-wave velocity of 7.7 to 7.9 km/sec and the mantle beneath to exhibit a compressional wave velocity of 8.0 to 8.2 km/sec.

Figure 21 shows a block of material of 2.70 gm/cm^3 density near the west end of the section that corresponds to Paleozoic and Mesozoic metamorphic sediments and volcanics of the Klamath Mountains. Rock of density 3.0 gm/cm^3 within the block corresponds to a band of ultramafic

intrusive rocks mapped by Wells and Peck (1961). A large intrusive body of 2.85 gm/cm^3 density rises asymmetrically to the surface along the east flank of the Klamath block and, as mapped by Wells and Peck (1961), consists of granitoid, gabbroid, and ultramafic rocks. The easterly dip and high density of this unit are consistent with the suggestion of Irwin (1966) that the large intrusive body may be the eroded lip of a mafic or ultramafic sheet whose roots lie buried beneath rocks of the eastern Klamath Mountains.

Along the surface the units with densities of 2.10 and 2.2 gm/cm^3 are indicative of sediment-filled basins and are consistent with the units mapped by Peterson and McIntyre (1970) and Walker (1977). The basins are bounded by faults on the eastern and/or western sides and are associated with pluvial deposits in Pleistocene lakes.

The western end of the 2.50 gm/cm^3 unit and the 2.70 gm/cm^3 unit west of 122°30' W. lon. correspond to the volcanics of the Western Cascade Mountains. The model section suggests these rocks may extend a considerable distance eastward beneath the Pliocene and Pleistocene sediments and volcanics of the Basin and Range Province which are at least 4 km thick at the Humble Thomas Creek No. 1 well.

The two units of 2.65 gm/cm^3 density west of Upper Klamath Lake are basaltic andesites of the High Cascades. These units overlie a layer of 2.50 gm/cm^3 density that represents andesites of Mt. McLoughlin. A density of 2.50 gm/cm^3 for Mt. McLoughlin is similar to the density of 2.54 gm/cm^3 determined for Mt. Shasta by LaFehr (1965).

The model section indicates that the sedimentary layer with a density of 2.20 gm/cm^3 extends eastward to Abert Rim and may cover a

series of step-like faults that form the western side of a graben. The model also suggests that this fault system extends to a depth of at least 3 km and displaces rocks with a density of 2.65 gm/cm^3.

The large irregularly shaped body with a density of 2.65 gm/cm^3 east of Klamath lake coincides with a large residual gravity anomaly (see Figure 16) located immediately south of the Sprague River Valley. The density and model configuration suggests a large buried intrusive body that might be the heat source for the thermal springs in the valley.

Between the irregular block with a density of 2.65 gm/cm^3 and the Humble Thomas Creek No. 1 well, a five-km-thick layer of 2.50 density coincides with the southern extent of a large negative residual gravity anomaly which extends northward to Yamsay Mountain. This unit may reflect, in part, low-density material in a synclinal basin. Peterson and McIntyre (1970) proposed a synclinal basin in the area of Yamsay Mountain, Sycan Marsh and the Sprague River valley. The data along the section are insufficient to delineate or determine the depth of such a basin.

The geologic maps of Wells and Peck (1961) and Peterson and McIntyre (1970) and the cross section in Figure 21 indicate that a series of step-like faults form the graben that contains Upper Klamath Lake. The model suggests that the sediments that fill the graben may be 1.2 km thick and that the graben floor may be downdropped a total of 1.6 km. These estimates depend on the densities assumed for the sediments and surrounding rocks. On the residual gravity anomaly map (Figure 16) the negative anomaly associated with the graben increases in width and

amplitude northwest of Upper Klamath Lake and decreases toward the south. Hence the displacements on the bounding faults and the thickness of sediment also increase toward the north and decrease toward the south.

Structural and Geothermal Implications of the Cascade Gravity Anomalies

The residual gravity anomalies in Figures 14, 15, and 16, and the consequent prominent lineations in Figure 17, 18, and 19 outline a major fault zone, herein called the Cascade fracture zone, that extends along and across the transition between the Western Cascades and High Cascades north of Crater Lake. South of 43°10' N. latitude the Cascades fracture zone passes through Mt. Mazama and includes the Fort Klamath Basin and Klamath Graben. South of Klamath Lake the fracture zone appears to extend south and/or southeasterly into northern California. An arm of the fracture zone may strike southwesterly from the northwest flank of Crater Lake.

The gravity anomaly minima and the consequent lineations that outline the 400-km (250-mi)-long fracture zone are interpreted as indicating normal faulting with the east side down. Recent geologic mapping in the area of Cougar Reservoir northeast of Oakridge (Priest and Woller, 1982) and in the North Santiam River area southwest of Mt. Jefferson (Hammond and others, 1982) confirms a large fault zone with vertical displacement. The down faulting and down-faulted blocks probably extend farther eastward than the gravity data suggest. The expected gravity low east of the observed low is quite likely obscured by the high-density material that overlies the down-faulted blocks and forms the basal units of the younger High Cascades. The gravity lows along the fracture zone reflect the brecciated material and low-density intrusions in the fracture zone and the low-density material of High Cascade origin that overlies and fills the graben formed by the down-faulted blocks. The sequence of parallel lineations, oriented N 10° E,

on the west side of the Cascades are interpreted as delineating the western side of a Cascades graben. The lineations, and hence the graben boundary, between 42°15' and 44°45' are remarkable for their linearity. Less prominent lineations east of the High Cascades suggest an eastern side of the graben that may actually lie east of Green Ridge, near the western ends of the Mutton Mts. and Blue Mts. anticlines, and between the Shukash and Paulina Basins. This eastermost boundary, if it exists, exists at depth and may actually be a monoclinal flexure in some areas rather than a fault. The lineations suggest the fault system or graben is approximately 60 km (40 mi) or more wide north of 43°30' N. latitude between Crater Lake and Mt. Hood. Many faults both east and west of the High Cascades occur within the graben and parallel the sides.

In addition to the north-trending faults which define the Cascades fracture zone and graben, many lineations, some very prominent, transect the graben structure in northeast-southwest and southwest-northeast directions. The residual gravity anomalies indicate that vertical displacement has occurred on these faults also, particularly on the west side of the High Cascades. Structural blocks defined by these complimentary faults and the N 10° E-trending faults have dropped to form small, generally filled grabens and basins.

Interestingly, most of the hot springs in the Western Cascades (indicated by the triangles in Figures 17, 18, and 19) seem to occur on or near northeasterly oriented faults or near the junction of the northeasterly striking faults and northerly or northwesterly striking faults.

In Figure 20, the material of density 2.27 gm/cm^3 represents High Cascades flows and pyroclastics that are porous and permeable. Water that penetrates these rocks would flow downward and westward where it would contact hot rock at relatively shallow depths beneath the High Cascades or percolate down graben faults which extend 4 km or more deep to deeper heat sources beneath the Western Cascades. After becoming heated and flowing generally westward, the water would rise to the surface along the faults that form and transect the western side of the Cascade Graben. If such geothermal systems prevail in the Cascade Range, exploration targets would include the larger transecting faults along the western side of the Cascade Graben that are still active or open. Further, if such systems have been active for long periods of time, extensive mineralization zones should exist along some of the faults or fault zones.

Acknowledgements

We appreciate the effort and dedication of the many people who assisted in the field measurements. We thank A. Griscom, J. Leutsher, H. Richard Blank, R. Blakely, D. Williams, and J. Van Deusen for access to their unpublished data and encouragement in the course of the studies. Steven Troseth and Josie Peper provided the cartographic and drafting efforts, and Donna Moore typed the manuscript.

This research was supported by the U.S. Geological Survey under Grant Number 14-08-0001-G-393 and by the U.S. Department of Energy through the Department of Geology and Mineral Industries of the State of Oregon under Cooperative Agreement Numbers DE-FC07-79ID12044 and DE-FC07-79ET27220.

References

Baldwin, E.M., 1959, Geology of Oregon: Eugene, Oreg., University of Oregon Cooperative Bookstore, 136 p.

------1980, Geology of Oregon (3rd ed.): Dubuque, Iowa, Kendall/Hunt, 170 p.

Barday, R.J., 1974, Structure of the Panama Basin from gravity data: Corvallis, Oreg., Oregon State University master's thesis, 99 p.

Barnes, D.F., 1968, Mount Hood calibration loop: Menlo Park, Calif., U.S. Geological Survey unpublished report.

Berg, J.W., Jr., and Thiruvathukal, J.V., 1965, Gravity base station network, Oregon: Journal of Geophysical Research, v. 70, no. 14, p. 3325-3330.

Blakeley, R.J., 1979, Medford gravity survey: Menlo Park, Calif., U.S. Geological Survey unpublished data.

Blank, H.R., Jr., 1965, Southwest Oregon gravity data: U.S. Geological Survey Open-File Report 65-17, 1 p., 63 computer printout sheets, 1 map.

------1968, Aeromagnetic and gravity surveys of the Crater Lake region, Oregon, in Dole, H.M., ed., Andesite Conference guidebook: Oregon Department of Geology and Mineral Industries Bulletin 62, p. 42-52.

Boler, F.M., 1979, Aeromagnetic measurements, magnetic source depths, and the Curie point isotherm in the Vale-Owyhee, Oregon, geothermal area: Corvallis, Oreg., Oregon State University master's thesis, 104 p.

Boler, F.M., Pitts, G.S., Connard, G.G., and Gemperle, M., 1978, Gravity and aeromagnetic data analysis, pt. 1, in Couch, R.W., Geophysical investigations of the Cascade Range in central Oregon: Technical Report No. 5 to the U.S. Geological Survey Extramural Geothermal Research Program.

Bowen, R.G., and Peterson, R.V., 1970, Thermal springs and wells [in Oregon]: Oregon Department of Geology and Mineral Industries Miscellaneous Paper 14, 1 sheet.

Braman, D.E., 1981, Interpretation of gravity anomalies observed in the Cascade Mountain province of northern Oregon: Corvallis, Oreg., Oregon State University master's thesis, 144 p.

Brenner, N., 1968, FOR2D subroutine package for multidimensional FFT: Boston, Mass., Massachusetts Institute of Technology, Lincoln Laboratory.

Briggs, I.C., 1974, Machine contouring using minimum curvature: Geophysics, v. 39, no. 1, p. 39-48.

Bullard, E.C., 1936, Gravity measurements in East Africa: Royal Society of London Philosophical Transactions, ser. A, v. 235, p. 445-531.

Chapman, R.H., and Bishop, C.C., 1968, Bouguer gravity atlas of California--Alturas sheet: California Division of Mines and Geology.

Cook, K.L., 1962, The problem of the mantle-crust mix--lateral inhomogeneity in the uppermost part of the earth's mantle: Advances in Geophysics, v. 9, p. 295-360.

------1966, Rift system in the Basin and Range Province, in Irvine, T.N., ed., The world rift system. International Upper Mantle Committee Symposium, Ottawa, 1965: Geological Survey of Canada Paper 66-14, p. 246-279.

Cooley, J.W., and Tukey, J.W., 1965, An algorithm for the machine calculation of complex Fourier series: Mathematics of Computation, v. 19, no. 89, p. 297-301.

Couch, R.W., and Gemperle, M., 1979, Gravity measurements in the area of Mount Hood, Oregon, in Hull, D.A. investigator, and Riccio, J.F., ed., Geothermal resource assessment of Mount Hood: Oregon Department of Geology and Mineral Industries Open-File Report O-79-8, p. 137-189.

Couch, R.W., Pitts, G.S., Braman, D.E., and Gemperle, M., 1981a, Free-air gravity anomaly map and complete Bouguer gravity anomaly map, Cascade Mountain Range, northern Oregon: Oregon Department of Geology and Mineral Industries Geological Map Series GMS-15.

Couch, R.W., Pitts, G.S., Gemperle, M., Veen, C.A., and Braman, D.E., 1982, Residual gravity maps of the northern, central, and southern Cascade Range, Oregon, 122° 30' to 121° 00' E. by 42° 00' to 45° 45' N.: Oregon Department of Geology and Mineral Industries Geological Map Series GMS-26.

Couch, R.W., Pitts, G.S., Veen, C.A., and Gemperle, M., 1981b, Free-air gravity anomaly map and complete Bouguer gravity anomaly map, Cascade Mountain Range, southern Oregon: Oregon Department of Geology and Mineral Industries Geological Map Series GMS-16.

Couch, R.W., Thrasher, G., and Keeling, K., 1976, The Deschutes valley earthquake of April 12, 1976: Oregon Department of Geology and Mineral Industries, Ore Bin, v. 38, no. 10, p. 151-161.

Dehlinger, P., Couch, R.W., and Gemperle, M., 1968, Continental and oceanic structure from the Oregon coast westward across the Juan de Fuca Ridge, in Symposium on continental margins and island arcs, 3rd, Zürich, 1967: Canadian Journal of Earth Sciences, v. 5, no. 4, p. 1079-1090.

Dehlinger, P., Couch, R.W., McManus, D.A., and Gemperle, M., 1970, Northeast Pacific structure, in Maxwell, A.E., ed., The sea: New York, N.Y., John Wiley, v. 4, pt. 2, p. 133-189.

Eaton, J.P., 1963, Crustal structure from San Francisco, California, to Eureka, Nevada, from seismic-refraction measurements: Journal of Geophysical Research, v. 68, no. 20, p. 5789-5806.

Farooqui, S.M., Beaulieu, J.D., Bunker, R.C., Stensland, D.E., and Thoms, R.E., 1981, Dalles Group: Neogene formations overlying the Columbia River Basalt Group in north-central Oregon: Oregon Department of Geology and Mineral Industries, Oregon Geology, v. 43, no. 10, p. 131-140.

Finn, C., 1980, Crater Lake gravity survey: Denver, Colo., U.S. Geological Survey unpublished data.

Gemperle, M., 1975, Program GRAV2DS: Corvallis, Oreg., Oregon State University Geophysics Program and Data Library, 9 p.

Griscom, A., 1974, Wart Peak gravity survey: Menlo Park, Calif., U.S. Geological Survey unpublished data.

------1975, Newberry Crater gravity survey: Menlo Park, Calif., U.S. Geological Survey unpublished data.

Hammond, P.E., Geyer, K.M., and Anderson, J.L., 1982, Preliminary geologic map and cross sections of the upper Clackamas and North Santiam Rivers area, northern Oregon Cascade Range: Portland, Oreg., Portland State University Department of Earth Sciences.

Hassemer, J.H., and Peterson, D.L., 1977, Principal facts for a gravity survey of Breitenbush Known Geothermal Resource Area, Oregon: U.S. Geological Survey Open-File Report 77-67-A, 2 p., 1 table.

Hayford, J.F., and Bowie, W., 1912, The effect of topography and isostatic compensation upon the intensity of gravity: U.S. Coast and Geodetic Survey Special Publication 10, 132 p.

Heiskanen, W.A., and Vening Meinesz, F.A., 1958, The earth and its gravity field: New York, N.Y., McGraw-Hill, 470 p.

Hill, D.P., 1963, Gravity and crustal structure in the western Snake River Plain, Idaho: Journal of Geophysical Research, v. 68, no. 20, p. 5807-5819.

------1972, Crustal and upper mantle structure of the Columbia Plateau from long-range seismic-refraction measurements: Geological Society of America Bulletin, v. 83, no. 6, p. 1639-1648.

Hill, D.P., Mooney, W.D., Fuis, G.S., and Healy, J.H., 1981, Evidence on the structure and tectonic environment of the volcanoes in the Cascade Range, Oregon and Washington, from seismic-refraction/reflection measurements [abs.]: Society of Exploration Geophysicists 51st Annual International Meeting, Los Angeles, Calif.

Hill, D.P., and Pakiser, L.C., 1967, Seismic-refraction study of crustal structure between the Nevada test site and Boise, Idaho: Geological Society of America Bulletin, v. 78, no. 6, p. 685-704.

Irwin, W.P., 1966, Geology of the Klamath Mountains Province, in Bailey, E.H., ed., Geology of northern California: California Division of Mines and Geology Bulletin 190, p. 19-38.

Kim, C.K., and Blank, H.R., Jr., 1973, Bouguer gravity atlas of California--Weed sheet: California Division of Mines and Geology.

Kohler, W., Healy, J.H., and Wegener, S., 1982, Upper crustal structure of the Mt. Hood, Oregon, region as revealed by time-term analysis: Journal of Geophysical Research, in press.

LaFehr, T.R., 1965, Gravity, isostasy, and crustal structure in the southern Cascade Range: Journal of Geophysical Research, v. 70, no. 22, p. 5581-5597.

Lawrence, R.D., 1976, Strike-slip faulting terminates the Basin and Range province in Oregon: Geological Society of America Bulletin, v. 87, no. 6, p. 846-850.

Leutsher, J., 1968, Newberry Crater gravity survey: Menlo Park, Calif., U.S. Geological Survey unpublished data.

Lu, R.S., and Keeling, K.M., 1974, A simplified program for the rapid calculation of theoretical marine magnetic anomalies: Science Reports of the National Taiwan University, no. 4, p. 105-114.

Ludwig, W.J., Nafe, J.E., and Drake, C.L., 1970, Seismic refraction, in Maxwell, A.E., ed., The sea: New York, N.Y., John Wiley, v. 4, pt. 1, p. 53-84.

McBirney, A.R., 1968, Petrochemistry of the Cascade andesite volcanoes, in Dole, H.M., ed., Andesite Conference guidebook: Oregon Department of Geology and Mineral Industries Bulletin 62, p. 101-107.

McLain, W.H., 1981, Geothermal and structural implications of magnetic anomalies observed over the southern Oregon Cascade Mountains and adjoining Basin and Range Province: Corvallis, Oreg., Oregon State University master's thesis, 151 p.

Nettleton, L.L., 1976, Gravity and magnetics in oil prospecting: New York, N.Y., McGraw-Hill, 464 p.

Newton, V.C., Jr., 1969, Subsurface geology of the lower Columbia and Willamette Basins, Oregon: Oregon Department of Geology and Mineral Industries Oil and Gas Investigation 2, 121 p.

Oliver, H.W., Griscom, A., Robbins, S.L., and Hanna, W.F., 1969, U.S. Geological Survey gravity data in California, part IV: Menlo Park, Calif., U.S. Geological Survey internal report, 41 p.

Pakiser, L.C., 1963, Structure of the crust and upper mantle in the western United States: Journal of Geophysical Research, v. 68, no. 20, p. 5747-5756.

Pakiser, L.C., and Hill, D.P., 1963, Crustal structure in Nevada and southern Idaho from nuclear explosions: Journal of Geophysical Research, v. 68, no. 20, p. 5757-5766.

Peck, D.L., Griggs, A.B., Schlicker, H.G., Wells, F.G., and Dole, H.M., 1964, Geology of the central and northern parts of the Western Cascade Range in Oregon: U.S. Geological Survey Professional Paper 449, 56 p.

Peterson, N.V., Groh, E.A., Taylor, E.M., and Stensland, D.E., 1976, Geology and mineral resources of Deschutes County, Oregon: Oregon Department of Geology and Mineral Industries Bulletin 89, 66 p.

Peterson, N.V., and McIntyre, J.R., 1970, The reconnaissance geology and mineral resources of eastern Klamath County and western Lake County, Oregon: Oregon Department of Geology and Mineral Industries Bulletin 66, 70 p.

Pitts, G.S., 1979, Interpretation of gravity measurements made in the Cascade Mountains and adjoining Basin and Range Province in central Oregon: Corvallis, Oreg., Oregon State University master's thesis, 186 p.

Pitts, G.S., and Couch, R.W., 1978, Complete Bouguer gravity anomaly map, Cascade Mountain Range, central Oregon: Oregon Department of Geology and Mineral Industries Geological Map Series GMS-8.

Plouff, D., 1977, Preliminary documentation for a FORTRAN program to compute gravity terrain corrections based on topography digitized on a geographic grid: U.S. Geological Survey Open-File Report 77-535, 45 p.

Priest, G.R., and Woller, N.M., 1982, Geology of the Cougar Reservoir area, in Priest, G.R., and Vogt, B.F., eds., Geology and geothermal resources of the Cascades, Oregon: Oregon Department of Geology and Mineral Industries Open-File Report O-82-7, in preparation.

Priestly, K.F., and Brune, J., 1978, Surface waves and the structure of the Great Basin of Nevada and western Utah: Journal of Geophysical Research, v. 83, no. 35, p. 2265-2272.

Priestly, K.F., Ryall, A.S., and Fezie, G.S., 1982, Crust and upper mantle structure in the northwest Basin and Range Province: Bulletin of the Seismological Society of America, v. 72, no. 3, p. 911-924.

Rayner, J.N., 1971, An introduction to spectral analysis: London, Pion Ltd., 174 p.

Robbins, S.L., and Oliver, H.W., 1970, On making inner-zone terrain corrections to gravity data: A contribution of the regional geophysics branch: Menlo Park, Calif., U.S. Geological Survey report to the U.S. Army Topographic Command.

Scheibe, D.M., and Howard, H.W., 1964, Classical methods for the reduction of gravity observations: U.S. Air Force Aeronautical Chart and Information Center Publication 12, 65 p.

Scholz, C.H., Barazangi, M., and Sbar, M.L., 1971, Late Cenozoic evolution of the Great Basin, western United States, as an ensialic interarc basin: Geological Society of America Bulletin, v. 82, no. 11, p. 2979-2990.

Shor, G.G., Jr., Dehlinger, P., Kirk, H.K., and French, W.S., 1968, Seismic refraction studies off Oregon and northern California: Journal of Geophysical Research, v. 73, no. 6, p. 2175-2194.

Stanley, W., 1981, Magnetotelluric survey of the Cascade volcanoes region, Pacific Northwest [abs.]: Society of Exploration Geophysicists 51st Annual International Meeting, Los Angeles, Calif., program, p. 16.

Swick, C.H., 1942, Pendulum gravity measurements and isostatic reductions: U.S. Coast and Geodetic Survey Special Publication 232, 82 p.

Talwani, M., Worzel, J.L., and Landisman, J., 1959, Rapid gravity computations for two-dimensional bodies with application to the Mendocino submarine fracture zone: Journal of Geophysical Research, v. 64, no. 1, p. 49-59.

Taylor, E.M., 1980, Volcanic and volcaniclastic rocks on the east flank of the central Cascade Range to the Deschutes River, Oregon, in Oles, K.F., Johnson, J.G., Niem, A.R., and Niem, W.A., eds., Geologic field trips in western Oregon and southwestern Washington: Oregon Department of Geology and Mineral Industries Bulletin 101, p. 1-7.

Thiruvathukal, J.V., 1968, Regional gravity of Oregon: Corvallis, Oreg., Oregon State University doctoral dissertation, 92 p.

Thiruvathukal, J.V., Berg, J.W., Jr., and Heinrichs, D.F., 1970, Regional gravity of Oregon: Geological Society of America Bulletin, v. 81, no. 3, p. 725-238.

Van Deusen, J.E., III, 1978, Mapping geothermal anomalies in the Klamath Falls, Oregon, region with gravity and aeromagnetic data: Eugene, Oreg., University of Oregon master's thesis, 86 p.

Veen, C.A., 1981, Gravity anomalies and their structural implications for the southern Oregon Cascade Mountains and adjoining Basin and Range Province: Corvallis, Oreg., Oregon State University master's thesis, 86 p.

Walker, G.W., 1977, Geologic map of Oregon east of the 121st meridian: U.S. Geological Survey Miscellaneous Investigations Series Map I-902.

Wegener, S.S., Mooney, W.D., and Healy, J.H., 1980, A long-range seismic-refraction study of the High Cascades, Oregon [abs.]: EOS (American Geophysical Union Transactions), v. 61, no. 6, p. 71.

Wells, F.G., and Peck, D.L., 1961, Geologic map of Oregon west of the 121st meridian: U.S. Geological Survey Miscellaneous Geologic Investigations Map I-325.

Williams, D.L., and Finn, C., 1981, Evidence from gravity data on the location and size of subvolcanic intrusions: Society of Exploration Geophysicists 51st Annual International Meeting, Los Angeles, Calif., oral presentation of preliminary results.

Williams, D.L., Hull, D.A., Ackerman, H.D., and Beeson, M.H., 1982, The Mt. Hood region: Volcanic history, structure, and geothermal energy potential: Journal of Geophysical Research, v. 87, no. B4, p. 2767-2781.

Woollard, G.P., and Rose, J.C., 1963, International gravity measurements: Madison, Wis., University of Wisconsin Geophysical and Polar Research Center, 518 p.

Figure Captions

Figure 1. Regional geology of the Pacific Northwest. Rectangles outline the areas of gravity surveys in the Cascade Range of northern, central, and southern Oregon.

Figure 2. Topography of the Cascade Range in northern Oregon. Elevation contours occur at 1000-foot intervals. A-A' shows the location of the seismic refraction line reported by Wegener and others, 1980, and Hill and others, 1981. B-B' shows the trace of the northern Cascade Range geophysical cross section shown in Figure 20.

Figure 3. Free-air gravity anomalies of the Cascade Range of northern Oregon. Heavy contours occur at 50-mgal intervals.

Figure 4. Complete Bouguer gravity anomalies of the Cascade Range of northern Oregon. Heavy contours occur at 10-mgal intervals.

Figure 5. Topographic map of the Cascade Range in central Oregon.

Figure 6. Free-air gravity anomaly map of the Cascade Range in central Oregon. Heavy contours occur at 50-mgal intervals.

Figure 7. Complete Bouguer gravity anomalies of the Cascade Range in central Oregon. Heavy contours occur at 10-mgal intervals.

Figure 8. Topography of the Cascade Range in southern Oregon. Elevation contours occur at 1000-foot intervals. C-C' shows the trace of the geophysical cross section shown in Figure 21.

Figure 9. Free-air gravity anomalies of the Cascade Range in southern Oregon. Heavy contours occur at 50-mgal intervals.

Figure 10. Complete Bouguer gravity anomalies of the Cascade Range in southern Oregon. Heavy contours occur at 10 mgal intervals.

Figure 11. Regional gravity anomalies of the Cascade Range in Oregon. Reduction density is 2.43 gm/cm^3. Map shows anomalies with wavelengths greater than 90 km. Dotted lines outline gravity survey areas.

Figure 12. Topographic and gravity anomaly profiles along the axis of the Cascade Range in Oregon.

Figure 13. West-to-east topographic and gravity profiles of High Cascade Volcanoes.

Figure 14. Residual gravity anomaly map of the Cascade Range in northern Oregon. Heavy contours occur at 10-mgal intervals.

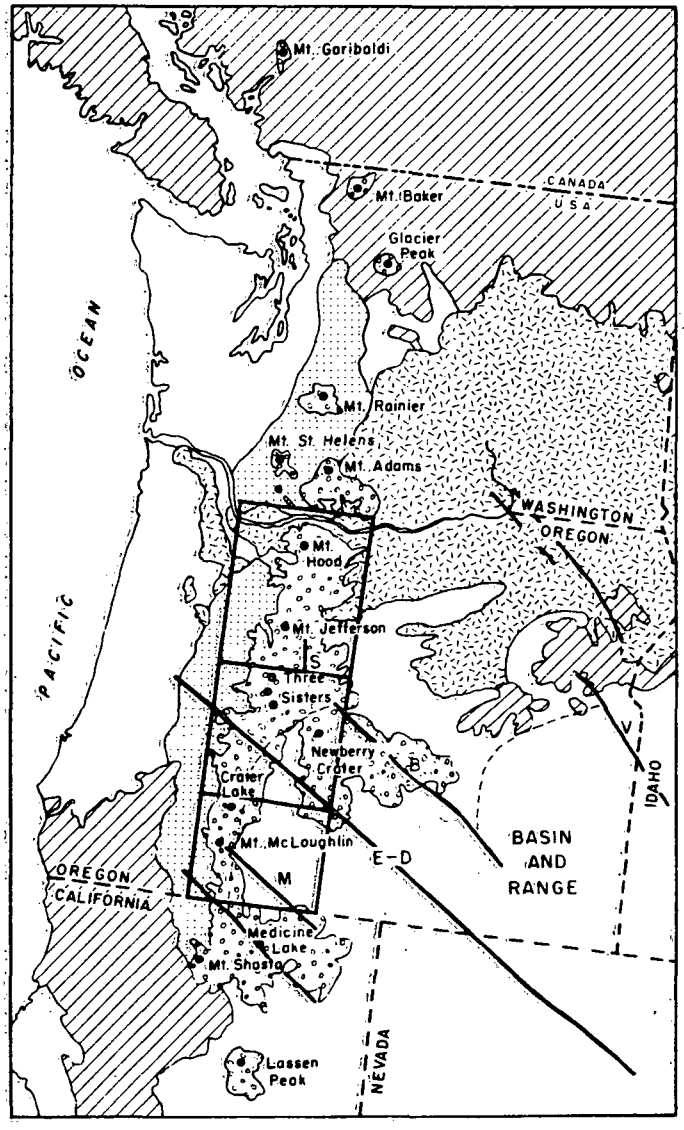

QUATERNARY VOLCANIC ROCKS

WESTERN CASCADES

COLUMBIA RIVER BASALTS

PRE-TERTIARY ROCKS

---- Boundary of Basin and Range

• Quaternary volcanic centers

—— Fault zones:

B = Brothers Fault Zone
E-D = Eugene-Denio Zone
M = McLoughlin Zone
V = Vale Zone
S = Sisters Fault Zone

Generalized geology after McBirney (1968).
Fault data after Lawrence (1976).

Figure 1.

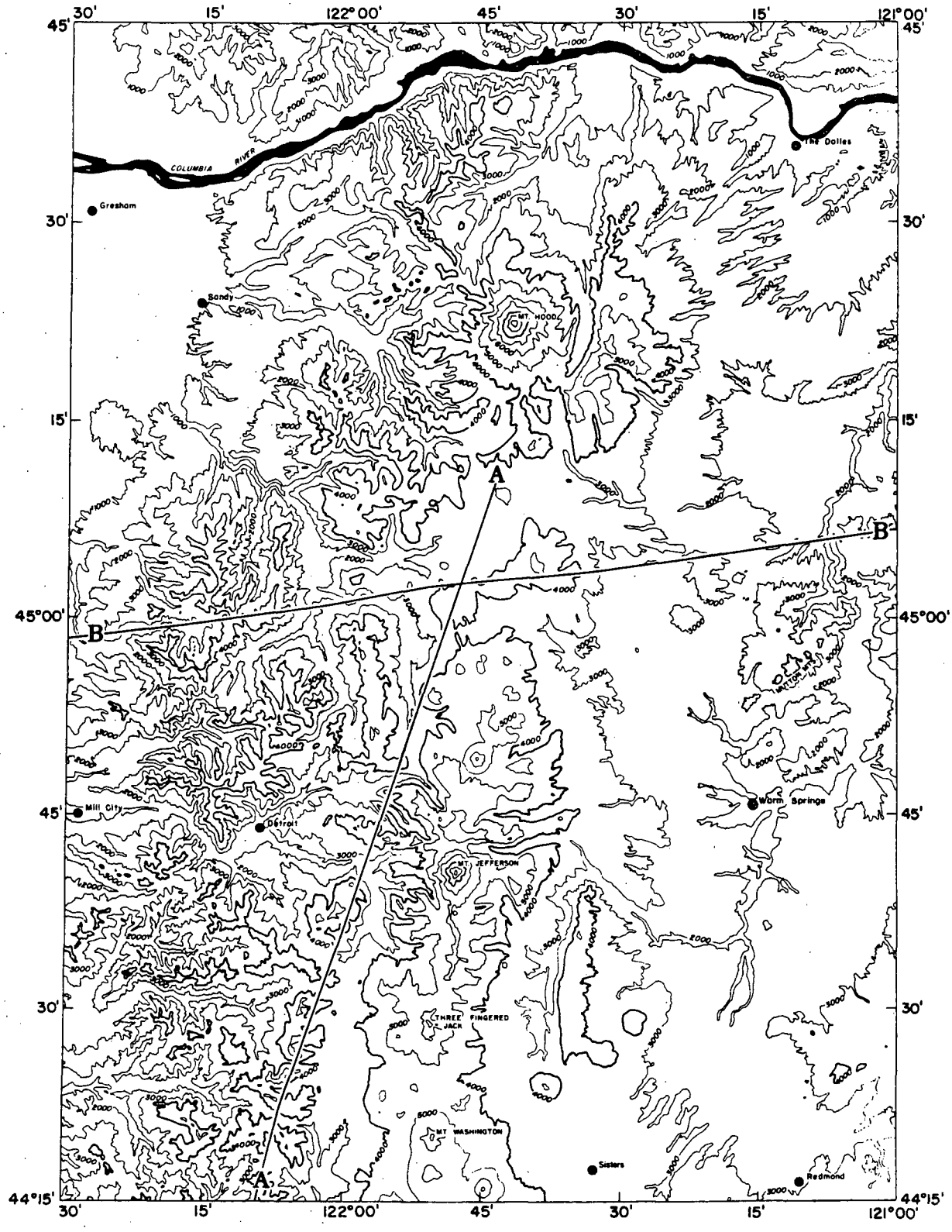

TOPOGRAPHIC MAP
CASCADE MOUNTAIN RANGE, NORTHERN OREGON

MAP LOCATION

DATA FROM USGS 1:250,000 QUADRANGLE MAPS
BEND NL 10-12
SALEM NL 10-11
VANCOUVER NL 10-8
THE DALLES NL 10-9

KILOMETERS
0 5 10 15 20
0 5 10
MILES

TRANSVERSE MERCATOR PROJECTION
CONTOUR INTERVAL 1000 FEET

OREGON STATE UNIVERSITY
DECEMBER, 1980

Figure 2.

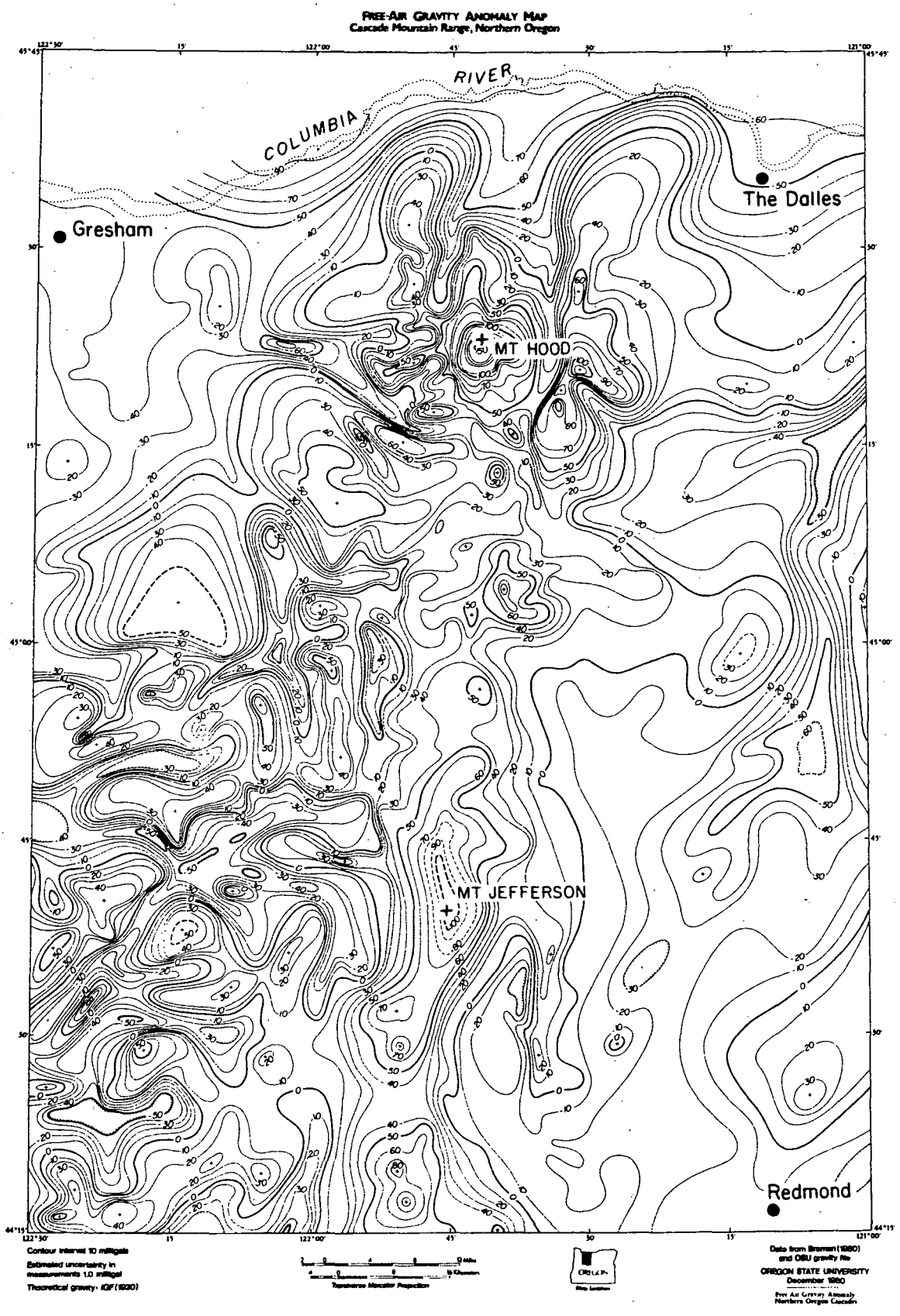
FREE-AIR GRAVITY ANOMALY MAP
Cascade Mountain Range, Northern Oregon
COLUMBIA RIVER
Gresham
The Dalles
MT HOOD
MT JEFFERSON
Redmond
Contour interval 10 milligals
Estimated uncertainty in measurements 1.0 milligal
Theoretical gravity: (GF 1930)
Transverse Mercator Projection
Data from Bremner (1980) and OSU gravity file
OREGON STATE UNIVERSITY
December 1980
Free Air Gravity Anomaly
Northern Oregon Cascades

Figure 3.

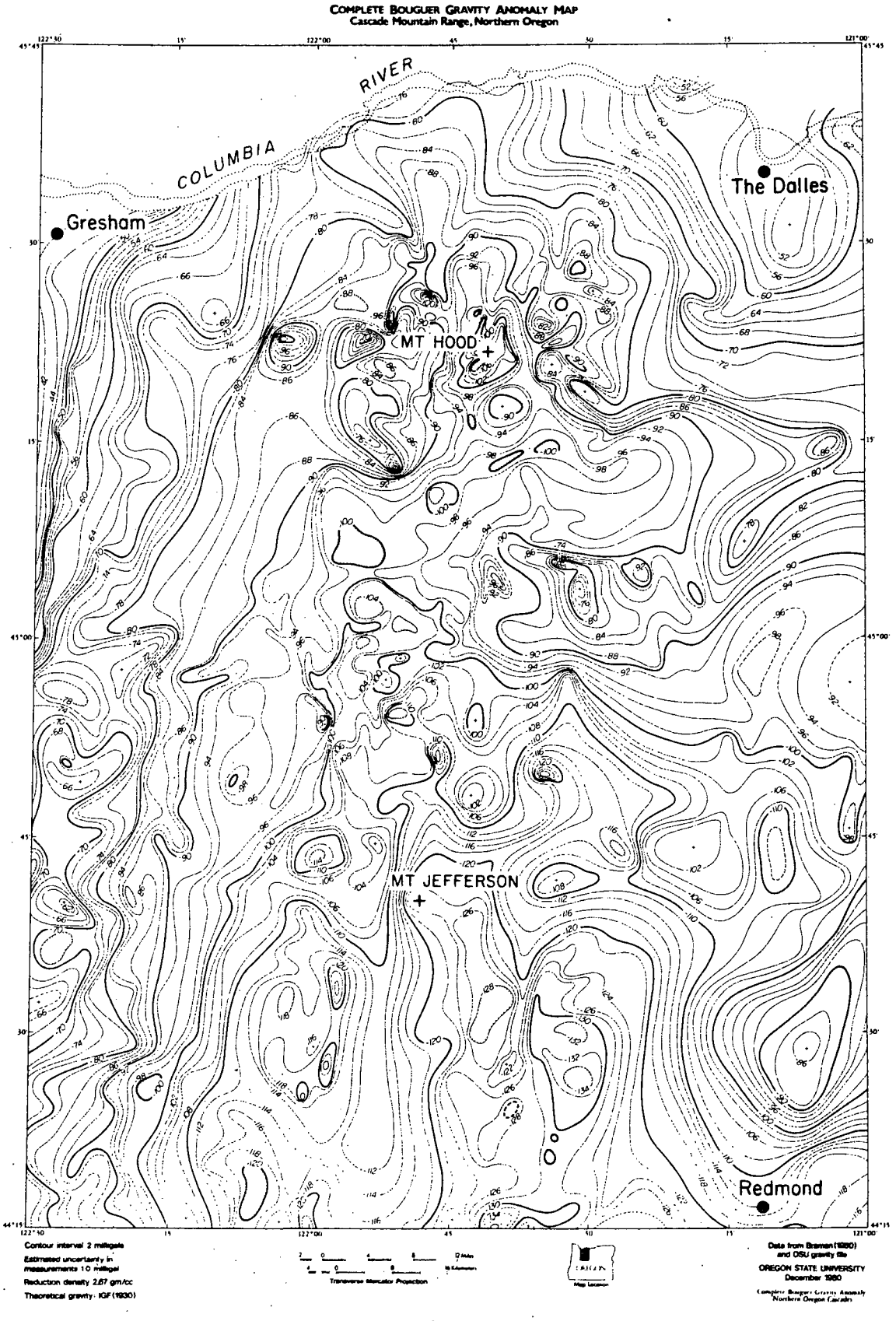
COMPLETE BOUGUER GRAVITY ANOMALY MAP
Cascade Mountain Range, Northern Oregon
COLUMBIA RIVER
Gresham
The Dalles
MT HOOD
MT JEFFERSON
Redmond
Contour interval 2 milligals
Estimated uncertainty in measurements 1.0 milligal
Reduction density 2.67 gm/cc
Theoretical gravity: IGF(1930)
Transverse Mercator Projection
Data from Bremner (1980) and OSU gravity file
OREGON STATE UNIVERSITY
December 1980

Figure 4.

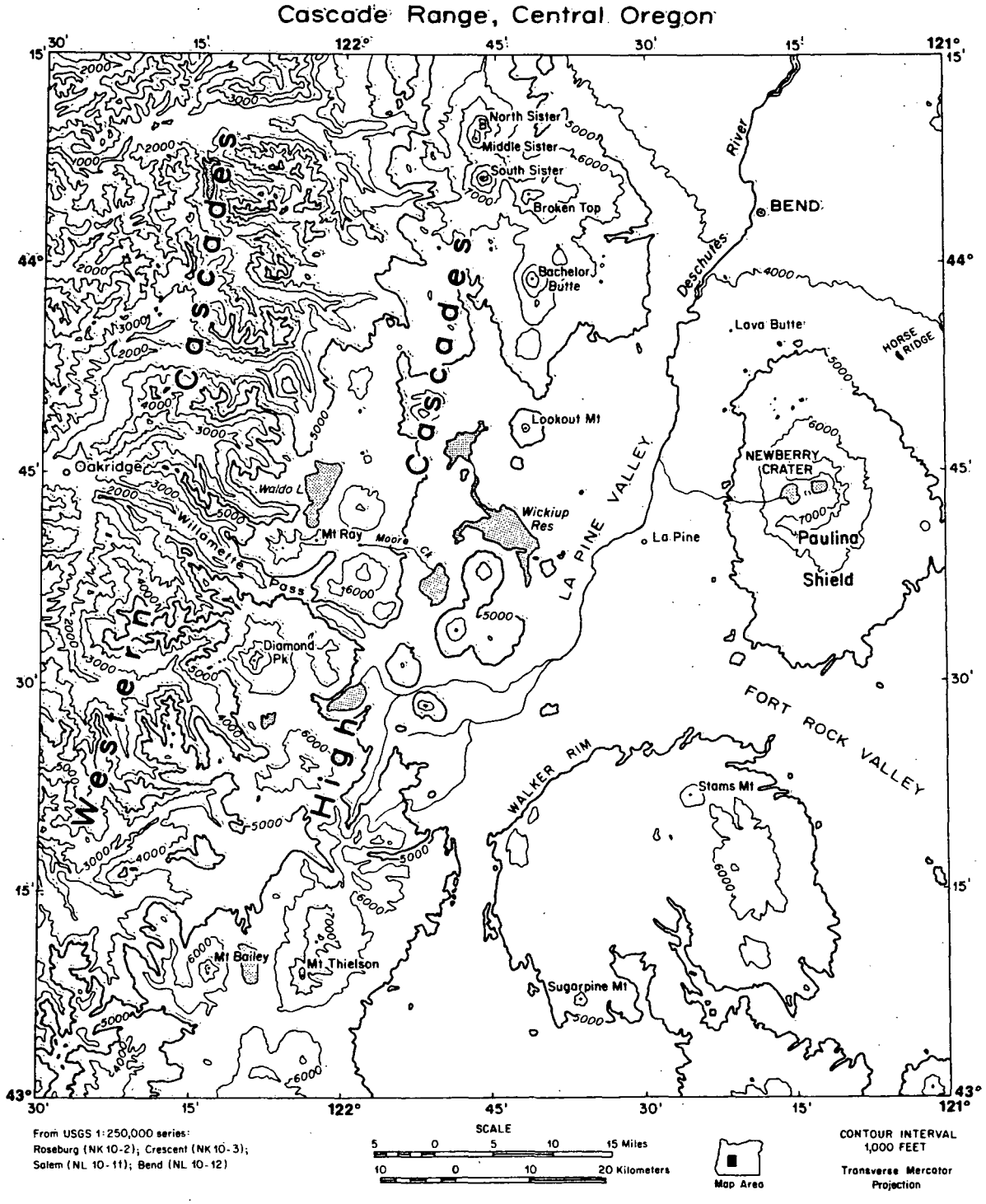
Cascade Range, Central Oregon
122° 45' 30' 15' 121° 15'
44° 45' 30' 43°
North Sister
Middle Sister
South Sister
Broken Top
Bachelor Butte
BEND
Deschutes River
Lava Butte
HORSE RIDGE
Lookout Mt
NEWBERRY CRATER
Paulina
Shield
La Pine
LA PINE VALLEY
Wickiup Res
Moore Ck
Mt Ray
Oakridge
Waldo L
Willamette Pass
Diamond Pk
Cascades
Western Cascades
High
FORT ROCK VALLEY
WALKER RIM
Stams Mt
Sugarpine Mt
Mt Bailey
Mt Thielson
From USGS 1:250,000 series:
Roseburg (NK 10-2); Crescent (NK 10-3);
Salem (NL 10-11); Bend (NL 10-12)
SCALE
5 0 5 10 15 Miles
10 0 10 20 Kilometers
Map Area
CONTOUR INTERVAL
1,000 FEET
Transverse Mercator
Projection

Figure 5.

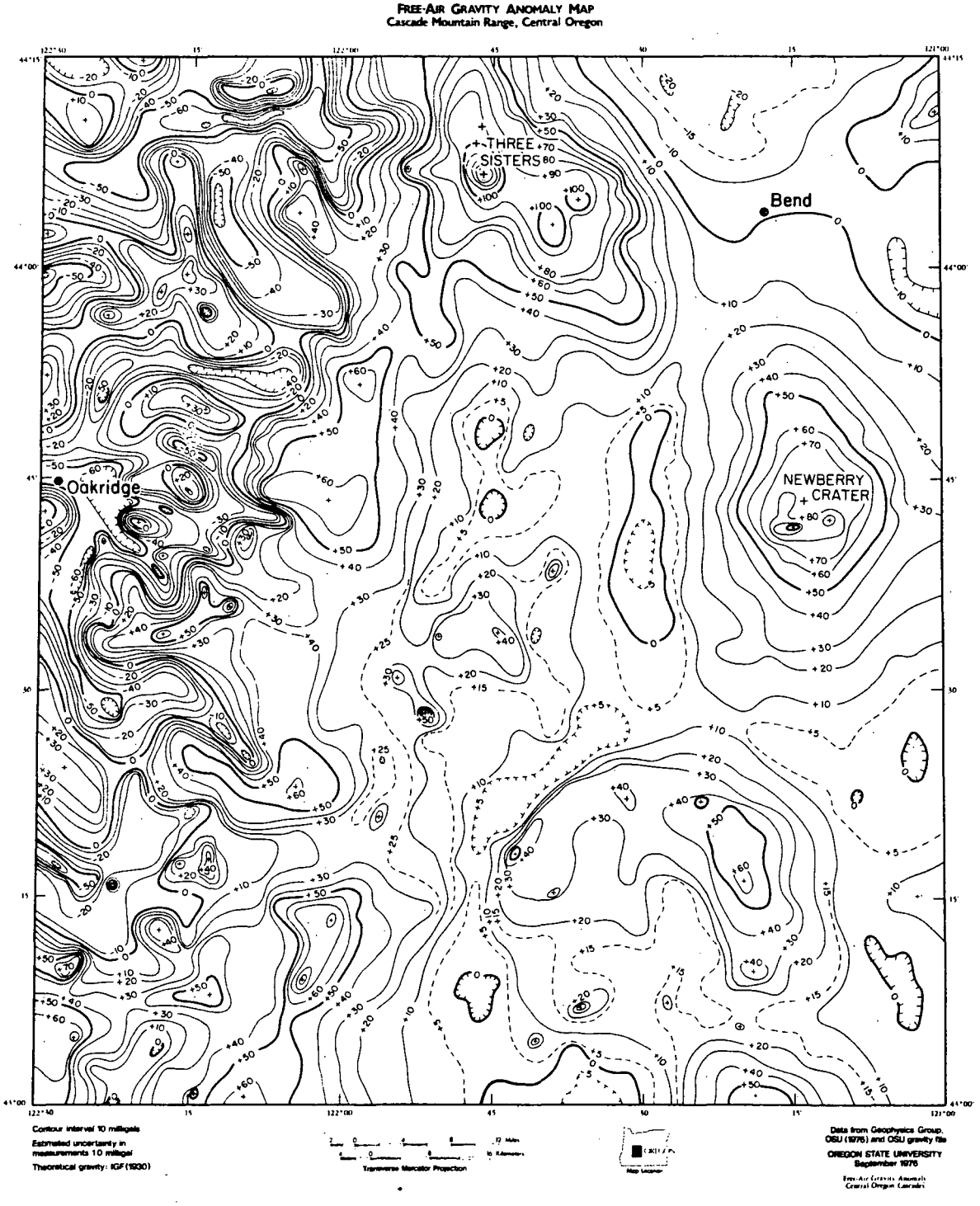
FREE-AIR GRAVITY ANOMALY MAP
Cascade Mountain Range, Central Oregon
THREE SISTERS
Bend
NEWBERRY CRATER
Oakridge
Contour interval 10 milligals
Estimated uncertainty in measurements 10 milligal
Theoretical gravity: IGF(1930)
Transverse Mercator Projection
Data from Geophysics Group, OSU (1976) and OSU gravity file
OREGON STATE UNIVERSITY
September 1976

Figure 6.

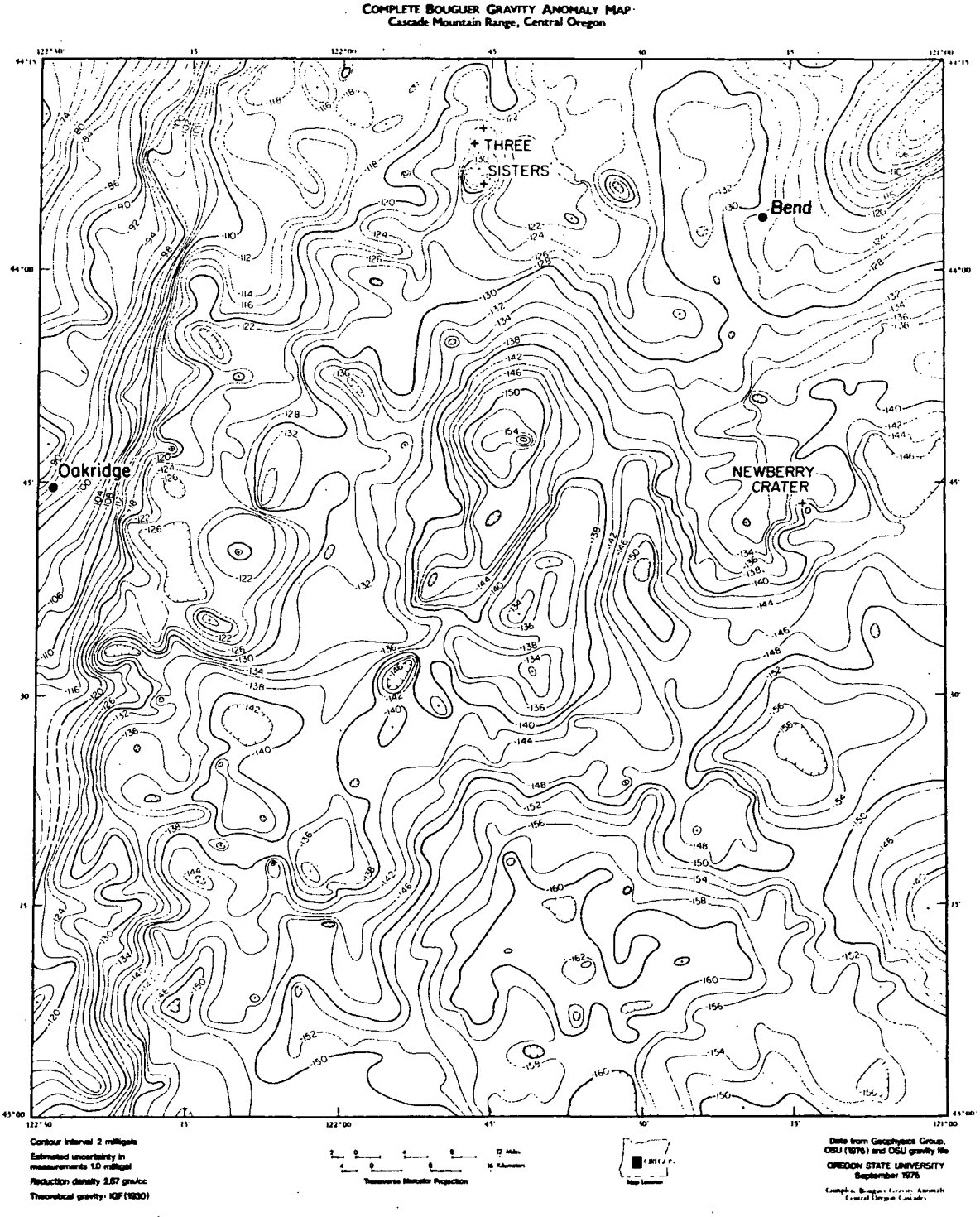
COMPLETE BOUGUER GRAVITY ANOMALY MAP
Cascade Mountain Range, Central Oregon
THREE SISTERS
Bend
Oakridge
NEWBERRY CRATER
Contour interval 2 milligals
Estimated uncertainty in measurements 1.0 milligal
Reduction density 2.67 gm/cc
Theoretical gravity: IGF(1930)
Data from Geophysics Group, OSU (1976) and OSU gravity file
OREGON STATE UNIVERSITY
September 1976

Figure 7.

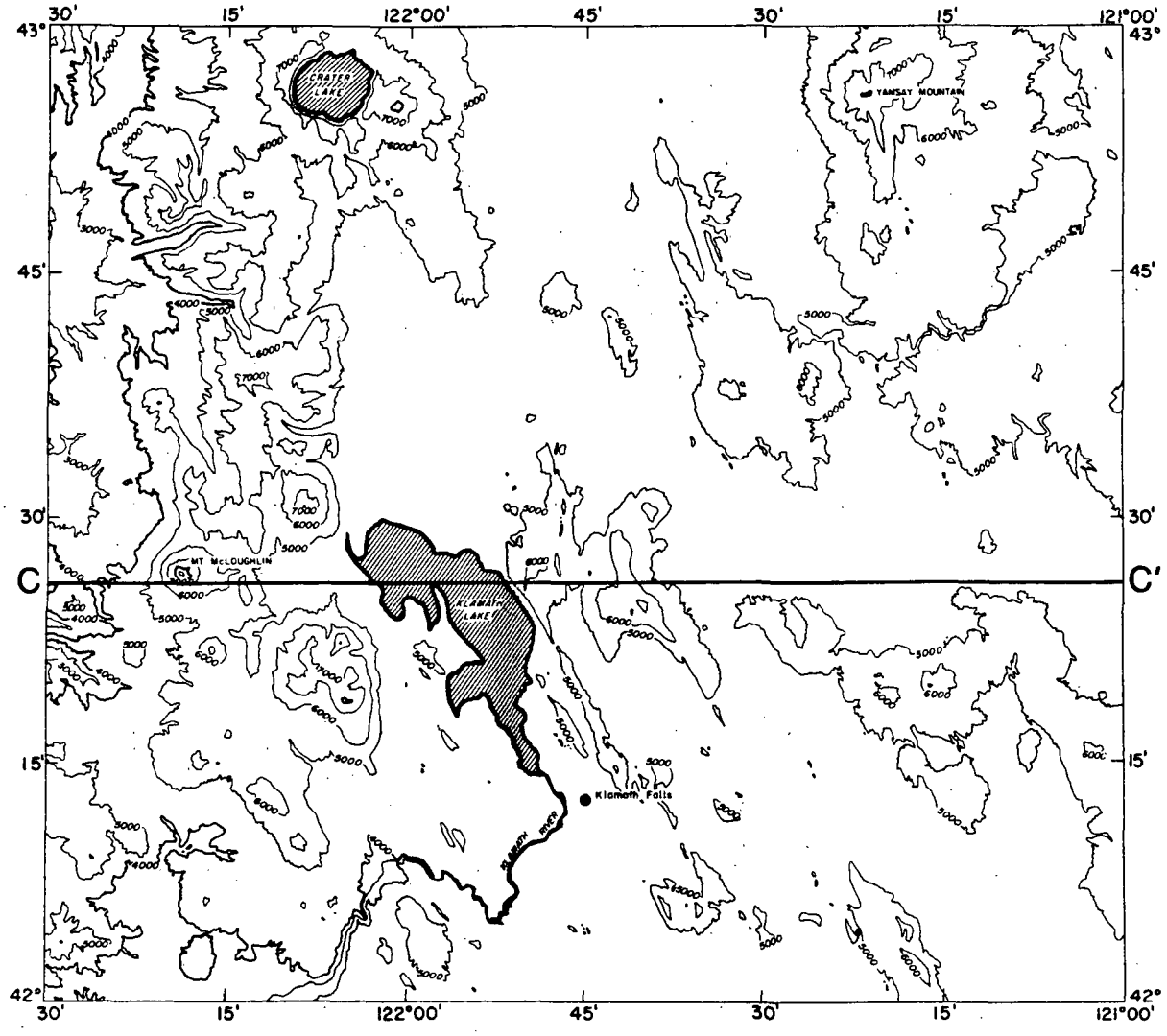

TOPOGRAPHIC MAP
CASCADE MOUNTAIN RANGE, SOUTHERN OREGON

DATA FROM USGS 1:250,000 QUADRANGLE MAPS
KLAMATH FALLS NK 10-6
MEDFORD NK 10-5

KILOMETERS
0 5 10 15 20
0 5 10
MILES

TRANSVERSE MERCATOR PROJECTION
CONTOUR INTERVAL 1000 FEET

OREGON STATE UNIVERSITY
DECEMBER, 1980

Figure 8.

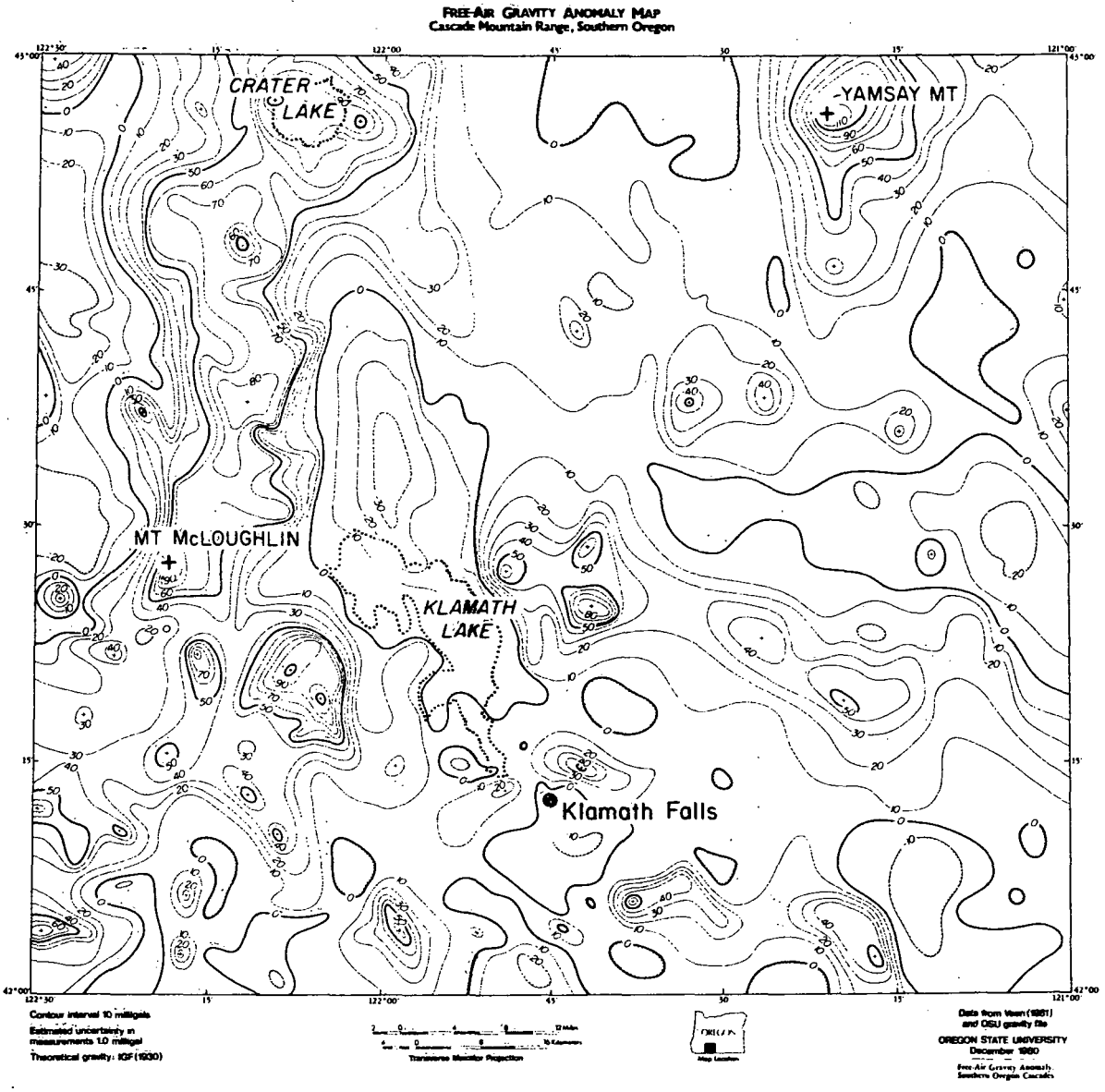
FREE-AIR GRAVITY ANOMALY MAP
Cascade Mountain Range, Southern Oregon
CRATER LAKE
YAMSAY MT
MT McLOUGHLIN
KLAMATH LAKE
Klamath Falls
Contour interval 10 milligals
Estimated uncertainty in measurements 1.0 milligal
Theoretical gravity: IGF(1930)
Transverse Mercator Projection
OREGON
Map Location
Data from Woollard (1951) and OSU gravity file
OREGON STATE UNIVERSITY
December 1980
Free-Air Gravity Anomaly, Southern Oregon Cascades

Figure 9.

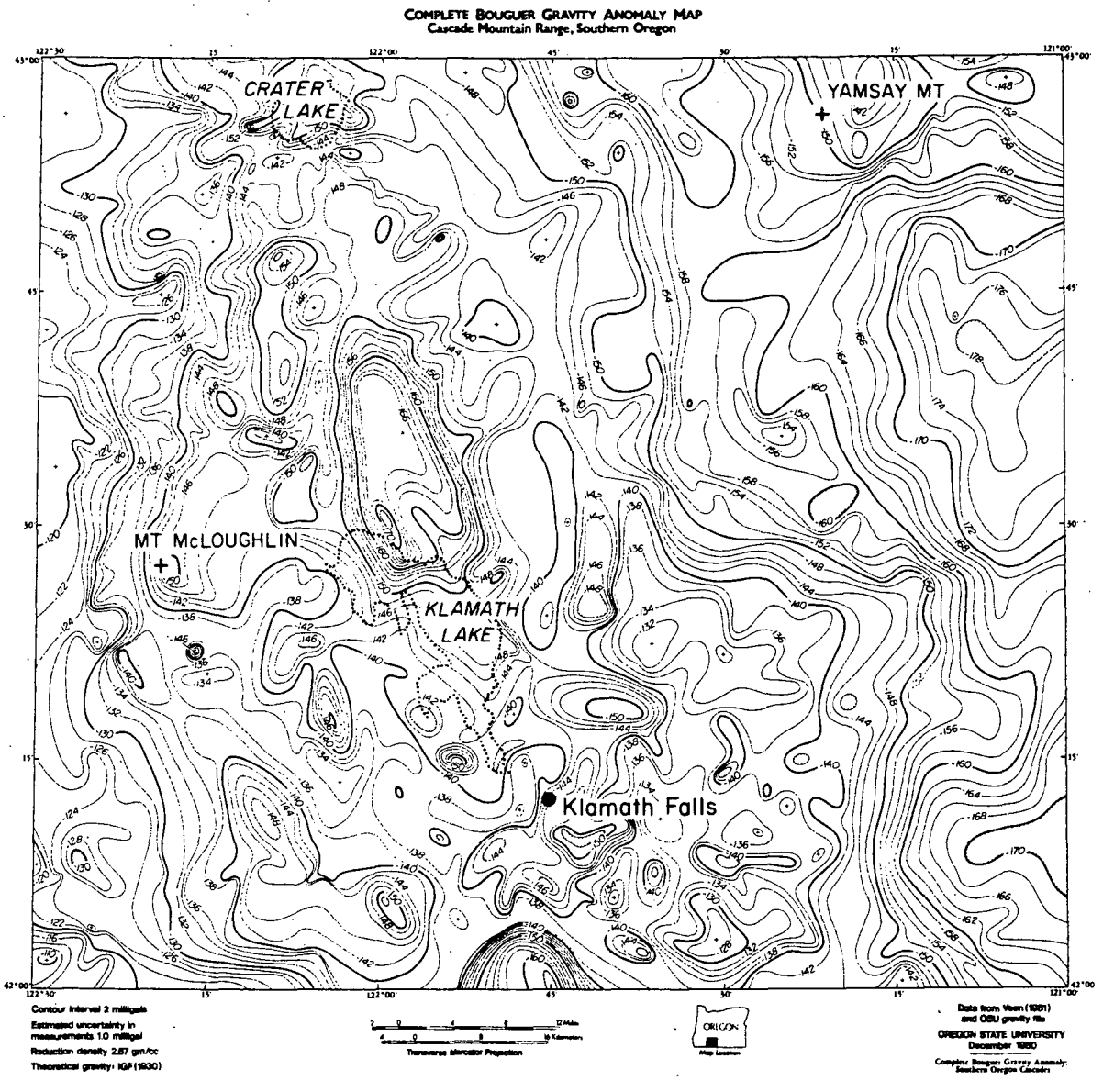
COMPLETE BOUGUER GRAVITY ANOMALY MAP
Cascade Mountain Range, Southern Oregon
CRATER LAKE
YAMSAY MT
MT McLOUGHLIN
KLAMATH LAKE
Klamath Falls
Contour interval 2 milligals
Estimated uncertainty in measurements 1.0 milligal
Reduction density 2.67 gm/cc
Theoretical gravity: IGF(1930)
Transverse Mercator Projection
OREGON
Data from Mean (1981) and OSU gravity file
OREGON STATE UNIVERSITY
December 1980

Figure 10.

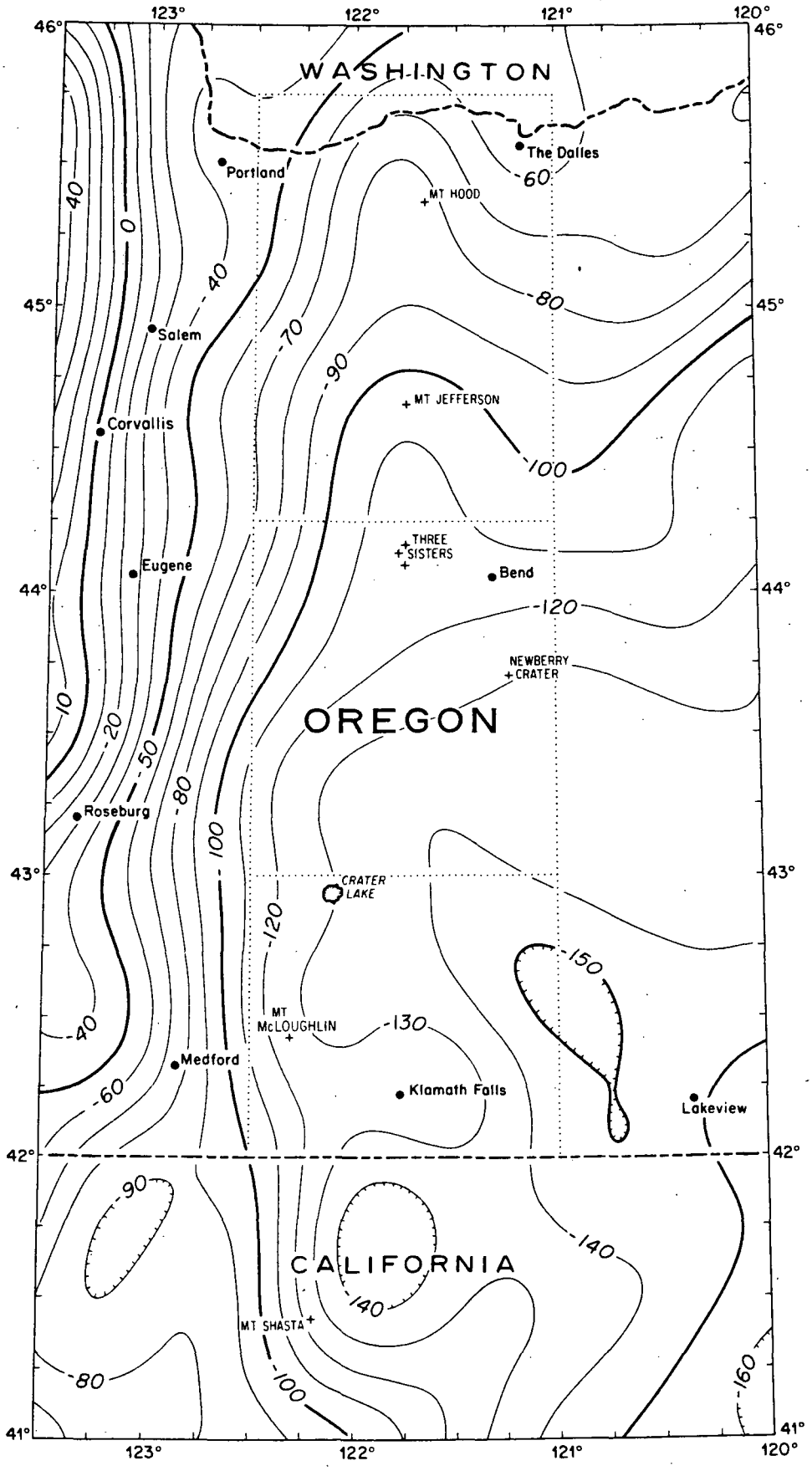
123°
122°
121°
120°
46°
45°
44°
43°
42°
41°
WASHINGTON
OREGON
CALIFORNIA
Portland
The Dalles
MT HOOD
Salem
Corvallis
MT JEFFERSON
THREE SISTERS
Bend
Eugene
NEWBERRY CRATER
Roseburg
CRATER LAKE
MT McLOUGHLIN
Medford
Klamath Falls
Lakeview
MT SHASTA
0
10
20
40
50
60
70
80
90
100
120
130
140
150
160

Figure 11.

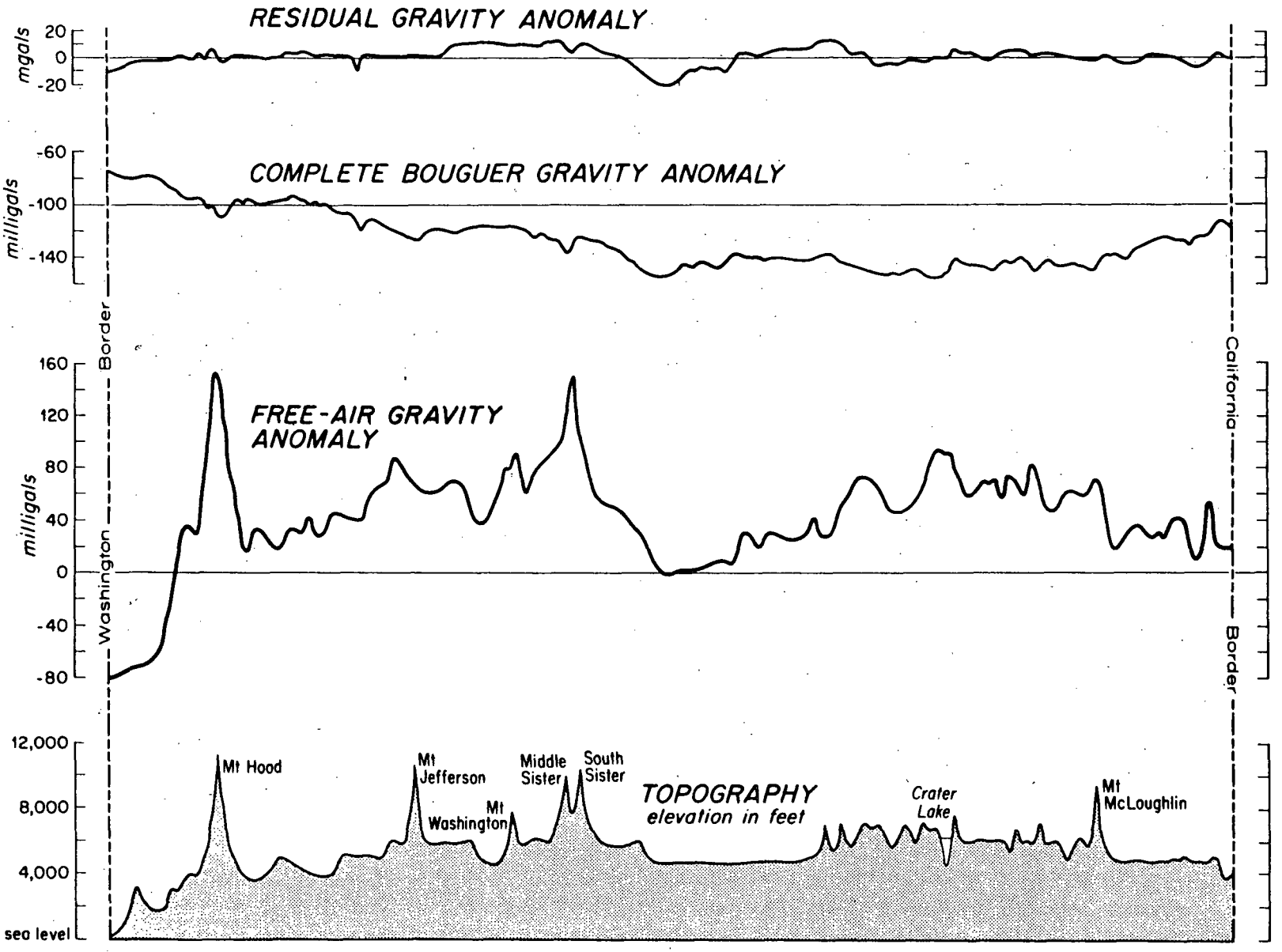
RESIDUAL GRAVITY ANOMALY
mgals
20
0
-20
COMPLETE BOUGUER GRAVITY ANOMALY
milligals
-60
-100
-140
Washington Border
California Border
FREE-AIR GRAVITY ANOMALY
milligals
160
120
80
40
0
-40
-80
TOPOGRAPHY
elevation in feet
12,000
8,000
4,000
sea level
Mt Hood
Mt Jefferson
Mt Washington
Middle Sister
South Sister
Crater Lake
Mt McLoughlin

Figure 12.

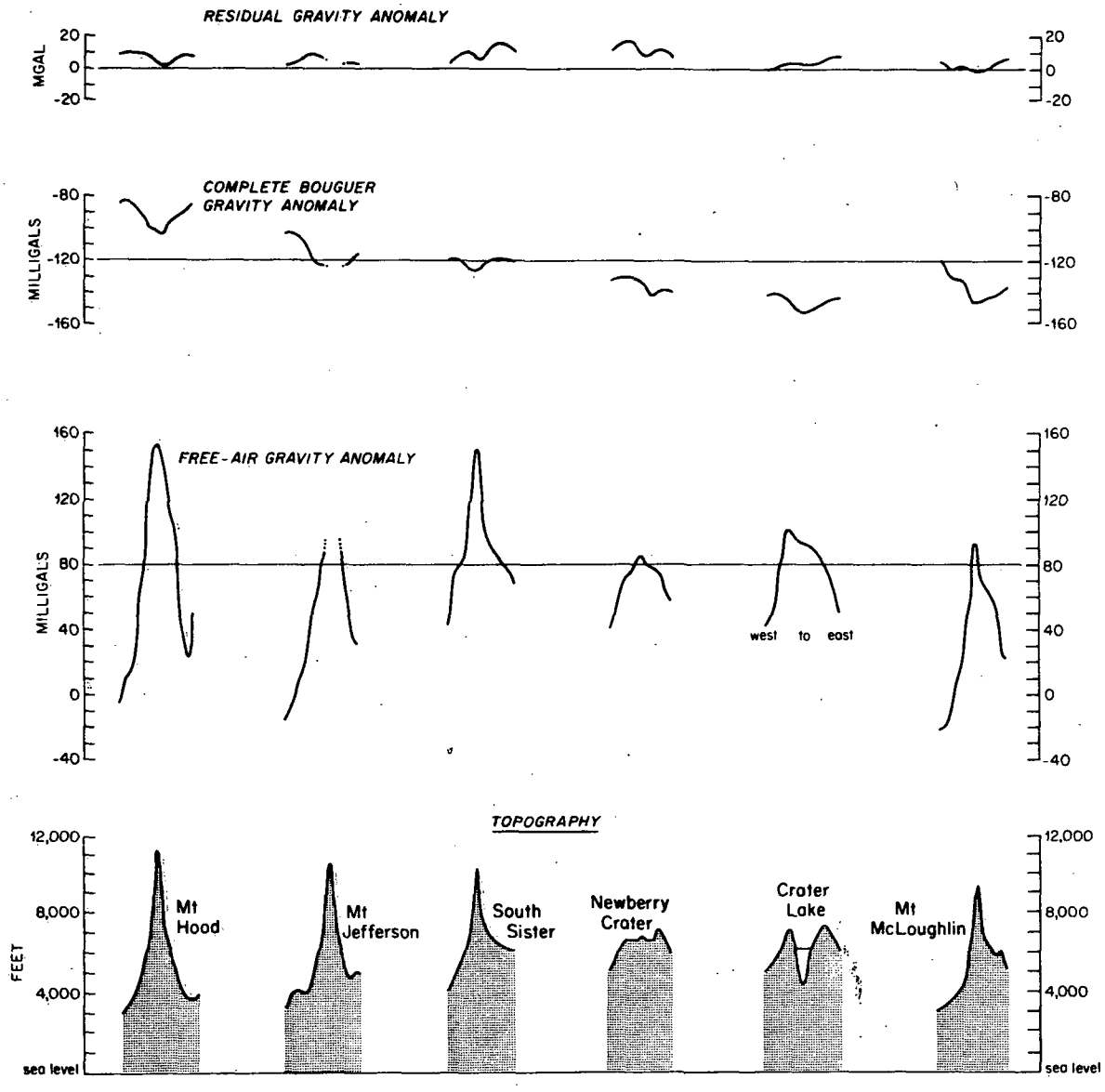
RESIDUAL GRAVITY ANOMALY
MGAL
20
0
-20
COMPLETE BOUGUER GRAVITY ANOMALY
MILLIGALS
-80
-120
-160
FREE-AIR GRAVITY ANOMALY
MILLIGALS
160
120
80
40
0
-40
west to east
TOPOGRAPHY
FEET
12,000
8,000
4,000
sea level
Mt Hood
Mt Jefferson
South Sister
Newberry Crater
Crater Lake
Mt McLoughlin

Figure 13.

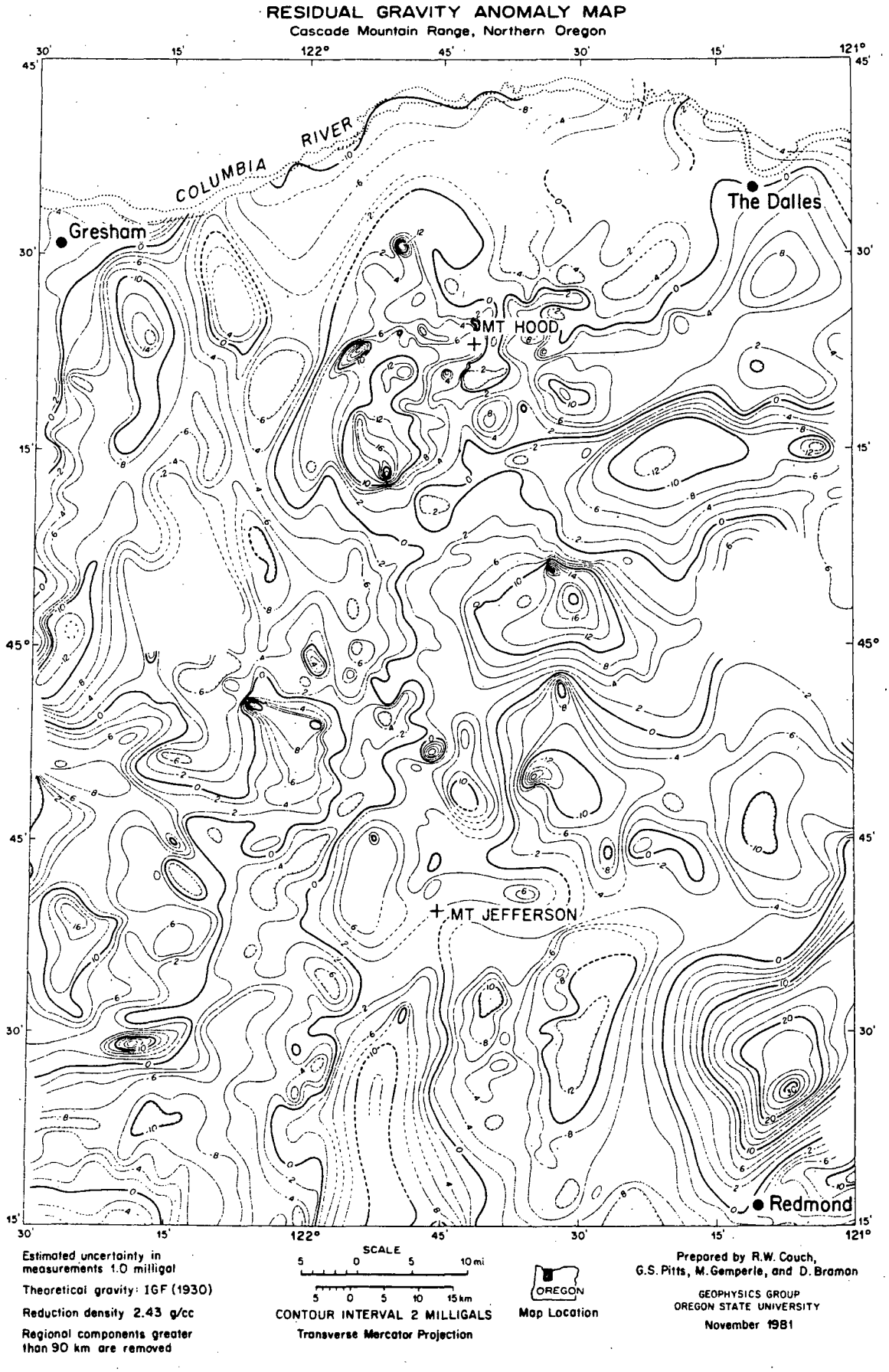
RESIDUAL GRAVITY ANOMALY MAP
Cascade Mountain Range, Northern Oregon
COLUMBIA RIVER
Gresham
The Dalles
MT HOOD
MT JEFFERSON
Redmond
30'
15'
122°
45'
121°
45°
Estimated uncertainty in measurements 1.0 milligal
Theoretical gravity: IGF (1930)
Reduction density 2.43 g/cc
Regional components greater than 90 km are removed
SCALE
5 0 5 10 mi
5 0 5 10 15 km
CONTOUR INTERVAL 2 MILLIGALS
Transverse Mercator Projection
OREGON
Map Location
Prepared by R.W. Couch, G.S. Pitts, M. Gemperle, and D. Braman
GEOPHYSICS GROUP
OREGON STATE UNIVERSITY
November 1981

Figure 14.

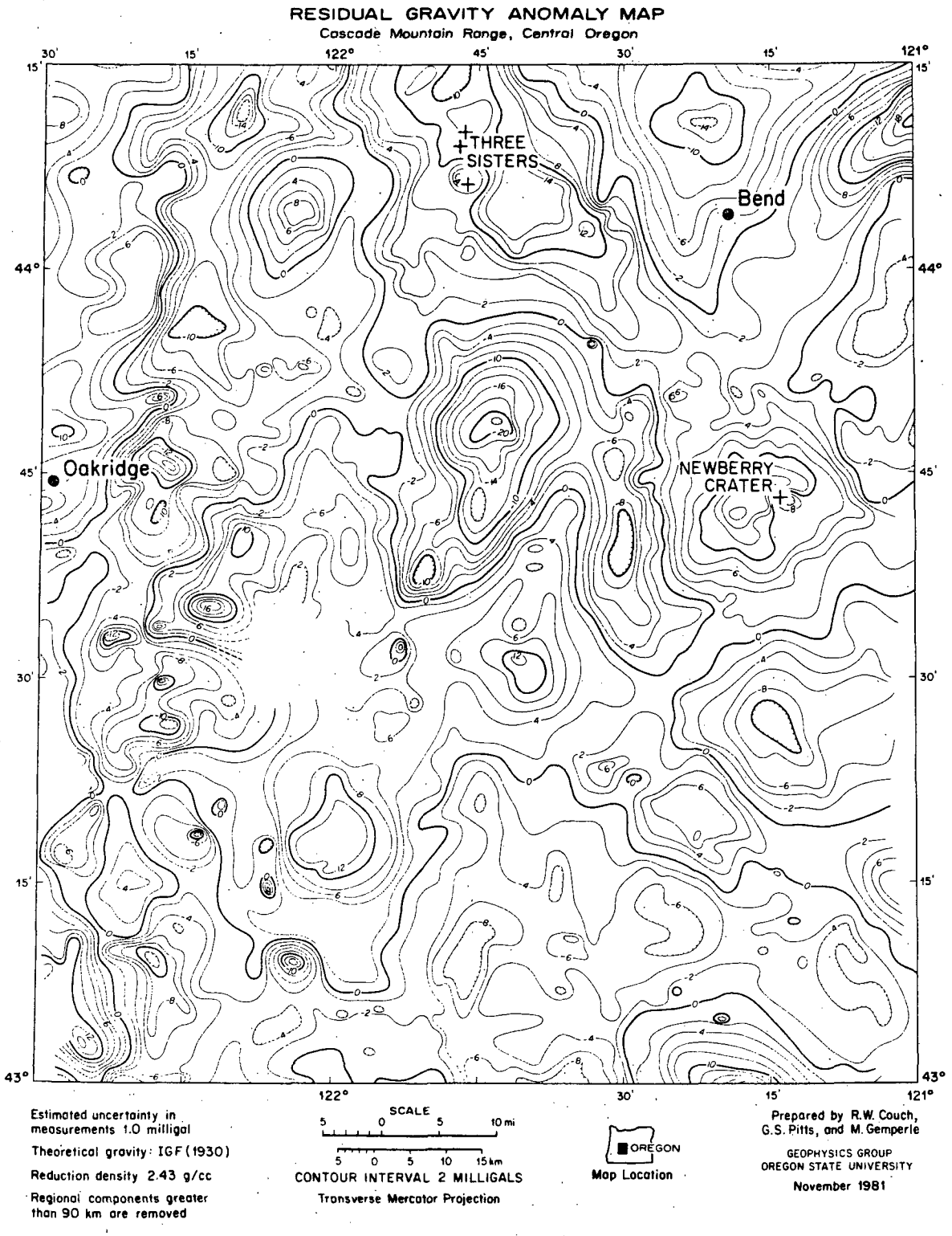
RESIDUAL GRAVITY ANOMALY MAP
Cascade Mountain Range, Central Oregon
30'
15'
122°
45'
30'
15'
121°
15'
44°
45'
30'
15'
43°
THREE SISTERS
Bend
Oakridge
NEWBERRY CRATER
Estimated uncertainty in measurements 1.0 milligal
Theoretical gravity: IGF (1930)
Reduction density 2.43 g/cc
Regional components greater than 90 km are removed
SCALE
5 0 5 10 mi
5 0 5 10 15 km
CONTOUR INTERVAL 2 MILLIGALS
Transverse Mercator Projection
OREGON
Map Location
Prepared by R.W. Couch, G.S. Pitts, and M. Gemperle
GEOPHYSICS GROUP
OREGON STATE UNIVERSITY
November 1981

Figure 15.

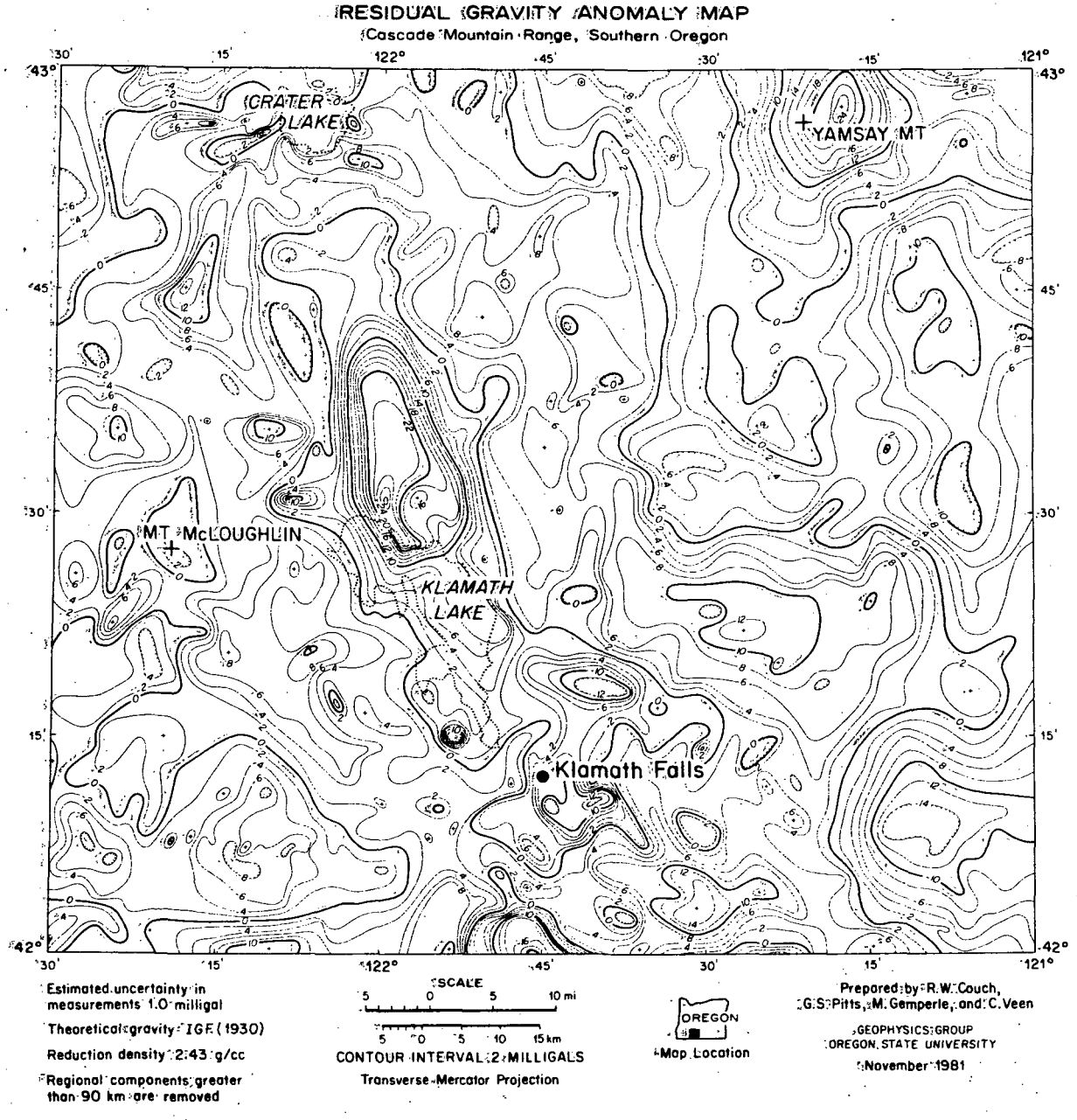
RESIDUAL GRAVITY ANOMALY MAP
Cascade Mountain Range, Southern Oregon
CRATER LAKE
YAMSAY MT
MT McLOUGHLIN
KLAMATH LAKE
Klamath Falls
Estimated uncertainty in measurements 1.0 milligal
Theoretical gravity IGF (1930)
Reduction density 2.43 g/cc
Regional components greater than 90 km are removed
SCALE
CONTOUR INTERVAL 2 MILLIGALS
Transverse Mercator Projection
OREGON
Map Location
Prepared by R.W. Couch, G.S. Pitts, M. Gemperle, and C. Veen
GEOPHYSICS GROUP
OREGON STATE UNIVERSITY
November 1981

Figure 16.

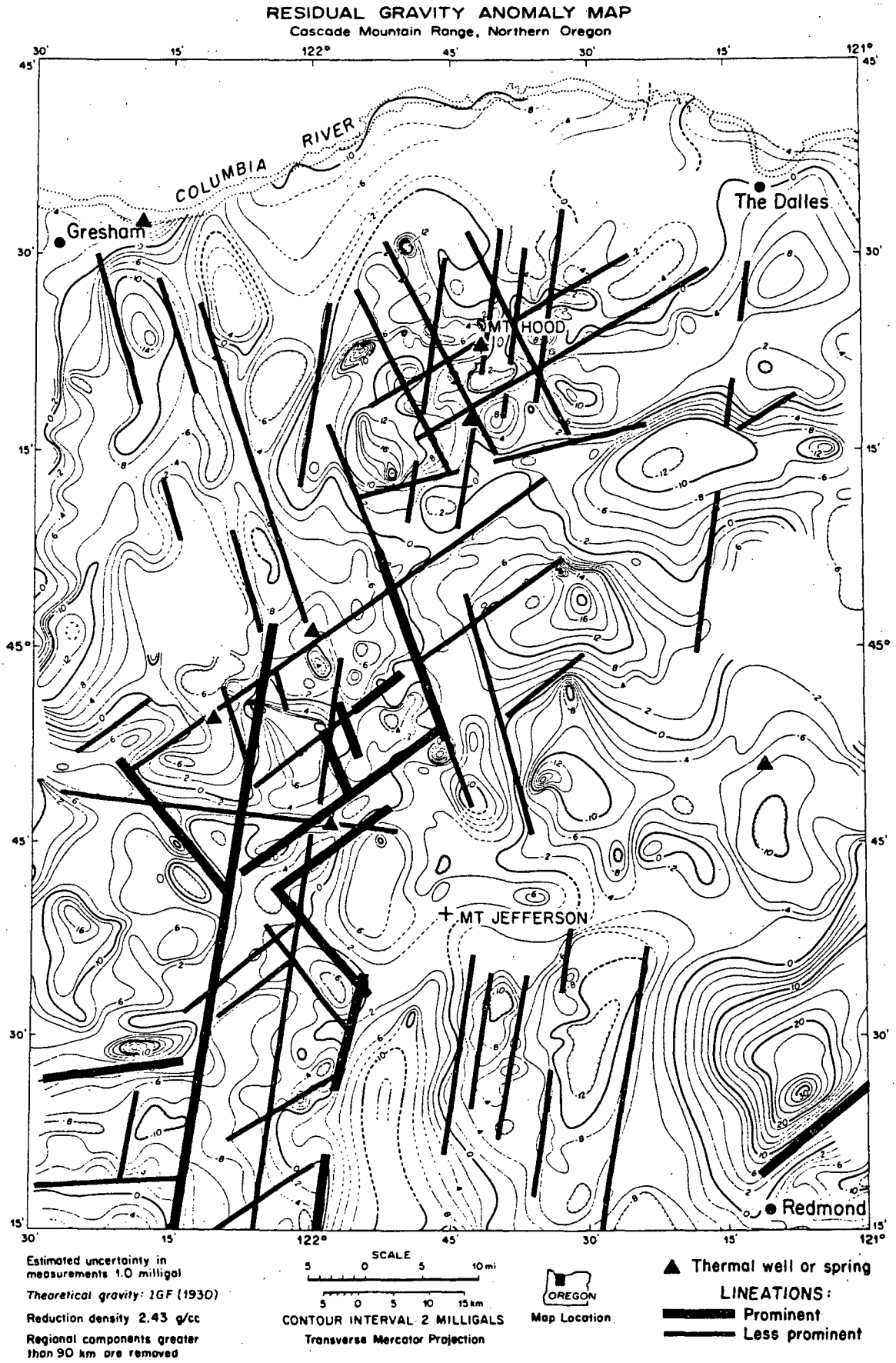
RESIDUAL GRAVITY ANOMALY MAP
Cascade Mountain Range, Northern Oregon
COLUMBIA RIVER
Gresham
The Dalles
MT. HOOD
MT JEFFERSON
Redmond
Estimated uncertainty in measurements 1.0 milligal
Theoretical gravity: IGF (1930)
Reduction density 2.43 g/cc
Regional components greater than 90 km are removed
SCALE
CONTOUR INTERVAL 2 MILLIGALS
Transverse Mercator Projection
OREGON
Map Location
Thermal well or spring
LINEATIONS:
Prominent
Less prominent

Figure 17.

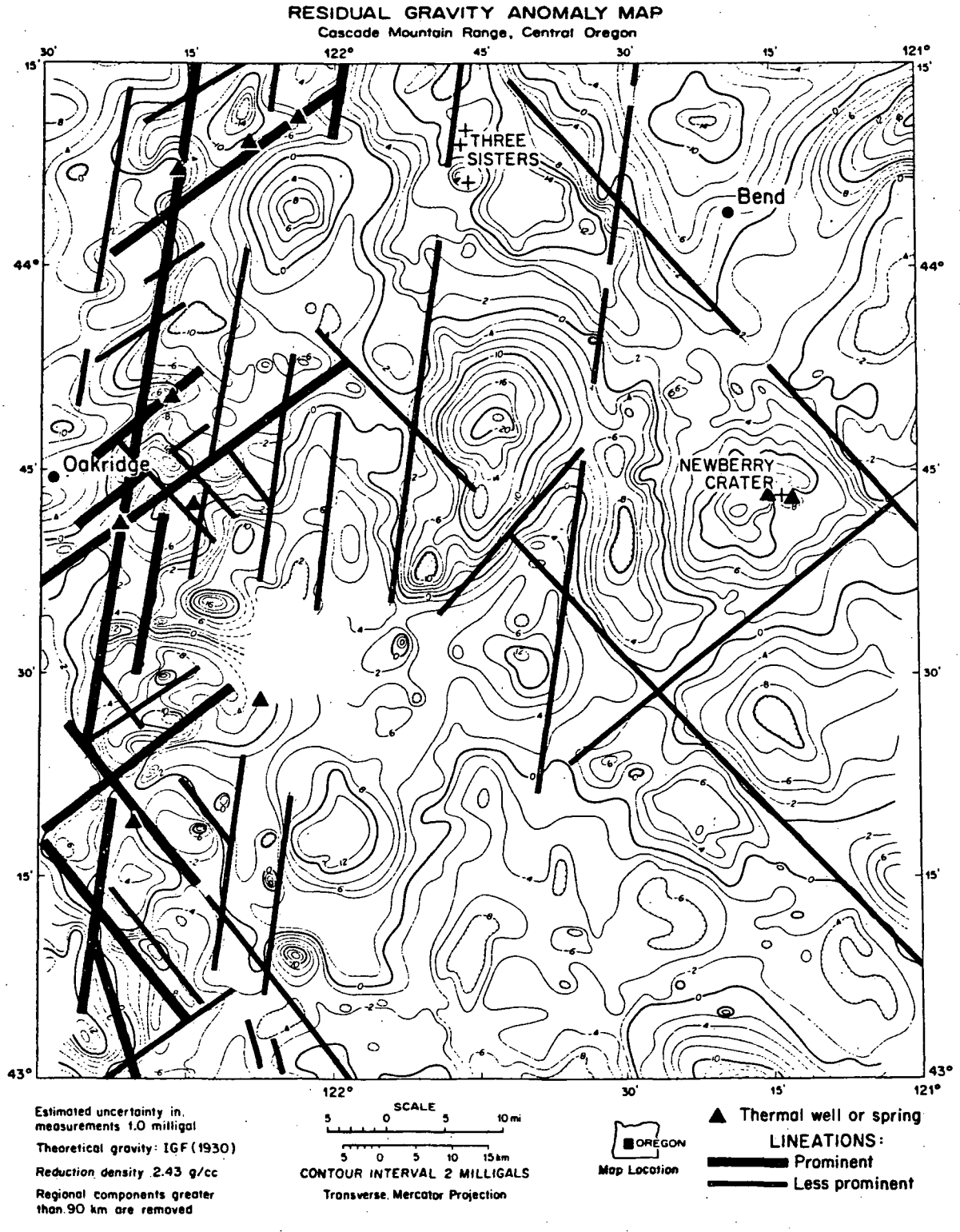
RESIDUAL GRAVITY ANOMALY MAP
Cascade Mountain Range, Central Oregon
30'
15'
122°
45'
30'
15'
121°
15'
44°
45'
30'
15'
43°
THREE SISTERS
Bend
Oakridge
NEWBERRY CRATER
Estimated uncertainty in measurements 1.0 milligal
Theoretical gravity: IGF (1930)
Reduction density 2.43 g/cc
Regional components greater than 90 km are removed
SCALE
5 0 5 10 mi
5 0 5 10 15 km
CONTOUR INTERVAL 2 MILLIGALS
Transverse Mercator Projection
OREGON
Map Location
Thermal well or spring
LINEATIONS:
Prominent
Less prominent

Figure 18.

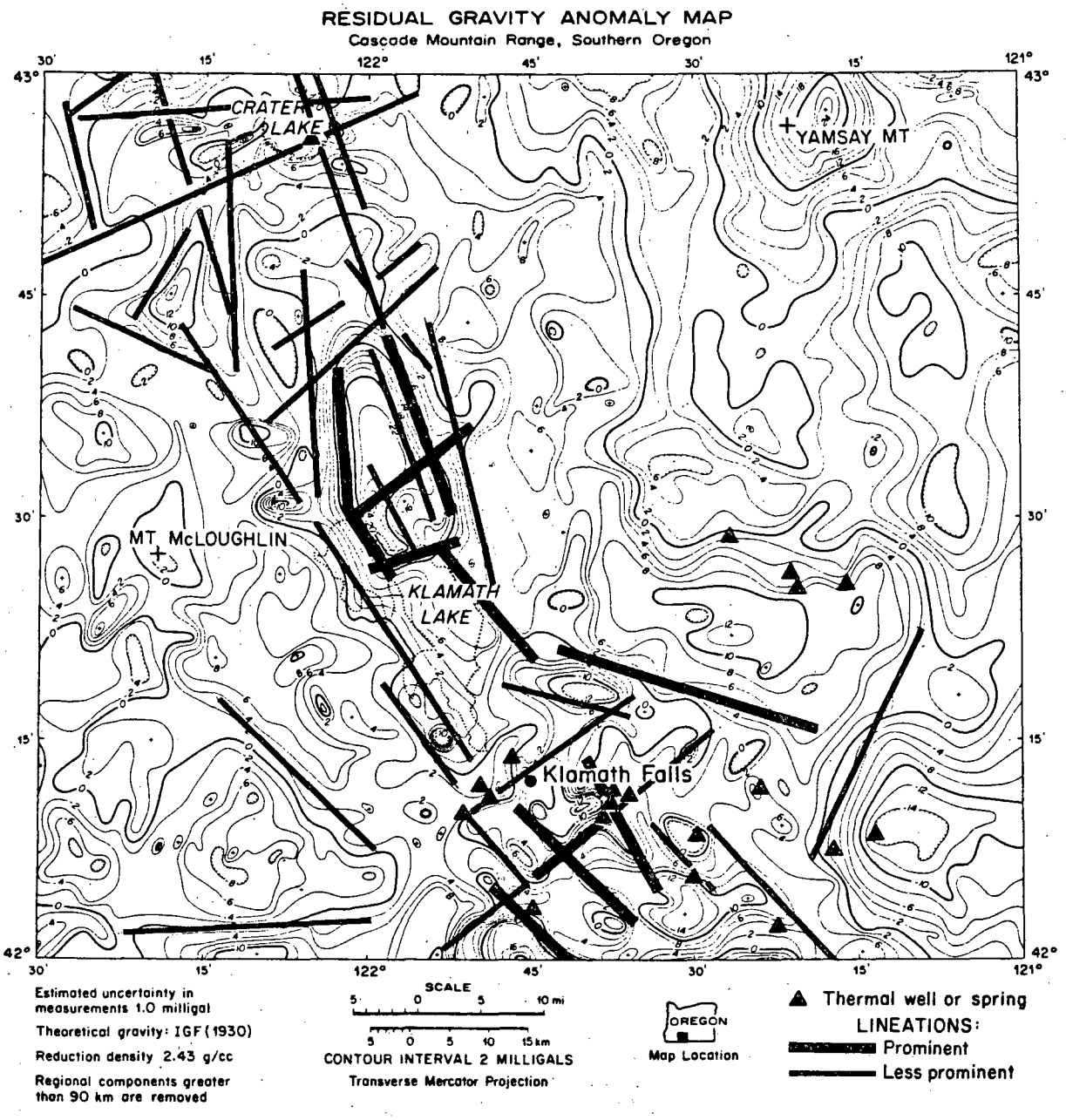
RESIDUAL GRAVITY ANOMALY MAP
Cascade Mountain Range, Southern Oregon
CRATER LAKE
YAMSAY MT
MT McLOUGHLIN
KLAMATH LAKE
Klamath Falls
Estimated uncertainty in measurements 1.0 milligal
Theoretical gravity: IGF (1930)
Reduction density 2.43 g/cc
Regional components greater than 90 km are removed
SCALE
CONTOUR INTERVAL 2 MILLIGALS
Transverse Mercator Projection
OREGON
Map Location
Thermal well or spring
LINEATIONS:
Prominent
Less prominent

Figure 19.

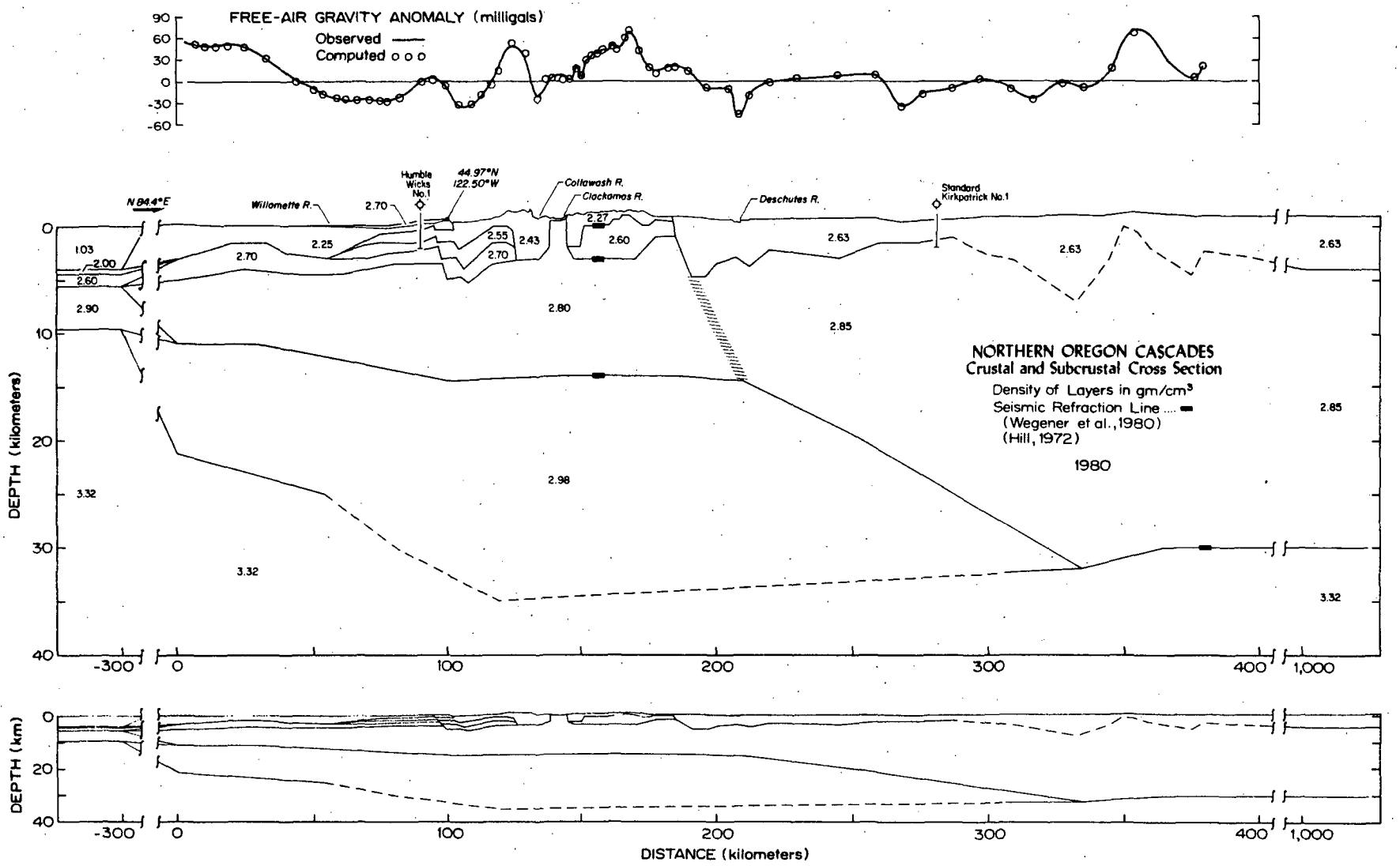
FREE-AIR GRAVITY ANOMALY (milligals)
Observed
Computed
90
60
30
0
-30
-60
N 84.4° E
Willamette R.
Humble Wicks No.1
44.97°N 122.50°W
Columbia R.
Clackamas R.
Deschutes R.
Standard Kirkpatrick No.1
2.70
2.27
2.25
2.55
2.43
2.70
2.60
2.63
2.63
2.63
1.03
2.00
2.60
2.90
2.80
2.85
2.85
2.98
3.32
3.32
3.32
NORTHERN OREGON CASCADES
Crustal and Subcrustal Cross Section
Density of Layers in gm/cm³
Seismic Refraction Line ....
(Wegener et al., 1980)
(Hill, 1972)
1980
DEPTH (kilometers)
DEPTH (km)
0
10
20
30
40
-300
0
100
200
300
400
1,000
DISTANCE (kilometers)

Figure 20.

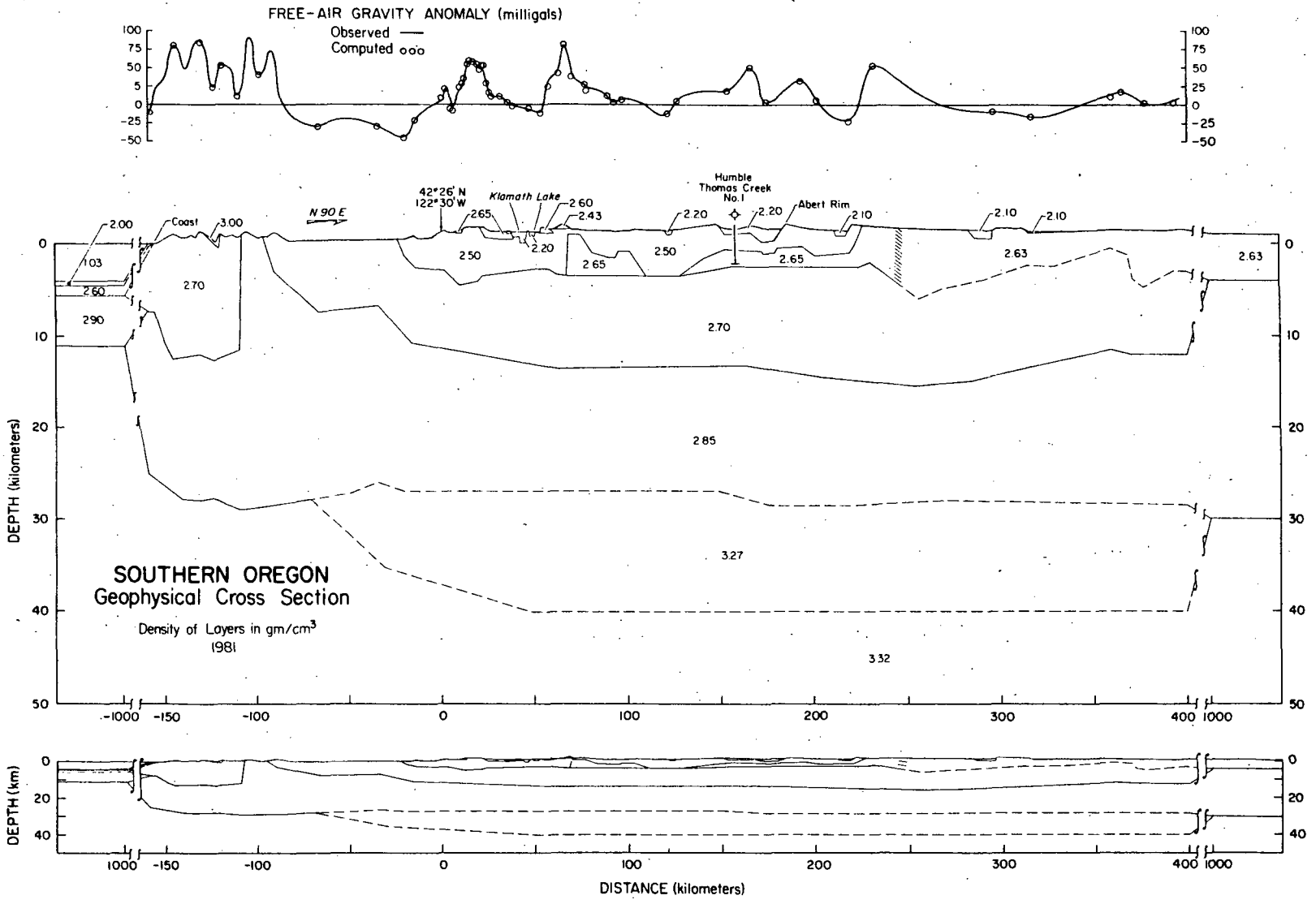
FREE-AIR GRAVITY ANOMALY (milligals)
Observed
Computed
100
75
50
25
0
-25
-50
42°26' N
122°30' W
Klamath Lake
Humble
Thomas Creek
No.1
Abert Rim
N 90 E
Coast
2.00
3.00
2.65
2.60
2.43
2.20
2.10
1.03
2.70
2.90
2.50
2.65
2.63
2.85
3.27
3.32
SOUTHERN OREGON
Geophysical Cross Section
Density of Layers in gm/cm³
1981
DEPTH (kilometers)
DEPTH (km)
-1000
-150
-100
0
100
200
300
400
1000
DISTANCE (kilometers)

Figure 21.